Building Stronger Synapses: Investigating the Structural Role of CaMKII in Long-Term Potentiation

Ashton Curtis

Submission of PhD Thesis

Department of Neuroscience, Physiology & Pharmacology
University College London
Gower Street
London
WC1E 6BT

I, Ashton Curtis confirm that the work presented in this thesis is my own. Where information has been derived from other sources, I confirm that this has been indicated in the thesis.

Impact statement

Long-lasting changes in synaptic strength underlie learning and cognition. In excitatory synapses, synaptic plasticity is typically triggered by the entry of Ca^{2+} through NMDA receptors. Large influxes of Ca^{2+} activate $Ca^{2+/}$calmodulin-dependent protein kinase II (CaMKII), which drives long-term potentiation (LTP) by phosphorylating key proteins to increase responses in postsynaptic spines. CaMKII also plays a structural role in the enlargement of dendritic spines that occurs during LTP, facilitated by its high abundance and dodecameric structure. During my research I have been able to illuminate this more enigmatic structural role of CaMKII. I found that - contrary to what might have been expected from earlier in vitro studies - interactions between CaMKII and the actin-crosslinking protein α-actinin-2 are elevated in dendritic spines following the induction of LTP using a chemical protocol. These interactions are established within 1-2 minutes, endure for hours, and are not affected by regulatory phosphorylation of CaMKII. I went on to provide a molecular explanation for the elevation of CaMKII-actinin interactions that involves docking of activated CaMKII to substrates including GluN2B subunits of NMDA receptors. I also show that a variant of CaMKII that is commonly used to investigate the role of negative feedback regulation of the kinase has a gain-of function ability to bind tightly to actinin irrespective of NMDA receptor activation. This calls for a re-interpretation of earlier studies employing this CaMKII variant.

The immediate impact of my findings will be on academic researchers who are interested in basic mechanisms underlying synaptic transmission and plasticity. I have been able to put forward a more coherent overall model of LTP that will help other researchers develop new ideas for investigation to deepen our knowledge in this field. It is less certain that the research will immediately impact medical research although this is conceivable. The synapse is a locus for mutations that underlie neurological disorders, and aberrations in synapse number and plasticity have been implicated in many conditions such as epilepsy, clinical depression, Alzheimer's, and autism to name only a few. Recently six de novo mutations in CaMKII have been identified in schizophrenic patients, therefore a precise understanding of CaMKII induced mechanisms that underlie changes in neuronal synapses might support future efforts to modify synapse formation in an attempt to treat conditions such as these.

Abstract

The process of learning and memory storage relies on long-lasting changes in the strength of synaptic connections. In excitatory synapses, long-term potentiation (LTP) is triggered by high Ca^{2+} influx through NMDA-type glutamate receptors (NMDARs). Activation of NMDARs leads to the stimulation of the abundant Ca^{2+}/CaM-dependent protein kinase II (CaMKII), which phosphorylates key proteins to increase postsynaptic responsiveness. In addition to its role in phosphorylating proteins, CaMKII also plays a structural role by supporting enlarged synapses through its ability to nucleate multivalent interactions with other proteins. In this study, I investigate the structural role of CaMKII with a focus on understanding how it mediates interactions that regulate spine morphology at a molecular level. I reveal that association of CaMKII with the actin cross-linking protein α-actinin-2 is elevated following NMDAR activation that induces LTP. Furthermore, I find that this interaction is necessary for the formation of structure of enlarged dendritic spines. CaMKII-α-actinin-2 association occurs within 2 minutes of NMDAR activation, persists for hours, and is not influenced by CaMKII autophosphorylation. I also examine a widely utilised phospho-deficient CaMKII mutant (T305A/T306A) and show that it has a gain-of-function ability to bind α-actinin-2 tightly, which has important implications for interpretations of earlier studies involving this CaMKII variant. Together, my research findings further our understanding of the role of CaMKII in LTP, revealing a new layer of sophistication to its function.

Acknowledgements

It is difficult to acknowledge everyone who has contributed to the completion of my project. However, I would like to start by saying thank you to Dr. Matthew Gold for not only hosting me to conduct this exciting project, but his enthusiasm, guidance and entertaining stories throughout my time in the lab. I would also like to thank Tim Church for his technical expertise, his persistent positive energy in the lab and his guidance on work/life balance! I am grateful to Ryan Dowsell for his company during long working hours, as well as his supply of milk and confectionaries in the office (tea & biscuits have been a vital energy source for the project!). My thanks also go to members of the Brodsky Lab, Salinas Lab, Smart lab & Dolphin lab for their technical advice on experimental procedures, as well as their reagents when we were waiting weeks for basic lab consumables.

To my family, I thank you for all the support you've given me. Despite not having any idea as to what I've been doing over the years and continuing to refer my workplace as 'school', you have kept me persistent to the project and I thank you for the visits into London. To my friends, you have all been great company and inspiration to me and I'm grateful to be in such a circle that reminds me of what a 'normal' life is like out of academia. Ben and Denis, I'm glad to have met you both during my PhD and I truly appreciate the tea breaks and Friday nights we've had over the years. Finally, Myra I thank you for understanding and supporting me through the busy days and weekend shifts.

Table of contents

List of Figures

Chapter 1. Introduction

Chapter 2. Methods

Chapter 3. Role of α-actinin-2-CaMKII interactions in structural LTP

List of Tables

Abbreviations

Abbreviation	Full name
ABD	Actin-binding domain of α-actinin-2
AIM	Auto-induction Media
AMPAR	AMPA- type glutamate receptor
BCA	Bicinchoninic acid
BSA	Bovine serum albumin
CaMKII	Ca^{2+}/calmodulin-dependent protein Kinase II
cLTP	Chemically induced LTP
CMV	Cytomegalovirus
C-tail	Cytoplasmic tail
densin-180c	densin-180 fragment (1266-1495)
Da	Dalton
D-APV	D-2-Amino-5-phosphonovaleric acid
DMEM	Dulbecco's modified eagle medium
DMSO	Dimethyl sulfoxide
DP	Differential power
DSS	Disuccinimidyl suberate
DTT	1,4-Dithiothreitol
EDTA	Ethylenediaminetetraacetic acid
EF1-4	EF hand motifs 1-4 of α-actinin-2
EF3-4	EF hand motifs 3-4 of α-actinin-2
GFP	Green Fluorescent protein
EGTA	Ethylene glycol-bis(β-aminoethyl ether)-N,N,N′,N′-tetraacetic acid
EM	Electron Microscopy
FBS	Fetal Bovine Serum
GluN2Bc	GluN2B C-tail fragment 1260-1492
GST	Glutathione s-transferase
HBSS	Hank's Balanced Salt solution
HEPES	4-(2-Hydroxyethyl)piperazine-1-ethanesulfonic acid
HRP	Horseradish peroxidase
IPTG	Isopropyl β-D-1-thiogalactopyranoside
ITC	Isothermal Titration Calorimetry
kDa	Kilo-Dalton
KO	Knock out
LB	Lysogeny broth
LC-MS/MS	Liquid chromatography tandem mass spectrometry
LTD	Long-term depression
LTP	Long-term potentiation
MAGUK	Membrane Associated Guanylate Kinases
MES	2-(N-morpholino)ethanesulfonic acid
MS	Mass spectrometry
MS/MS	Tandem mass spectrometry
MWCO	Molecular weight cut-off
Ni-NTA	Nickel nitrilotriacetic acid agarose
NMDAR	NMDA type glutamate receptor

ND	Not Determined
OD_{600}	Optical density at 600 nm
PBS	Phosphate buffered saline
PDZ	Post synaptic density protein (PSD95), Drosophila disc large tumor suppressor (Dlg1) Zonula occludens-1 protein (zo-1)
pIRES	Plasmid Internal Ribosome Entry site
PLA	Proximity Ligation Assay
PSD	Postsynaptic density
Rep	Replicate
RT	Room temperature
SDS-PAGE	Sodium Dodecyl Sulphate Polyacrylamide gel electrophoresis
SEC	Size-Exclusion Chromatography
sLTP	Structural LTP
SOB	Super optimal broth
SynGAP	Synaptic Ras GTPase activating protein
Tris	Tris(hydroxymethyl)aminomethane
TTX	Tetrodotoxin
v/v	Volume by volume
w/v	Weight by volume
WT	Wild-type
XL-MS	Cross-linking couple to mass spectrometry
αA2	α-actinin isoform 2

Chapter 1. Introduction

1.1. Learning, memory and synaptic plasticity

One of the most fascinating features of the brain is its ability to process information from external stimuli and generate new behavioural responses. Whether this is categorising certain foods as poisonous or developing hand-made tools for hunting and defence, the capacity to learn from external cues in the environment has been vital for animal adaptability and survival. But how exactly does the brain learn and store information? It is now accepted that information is encoded in patterns of synaptic connections between neuronal networks in the brain, and changes in these connections, known as synaptic plasticity, are a fundamental component of learning.

The first origins of synaptic theory stem from neuronal drawings undertaken by Santiago Ramon y Cajal. Alongside his hypothesis for the neuron doctrine - that neurons are connected by small gaps rather than existing as singular cytoplasmic continuity – Cajal suggested that changes in synaptic efficiency might underlie learning (Ramon y Cajal, 1894). The psychologist Donald Hebb later elaborated on this idea in 1949 when he postulated the following mechanism for changes in synaptic strength: "When axon of cell A is near enough to excite a cell B, and repeatedly or persistently takes part in firing it, some growth process or metabolic change takes place in one or both cells such that A's efficiency, as one of the cells firing B, is increased"- in other words synapses can grow stronger when neurons are activated together, often simplified to the common phrase "neurons which fire together wire together" (Cobb, 2021).

It wasn't until 1970, with the advent of molecular biology that knowledge of the potential cellular basis of learning & memory began to emerge, with influential studies conducted by Eric Kandel and colleagues using *Aplysia californica* (sea slug). Innovative behavioural experiments showed that the animal learned to withdraw its gills in response to noxious stimuli, with a concomitant increase in the strength of synapses involved in this process uncovered using electrophysiology (Kandel et al., 1970). However, the first example of synaptic plasticity in a mammalian synapse was revealed in 1973 by Tim Bliss and Terje Lømo. Recording rabbit hippocampi *in vivo*, they applied repetitive high-frequency stimulations to perforant path fibres innervating the dentate gyrus from which they recorded excitatory postsynaptic potentials (EPSPs) (**Figure 1.1A**). Lømo and Bliss found these repeated stimulations triggered a potentiation of the excitatory response in

the target granule cells which lasted from 30 mins to 10 hours after stimulation. They coined this phenomenon long-term potentiation (LTP) (Bliss and Lomo, 1973)

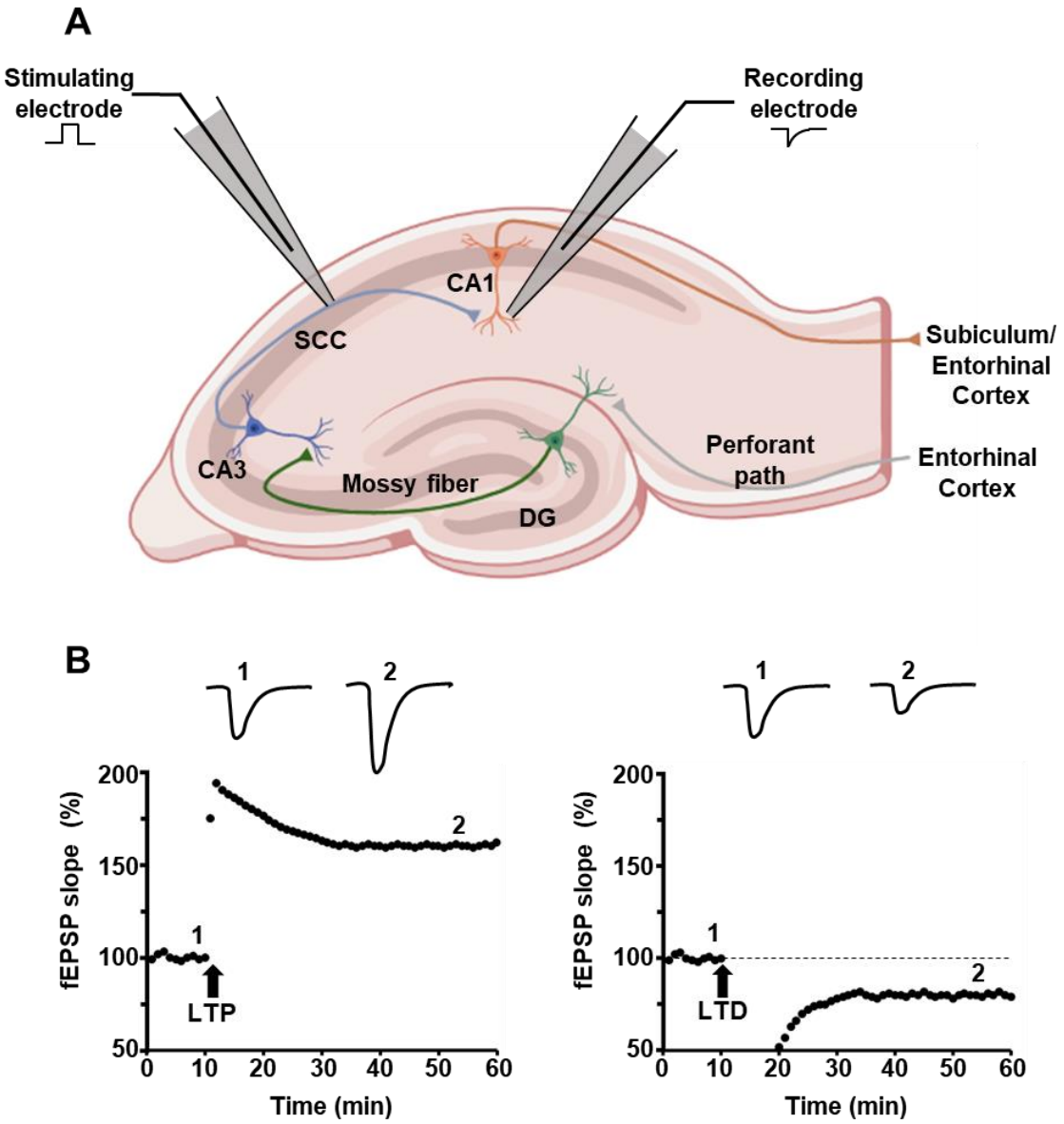

Figure 1.1. Tri-synaptic circuitry of the hippocampus and LTP/LTD field recordings. A) Cellular organisation in the hippocampus**.** Axonal projections from the entorhinal cortex innervate granule cells in the dentate gyrus (DG) via the perforant path. Cells within DG terminate on pyramidal neurons in CA3 region which in turn excite pyramidal neurons in the CA1 through the Schaffer collateral-commissural path (SCC). LTP and LTD have been most intensively studied in the CA1 region with stimulation of Schaffer collaterals emanating from CA3 and recording of postsynaptic potentials in CA1. **(B)** An illustration of NMDAR-dependent LTP and LTD induction in the CA1 region of the hippocampus**.** The synaptic strength is defined as the initial slope of the field excitatory postsynaptic potential (fEPSP; normalized to baseline) and is plotted as a function of time. Left panel demonstrates LTP elicited by high-frequency tetanic stimulation; right panel illustrates LTD elicited by low-frequency stimulation.

1.2. Synaptic plasticity in the hippocampus

Since the discovery of LTP in 1973, the hippocampus has served as the leading model for studying synaptic plasticity due to its simple highly parallel circuitry that facilitates experimentation (**Figure 1.1A**) and its clear function in learning and memory (Morris et al., 1990; Scoville and Milner, 1957). In particular, the CA3-CA1 synapse has served as the leading prototype for understanding how LTP is brought about at the molecular level, with three key features of synaptic plasticity uncovered by focusing on this synapse. First, the induction of LTP in the CA1 region was shown to be N-methyl-D-aspartate receptor (NMDAR)-dependent, as applying the competitive NMDAR antagonist 2-amino-5-phosphonovalerate (APV), or non-competitive channel blocker MK-801 abolished LTP induction (Collingridge et al., 1983). Second, LTP was shown to be Ca^{2+}-dependent, as intracellular injection of the Ca^{2+} chelator EGTA abolished LTP induction (Lynch et al., 1983). Third, the opposite form of LTP - long-term depression (LTD) - was first revealed in the CA3-CA1 pathway following low-frequency stimulations. Like LTP, LTD was found to be NMDAR-dependent, saturable and reversible (Dudek and Bear, 1992). Since the unearthing of LTP and LTD, these forms of plasticity have been the most extensively studied in the hippocampal CA1 region and form the basis of the canonical NMDAR-dependent bi-directional synaptic plasticity model.

1.2.1. Non-canonical models of plasticity

The focus of this dissertation is elucidating the molecular details for the canonical NMDAR-dependent form of synaptic plasticity that occurs in excitatory synapses. However, before providing further background information relevant to this overarching aim, it is important to note that other forms of synaptic plasticity are important in the brain. For example, LTP induction in mossy fiber synapses onto hippocampal area CA3 are not inhibited in the presence of glutamate receptor antagonists: this form of LTP is thought to be induced and expressed pre-synaptically with Ca^{2+} influx via voltage-gated Ca^{2+} channels leading to alterations in the quantity of neurotransmitter release (Barnes et al., 2010). Type I metabotropic glutamate receptors are also essential to some forms of synaptic plasticity (Wang et al., 2016). It is also worth noting that although the focus of this thesis is CA3-CA1 synapses, synaptic plasticity is thought to at least contribute to learned behaviours involving almost all brain regions. Examples include plasticity in connections between the ventral tegmental area and nucleus accumbens that underlie addiction (Huijstee and Mansvelder, 2015), plasticity in the amygdala that mediates

associations including fear conditioning (Mahan and Ressler, 2012), and changes in spinal horn synapses and nociceptive circuits that are involved in chronic pain (Kuner and Flor, 2016). It is anticipated that understanding synaptic plasticity in great depth by focusing on the CA1-CA3 prototype synapses will ultimately undercover general characteristics of synaptic plasticity that are employed throughout the central nervous system.

1.2.2. Key features of NMDAR-dependent synaptic plasticity

As glutamate is the major excitatory neurotransmitter in the CNS, it is easy to conceive that controlling the population of glutamate receptors at the synapse would be ideal for regulating synaptic strength across the brain. As well as NMDARs, the postsynaptic membrane contains another predominant glutamate receptor subtype- α-amino-3-hydroxy-5-methyl-4-isoxazolepropionic acid receptors (AMPARs). While both receptor subtypes share similar structures, their kinetics and channel properties differ: AMPARs exhibit fast excitatory currents with time to peak at ~200 μs and decay constants of ~2-3 ms. In comparison, NMDAR kinetics are slow, with time to peak at ~10 ms and a decay constant of ~100 ms (**Figure 1.2A**). Most AMPARs are only Na^+-permeable and are voltage-independent. On the other hand, NMDARs are permeable to both Na^+ and Ca^{2+}. Furthermore, NMDARs are subject to extracellular Mg^{2+} block at resting membrane potentials, which confers them with an indirect sensitivity to changes in membrane voltage (McBain and Mayer, 1994). The unique properties of each receptor subtype are aligned to their different roles in synaptic transmission: following glutamate release into the synaptic cleft, membrane depolarisation arises predominantly from AMPARs by virtue of their voltage-independence and fast kinetics. This has the knock-on effect of expelling Mg^{2+} from NMDARs, allowing relatively slow fluxes of Ca^{2+} into the postsynaptic spine for signalling underlying synaptic plasticity (**Figure 1.2B**). As both agonist binding and membrane depolarisation are necessary to activate NMDARs, these receptors act as coincident detectors for both pre- and postsynaptic activity, allowing the rules of Hebbian learning "neurons which fire together wire together" to be understood on a molecular level. This coincidence detection promotes tight control of Ca^{2+} influx, whereby high or low levels of Ca^{2+} influx drive LTP or LTD respectively (**Figure 1.2C)** (Bear, 2003) .Coincidence detection also allows for NMDARs to mediate spike-timing dependent plasticity, whereby the relative timings of presynaptic and post synaptic activity determines the direction of plasticity (Markram et al., 1997)

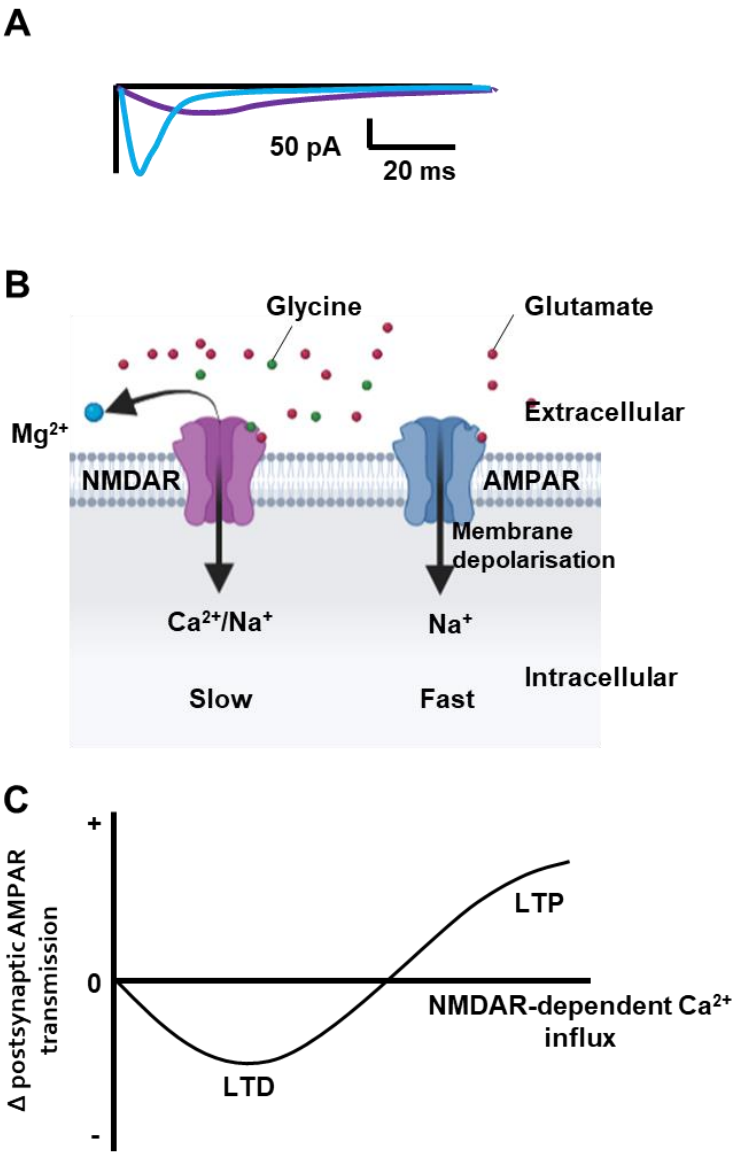

Figure 1.2. Synaptic transmission through glutamate receptors. **(A)** Typical intracellular recordings of excitatory postsynaptic currents mediated from AMPAR (blue) and NMDAR (purple). **(B)** Coincidence detection of NMDAR at the synapse. Glutamate activation of AMPARs mediate fast excitatory transmission and membrane depolarisation, resulting in the expulsion of Mg^{2+}. Only when Mg^{2+} channel-block is relieved from postsynaptic membrane de-polarisation and both agonist/ co-agonists are released from presynaptic neuron; does NMDARs activate. This mechanism allows NMDARs to act as coincidence detectors of presynaptic and postsynaptic activity. **(C)** Postsynaptic NMDAR-dependent Ca^{2+} influx can mediate bidirectional changes in synaptic transmission in canonical models of synaptic plasticity.

Hippocampal synapses undergoing NMDAR-dependent LTP or LTD are associated with long-lasting dendritic spine enlargement (Van Harreveld and Fifkova, 1975; Matsuzaki et al., 2004) or shrinkage (Zhou et al., 2004) respectively. This aspect of LTP – specifically concerned with morphological changes in the structure of dendritic spines rather than their responsiveness to neurotransmitters – is known as structural LTP (sLTP). LTP and LTD processes also correlate to key physiological changes that are depicted in **figure 1.3**. In brief, these effects are mainly the increase/decrease of AMPAR density at the synapse as well as their channel conductance. As mentioned previously, the key second messenger in NMDAR-dependent plasticity is Ca^{2+}, that drives signalling cascades through the activation of the intermediary Ca^{2+} sensitive protein calmodulin (CaM). During LTP, high-levels of Ca^{2+} influx activates CaM in turn stimulating several kinases with the main kinase being Ca^{2+}-CaM dependent protein kinase II (CaMKII). CaMKII has several effects in LTP (discussed later) including the phosphorylation of the AMPAR subunit GluA1 at S831, thereby elevating single-channel conductance (**Figure 1.3**, right panel). Protein Kinase C (PKC) is also activated in LTP and can directly phosphorylate residues S816 and S818 of the GluA1 subunit, promoting AMPAR trafficking to the membrane (Lin et al., 2009). Opposite to LTP, low levels of Ca^{2+} influx during LTD activates CaM, which triggers the action of phosphatases such as calcineurin leading to the dephosphorylation of PKA primed substrate GluA1 S845 (Bear, 2003; Lee et al., 1998). This causes the removal of AMPARs from the membrane and its internalisation (**Figure 1.3**, left panel) (Ehlers, 2000).

So how can one signalling messenger – Ca^{2+} – lead to polar-opposite effects in NMDAR-dependent plasticity? The answer is most likely in the position of key LTP/LTD mediating proteins from NMDAR ion-pore to detect spatio-temporal subtleties in Ca^{2+}-influx.

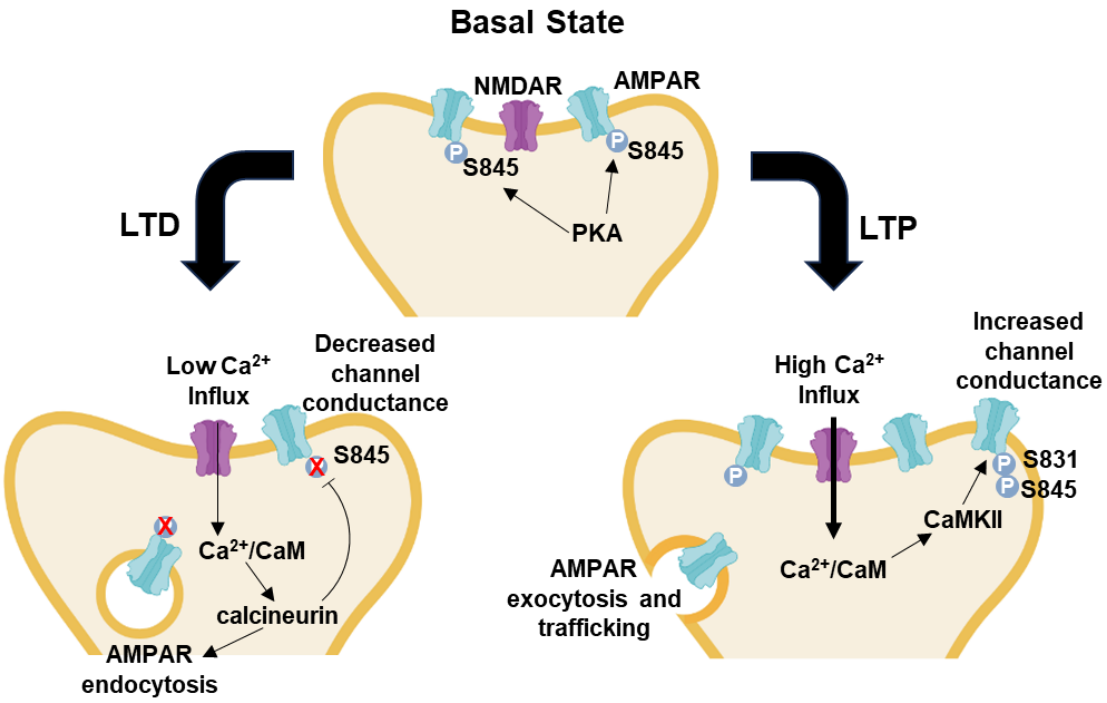

Figure 1.3. Signalling mechanisms underlying NMDAR-dependent synaptic plasticity. NMDARs are shown in purple and AMPARs are shown in blue, which predominantly allow Ca^{2+} and Na^{2+} influx, respectively. During the basal state GluA1 subunits are phosphorylated at S845 by PKA. Left panel- low synaptic activity in LTD induction causes low Ca^{2+} influx through NMDARs driving signalling pathways to mediate decreased channel conductance and AMPAR endocytosis. Right panel- high synaptic activity in LTP mediates large Ca^{2+} influx through NMDARs, activating signalling pathways to increase AMPAR channel conductance and trafficking to the synapse.

1.3. Overview of the postsynaptic density

Receptors and signalling proteins that underlie changes in synaptic strength are concentrated in a proteinaceous specialisation of dendritic spines known as the postsynaptic density (PSD). The PSD derives its name from electron microscopy (EM) studies of postsynaptic neurons at excitatory synapses where it appears as electron rich densities (Gray, 1959; Palay and Palade, 1955). The PSD is a disk-like structure with a diameter of 300-500 nm and a thickness of 30-60 nm that is located at the head of a dendritic spine (Harris et al., 1992; Spacer and Harris, 1998). The mass of an average PSD is approximately 1.1 GDa corresponding to over 1000 membrane and cytoplasmic proteins. These proteins link Ca^{2+} influx to LTD and LTP as well as positioning glutamate receptors directly across from the active zones of axon terminals (Chen et al., 2005; Okabe, 2007).

The low-resolution structure of the PSD consists of a lattice of vertical and horizontal filaments (**Figure 1.4**). The vertical filaments correspond to membrane-associated

guanylate kinase (MAGUK) proteins PSD-95 and SAP-97, which are spaced ~15 nm apart and linked to horizontal filaments including SHANK and homer (Chen et al., 2008). Together these filaments form the higher order complex of the PSD. The structure itself can be categorised into two layers: The PSD 'core' layer typically within 30 nm from the postsynaptic membrane where NMDARs, AMPARs, MAGUKs and α-actinins typically reside. The deeper layer is known as the 'pallium' typically ~50 nm from the membrane, comprised of the cytoplasmic facing horizontal filaments, homer and shank, linking the PSD to actin cytoskeleton (Dosemeci et al., 2016).

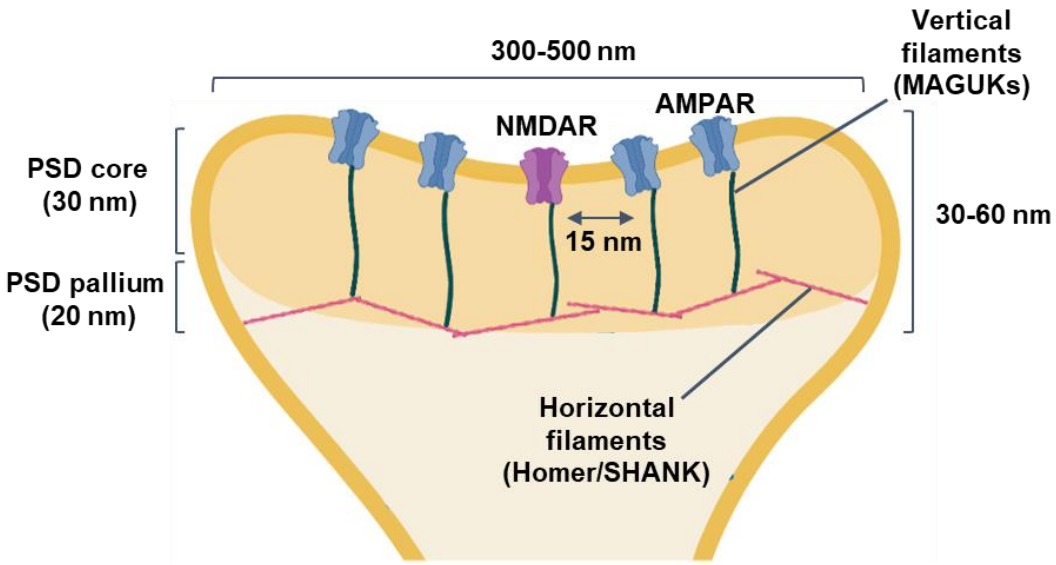

Figure 1.4. PSD structure. PSDs are typically 30-60 nm in depth, and 300-500 in diameter with a PSD "core" and "pallium" layer. The PSD is tethered to F-actin (blue) through its interaction with shank, that is part of the horizontal filaments in the PSD (red). Vertical filaments (black) are composed of MAGUK, which tether receptors and horizontal filaments.

The most prevalent protein in the PSD is CaMKII, which alone counts for ~ 9 % total PSD mass (Cheng et al., 2006). The filament proteins PSD-95, synaptic GTPase (SynGAP), SHANK, and Homer are also highly abundant with AMPAR & NMDAR receptor subunits completing the 'core' components of the PSD (Cheng et al., 2006). Due to rich density of proteins, the signalling mechanisms and structure in the PSD remain challenging to solve (Gold, 2012). However, CaMKII has emerged as the lead candidate for organising structural changes in the PSD following LTP (Hell, 2014).

1.4. CaMKII: structure & activation mechanism

CaMKII, despite its nomenclature, was actually the first Ca^{2+}/CaM kinases to be identified (Schulman, H.; Greengard, 1978a; Schulman and Greengard, 1978b), with CaMKI described for the first time a year later (Huttner and Greengard, 1979). CaMKII is one of, if not the single most highly expressed proteins in neurons, constituting 1 % of all proteins expressed in the forebrain and 2 % in the hippocampus and neocortex (Erondu and Kennedy, 1985). Since its discovery, it has been touted as the memory molecule and the central organiser for LTP. In this section, I will first explain the current understanding of the structure and activation mechanism of CaMKII and its importance in LTP. I go on to cover the enzymatic (**Section 1.5**) and structural (**Section 1.6**) roles of CaMKII in LTP, before describing the aims of my project (**Section 1.7**).

1.4.1. CaMKII subunit structure and holoenzyme assembly

The mammalian CaMKII family comprises four gene homologs (α, β, δ, γ). The α and β isoforms are largely brain-specific, with the forebrain containing α:β isoforms at a ratio of 3:1 and the inverse ratio of these subunit in the cerebellum (Miller and Kennedy, 1985). CaMKIIδ is ubiquitously expressed across all tissues, but particularly predominates in the heart, whereas CaMKIIγ is found in multiple organs including the liver and gallbladder (Tombes et al., 2003). Each CaMKII isoform has the same basic topology comprised of an N-terminal kinase domain, a regulatory segment, a linker, and a C-terminal association domain (**Figure 1.5A**). The kinase and association domains of each gene are the most conserved across the family with amino acid homologies of 90 % and 75 % across all isoforms, respectively. The linker region connecting the regulatory segment to the association domain is the most variable in length and amino acid composition with further variation arising within each isoform due to alternative splicing in this region (Sloutsky et al., 2020).

Like all mammalian serine/threonine protein kinases, the kinase domain of CaMKII consists of a small N-lobe and large C-lobe with ATP binding to a cleft between the two. The regulatory segment contains a Ca^{2+}/CaM binding site that overlaps with a CaMKII pseudo-substrate sequence that docks to the kinase domain to occlude substrate access in the inhibited kinase (Chao et al., 2011). Through its association domain, each CaMKII subunit oligomerises to form dodecameric holoenzymes (12- subunits) with a small population assembling as tetradecamers (14-subunits) (Myers et al., 2017). The holoenzyme consists of two hexameric rings stacked on top of one another with the inner

ring comprised of oligomerised association domains (blue, **Figure 1.5B**) from which the kinase domains emanate (green, **Figure 1.5B**) (Myers et al., 2017).

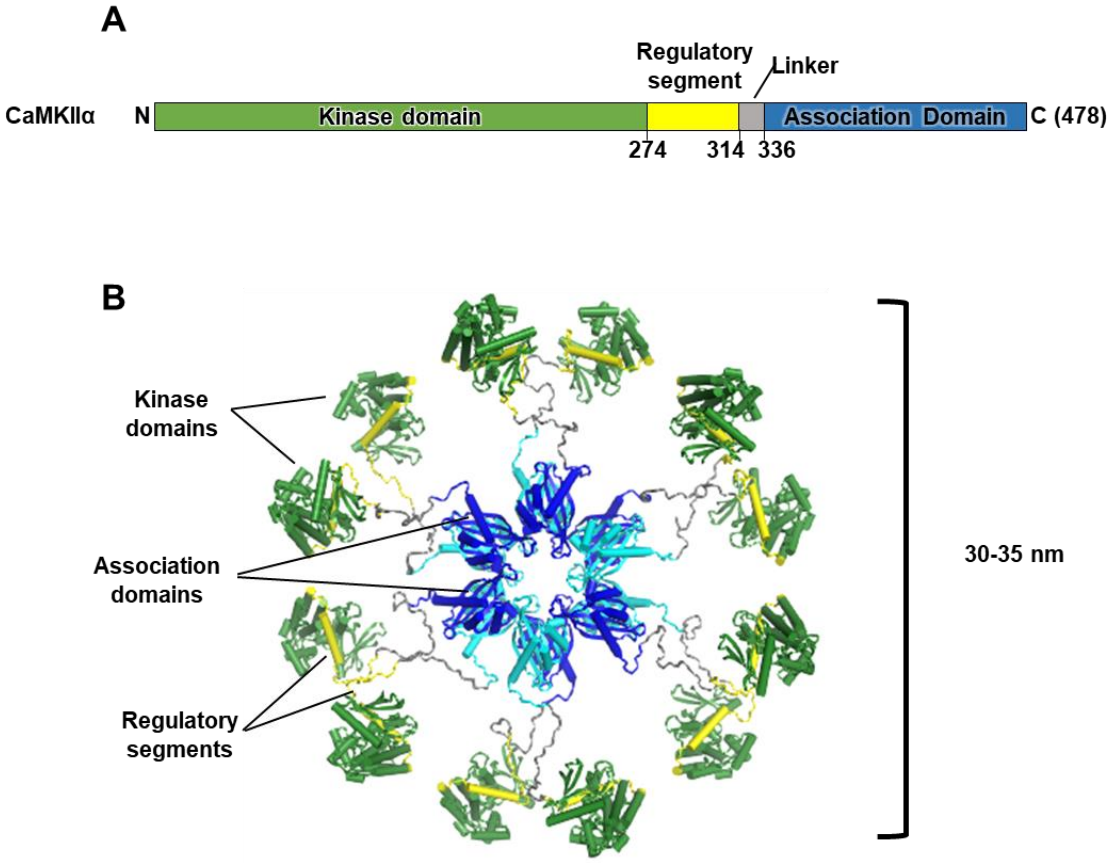

Figure 1.5. CaMKIIα structure. (A) Topology of a single CaMKII monomer. Kinase domain (green), regulatory segment (yellow), flexible linker region (grey) and association domain (blue). **(B)** Cryo-EM reconstitution of CaMKII full-length holoenzyme (PDB: 5U6Y).

1.4.2. CaMKII activation mechanism and autonomy

In contrast to other canonical kinases that are typically activated by the phosphorylation of an "activation loop" to render correct folding of the ATP binding pocket, CaMKII activity is regulated through binding and release of the pseudo-substrate regulatory segment that occupies the substrate binding groove in the autoinhibited kinase (**Figure 1.6A**). Activation is triggered by association of Ca^{2+}/CaM with the CaMKII regulatory segment causing its displacement from the kinase, thereby exposing the active site for substrate binding and phosphorylation (**Figure 1.6A**). An important feature of this activation mechanism is that at sufficient Ca^{2+}/CaM concentrations, where two or more Ca^{2+}/CaM molecules are bound to adjacent subunits; the kinase domain of one subunit can trans-autophosphorylate T286 from the regulatory segment of an adjacent subunit (**Figure 1.6C**, right panel) (Hanson et al., 1994). The consequence of this T286

autophosphorylation is that the regulatory segment is no longer able to so efficiently block substrate access to the active site even after Ca^{2+}/CaM dissociation, thereby rendering CaMKII autonomously active (Kuret and Schulman, 1985; Miller et al., 1988). Studies have demonstrated autonomous activity at 15-65 % compared to maximal Ca^{2+}/CaM activity depending on the substrate peptide used for the assay (Coultrap et al., 2010).

.

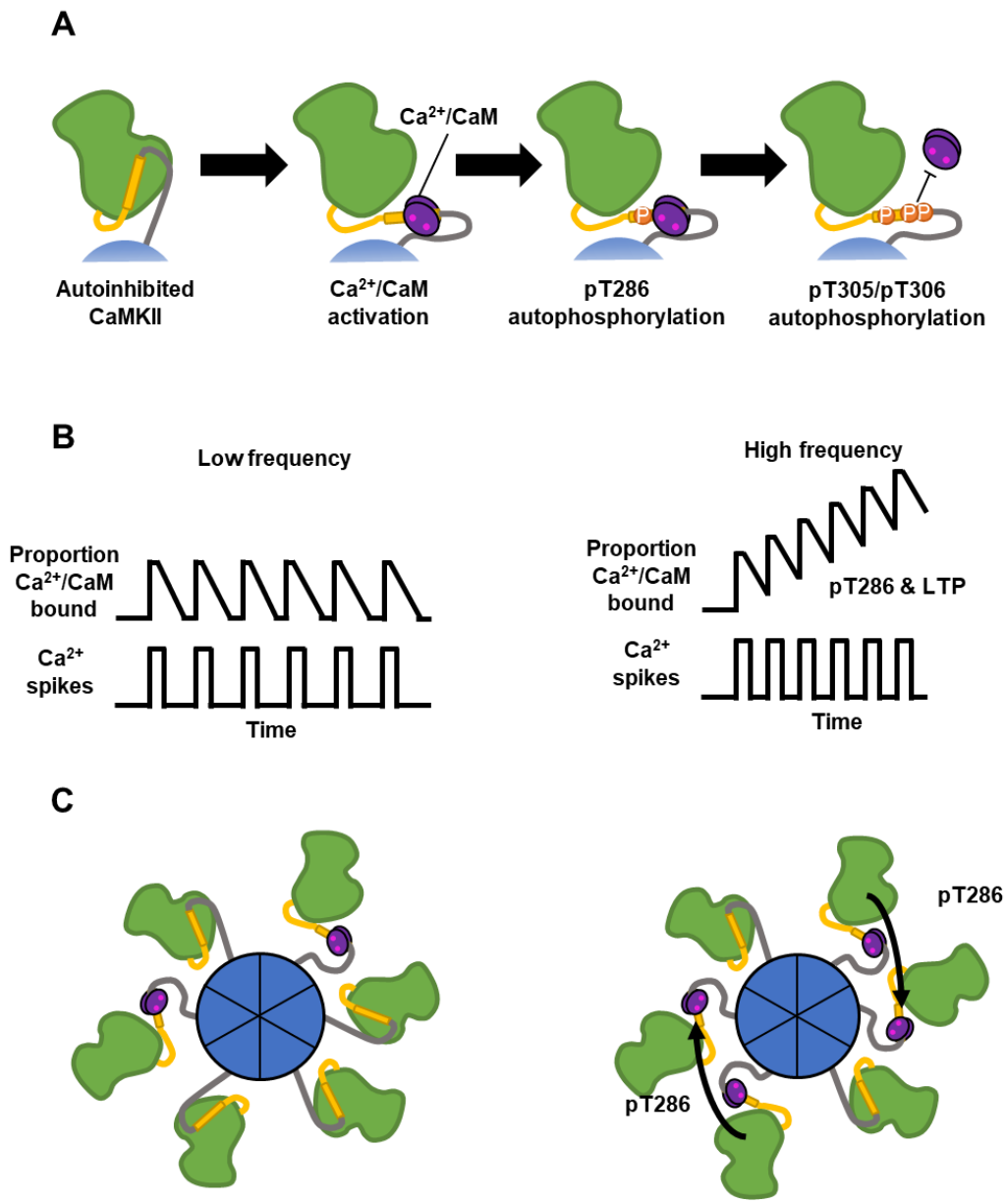

Figure 1.6. CaMKII activation, autonomy and frequency detection. **(A)** Ca^{2+}/CaM (purple) binds to and displaces the CaMKII regulatory segment (yellow) from its docking site on the kinase domain (green) exposing T286 for trans-autophosphorylation by an adjacent kinase domain. Subsequent dissociation of Ca^{2+}/CaM leads to autophosphorylation at residues T305/T306, thereby preventing further Ca^{2+}/CaM re-association. **(B)** The dual role of Ca^{2+}/CaM and Thr286 phosphorylation allows frequency detection of threshold to induce autonomous activity. Left-At low frequency Ca^{2+} spikes, Ca^{2+}/CaM can bind to CaMKII and dissociate between intervals. Right- At higher frequencies with spike intervals in the range of Ca^{2+}/CaM dissociation time, additional Ca^{2+}/CaM molecules can bind to adjacent CaMKII subunits before all the initial Ca^{2+}/CaM molecules dissociate. **(C)** The presence of Ca^{2+}/CaM binding to adjacent CaMKII subunits during LTP increases the probability of T286 trans-autophosphorylation. Experimental data to show this phenomenon have been reported (Chang et al., 2019).

The autonomous activity generated by T286 autophosphorylation allows CaMKII to act as a frequency detector as illustrated in **figure 1.6**. During sub-maximal Ca^{2+} spikes, Ca^{2+}/CaM binds to some of the subunits within the CaMKII holoenzyme and fully dissociate during spike intervals. At sub-threshold frequencies, these Ca^{2+}/CaM binding and complete release cycles repeat (**Figure 1.6 B** & **C**, left panel). However, at higher frequencies with spike intervals in the range of Ca^{2+}/CaM dissociation time; bound Ca^{2+}/CaM accumulates within the holoenzyme, which increases the chance of T286 autophosphorylation (**Figure 1.6 B** & **C**, right panel). In this way, higher frequency Ca^{2+} spikes – such as occur in some LTP-induction protocols – can elicit T286 autophosphorylation. T286 phosphorylation is thought to serve as a "molecular memory" as it allows sustained CaMKII activity following the depletion of Ca^{2+} such as occurs after completion of a spike train. While this activity outlasts initial Ca^{2+} transients, imaging results show CaMKII activity peaks ~10 s following LTP stimuli and returns to baseline levels at least within 2 min following LTP stimuli (Chang et al., 2017; Lee et al., 2009). In this way, pT286 phosphorylation is thought to be essential for LTP induction by naturalistic stimuli but probably is not necessary for the long-term maintenance of LTP beyond the induction phase (Buard et al., 2010; Yasuda et al., 2022). The role of T286 phosphorylation in LTP induction was first demonstrated in hippocampal CA1 region from knock-in mice with the phospho-deficient mutation T286A in CaMKIIα (Giese et al., 1998). These T286A mice failed to induce NMDAR-dependent LTP and exhibited deficits in the Morris water maze, which is a spatial learning paradigm. However, it should be noted that NMDAR-independent forms of LTP can be induced in the presence of T286A (Villers et al., 2014).

1.4.3. Inhibitory CaMKII autophosphorylation residues

Following Ca^{2+}/CaM dissociation of a T286-phosphorylated CaMKII subunit, two other residues within the regulatory segment, T305 & T306, can undergo autophosphorylation (Colbran and Soderling, 1990a; Patton et al., 1990). Autophosphorylation at T305 or T306 prevents Ca^{2+}/CaM re-association following re-occurring Ca^{2+} influx and has been postulated to represent a form of negative feedback (**Figure 1.6A**). Autophosphorylation at these sites is also thought to mediate release of CaMKII from the PSD. Consistent with this notion, mice expressing double T305V/T306A mutant variants of CaMKIIα exhibit 3-fold higher levels of CaMKII in PSD fractions compared to WT (Wild-Type) CaMKIIα. These CaMKIIα T305V/T306A mutants also display lower thresholds for hippocampal

LTP (Elgersma et al., 2002). Moreover, phosphodeficient CaMKIIα T305A/T306A hippocampal neurons display slower PSD dissociation rates compared to their WT counterparts (Shen et al., 2000). Additionally, mice expressing a phosphomimetic T305D variant of CaMKII show decreased levels of CaMKII in the PSD, and these mice are also resistant to induction of LTP and have learning deficiencies (Elgersma et al., 2002). More recently T305/T306 autophosphorylation has been implicated in the targeting of CaMKII phosphorylation in LTD-related substrates; expression of the triple-phosphomimetic T286D/305D/306D CaMKII mutant reduces synaptic transmission to the point where LTD was occluded, and LTP cannot be generated. On the other hand, the T286D/305A/306A variant exhibits maximally potentiated synapses at baseline that cannot undergo LTD (Pi et al., 2010). Therefore T305/T306 autophosphorylation could provide another switch to decide whether CaMKII mediates LTP and LTD. However, ss I will show later in this thesis, the T305A/T306A phospho-deficient mutant possesses properties beyond regulation of CaMKII activity that call in to question the interpretation of previous experiments with this variant.

1.4.4. CaMKII is essential for the induction of LTP

The possibility that CaMKII activity is necessary for inducing LTP has been investigated for almost 40 years. The first experiments to test this hypothesis were made possible by the development of CaMKII specific inhibitors (analogous to the first experiments uncovering the key role of NMDARs with receptor antagonists). Peptides modelled after the CaMKII regulatory segment which block CaMKII activity were found to block the induction of LTP in hippocampal slices (Malinow et al., 1989). Furthermore, standard protocols to induce hippocampal LTP in CaMKIIα-deficient mice failed to generate a rise in EPSP responses as compared to control mice (Silva et al., 1992). Moreover, expression of a constitutively active form of CaMKIIα (1-290) was found to elevate basal synaptic conductance to a level comparable to control groups that had undergone LTP and to an extent that no further LTP could be generated (Pettit et al., 1994). Together these initial experiments demonstrated the importance of CaMKII in mediating LTP induction. Subsequent work has revealed that both the ability of CaMKII to phosphorylate postsynaptic substrates, and its ability to nucleate protein-protein interaction networks, are integral to its function in LTP. I will first describe the catalytic role of CaMKII in LTP before considering its structural role in more detail (**Section 1.6**) since this is more pertinent to the studies that I have undertaken.

1.5. Enzymatic role of CaMKII in LTP

CaMKII has broad inherent substrate specificity (Kennedy and Greengard, 1981; Payne and Sorderling, 1980; Yamauchi and Fujisawa, 1981), which is compatible with the kinase phosphorylating a wide range of substrates during LTP. The enhancement of AMPAR-mediated transmission during LTP occurs through two processes: the first is the enhancement of single channel conductance; the second involves the increase in number of AMPARs at the synapse. CaMKII phosphorylates GluA1 subunits of AMPAR receptors at S831 to increase channel conductance and this phosphorylation can be blocked by the CaMKII inhibitor KN-62 (Barria et al., 1997; Mammen et al., 1997). As well as GluA1, CaMKII can mediate LTP effects through phosphorylation of the AMPAR auxiliary subunit stargazing, which is known to tether AMPARs to the synapse through its interaction with PSD-95 (Bats et al., 2007). Using single-particle tracking of AMPARs, CaMKII activity has been shown to induce synaptic trapping of AMPARs at the membrane, dependent on the phosphorylation stargazin (at residue S9) and stargazin binding to PSD-95 (Opazo et al., 2010).

CaMKII kinase activity can also indirectly promote AMPAR membrane insertion through the regulation of small GTPase Ras via phosphorylation of SynGAP, which is a Ras GTPase-activating protein (Chen et al., 1998). Proteomic analysis reveals at least 10 CaMKII phosphorylation sites within the disordered region of SynGAP (Oh et al., 2004; Walkup et al., 2015). SynGAP phosphorylation by CaMKII results in the disinhibition of Ras, which can in turn activate extracellular regulated kinases (ERKs) to promote AMPAR exocytosis (Araki et al., 2015; Zhu et al., 2002).

Besides its role in increasing receptor function at the synapse, CaMKII kinase activity can mediate dendritic spine enlargement through triggering actin re-organisation. Specifically, CaMKII can indirectly induce actin-cytoskeletal changes through TIAM-1, which is a guanylate-exchange factor (GEF) for the small G-protein Rac. The interaction between TIAM-1 and CaMKII causes permanent TIAM-1 phosphorylation and activation of Rac, which can promote actin elongation during sLTP (Kojima et al., 2019; Saneyoshi et al., 2019a). Overall, phosphorylation by CaMKII regulates multiple facets of synaptic function to bring about LTP.

1.6. Structural Role of CaMKII in LTP

As mentioned, synapses undergoing synaptic potentiation can undergo physiological changes, but also long term structural changes- sLTP. This consists of changes in the structure of dendritic spines resulting in larger spine heads that arise from postsynaptic cytoskeletal actin re-organisation (Okamoto et al., 2007). In addition to its enzymatic role, CaMKII plays an essential structural role in supporting the structure of enlarged postsynaptic spines by virtue of its dodecameric structure and high abundance (Hell, 2014). CaMKIIβ directly associates with F-actin (O'Leary et al., 2006) and this interaction bundles and stabilises the structure of F-actin in potentiated spines (Okamoto et al., 2007; Wang et al., 2019). The α isoform of CaMKII can also interact with actin adaptor protein α-actinin and it is thought that CaMKII α/β dodecamer can form multivalent interactions with actinin and actin to form stabilised enlarged synapses. Although, how CaMKII can mediate sLTP through its interaction partners remains unexplored. The interaction partners of CaMKII in the PSD are outlined in **table 1.1**. The PSD partners that are the focus of my project are GluN2B subunits of NMDARs, α-actinin-2 and densin-180. Next I will briefly describe the structure and role of these CaMKII interaction partners at the synapse and highlight the multivalent interactions between CaMKII and its PSD binding partners.

CaMKII region (α isoform numbering)	Interaction partner	Ca^{2+}/CaM sensitivity	Effect of interaction	Method of detection
Kinase domain (1-275)	GluN2B subunit of NMDARs (839-1482)	Binding occurs following Ca^{2+}/CaM activation	Translocation to the PSD core and synaptic tagging of CaMKII. Maintenance of synaptic strength.	GST pull-down assay (Bayer et al., 2001; Robison et al., 2005a; Strack and Colbran, 1998). Immunofluorescence studies in HEK cells and neurons (Bayer et al., 2001). Mutagenesis in organotypic slices (Barcomb et al., 2016).
Kinase domain (1-275)	'densin-IN' domain (793-824) of densin-180	Binding occurs following Ca^{2+}/CaM activation	Substrate selective inhibition of GluA1 Ser 831 phosphorylation	GST pull-down assay (Jiao et al., 2011). Isothermal-titration calorimetry and X-ray crystallography (Özden et al., 2022)
Kinase domain (1-275)	Tiam-1 carboxy-tail (1541-1559)	Binding occurs following Ca^{2+}/CaM activation	Activation of Rac1 and modulation of F-actin dynamics. Maintenance of synaptic strength.	Flag-pulldown assay (Saneyoshi et al., 2019b). Isothermal titration calorimetry and X-ray crystallography (Özden et al., 2022)
Kinase domain (1-275)	CaMKII natural inhibitor protein (CaMKIIN)	Binding occurs following Ca^{2+}/CaM activation	Inhibition of CaMKII activity	Pulldown and kinase assay (Vest et al., 2007)
Regulatory segment (276-314)	alpha-actinin-2 EF hands 3-4 (819-894)	Ca^{2+}/CaM competes for binding*	Substrate selective phosphorylation of GluN2B	GST pull-down assays (Jalan-Sakrikar et al., 2012; Robison et al., 2005a)
Linker region-β subunit only (315-339)	F-actin	Binding inhibited following Ca^{2+}/CaM activation	Modulation of F-actin turnover rate and bundling	Co-sedimentation assay, electron microscopy fluorescence imaging, fluorescence recovery after photobleaching (O'Leary et al., 2006)
Association domain (340-478)	densin-180 C-terminus (1354-1404)	No Ca^{2+}/CaM dependency-constitutively bound	Effect of interaction not explored.	GST pull-down assay (Jiao et al., 2011; Robison et al., 2005b)

Table 1.1. Existing knowledge of CaMKII interaction partners in the PSD. Current literature of CaMKII interaction partners is the PSD, their binding conditions, known effect on interactions, as well as their method of interactions. *As discussed later, there is nuance to interplay between Ca^{2+}/CaM and alpha-actinin-2.

1.6.1. CaMKII association with NMDARs: LTP maintenance and synaptic tagging

Docking of CaMKII with GluN2B subunits of NMDARs is thought to play a fundamental role in initiating structural changes in dendritic spines following the induction of LTP. Prior to stimulations that elicit LTP, the majority of CaMKII is thought to reside outside of the PSD in an F-actin bound state (Feng et al., 2011; Shen and Meyer, 1999). Once activated by Ca^{2+}/CaM, CaMKII translocates to both the core and the pallium of the PSD (**Figure 1.4**) (Tao-Cheng, 2020). The driving forces for CaMKII translocation are diffusion and binding to synaptic CaMKII anchoring proteins – foremost among these is an interaction with the intracellular region/cytoplasmic tail (C-tail) of the NMDAR GluN2B subunit (Bayer et al., 2001; Leonard et al., 1999; Strack and Colbran, 1998).

Once activated by Ca^{2+}/CaM, the exposed kinase domain of CaMKII binds to two different regions within the GluN2B C-tail: a 'distal' site further from the membrane spanning regions in the primary sequence (1290-1309) that contains a CaMKII phosphorylation site at Ser1303; and a less well-defined 'proximal' site (839-1120) that does not undergo phosphorylation (**Figure 1.7**) (Leonard et al., 1999; Strack et al., 2000a). CaMKII interactions with the distal site only requires Ca^{2+}/CaM activation whereas binding to the proximal site requires T286 autophosphorylation in addition to Ca^{2+}/CaM binding (Bayer et al., 2001). When CaMKII-GluN2B binding is established, the complex can endure for hours even after the dissociation of Ca^{2+}/CaM to CaMKII (Bayer, 2006).

The distal CaMKII interaction site in the GluN2B subunit C-tail has been shown to bind to the CaMKII kinase substrate binding groove and the interaction results in the displacement of the CaMKII regulatory segment (Bayer et al., 2001; Özden et al., 2022). Docking to GluN2B supports access of some substrate sequences to the catalytic site although the activity is negligible compared to fully activated CaMKII (Bayer et al., 2001) – presumably because the substrate binding groove is largely occupied - therefore it is not generally considered to have a role in maintaining CaMKII enzymatic activity. Instead, the consensus is that CaMKII-GluN2B interactions serve a role in "synaptic tagging", with synapses that will undergo long-lasting structural changes characteristic of LTP marked with GluN2B-CaMKII complexes. Consistent with an important role for CaMKII-GluN2B interactions, it is not possible to induce LTP in slices derived from GluN2B R1300Q/S1303D knock-in mice (Halt et al., 2012) – this GluN2B variant is unable to associate with CaMKII through the major distal interaction site. An important

outstanding goal in research of synaptic plasticity is to define the downstream steps following synaptic tagging of this type (Yasuda et al., 2022).

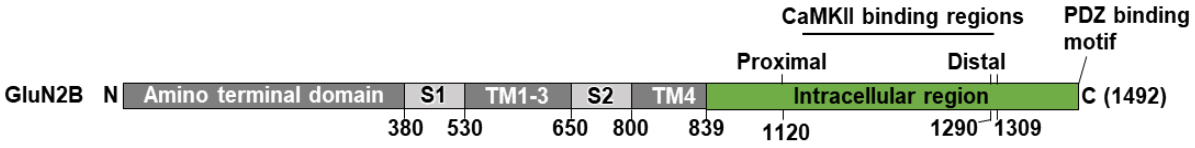

Figure 1.7. Topology of NMDAR GluN2B subunit. Proximal and distal CaMKII binding regions in the intracellular C-tail of the subunit are highlighted.

1.6.2. CaMKII interaction with α-actinin-2

An important role is also emerging for interactions between CaMKII and a family of actin cross-linking proteins called α-actinins. α-actinins primarily serve as adaptor proteins to build cytoskeletal assemblies, but also bridge the cytoskeleton to cellular signalling pathways (Sjöblom et al., 2008). There are four α-actinin isoforms - α-actinins 1, 2 and 4 are expressed in the brain (Marcora et al., 2007). The four α-actinin isoforms are highly homologous and bear the same topology with an N-terminal actin binding domain (ABD), followed by 4 spectrin repeats, 4 EF-hand motifs, and a C-terminal PDZ domain binding motif (**Figure 1.8**) (Ribeiro et al., 2014). The most divergent region within the family is the EF-hand region: α-actinin-2 and -3 possess Ca^{2+}-insensitive EF-hands whereas α-actinin-1 and -4 are Ca^{2+} sensitive. α-actinins self-assemble into anti-parallel dimers that can bind actin at either end. This property is essential to their ability to cross-link F-actin (Sjöblom et al., 2008), best known in the assembly of Z-disks within skeletal muscle cells (Masaki et al., 1967). Importantly, they are also found in the PSD, where in particular α-actinin-2 is involved in supporting the structure of dendritic spines. For example, overexpression of α-actinin-2 leads to an increase length and dendritic protrusions in cultured hippocampal neurons (Nakagawa et al., 2004).

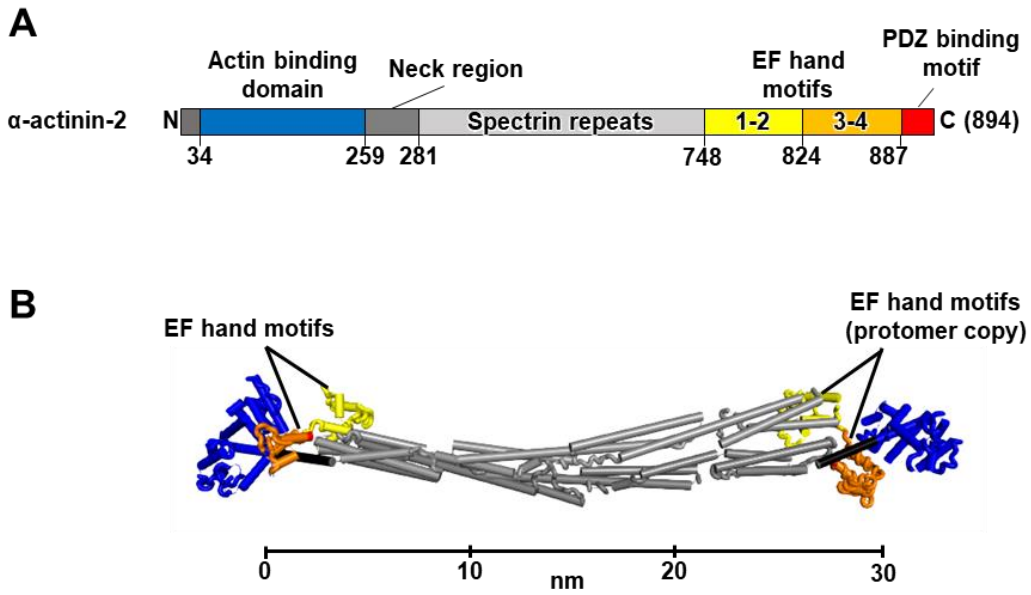

Figure 1.8. α-actinin-2 structure. **A)** Topology of α-actinin-2 and **B)** Crystal structure of α-actinin-2 anti-parallel dimer**.** Colour schemes of both panels are identical. Modelled from PDB: 4D1E.

The importance of α-actinin-2 in the PSD was first demonstrated by Wysynski and co-workers, who identified interactions between the spectrin repeats of α-actinin-2 and the C-terminal tails of NMDAR GluN1 and GluN2B subunits (Wyszynski et al., 1997). In this study, they showed co-precipitation of α-actinin-2 and NMDAR subunits from fractions of forebrain tissue, highlighting the importance of α-actinin-2 as a core PSD protein. Interaction between α-actinin-2 and NMDARs has been suggested to connect the receptors to the actin cytoskeleton. Some evidence in support of this notion has been provided by experiments with latrunculin-A. Treatment of primary hippocampal cultures with the actin destabiliser latrunculin-A causes NMDAR and α-actinin-2 clusters to disperse from synapses and coalesce into large non-synaptic cell body clusters (Allison et al., 1998). α-actinin demonstrated in the PSD is the tethering of PSD-95 to postsynaptic sites. Specifically, the very N-terminus (amino acids 1-13) of PSD-95 was shown to bind to α-actinin-2 and disrupting this interaction led to reduced accumulation of PSD-95 and AMPAR receptors at the synapse (Matt et al., 2018). Finally, α-actinin-2 knockdown in primary hippocampal cultures display immature filapodial like spine structures which cannot develop into mushroom type spines. The Ca^{2+}-insensitive EF hands are believed to be essential for regulating the PSD structure and spine morphology as exchanging this domain with the Ca^{2+}-sensitive EF hands from α-actinin-4 inhibits this function (Hodges et al., 2014).

Other than Ca^{2+}/CaM, α-actinin-2 is the only protein known to interact with the regulatory segment of CaMKIIα and this Ca^{2+} -independent binding is thought to be mediated principally through the third and fourth EF hands (EF3-4) of α-actinin-2 (Robison et al., 2005a). Association with α-actinin-2 only weakly activates CaMKII activity towards GluN2B, and actually inhibits its activity towards GluA1 subunits (Jalan-Sakrikar et al., 2012). Therefore, interactions between CaMKII and α-actinin-2 are thought to fulfil a structural role in LTP. While no three-dimensional structural information showing the mode of α-actinin-2-CaMKII binding is available, structural modelling (Jalan-Sakrikar et al., 2012) has been attempted by superimposing α-actinin-2 EF3-4 on the CaM C-lobe according to the binding mode observed a crystal structure of Ca^{2+}/CaM in complex with CaMKII regulatory segment (PDB: 1CM1). This modelling suggests that α-actinin-2 can fully access the regulatory segment of CaMKII in its autoinhibited state. Phosphorylation of CaMKII at T305 & T306 has distinct effects on Ca^{2+}/CaM and α-actinin-2 binding: either T305 or T306 autophosphorylation inhibits Ca^{2+}/CaM binding whereas α-actinin-2 association is only reduced by T306 autophosphorylation (Jalan-Sakrikar et al., 2012). Finally, the work of Jalan-Sakrikar and colleagues hints at CaMKII T305A/T306A mutant elevating association with α-actinin-2 compared to CaMKII WT (Jalan-Sakrikar et al., 2012, see supplementary Figure 4B). I explore this phenomenon further in my thesis to highlight consequences of T305A/T306A mutant besides preventing regulatory phosphorylation.

1.6.3. CaMKII interaction with densin-180

Another key PSD interaction partner for CaMKII is densin-180. Densin-180, also known as leucine-rich repeat 7 (LRRC7), was first characterised from rat forebrain extracts as a 167 kDa O-sialoglycoprotein (Apperson et al., 1996). Like CaMKII and α-actinin-2, densin-180 is enriched in the PSD. After its discovery, densin-180 was initially assumed to be a transmembrane protein with a large extracellular domain since it contains 16 leucine rich repeats (LRR) and most LRR proteins either contain a single transmembrane domain or are secreted (Apperson et al., 1996). However, biotinylation and immunofluorescent studies have subsequently revealed that densin-180 is actually an intracellular protein (Liu et al., 2013). Densin-180 is attached to the inner face of the cell membrane through palmitoylation at cysteine residues at position 14 and 16, and it is enriched in the PSD core with a median distance of ~27 nm from the postsynaptic membrane according to immunogold labelling (Dosemeci et al., 2018). Densin-180

remains an enigmatic protein with no high-resolution structural information available for the protein (**Figure 1.9**) (Quitsch, 2005; Thalhammer et al., 2009; Walikonis et al., 2001).

Despite its poor structural characterisation, there is evidence that densin-180 fulfils an important role in neurons. Densin-180 knockout (KO) mice display abnormal behaviours correlated to autism and schizophrenia, with reduced levels of α-actinin, DISC1 and metabotropic glutamate receptors (mGluRs) in PSD fractions. Electrophysiological recordings from hippocampi of densin-180 KO mice reveal an impairment of mGluR and NMDAR-dependent forms of LTD (Carlisle et al., 2011). Moreover, densin-180 has been found to enhance the cell surface trafficking and postsynaptic localization of Cav1.2 L-type Ca^{2+} channels in neurons, illustrating its crucial role in neuronal excitability and synaptic transmission (Wang et al., 2017).

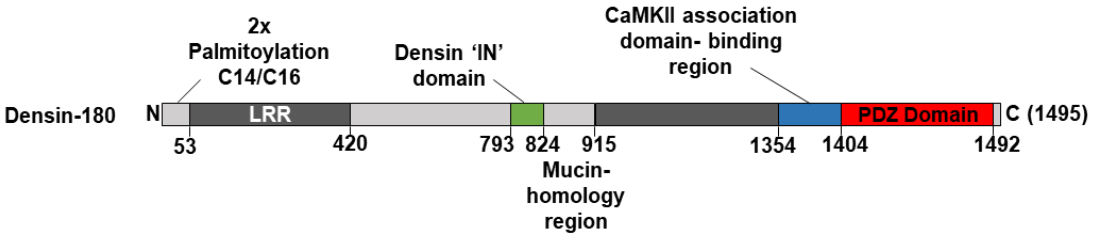

Figure. 1.9. Topology of densin-180 and the current identified domains.

Densin-180 is thought to be essential for the correct positioning of CaMKII in the PSD. The C-terminal ~150 amino acids of densin-180 can bind to the association domain of CaMKIIα but not CaMKIIβ, in a Ca^{2+}/CaM independent manner (Robison et al., 2005a; Walikonis et al., 2001). Densin-180 is the only known interaction partner for the CaMKII association domain (Penny and Gold, 2018). This interface does not depend on the activity state of CaMKII. However, the exact stoichiometry CaMKII-densin-180 interactions and its role in synaptic plasticity remains to be explored. Densin-180 also engages with the kinase domain of activated CaMKII via an internal region known as the densin-IN domain (**Figure 1.9**). This second binding interface has been shown to modulate CaMKII phosphorylation to certain substrates *in vitro*: densin-IN binding can selectively inhibit the phosphorylation of AMPAR GluA1 subunits, whilst having no effect on NMDAR GluN2B phosphorylation (Jiao et al., 2011).

1.6.4. Multivalent interactions underlying the structural role of CaMKII

In this section, I have introduced three essential interaction partners for CaMKII that are thought to support the structural function of CaMKII in postsynaptic spines. To complicate matters, all three of these proteins are also capable of interacting with each other. The last four amino acids of α-actinin-2 (ESDL) create a PDZ ligand that has been shown to bind to the C-terminal PDZ domain of densin-180 *in vitro*, and cooperative interactions between CaMKII-α-actinin-2-densin-180 have been proposed as a mechanism to support the formation of ternary complexes comprised of the three proteins (Robison et al., 2005a). Also mentioned earlier, α-actinin-2 can interact with both GluN1 and GluN2B subunits through its spectrin repeats (Wyszynski et al., 1997). The availability of multiple binding partners for CaMKII and its partners suggest that is likely there is co-operativity in these interactions. However, this has not been fully explored in a physiological setting before. The full complexity of interactions between CaMKII and its binding partners in dendritic spines is illustrated in **figure 1.10**.

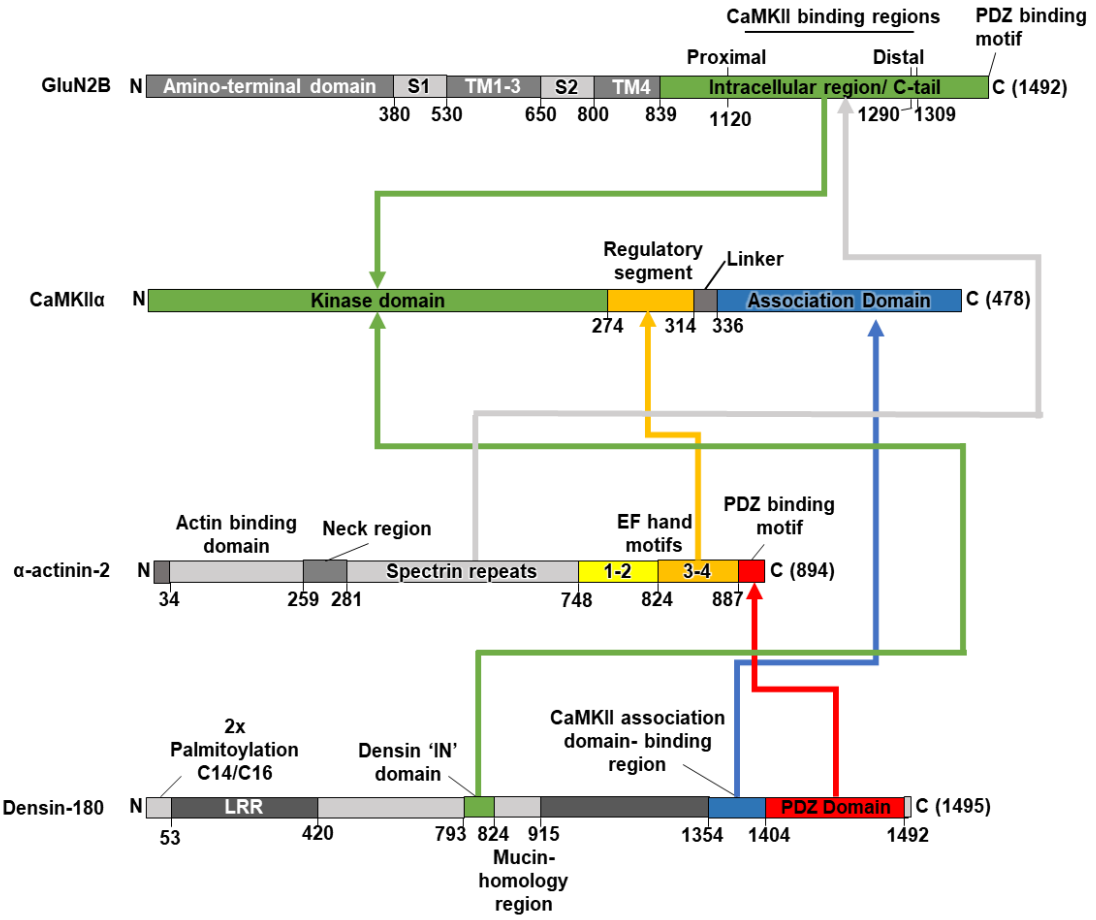

Figure 1.10. Multivalent interactions between CaMKII, α-actinin-2, densin-180 and GluN2B. CaMKII can interact with densin-180 through its association domain; bind to α-actinin-2 EF hand motifs through its regulatory segment; and associate with GluN2B C-tail/densin-180 densin-IN domain through its kinase domain following activation. α-actinin-2 can bind to densin-180 through PDZ interactions, and also to GluN2B intracellular region through its spectrin repeats.

1.7. Outstanding questions concerning the structural role of CaMKII in LTP

A clear structural role for CaMKII is emerging from synaptic plasticity research. However, there are inconsistencies and holes in knowledge regarding exactly how the kinase supports long-lasting increases in the size of postsynaptic spines following LTP induction. Docking of CaMKII to GluN2B subunits is emerging as a strong candidate for the initiator step in structural changes, however it is not clear how this is linked to 'follower-type' interactions that would modify the structure of the cytoskeleton (Yasuda et al., 2022). Interactions with the actin cross-linking protein α-actinin-2 are an obvious candidate for linking CaMKII activation to changes in spine size, however existing evidence indicates that Ca^{2+}/CaM competes with α-actinin-2 for binding to the CaMKII regulatory segment (Robison et al., 2005b), which is not consistent with this mechanism. There have been few attempts to monitor CaMKII interactions *in situ* at different times following LTP induction. Furthermore, there is some evidence that the double phospho-null CaMKIIα mutation T305A/T306A causes tighter binding to α-actinin-2 in the test tube (Jalan-Sakrikar et al., 2012). This property has not been properly investigated, especially in the context of intact neurons, and could call for a re-assessment of the function of phosphorylation at sites 305 and 306.

1.8. Aims

The overarching aim of this thesis was to understand how CaMKII supports structural changes in LTP. To this end, I pursued three specific aims:

Aim 1. To understand when CaMKII & α-actinin-2 interact during LTP and the importance of this interaction to changes in spine morphology that occur in LTP (Chapter 3).

Aim 2. To understand how CaMKII and α-actinin-2 interact during LTP at the molecular level (Chapter 4).

Aim 3. To investigate whether the double substitution T305A/T306A in CaMKII alters its ability to interact with α-actinin-2 and to determine the significance of this behaviour in terms of regulation of spine morphology (Chapter 5).

Chapter 2. Methods & Materials

2.1. Basic molecular biology methods

2.1.1. *E.coli* culturing

All *Escherichia. coli (E. coli)* were cultured in either lysogeny broth (LB) or auto-induction media (AIM) (Studier, 2005). LB was prepared using 10 g/L tryptone, 5 g/L yeast extract, and 5 g/L NaCl. AIM contained the following components:10 g tryptone/L, 5 g yeast extract/L, 1 part in 25 of 25 x M solution (1.25 M Na_2HPO_4, 1.25 M KH_2PO_4, 2.5 M NH_4Cl, 0.25 M Na_2SO_4), 1 part in 50 of 50 x 5052 solution (25 % (w/v) glycerol, 25 g/L glucose, 100 g/L α-lactose monohydrate), 2 mL of 1 M $MgSO_4$, 0.2 mL 1000 x trace elements (50 mM $FeCl_3$, 20 mM $CaCl_2$, 10 mM $MnCl_2$,10 mM $ZnSO_4$, 2 mM $CoCl_2$, 2 mM $CuCl_2$, 2 mM $NiCl_2$, 2 mM Na_2MoO_4, 2 mM Na_2SeO_3, 2 mM H_3BO_3).

2.1.2. Production of chemically-competent *E.coli*

Chemically-competent *E. coli* were produced using a rubidium chloride-based method. Starter cultures of the relevant *E.coli* strain were grown in 100 mL LB overnight at 37 ^oC. On the following morning, 100 mL was inoculated with 0.3 mL of the starter culture and shaken at 37 ^oC until the culture had reached an optical density at 600 nm (OD_{600}) of ~ 0.35. At this point the culture was cooled on ice, pelleted at 1560 x *g* for 10 min and resuspended in 40 mL solution A (30 potassium acetate, 10 mM RbCl, 10 mM $CaCl_2$, 50 mM $MnCl_2$, 15 % (w/v) glycerol, adjusted to pH 5.8 with acetic acid, sterile filtered). After 10 min, the bacteria were resuspended and pelleted once more. The pellets were then resuspended in 4 mL solution B (10 mM MOPS, 10 mM RbCl, 75 mM $CaCl_2$, 15 % (w/v) glycerol, adjusted to pH 5.8 with KOH, sterile filtered). The chemically-competent *E.Coli* were finally aliquoted and flash frozen in liquid N_2 for storage at -80 ^oC.

2.1.3. Generation of recombinant DNA vectors

Many novel expression vectors were generated during the research, typically using polymerase chain reaction (PCR) to amplify sequences before insertion into vectors using restriction digestion and ligation. In some cases, Gibson assembly was employed to generate new vectors, and site-directed mutagenesis was also utilised for introducing targeted mutations. A complete list of DNA oligonucleotide primers employed in this study is provided in **table 2.1** and a list of the newly designed constructs and their entry vectors are provided in **table 2.2**. Required inserts were amplified using Phusion polymerase and purified using Qiagen gel purification reagents. Inserts and vectors were

digested using the appropriate enzymes purchased from New England Biolabs for 3 hours at 37 ^{o}C, including supplementation with Shrimp Alkaline Phosphatase for the final 30 min for vector digestion. Ligation reactions with T4 DNA ligase were incubated overnight at 4 ^{o}C.

Ligation mixtures were transformed into One Shot® TOP10 Chemically Competent *E. coli*. Briefly 50 ng of ligated DNA were inoculated with 50 μL thawed cells on ice for 30 min before a 30 sec heat-shock at 42 ^{o}C. Following heat shock cells were immediately placed on ice for 2 min and were inoculated with 200 μL S.O.C medium (super optimal broth with Catabolite repression- Thermo Fisher) for 1 hour with gentle shaking. After incubation, cells were spread on a pre-warmed agar plate containing the relevant antibiotic before overnight incubation at 37 ^{o}C. Single colonies were selected for overnight culture before plasmid DNA purification using a DNA miniprep kit (Qiagen). Novel DNA vectors were verified using Sanger sequencing performed by Source Biosciences..

I am grateful to many other investigators for providing DNA coding sequences in support of this research. Template DNA for GluN2B-iHA vector development was provided by Andres Barria & Robert Malinow (RRID:Addgene_45447)(Barria and Malinow, 2002), and α-actinin-2 coding sequence by Kristina Djinović-Carugo (Ribeiro et al., 2014). For expression of CaMKIIα 1-315, the corresponding coding sequence was cloned into pNH-TrxT (gift of Opher Gileadi, RRID:Addgene_26106)(Savitsky et al., 2010). Template DNA for densin-180 was provided by Roger Colbran (Strack et al., 2000b, 2000a). Recombinant His_6-CaMKIIα (336-C) was generated by Dr. Christopher Penny, a previous member of the Gold lab.

Primer Name	Sequence (5’ to 3’)
EcoRI_FLAG_actinin_1	CTTGAATTCCACCATGGACTATAAGGATGACGATGACAAAATGAACCAG ATAGAGCCCGG
EcoRI_FLAG_actinin_747	CTTGAATTCCACCATGGACTATAAGGATGACGATGACAAAGCGAAGGGC ATCACCCAG
actinin_894stop_SalI	CTTGTCGACTCACAGATCGCTCTCCCCG
actinin_890stop_SalI	CTTGTCGACTCACCCGTAGAGTGCGGAAGAGAA
actinin_748stop_SalI	CTTGTCGACTCACTTCGCATCTCTCGTCAGGATCT
L854R_F	GAGGAGCTGCGTCGGGAGCGGCCCCCGGATCAGGCCCAG
L854R_R	CTGGGCCTGATCCGGGGGCCGCTCCCGACGCAGCTCCTC
pNH-Trx CaMKIIα 1-315_F	TACTTCCAATCCATGGCTACCATCACCTGCACC
pNH-Trx CaMKIIα 1-315_R	TATCCACCTTTACTGTCATCGGGAGAAGTTCCTGGTGGC
EcoRI_actinin_747	TACTTGAATTCGCGAAGGGCATCACCCAG
actinin_Term_Not1	TAAATCGCGGCCGCTCACAGATCGCTCTCCCC
EF3-4_F	TACTTCCAATCCAATCCAATGCAACCGACACTGCCGAGCAGGTCATC
EF3-4_R	TTATCCACTTCCAATGTTATTATCATCACAGATCGCTCTCCCCG
EcoRI_6HisCaMKIIα	CATGAATTCCACCATGCACCACCATCACCACCATATGGCTACCATCACCT GCAC
CaMKIIα_Term_XhoI	CACTCGAGTCAATGCGGCAGGACG
BamHI_GluN2B_1260	AGCGGCGGATCCCTGCAGGAACTGGACCAG
GluN2B_Term_EcoRI	CCGGGAGCTGCATGTGTCAGAGG
T286A_F	GCCTGCATGCACAGACAGGAGGCCGTGGACTGCCTG
T286A_R	GAACTTCTTCAGGCAGTCCACGGCCTCCTGTCTGTG
T305A_F	GGAAACTGAAGGGAGCCATCCTCGCCACTATGCTGGCCACCAGGAAC
T305A_R	GTTCCTGGTGGCCAGCATAGTGGCGAGGATGGCTCCCTTCAGTTTCC
T306A_F	GGAAACTGAAGGGAGCCATCCTCACCGCTATGCTGGCCACCAGGAAC
T306A_R	GTTCCTGGTGGCCAGCATAGCGGTGAGGATGGCTCCCTTCAGTTTCC
T305A/T306A F	GGAAACTGAAGGGAGCCATCCTCGCCGCTATGCTGGCCACCAGGAAC
T305A/T306A R	GTTCCTGGTGGCCAGCAT AGCGGC GAGGATGGCTCCCTTCAGTTTCC
BamHI_V5_CaMKIIα_F	AGCGGCGGATCCCACCATGGGTAAGCCAATCCCAAACCCCTTGCTGGGT CTCGATAGCACAATGGCTACCATCACCTGCACCCGATTCACAGAA
CaMKIIα_Term_SalI_R	AGCAGGTCGACACGCGTCGTACGTCAATGCG
AgeI_4gHA4g_F	CCTCGACCGGTCTGGGGGAGGCGGAGGTTACCCATACGATGTTCCAGATT ACGCTGGTGGAGGGGGTGGCAACTTCTGCCGCAGCTGTCCTTCC
EcoRI_GluN2B_R	CGGCAAGAATTCAGTGAAAGC
GluN2B_AQ_F	CGGAACAAAGCGCGCCAGCAGCATTCCTACGACACC
GluN2B_AQ_R	CTGCTGGCGCGCTTTGTTCCGATTCTTCTTCTGAGC
EF1-4_F	TACTTGAATTCGCGAAGGGATCACCAG
EF1-4_R	TAAATCGCGGCCGCTCACAGATCGCTCTCCCC

BaMHI_densin180_1266_F	TGGGATCCGAGAGCTGTGGCAAAATGCCGG
densin180_Term_EcoRI_R	AGAATTCTTAGACAGTAAGCTCACGTTGAATAC

Table 2.1. Oligonucleotide primer sequences.

Insert	Backbone	Primers used to construct
FLAG-α-actinin-2 WT	pIRES2-eGFP	EcoRI_FLAG_actinin_1 & actinin_894stop_SalI
FLAG-α-actinin-2 ΔPDZ	pIRES2-eGFP	EcoRI_FLAG_actinin_1 & actinin_890stop_SalI
FLAG-α-actinin-2 EF hand 1-4	pIRES2-eGFP	EcoRI_FLAG_actinin_747 & actinin_894stop_SalI
FLAG-α-actinin-2 EF hand 1-4 ΔPDZ	pIRES2-eGFP	EcoRI_FLAG_actinin_747 & actinin_890stop_SalI
FLAG-α-actinin-2 EF ΔEF hand 1-4	pIRES2-eGFP	EcoRI_FLAG_actinin_1 & actinin_748stop_SalI
FLAG-α-actinin-2 EF hand 1-4 L854R	pIRES2-eGFP	L854R_F & L854R_R
His_6_GST_TEV_α-actinin-2 EF hand 3-4	pET28x	EF3-4_F & EF3-4 R
GST_TEV_α-actinin-2 EF hand 1-4	pGEX-6P-1	EcoRI_actinin_747 & actinin_Term_NotI
His_6-TrxA-CaMKIIα 1-315 WT	pNH-TrxT	pNH-Trx CaMKIIα 1-315_F & pNH-Trx CaMKIIα1-315_R
His_6-TrxA-CaMKIIα 1-315 T305A	pNH-TrxT	T305A_F & T305A_R
His_6-TrxA-CaMKIIα 1-315 T306A	pNH-TrxT	T306A_F & T306A_R
His_6-TrxA-CaMKIIα 1-315 T305A/T306A	pNH-TrxT	T305A/T306A_F & T305A/T306A_R
His_6-CaMKIIα FL WT	pCDNA3.1	EcoRI_6HisCaMKIIα & CaMKIIα_Term_XhoI
V5-CaMKII WT	pIRES2-eGFP	BamHI_V5_CaMKII_F & CaMKII_Term_SalI_R
V5-CaMKII T286A	pIRES2-eGFP	T286A_F & T286A_R
V5-CaMKII T305A	pIRES2-eGFP	T305A_F & T305A_R
V5-CaMKII T306A	pIRES2-eGFP	T306A_F & T306A_R
V5-CaMKII T305A/T306A	pIRES2-eGFP	T305A/T306A_F & T305A/T306A_R
GluN2B (1260-C)	pGEX-6P-1	BamHI_GluN2B_1260 & GluN2B_Term_EcoRI
densin-180 (1266-C)	pGEX-6P-1	BaMHI_densin180_1266_F & densin180_Term_EcoRI_R
GluN2B-iHA WT	GFP-GluN2B	AgeI_4gHA4g_F & EcoRI_GluN2B_R
GluN2B-iHA WT ΔCaMKII	GFP-GluN2B	GluN2B_AQ_F & GluN2B_AQ_R

Table 2.2. DNA constructs generated during the course of the research.

2.2. Protein expression & purification

2.2.1. Expression in *E.coli*

A summary of *E.coli* protein expression conditions is shown in **table 2.3**. Starter cultures were inoculated from single colonies and grown in 100 mL LB overnight at 37 ºC. Large cultures (6 x 800 mL) were inoculated on the following morning with 1 part in 100 starter culture in 2 L conical flasks. All cultures were supplemented with the appropriate antibiotics for the plasmid and *E.coli* strain (ampicillin 0.1 mg/mL, kanamycin 0.05 mg/mL, chloramphenicol 0.034 mg/mL).

Protein	*E.Coli* strain	Media	OD_{600} density at induction	Final IPTG concentration (mM)	Expression temperature (ºC)
His_6-TrxA-Tev-CaMKIIα 1-315 WT	Rosetta™ (DE3) pLysS	LB	~0.5	0.2	18
His_6-TrxA-Tev-CaMKII 1-315α T305A	Rosetta™ (DE3) pLysS	LB	~0.5	0.2	18
His_6-TrxA-Tev-CaMKII 1-315α T306A	Rosetta™ (DE3) pLysS	LB	~0.5	0.2	18
His_6-TrxA-Tev-CaMKIIα 1-315 T305A/T306A	Rosetta™ (DE3) pLysS	LB	~0.5	0.2	18
His_6-GST-Tev-α-actinin-2 EF hands 3-4	Rosetta™ (DE3) pLysS	LB	~0.7	1	20
GST-α-actinin-2 EF hands 1-4	Rosetta™ (DE3)pLsS	AIM	N/A	N/A	37
GST-GluN2B (1260-C)	Tuner™ (DE3)pLsS	AIM	N/A	N/A	37
GST-densin-180 (1266-C)	Star™ (DE3)	AIM	N/A	N/A	37
CaM	(DE3)	AIM	N/A	N/A	37
His_6-FL-α-actinin-2	(DE3)	AIM	N/A	N/A	37
His_6-CaMKII association domain (336-478)	(DE3)	AIM	N/A	N/A	37

Table 2.3 Conditions for protein overexpression in *E.coli* BL21 strains.

2.2.2. Expression in mammalian cells

N-terminally His_6-tagged *Mus musculus* CaMKIIα was expressed in adherent HEK293T cells (ATCC, Cat# CRL-3216) using transient transfection. HEK293T cells were routinely cultured in DMEM (Dulbecco's Modified Eagle Medium), supplemented with 10 % fetal bovine serum, and penicillin/streptomycin (Thermo Fisher). HEK293T cells were transfected in batches of 20 x 10-cm plates. Cells were transfected at 60-70 % confluency using 10 µg DNA and 60 µg polyethlyenimine (linear, MW 25k, transfection grade-polysciences) per 10-cm plate in DMEM lacking penicillin/streptomycin (Curtis et al., 2022). The media was then replaced the following day with routine culture DMEM to prevent polyethylenimine toxicity. After 3 days, the cells were washed twice in PBS (Phosphate-Buffered Saline), then transferred to -80 ^{o}C for storage prior to protein extraction and purification.

2.2.3. Purification of full-length CaMKIIα

For His_6-CaMKIIα purification (**Figure 2.1**), HEK293T cells were lysed by Dounce homogenisation in lysis buffer (20 mM HEPES pH 8.0, 20 mM NaCl, 2 mM DTT, 1 mM EDTA, 1 cOmplete protease inhibitor tablet/100 mL) and clarified by centrifugation for 30 min at 45,000 x *g*. CaMKII was initially enriched using anion exchange with Q Sepharose Fast Flow resin (GE healthcare), eluted in high salt buffer (20 mM HEPES pH 7.5, 500 mM NaCl, 2 mM DTT and 1 mM EDTA) following 2 hour incubation. This eluate was exchanged into Ni-NTA buffer A (500 mM NaCl, 25 mM Tris pH 8, 1 mM Benzamidine, 20 mM imidazole) using a HiPrep desalting column (Cytiva) for binding to Ni-NTA agarose. His-CaMKIIα was eluted from the Ni-NTA agarose using a gradient into Ni-NTA buffer B (500 mM NaCl, 25 mM Tris pH 7.5, 1 mM Benzamidine, 300 mM imidazole), and finally exchanged into storage buffer (25 mM HEPES pH 7.5, 150 mM NaCl, 10 % (w/v) glycerol).

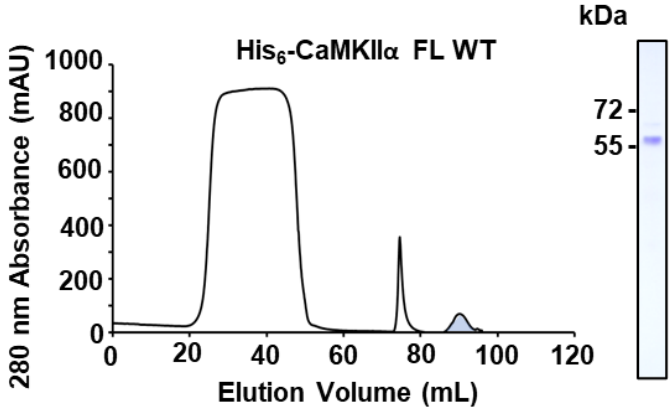

Figure 2.1. CaMKIIα WT purification. The chromatogram of the final size exclusion purification step is shown alongside a Coomassie stained SDS-PAGE gel corresponding to 1 µg His_6 CaMKIIα WT from the peak fraction.

2.2.4. Purification of CaMKIIα fragments

All CaMKIIα 1-315 variants and CaMKII association domain (336-C) were purified using a similar protocol, and their final chromatograms and purities are shown in **figure 2.2**. Cells were lysed in Ni-NTA Buffer A (25 mM Tris pH 8, 500 mM NaCl, 1 mM benzamidine, 20 mM imidazole) supplemented with 0.1 mg/mL lysozyme and 1 Complete EDTA-free protease inhibitor tablet/100 mL. His_6-Trx-CaMKIIα (1-315) was initially purified by affinity to Ni-NTA agarose, eluting with a gradient into Nickel Buffer B. The eluate was exchanged into anion exchange buffer A (20 mM Tris pH 8.8, 20 mM NaCl, 1 mM DTT, 1 mM EDTA) using a HiPrep 26/10 desalting column to enable binding to a Q Fast Flow column (Cytiva). Protein was eluted using a gradient into anion exchange buffer B (20 mM Tris, pH 8, 500 mM NaCl, 1 mM DTT, 1 mM EDTA). Finally, size exclusion was performed using a HiLoad Superdex 75 column equilibrated in gel filtration buffer (20 mM HEPES pH 7.5, 150 mM NaCl, 1 mM DTT) with the exception of CaMKII association domain which was purified with a Superdex 200 SEC column.

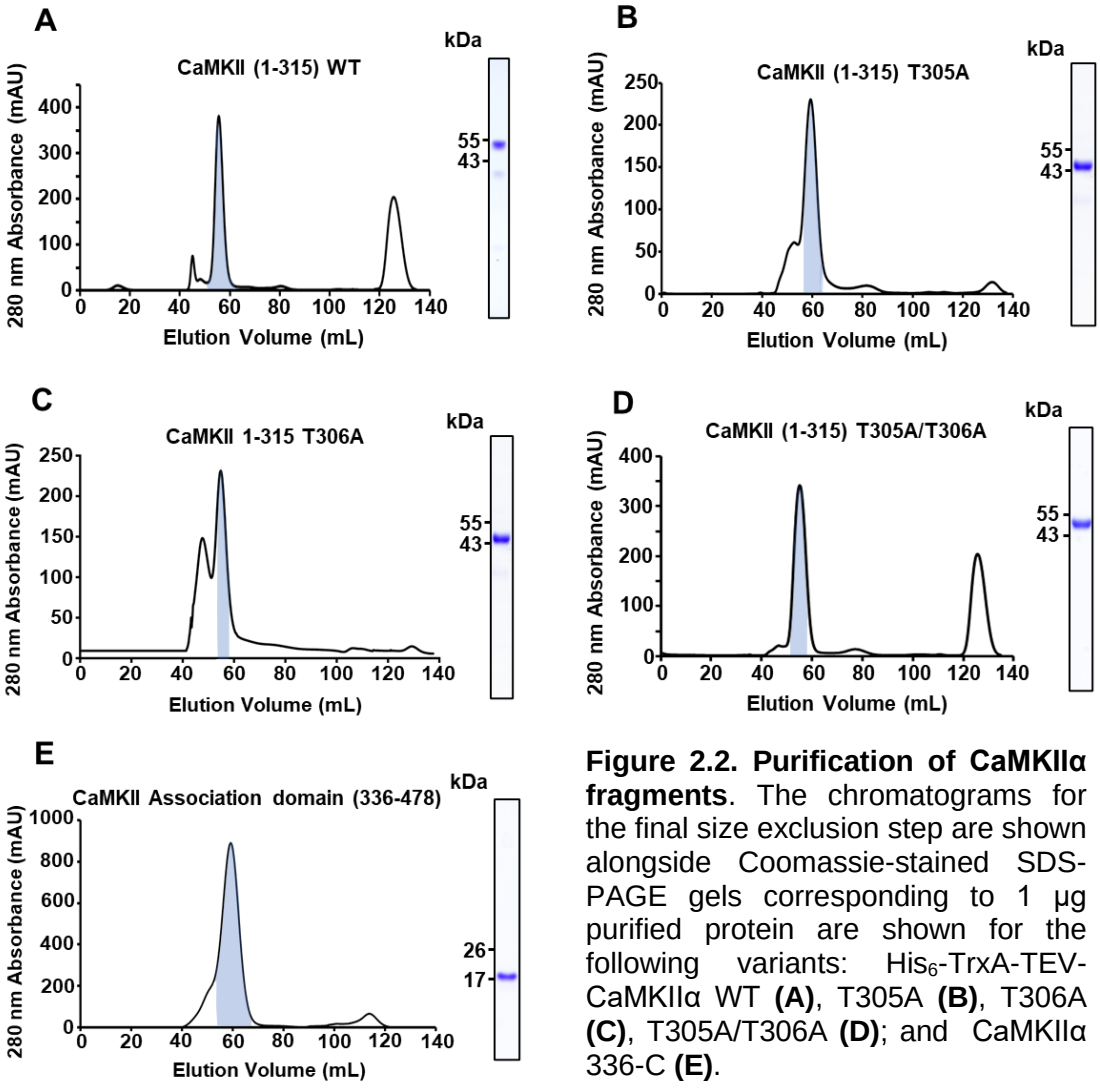

Figure 2.2. Purification of CaMKIIα fragments. The chromatograms for the final size exclusion step are shown alongside Coomassie-stained SDS-PAGE gels corresponding to 1 µg purified protein are shown for the following variants: His_6-TrxA-TEV-CaMKIIα WT **(A)**, T305A **(B)**, T306A **(C)**, T305A/T306A **(D)**; and CaMKIIα 336-C **(E)**.

2.2.5. Purification of full-length α-actinin-2

For the purification of His_6-α-actinin-2 (**Figure 2.3**), cells were lysed in Ni-NTA Buffer A (25 mM Tris pH 8, 500 mM NaCl, 1 mM benzamidine, 20 mM imidazole) supplemented with 0.1 mg/mL lysozyme and 1 Complete EDTA-free protease inhibitor tablet/100 mL. and first purified with to Ni-NTA agarose, and eluted with Nickel Buffer B (25 mM Tris pH 7.5, 500 mM NaCl, 1 mM benzamidine, 20 mM imidazole). The eluate was exchanged into anion exchange buffer A (20 mM Tris pH 8.8, 20 mM NaCl, 1 mM DTT, 1 mM EDTA) using a HiPrep 26/10 desalting column to enable binding to a Q Fast Flow column (Cytiva). Protein was eluted using a gradient into anion exchange buffer B (20 mM Tris, pH 8, 500 mM NaCl, 1 mM DTT, 1 mM EDTA). Finally, size exclusion was performed using a HiLoad Superdex 200 column equilibrated in gel filtration buffer (20 mM HEPES pH 7.5, 150 mM NaCl).

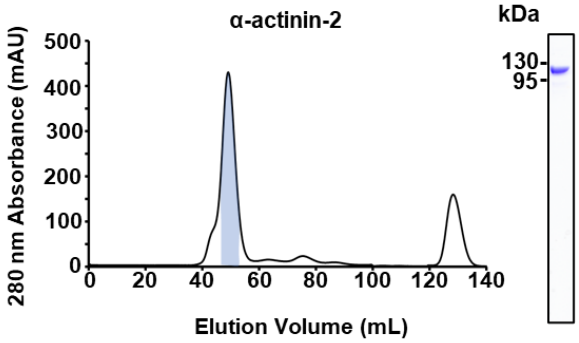

Figure 2.3. Purification of full-length α-actinin-2. The chromatogram of the final size exclusion chromatography purification step is shown alongside a Coomassie staining SDS-PAGE gel corresponding to 1 µg purified protein of the peak fractions.

2.2.6. Purification of α-actinin-2 fragments

For the purification of α-actinin-2 EF hands 1-4, bacteria were first lysed by sonication in lysis buffer (25 mM HEPES pH 7.5, 500 mM NaCl, 1 mM Benzamidine, 1 mM DTT, 1 mM EDTA) supplemented with 1 cOmplete protease inhibitor tablet/100ml and 0.1 mg/mL lysozyme, then clarified by centrifugation at 40,000 x *g*. Lysates were incubated with 3 mL Glutathione Sepharose 4B for 3 hours, washed and cleaved from immobilised GST fusion tag by overnight incubation with PreScission protease at 4 °C. Finally, the proteins were subjected to size-exclusion chromatography with a HiLoad 16/600 Superdex 75 column equilibrated in 25 mM HEPES pH 7.5 and 150 mM NaCl (**Figure 2.4A**). Cells expressing His_6-TrxA-Tev-α-actinin-2 EF hands 3-4 were lysed in Ni-NTA buffer A (25 mM Tris pH 8, 500 mM NaCl, 1 mM Benzamidine, 30 mM imidazole) supplemented with 1 cOmplete protease inhibitor tablet/100ml and 0.1 mg/mL lysozyme, then clarified by centrifugation at 40,000 x *g*. The clarified lysate was incubated with Ni-NTA agarose beads (Qiagen) for 1.5 hours. Following incubation, beads were washed and eluted (500 mM NaCl, 25 mM Tris pH 7.5, 1 mM Benzamidine, 300 mM imidazole).

The resulting eluate was buffer exchanged into Glutathione Sepharose binding buffer (25 mM HEPES pH 7.5, 500 mM NaCl, 1 mM DTT, 0.5 mM EDTA) and incubated with glutathione Sepharose 4B beads for 3 hours, washed and cleaved overnight at 4 °C with Tev protease. Following overnight cleavage, samples were further purified by size-exclusion chromatography with a HiLoad 16/600 Superdex 75 column equilibrated in 20 mM Na HEPES pH 7.5, 0.15 M NaCl, and 1 mM DTT (**Figure 2.4B**).

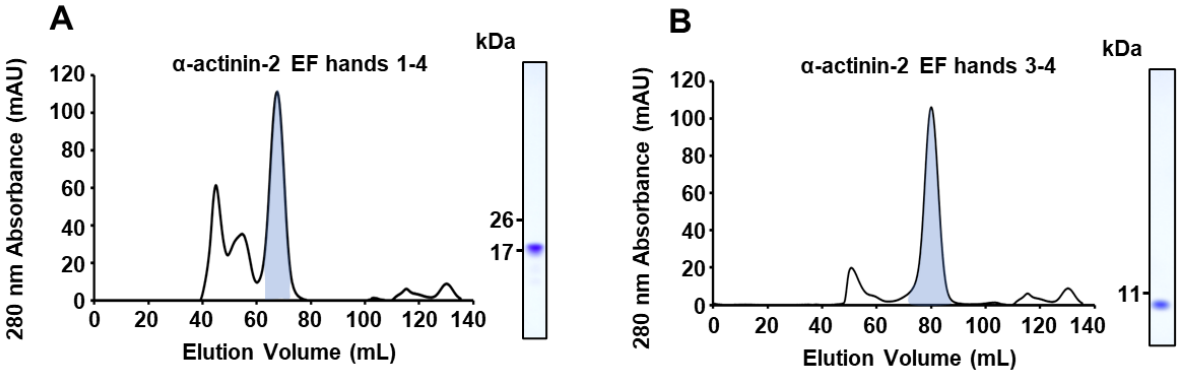

Figure 2.4. Purification of α-actinin-2 EF hand constructs. (A) EF1-4 purification, **(B)** EF3-4 purification. In each panel, the chromatogram of the final size exclusion chromatography purification step is shown alongside a Coomassie staining SDS-PAGE gel corresponding to 1 µg purified protein of the peak fractions.

2.2.7. Purification of densin-180 fragment & GluN2B C-tail

GluN2B (1260-C) and densin-180 (1266-C) were purified in the same way and their final chromatograms and purity are shown in **figure 2.5**. Bacteria were first lysed by sonication in lysis buffer (25 mM HEPES pH 7.5, 500 mM NaCl, 1 mM Benzamidine, 1 mM DTT, 1 mM EDTA) supplemented with 1 cOmplete protease inhibitor tablet/100ml and 0.1 mg/mL lysozyme, then clarified by centrifugation at 40,000 x *g*. Lysates were incubated with 3 mL Glutathione Sepharose 4B for 3 hours, washed and cleaved from immobilised GST fusion tag by overnight incubation with PreScission protease at 4 °C. Finally, the proteins were subjected to size-exclusion chromatography with a HiLoad 16/600 Superdex 75 column equilibrated in 25 mM HEPES pH 7.5 and 150 mM NaCl.

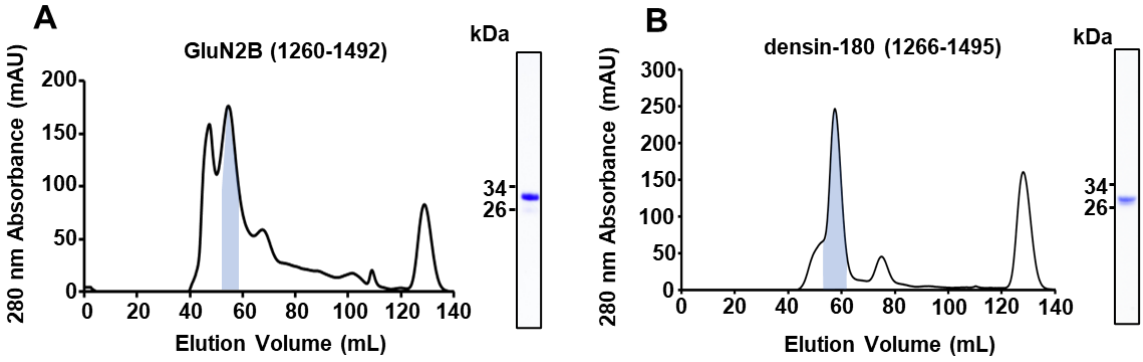

Figure 2.5. Purification of GluN2B and densin-180 fragments. **(A)** GluN2B 1260-C, **(B)** densin-180c (1266-C). In each panel, the chromatogram of the final size exclusion chromatography purification step is shown alongside a Coomassie staining SDS-PAGE gel corresponding to 1 µg purified protein of the peak fractions.

2.2.8. Purification of CaM

CaM was purified as described previously (Patel et al., 2017). Briefly, CaM was first purified by affinity to phenyl sepharose (GE Life Sciences) in the presence of 5 mM $CaCl_2$. CaM was eluted in buffer containing 1 mM EDTA then further purified using anion exchange with a Resource Q column (**Figure 2.6**) (GE Life Sciences) before dialysis into water and lyophilisation in a vacuum concentrator.

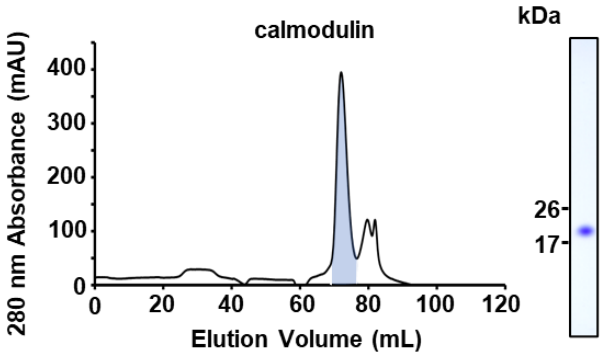

Figure 2.6. CaM purification. The chromatogram shows the final size exclusion chromatography purification step with a Superdex 75 column, alongside a Coomassie staining SDS-PAGE gel corresponding to 1 µg purified protein of the peak fractions.

2.2.9. Determining protein concentrations

Following purification, all proteins were concentrated with 10k or 30k MWCO vivaspin 15 turbo centrifugal concentrators (Sartorius). Protein concentrations were then determined and aliquots were stored at -80 ^{o}C until use. Protein concentrations were measured using absorbance at 280 nm with reference to theoretical extinction coefficients with the exception of CaM whose concentration was determined by bicinchoninic acid (BCA) assay.

Bovine serum albumin (BSA) standard concentrations were used for verifying protein concentrations. For BCA assays, these were prepared at 2, 1, 0.5, 0.25, 0.125, 0.0625, and 0.03125 mg/mL by serial dilution. Concentrated CaM was serially diluted in factors of 2. Protein and standard samples were dispensed into half-area 96-well plates (Thermo Fisher) with 20 uL solutions of either BSA standard or CaM test solution added per well before addition of 200 μL dye mixture comprised of a 1:50 mixture of cupric sulphate to bicinchoninic acid (Santa Cruz biotechnology). The plate was covered in clingfilm and placed in a 37 ^{o}C incubator for 30 min before 540 nm absorbance was measured using a FluoSTAR plate-reader (BMG LabTech). Measurements with protein standards were used to generate a standard line of best fit. Protein concentration was determined using concentrations fell within the linear part of the standard concentation series.

Protein absorbances at 280 nm were determined using a Nanodrop^{TM} 2000 spectrophotometer (Thermo Fisher) and used to calculate protein concentrations with reference to the theoretical extinction coefficient calculated by the Expasy Protparam tool (Gasteiger et al., 2003). The amino acids tyrosine and tryptophan, and to some extent cysteine absorb light with at 280 nm. This absorption is proportional to the concentration of these residues in a solution, and can be estimated for a given protein using the formula: $\varepsilon = (nW \times 5500) + (nY \times 1490) + (nC \times 125)$ in which ε is the calculated molar extinction coefficient for a protein. All protein concentrations were additionally verified using Coomassie staining of proteins separated by SDS-PAGE and run alongside proteins of known concentration.

2.3. Primary hippocampal neuron cultures & chemical LTP induction

2.3.1. Culture of primary hippocampal neurons

All procedures involving animals were conducted according to the Animals Scientific Procedures Act UK (1986) and in compliance with the ethical standards at University College London (UCL). Primary hippocampal cultures were prepared from E18 Sprague-Dawley rat embryos. Brains were removed and placed into a 35 mm dish containing pre-chilled 1 x Ca^{2+} and Mg^{2+}-free HBSS (Hanks' Balanced Sodium Solution - Thermo Fisher) then separated into single hemispheres with the cerebellum removed. Using a dissecting microscope and a pair of fine forceps, the meninges was removed from each hemisphere before the hippocampi were extracted by carefully cutting around their outline. Isolated hippocampi were washed four times with HBSS to remove residual

fibroblasts. Washed hippocampi were next incubated in pre-warmed 0.1 % (w/v) trypsin in Ca^{2+} and Mg^{2+}-free HBSS for 10 min at 37 ºC before digestion was terminated by washing cells twice in plating media (DMEM containing 2 mM L-glutamine, 20 mM glucose, penicillin/streptomycin, 10 % FBS (Fetal Bovine Serum) - all components supplied by Thermo Fisher Scientific) and twice in Ca^{2+} and Mg^{2+}-free HBSS. The tissue was then triturated using fire-polished Pasteur pipettes with progressively smaller apertures in 3 mL plating media and centrifuged at 500 x g for 5 min. Homogeneous cells were then resuspend in 5 mL of fresh plating media, counted on a haemocytometer and adjusted to a final density of 10^6 cells/mL. Cells were then plated onto 13 mm coverslips, pre-treated with Poly-L-Lysine (1 mg/mL) at a density of 1×10^5 cells per coverslip and placed in 5 % CO_2 incubator for 3 hours to allow cell attachment to coverslips. Plating media was then aspirated and replaced with 500 µL maintenance media (Neurobasal medium supplemented with supplemented with 0.5 % (v/v) GlutaMAX supplement, 1 % (v/v) B-27 supplement, 35 mM glucose and 1 x penicillin/streptomycin- all from Thermo Fisher). 50 % of the cultured media was exchanged with fresh maintenance media every four days to replenish nutrients.

2.3.2. Transfection of neuronal cultures

Neurons were transfected after 10 days *in vitro* (DIV) with a total of 0.8 µg DNA and 2 µL Lipofectamine-2000 (Thermo Fisher) per 13 mm coverslip. Neurons were transfected with pIRES2-eGFP vectors containing N-terminally FLAG-tagged α-actinin-2 constructs, and/or V5-tagged CaMKIIα variants, and/or GluN2B-iHA variant and/or empty pIRES2-eGFP vectors. In conditions where two vectors were transfected in neurons, each vector was added at a 1:1 mass ratio. Briefly, DNA and Lipofectamine 2000 were inoculated in opti-MEM for 5 min at room temperature (RT) in separate Eppendorf tubes. DNA and lipofectamine 2000 were then mixed and left for 15-20 min at room temperature, during which time the neurons were washed with opti-MEM media. The DNA-Lipofectamine 2000 mixture was then added directly to coverslips and incubated for 6-8 hours before replacing the mixture with fresh maintenance media. Neurons were then left to express transgenic proteins until 14 DIV.

2.3.3. Chemical LTP induction and neuron fixing

Chemical LTP (cLTP) was induced in cultured hippocampal neurons by activating NMDARs with glycine as described previously (Fortin et al., 2010; McLeod et al., 2018). Primary hippocampal neurons were first transferred into control solution (5 mM HEPES

pH 7.4, 125 mM NaCl, 2.5 mM KCl, 1 mM $MgCl_2$, 2 mM $CaCl_2$, 33 mM D-glucose, 20 μM D-APV, 3 μM strychnine, 20 μM bicuculline, 0.5 μM TTX) for 20 min at RT. cLTP was induced by incubating for 10 min at RT in cLTP solution (5 mM HEPES pH 7.4, 125 mM NaCl, 2.5 mM KCl, 2 mM $CaCl_2$, 33 mM D-glucose, 3 μM strychnine, 20 μM bicuculline, 0.2 mM glycine). Following cLTP induction, neurons were returned to control solution for between 1 and 4 hours before fixation. For PLA assays, neurons were fixed two hours after cLTP induction, other than in the time-course experiment in which they were fixed either 10, 30, 120, 600, or 3600 s after the initial addition of cLTP solution. Cells were fixed with PBS supplemented with 4 % paraformaldehyde PFA, 4 % sucrose, 0.2 % Glutaraldehyde for 5 min at RT, washed with PBS containing 30 mM glycine to quench excess fixative and washed two times with just PBS alone.

2.4. Isothermal Titration Calorimetry

2.4.1. Overview of Isothermal Titration Calorimetry

Isothermal titration Calorimetry (ITC) is a technique used to determine the enthalpy and entropy, as well as the stoichiometry, of molecular interactions by measuring heat changes when two molecules associate. A key advantage of ITC is the ability to measure binding thermodynamics of proteins in their native state in solution with no requirement for labels, tags or immobilisation.

ITC is conducted with calorimeters that consist of two highly-insulated cells: a reference cell with distilled water and a sample cell filled with a buffer containing the 'receptor' molecule (**Figure 2.7A**). When the 'ligand' molecule is injected from the syringe into the sample cell, small heat changes are detected upon association with the receptor molecule (**Figure 2.7 B** & **C**). The calorimeter detect the heat difference and returns the sample and reference cells back to equal temperatures. As the experiment is conducted at in a closed thermal system, one can calculate the precise heat energy changes during binding. The differential power potential (DP) is the difference between the reference cell and the sample cell and can directly be used to calculate energy changes as:

$$power \times time = energy$$

In an ITC experiment, the total area of each heat deflection is calculated as the ligand is titrated into the cell through the injector. Factoring in the size of the heat changes with the concentrations of the ligand and proteins, the total enthalpy change (ΔH) can be calculated for each injection. Plotting the heat changes against the cumulative concentration of the ligand enables the stoichiometry (n) and disassociation constant (K_d)

of the interaction to be determined. From these parameters it is possible to calculate the Gibbs free energy (ΔG) and entropy (ΔS) for the interaction according to the following equations:

$$\Delta G = -RT \ln K_d$$

$$\Delta G = \Delta H - T\Delta S$$

where R is the universal gas constant (8.314 J mol-1 K-1) and T is the temperature at which the experiment was conducted in Kelvin. It should be noted that the gradient of the integrated isotherm (**Figure 2.7C**) determines the K_d of binding with a steep slope resulting in a low K_d (or high association constant K_a) meaning higher affinity. On the other hand shallow slopes yield greater K_d values meaning a weaker affinity.

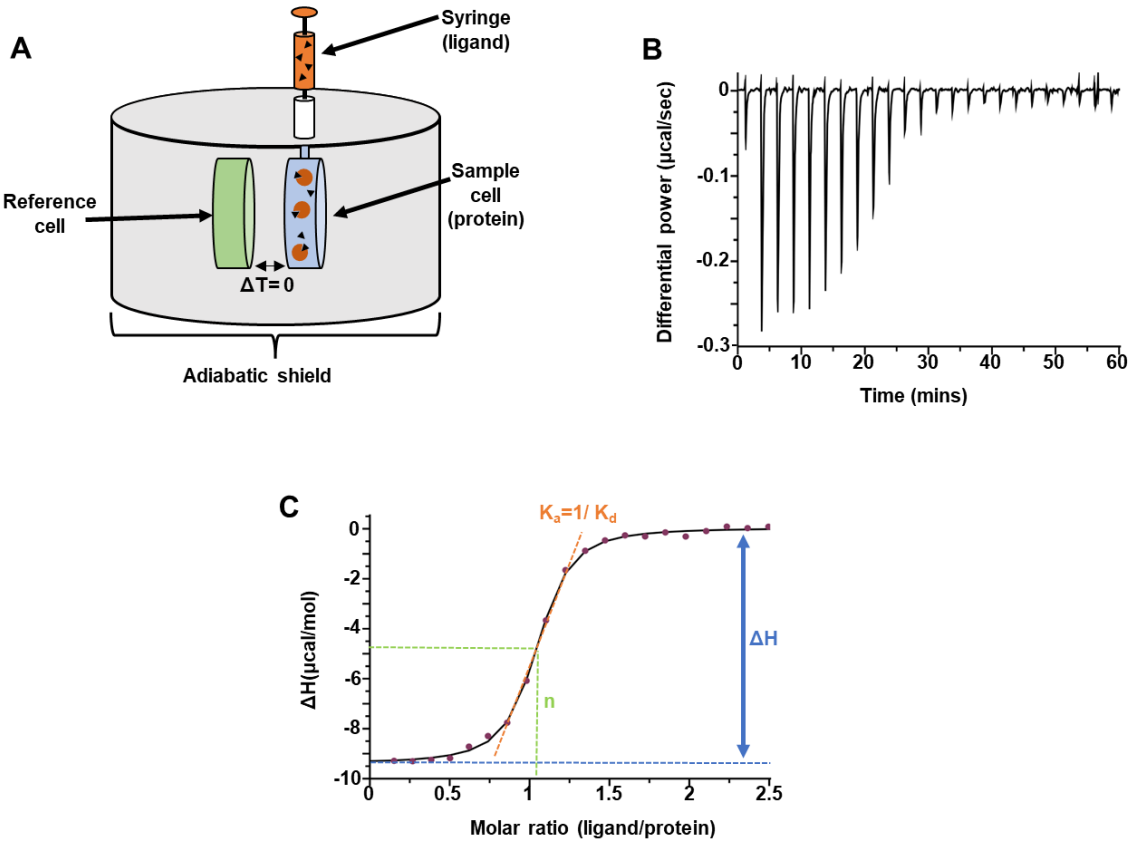

Figure 2.7. Principles of Isothermal Titration Calorimetry (ITC). **(A)** Schematic of a microcalorimeter. The sample cell (protein solution) and the reference cell (degassed water) are thermally insulated by the surrounding adiabatic shield. The syringe contains the ligand of interest at a concentration typically 10x higher than protein in the sample cell. During an ITC run, the ligand is injected at set volumes into the sample cell where heat changes are monitored. The reference cell is then heated/cooled to match the temperature of the sample cell, and the differential power (DP) for each injection is calculated. **(B)** Example raw isotherm of a typical exothermic binding reaction. DP for sequential injections decrease overtime as the ligand saturates protein in sample cell resulting in smaller heat changes. **(C)** Example of an integrated isotherm. As the concentration of the ligand and protein are known in the experiment the total enthalpy change (y-max), stoichiometry (half y-max) and dissociation constant (slope) can be calculated.

2.4.2. ITC sample preparation and experimental parameters

On days prior to conducting ITC measurements, samples were dialysed in 2 L of their respective buffers overnight at 4 ^{o}C using D-tube^{TM} dialyser 3500Da MWCO kits (Merck). On the morning of experiments, proteins were recovered from the dialysers and their concentrations were determined using a nanodrop 2000 or by BCA assay using a FluoSTAR Omega plate reader (BMG) with BCA assay kit. All ITC experiments were performed with a MicroCal PEAQ^{TM} (Malvern Panalyticial instruments) with 2 μL ligand injected at 120 s intervals with a constant mixing speed of 750 rpm. ITC data were collected and analysed using MicroCal Origin software (Malvern Panalytical Instruments). Heat change data series were corrected by subtracting basal heats of injection that were most clearly evident following saturation of binding. Heat change data were fitted to single binding models using a non-linear least-squares minimisation algorithm. Full details of the protein concentrations, buffers, and temperatures employed in ITC experiments are shown in **table 2.4**.

Binding Partner A	**Binding Partner B**	**Concentration A (μM)**	**Concentration B (μM)**	**Experimental temperature (ºC)**	**Buffer**
α-actinin-2 EF hands 3-4	CaMKIIα regulatory peptide 294-315 WT	50	500	25	150 mM NaCl, 25 mM HEPES pH7.5
α-actinin-2 EF hands 3-4	CaMKIIα regulatory peptide 294-315 T305A	50	500	25	150 mM NaCl, 25 mM HEPES pH7.5
α-actinin-2 EF hands 3-4	CaMKIIα regulatory peptide 294-315 T306A	50	500	25	150 mM NaCl, 25 mM HEPES pH7.5
α-actinin-2 EF hands 3-4	CaMKIIα regulatory peptide 294-315 T305A/T306A	50	500	25	150 mM NaCl, 25 mM HEPES pH7.5
α -actinin-2 EF hands 3-4	CaMKIIα regulatory peptide 299-315 WT	50	500	25	150 mM NaCl, 25 mM HEPES pH7.5
α -actinin-2 EF hands 3-4	CaMKIIα regulatory peptide 290-309 WT	50	500	25	150 mM NaCl, 25 mM HEPES pH7.5
α -actinin-2 EF hands 3-4	CaMKIIα regulatory peptide 290-309 T305A/T306A	50	500	25	150 mM NaCl, 25 mM HEPES pH7.5
α -actinin-2 EF hands 1-4	CaMKIIα regulatory peptide 294-315 WT	50	500	25	150 mM NaCl, 25 mM HEPES pH7.5
CaM	CaMKIIα regulatory peptide 294-315 WT	30	300	10	150 mM NaCl, 25 mM HEPES pH7.5, 1 mM $CaCl_2$
CaM	CaMKIIα regulatory peptide 294-315 T305A/T306A	30	300	10	150 mM NaCl, 25 mM HEPES pH7.5, 1 mM $CaCl_2$
CaM	CaMKIIα regulatory peptide 299-315 WT	50	500	10	150 mM NaCl, 25 mM HEPES pH7.5, 1 mM $CaCl_2$
CaMKII 1-315 WT	α -actinin-2 EF hands 3-4	30	300	25	150 mM NaCl, 25 mM HEPES pH7.5, 1 mM ADP, 2 mM $MgCl_2$
CaMKII 1-315 T305A	α -actinin-2 EF hands 3-4	30	300	25	150 mM NaCl, 25 mM HEPES pH7.5, 1 mM ADP, 2 mM $MgCl_2$
CaMKII 1-315 T306A	α -actinin-2 EF hands 3-4	30	300	25	150 mM NaCl, 25 mM HEPES pH7.5, 1 mM ADP, 2 mM $MgCl_2$
CaMKII 1-315 T305A/T306A	α -actinin-2 EF hands 3-4	30	300	25	150 mM NaCl, 25 mM HEPES pH7.5, 1 mM ADP, 2 mM $MgCl_2$
CaMKII 1-315 WT	α -actinin-2 EF hands 1-4	30	300	25	150 mM NaCl, 25 mM HEPES pH7.5, 1 mM ADP, 2 mM $MgCl_2$
CaMKII 1-315 WT	CaM	30	300	10	150 mM NaCl, 25 mM HEPES pH7.5, 1 mM ADP, 1mM $CaCl_2$, 2 mM $MgCl_2$

CaMKII 1-315 T305A/T306A	CaM	30	300	10	150 mM NaCl, 25 mM HEPES pH7.5, 1 mM ADP, 1 mM $CaCl_2$, 2 mM $MgCl_2$
CaMKIIα association domain (336-C)	densin-180 (1266-C)	30	300	25 and 10	150 mM NaCl, 25 mM HEPES pH7.5
densin-180 (1266-C)	α -actinin-2 EF hands 1-4	20	200	25	150 mM NaCl, 25 mM HEPES pH7.5

Table 2.4. Experimental conditions for ITC experiments

2.5. Cross-linking coupled to mass spectrometry

2.5.1. Overview of the technique

Cross-linking coupled to mass spectrometry (XL-MS) is a method whereby proteins of interest in a sample are chemically cross-linked and subsequently digested into peptides. The peptides are then sequenced by tandem MS to determine the exact positions of cross-linked amino acids. Since cross-links will only occur between amino acids that are within a certain distance, XL-MS provides information concerning the positions of different elements within large proteins or protein complexes: intra-links indicates the orientation of different regions within a protein, while inter-links reveal how proteins in complexes are oriented with respect to one another. This technique is particularly useful for structural analysis of large protein complexes, dynamic proteins, and heterogeneous protein samples that might be less amenable to structural approaches such as crystallography and electron microscopy. The generalised workflow of XL-MS is shown in **figure 2.8**.

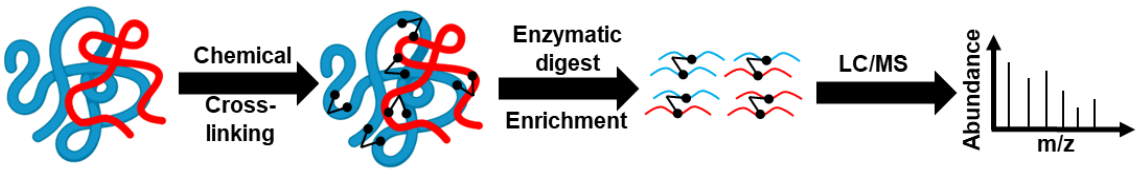

Figure 2.8. Overview of XL-MS. Proteins are cross-linked in their native state, typically using an amine-reactive cross-linker such as DSS. Following this, the protein mixture is enzymatically digested to create peptides using proteases such as trypsin. Finally, the peptides are subsequently analysed by liquid chromatography - tandem MS.

I used H_{12}/D_{12}-isotopically labelled disuccinimidyl suberate (DSS) for XL-MS. DSS is a non-cleavable cross-linker that contains amine-reactive N-hydroxysuccinimide (NHS) ester groups at each end of an 8-carbon spacer arm. At pH 7-9 the NHS groups target the primary amine groups of lysine residues and the N-terminus of polypeptides to form stable amide bonds. When fully extended, the spacer arm of DSS is ~ 11.4 Å long, allowing C_α (alpha carbon of protein backbone) of up to 24 Å apart to be cross-linked from lysine residues. However, taking into account the flexibility of proteins in aqueous solutions, typically a maximum distance of up to 30 Å between C_α atoms is expected when cross-referencing to static protein structures determined by techniques such as protein crystallography (Merkley et al., 2014). NHS groups of DSS are susceptible to rapid hydrolysis in aqueous solution under typical biological conditions and temperature with a half-life in order of tens of minutes (Leitner et al., 2010). Once DSS is solubilised, I immediately added the cross-linker to solutions to prevent loss of activity.

For XL-MS experiments, I performed purification, mixing, and cross-linking of the proteins were handled in our lab. Digestion, enrichment, LC-MS/MS and initial processing by xQuest/xProphet/xTract was carried out by our collaborator, Florian Stengel at the University of Konstanz. Analysis of data output by xQuest/xProphet/xTract was performed collaboratively.

2.5.2. Sample preparation and cross-linking

To facilitate identification of cross-linked peptides by MS, I used the commercially-available cross-linker H_{12}/D_{12} DSS (creative molecules), in which half of the DSS molecules contain deuterium in place of hydrogen at 12 positions resulting in a mass shift of 12.075 Da. The different masses of the heavy and light cross-linkers appear as a mass-shifted doublet on the spectrum to aid in the identification of peptides (Rinner et al., 2008).

Cross-linking experiments with CaMKIIα/CaM/α-actinin-2 ± GluN2B (1260-C) were performed at a 3:3:1:3 respective molar ratio. Master mix samples were prepared in a in basic buffer (25 mM HEPES pH 7.5, 150 mM NaCl). Mixtures were aliquoted in two separate Eppendorf tubes and supplemented with either a 10 x Ca^{2+}-additive (20mM $CaCl_2$, 20 mM DTT) or 10 x no Ca^{2+}-additive (20 mM DTT) and incubated at 4 ^oC for 30 min to allow association of proteins before adding EGTA (final concentration 2.5 mM). Samples were aliquoted into three tubes (biological replicates) and immediately incubated with 0.5 mM (final concentration) of H_{12} /D_{12} DSS solubilised in DMSO. The cross-linking reaction was then carried out by incubating proteins at 30 ^oC for 30 min, shaking at 500 RPM. The reaction was terminated with the addition of ammonium bicarbonate (50 mM final concentration). Reaction mixtures were then flash-frozen and sent to the Stengel lab for analysis. Each replicate sent off for mass spectrometry corresponded to 80 μg total protein at a concentrations of 1 mg/mL.

For western blot analysis of cross-linked samples, I employed the following western blotting detection approach: CaMKIIα was detected using anti-CaMKII antibody (RRID_Ab: 626787, 1:5000 dilution); α-actinin-2 was detected using anti-α-actinin-2 antibody (RRID_Ab: 11157538, 1:5000 dilution); CaM was detected using anti-CaM antibody (RRI_Ab: 2069438, 1:5000 dilution). Anti-mouse HRP (RRID_Ab: 228307, 1:5000 dilution) or anti-rabbit HRP (RRID_Ab: 228341, 1:5000 dilution) secondary

antibodies were then utilised as appropriate. As no antibody was available to detect GluN2Bc, the construct was monitored using Coomassie staining.

To prepare samples for MS (these steps were performed at the University of Konstanz), samples were first dessicated, then dissolved in 8 M urea, reduced with 2.5 mM urea/tris(2-carboxyethyl) phosphine (TCEP) and alkylated with 5 mM (final concentration) iodoacetamide. The samples were next digested with trypsin (1:40) overnight in 1 M urea. The trypsinised peptide mixtures were separated from the solution via solid phase extraction (SepPak, waters) and subsequently enriched by SEC using a Superdex^{TM} Peptide 3.2/300 column (GE healthcare) in 69.9 % water, 30 % acetonitrile, and 0.1 % trifluoroacetic acid. The peptides were collected in 100 μL fractions, which were individually processed on the LC-MS/MS.

2.5.3. Cross-linked peptide identification by MS

Cross-linked peptides were analysed by tandem MS. First, peptides were "softly ionised" by electrospray ionisation (ESI) to prevent peptide fragmentation in the ionisation process. During ESI peptides are transferred into a polar volatile solvent and forced through the tip of a high voltage spraying nozzle, which vaporises the liquid droplets releasing peptides that are charged. The mass-spectrometer used for the first MS phase (MS1) was the orbitrap spectrometer (Thermo Fisher) which consists of a central rod-like electrode surrounded by a barrel-like electrode. As ions enter the orbitrap chamber they swirl around the central electrode oscillating at different frequencies according to their mass/charge (m/z) ratio and the m/z is determined using the harmonic oscillations in combination with Fourier transform. Following orbitrap (MS1) charged ions are subsequently analysed MS2, where peptides are subject to collision induced dissociation (CID). During CID, accelerated ionised peptides are collided with neutral gas to induce breakages in the peptide which normally occur between amino acids in the peptide bond. This produces fragments of different masses that can be analysed in relation to one another to provide greater coverage of the peptide sequence.

2.6. Confocal imaging and Proximity Ligation Assays

2.6.1. Principles of the Proximity ligation assay

The Proximity Ligation Assay (PLA) is a powerful technique that may be employed for *in situ* labelling of intact fixed specimens (Fredriksson et al., 2002) to analyse co-localisation with resolution of less than 40 nm. The basis of PLA shown in **figure 2.9**. Antibodies to two proteins of interest are conjugated to single stranded oligonucleotides. When the two proteins are associated within cells, DNA hybridisation can occur enabling rolling circle amplification with fluorogenic oligonucleotides to produce fluorescent puncta that are visible using confocal microscopy. The two proteins of interest are detected with primary antibodies raised in different species. In turn, species-specific secondary antibodies conjugated to either a 'PLUS' (5' to 3') or 'MINUS' (3' to 5') oligonucleotide are added. If the epitopes of the two proteins are within 40 nm, the PLUS and MINUS oligonucleotides can hybridise and ligate to form a closed circular DNA upon addition of DNA ligase. In the final stage, the closed circular DNA acts as a template for rolling circle amplification with DNA polymerase and fluorogenic oligonucleotides, which boosts the PLA signal by ~1000-fold such that it can be directly visualised by confocal microscopy as a discrete puncta (Alam, 2018). PLA is often taken as a readout of direct protein-protein interactions, although this is not necessarily the case. In this project, the general approach was to perform control experiments including binding-deficient variants to determine to what extent PLA signals were likely to represent detection of direct protein-protein interactions as opposed to close co-localisation of the proteins of interest by indirect means.

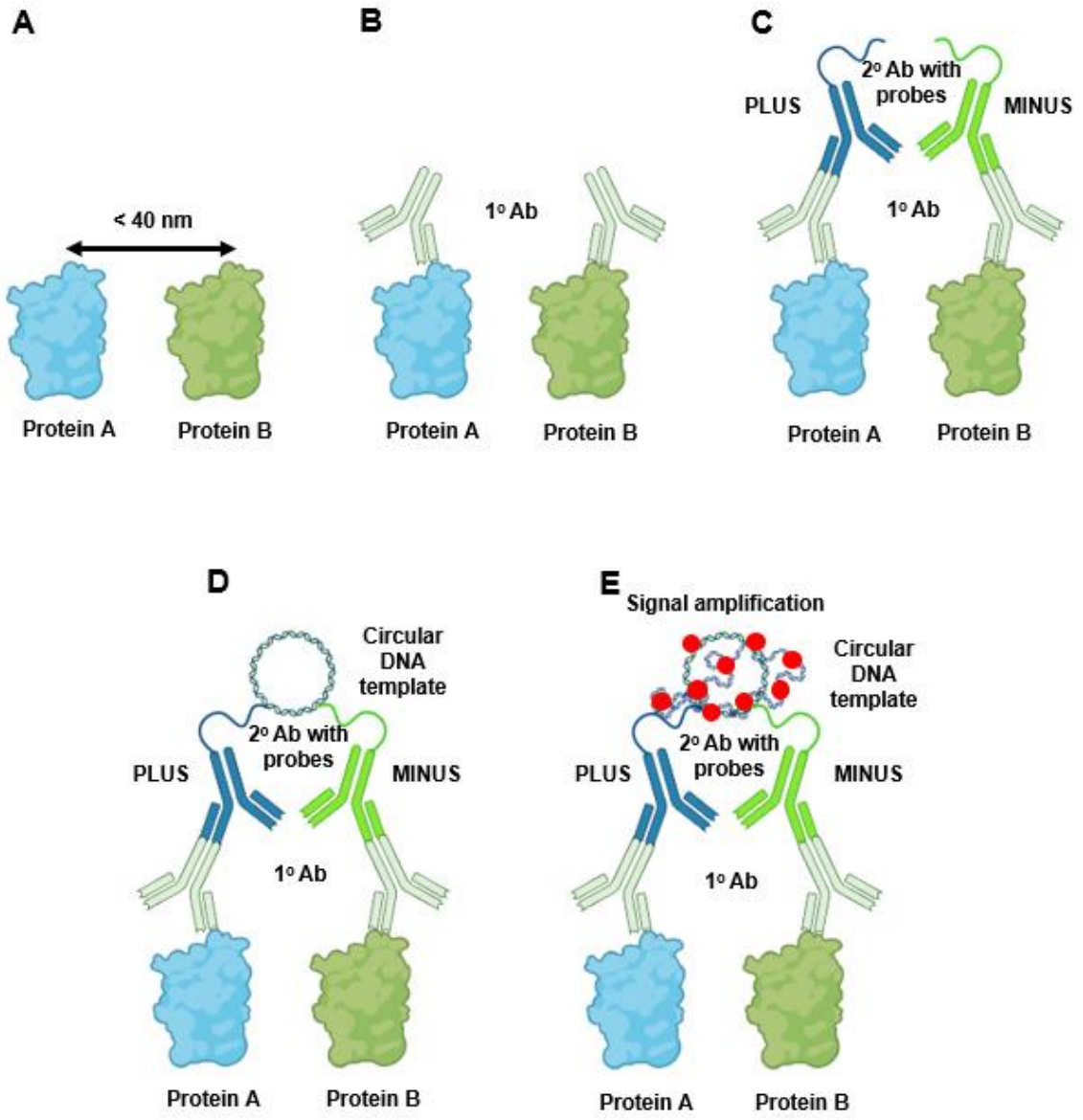

Figure 2.9. Basis of the proximity ligation assay. (A) Two proteins are in proximity. **(B)** Primary antibodies raised in different species bind to their respective epitopes in target proteins. **(C)** A pair of oligonucleotide-conjugated antibodies (PLA probes bind to primary antibodies. **(D)** When PLA probes are in proximity, hybridizing connector oligos join PLA probes following the edition of ligase, to form a closed circle DNA template for amplification. **(E)** DNA template is then amplified with the addition of DNA polymerase where it is hybridized with labelled oligos to form a fluorescent signal localised at a discrete spot.

2.6.2. PLA protocol

PLAs were performed using reagents from a Duolink In Situ PLA kit. Fixed neurons were permeabilised for 5 min at RT in PBS supplemented with 1 % BSA/0.1 % Triton X-100, and blocked for 1 hour in PBS supplemented with 10 % BSA before overnight incubation at 4°C with primary antibodies (**table 2.5**) in PBS supplemented with 1 % BSA. On the following morning, neurons were incubated with the corresponding Duolink probes (**table 2.5**) and goat anti-rabbit Alexa Fluor (Thermo Fisher) at 37 °C for 1 hour. Probes were ligated at 37 °C for 30 min and signals were amplified at 37 °C for 100 min. Coverslips were mounted on glass slides with ProLong Gold antifade mountant (Thermo Fisher) and sealed with generic nail varnish. Coverslips were imaged within 3 days after PLA labelling.

2.6.3 Preparation of coverslips for analysing dendritic spine width

Fixed neurons transfected with pIRES2-eGFP α-actinin-2 EF hands 1-4 WT or L854R mutant, cells were directly mounted on to coverslip glass slides with ProLong gold anti-fade mountant sealed with nail varnish. Fixed neurons transfected with pIRES2-eGFP FLAG-FL-α-actinin-2 and/or pIRES2-eGFP-V5-CaMKIIα were permeabilised and labelled with Chicken anti-GFP and Anti-chicken Alexa Fluor 488 as described in **section 2.6.2** and mounted on glass slides with ProLong gold anti-fade mountant (Thermo Fisher).

PLA Target Pairing	Primary Antibodies	Secondary Probes/Antibodies
Endogenous CaMKIIα *with* FLAG-α-actinin-2 variants	Mouse anti CaMKIIα RRID_Ab: 626787 1:400 dilution	Duolink In situ Anti-PLA probe mouse MINUS probe (DUO 92004)
	Goat anti-FLAG RRID_Ab: 10000565 1:200 dilution	Duolink In Situ PLA probe Anti-goat PLUS (DUO92003)
	Rabbit anti-GFP, RRID_Ab: 2750576. 1:300 dilution	Goat anti-rabbit Alexa Fluor 405. RRID_Ab: 221605. 1:500 dilution
N-V5-CaMKIIα variants *with* FLAG-α-actinin-2	Mouse anti-V5 RRID_Ab: 10977225 1:500 dilution	Duolink In situ Anti-PLA probe mouse MINUS probe (DUO 92004)
	Goat anti-FLAG RRID_Ab: 10000565 1:500 dilution	Duolink In Situ Anti-goat PLUS (DUO92003)
	Chicken Anti-GFP, RRID_Ab: 300798 1:500 dilution	Rabbit anti-chicken Alexa Fluor 488. RRID_Ab:2339327. 1:500 dilution
GluN2B-iHA variants *with* FLAG-α-actinin-2	Rabbit anti-HA RRID:Ab_307019 1:500	Duolink In Situ Anti-rabbit MINUS (DUO92005)
	Goat anti-FLAG RRID_Ab: 10000565 1:500 dilution	Duolink In Situ Anti-goat PLUS (DUO92003)
	Chicken Anti-GFP, RRID_Ab: 300798 1:500 dilution	Rabbit anti-chicken Alexa Fluor 488. RRID_Ab:2339327. 1:500 dilution
Glun2B-iHAand endogenous CaMKII	Rabbit anti-HA RRID:Ab_307019 1:500	Duolink In Situ Anti-rabbit PLUS (DUO92002)
	Mouse anti CaMKIIα RRID_Ab: 626787 1:400 dilution	Duolink In situ Anti-PLA probe mouse MINUS probe (DUO 92004)
	Chicken Anti-GFP, RRID_Ab: 300798 1:500 dilution	Rabbit anti-chicken Alexa Fluor 488. RRID_Ab:2339327. 1:500 dilution

Table 2.5. List of primary and secondary antibodies used for PLAs

2.6.4. Image acquisition by confocal microscopy

Imaging was performed using a 60 x oil objective (Numerical Aperture=1.40) and Zeiss acquisition software with either a Zeiss LSM 700 inverted microscope (imaging shown in Chapter 3) or a LSM 780 microscope (imaging shown in Chapters 4 & 5). 16-bit depth, Z-stack (optical slice of 0.38 μm) images were taken at 1024 x 1024 pixel resolution with

scan speeds of 6 (corresponding to a dwell time of 2.05 μs) and averaging images per scan. Laser power, detector gain and offset were kept constant throughout experimental conditions.

For PLA experiments to detect interactions with FLAG-α-actinin-2 variants and endogenous CaMKIIα, images were collected using 405 nm excitation/421 nm emission for detecting anti-GFP labelling, and 594 nm excitation/619 nm emission for PLA puncta. For the rest of the PLA experiments, images were collected using 488 nm excitation/421 nm emission for detecting anti-GFP labelling, and 594 nm excitation/619 nm emission for detecting PLA puncta. For imaging neurons transfected with α-actinin-2 EF1-4 disruptors, intrinsic GFP fluorescence was imaged using 488 nm excitation/509 nm emission. Data were obtained from three independent neuronal cultures with the exception of FLAG- α-actinin-2 ΔEF1-4 transfected neurons in chapter 3 (one culture) and PLA experiments comparing V5-CaMKII WT and V5-CaMKII T305A/T306A variants in chapter 5 (two cultures).

2.6.5. Data analysis

For PLA puncta analysis Image J software (NIH-version 1.52) was used with the Distance Analysis (DiAna) plugin (Gilles et al., 2017) for ImageJ. Z-stacks for the GFP channel of each image was superimposed to aid outlining the dendritic region of interest (ROI) which was saved and used on non-superimposed images for the PLA channel thereafter. DiAna plugin was then used to generate binarised images to detect of the number of PLA dots within the ROI. The number of PLA dots colocalised to synapses were then quantified within the total dendritic length of the ROI to calculate number of puncta per 10 μm of dendritic length. Images for spine width data and classification were analysed using the automated NeuronStudio software (Icahn School of Medicine at Mount Sinai) to determine spine width and morphology.

2.7. Pull-down assays with magnetic beads

For pull-down experiments to investigate the effect of GluN2B (1260-C) on CaMKII association with α-actinin-2 EF1-4 (Chapter 4), 0.25 μg of Pierce Glutathione Magnetic Agarose Beads were charged with 4 mg GST or GST-EF1-4 in basic binding buffer (25 mM HEPES pH 7.5, 150 mM NaCl, 0.05 % Tween-20, 10 mM $MgCl_2$, 0.5 mM ADP, 2 mM DTT) for 2 hours at 4 °C. Protein mixtures containing CaMKII, CaM, and GluN2B (1260-C) (as appropriate) were separately pre-incubated for one hour in basic binding

buffer supplemented with $CaCl_2$. These mixtures were diluted with equal volumes of basic binding buffer containing 4 % BSA to achieve final concentrations of 2 mM $CaCl_2$, 2 % BSA, 0.1 μM CaMKIIα, 3 μM CaM, and 1.5 μM GluN2B (1260-C) as appropriate. For each assay, 100 μL protein mixture was incubated with GST/GST-EF1-4 magnetic beads for 20 min before the reactions were supplemented with either 10, 2.5, or 1.8 mM EGTA. Free Ca^{2+} concentrations were estimated using maxchelator (Bers et al., 2010). Following 20 min further incubation, each pull-down was washed with 3 x 500 μL basic binding buffer supplemented with 2 mM $CaCl_2$ and the appropriate concentration of EGTA. Proteins were eluted from the beads by incubation with 50 μL 1 x LDS loading buffer (5 min heating at 65 °C). CaMKII and GST/GST-EF1-4 were detected using immunoblotting with mouse anti-CaMKIIα and rabbit anti-GST antibodies.

For pull-down experiments determining the effect of densin-180c (1266-C) (Chapter 3), 0.25 μg of Pierce Glutathione Magnetic Agarose Beads were charged with 4 μg GST or GST-EF1-4 in basic binding buffer (25 mM HEPES pH 7.5, 150 mM NaCl, 0.05 % Tween-20, 2 mM DTT) for 2 hours at 4 °C. Protein mixtures containing CaMKII (1 μM final) and densin-180 (15 μM final) were then pre-incubated for one hour in basic binding with 2 % BSA. For each assay, 100 μL protein mixture was incubated with GST/GST-EF1-4 magnetic beads for 30 min before each pull-down was washed with 3 x 500 μL basic binding buffer. Proteins were eluted from the beads by incubation with 50 μL 1 x LDS loading buffer (5 min heating at 65 °C). CaMKII and GST/GST-EF1-4 were detected using immunoblotting with mouse anti-CaMKIIα and rabbit anti-GST antibodies.

2.8. Statistical Analysis

Data were analysed on Graphpad Prism and assessed for normality using Kolmogorov-Smirnov testing. Normally distributed data were analysed using unpaired two-tailed Student's t-tests whereas Mann-Whitney tests were applied for non-parametric data where $*p < 0.05$, $**p < 0.01$, $***p < 0.001$. Two-way ANOVA was utilised to analyse PLA measurements with neurons expressing GluN2B-iHA. Non-linear curve fitting by iterative least squares minimization was performed in Origin (Matlab) to fit PLA time course data to a Hill function.

Chapter 3. Role of α-actinin-2-CaMKII interactions in structural LTP

In this chapter, I focus on understanding how interactions between CaMKII and α-actinin-2 contribute to structural changes in dendritic spines following the induction of LTP. As explained in the introduction, α-actinin-2 is an actin cross-linking protein so an obvious candidate for linking CaMKII to the actin cytoskeleton following LTP induction. However, this is not consistent with the observation that Ca^{2+}/CaM competes with α-actinin-2 for binding to the CaMKII regulatory segment (Robison et al., 2005b). I conducted *in situ* imaging experiments to determine whether CaMKII interactions with actinin are altered during LTP (**Section 3.1**). Next, I investigated whether densin-180 can contribute to CaMKII-actinin interaction *in vitro* (**Section 3.2**). I also monitored how quickly CaMKII-actinin interactions are modified following LTP (**Section 3.3**). Finally, I investigated the effect of expressing a truncated fragment of α-actinin-2 that disrupts actinin-CaMKII interactions on changes in dendritic spine architecture following LTP (**Section 3.4**).

3.1. The association between α-actinin-2 and CaMKII is elevated following LTP induction

To investigate α-actinin-2 association with CaMKII in neurons, I utilised proximity ligation assays (PLAs, see **Section 2.6**) in rat primary hippocampal neurons. For these experiments, I developed a set of vectors for mammalian expression of different α-actinin-2 fragments in tandem with GFP: each α-actinin-2 construct contains an N-terminal FLAG tag, so association with endogenous CaMKII can be monitored by PLA using paired anti-FLAG and anti-CaMKIIα antibodies. I transfected each construct after 10 days *in vitro* (DIV10) and fixed mature neurons on DIV14. Before fixing, a subset of neurons was subject to a chemical model of LTP (cLTP), using glycine to activate NMDARs and trigger spine head enlargement during LTP (Fortin et al., 2010). This is considered a relatively realistic chemical model for LTP that mimics other features including an increase in mini excitatory postsynaptic current amplitude following NMDAR stimulation (Lu et al., 2001). Following fixation, neurons were subsequently labelled with appropriate anti-GFP antibody and PLA probes for imaging anti-GFP immunofluorescence and α-actinin-2-CaMKIIα PLA puncta respectively. It should be noted that hippocampal neurons were fixed and analysed 4 hours after cLTP induction.

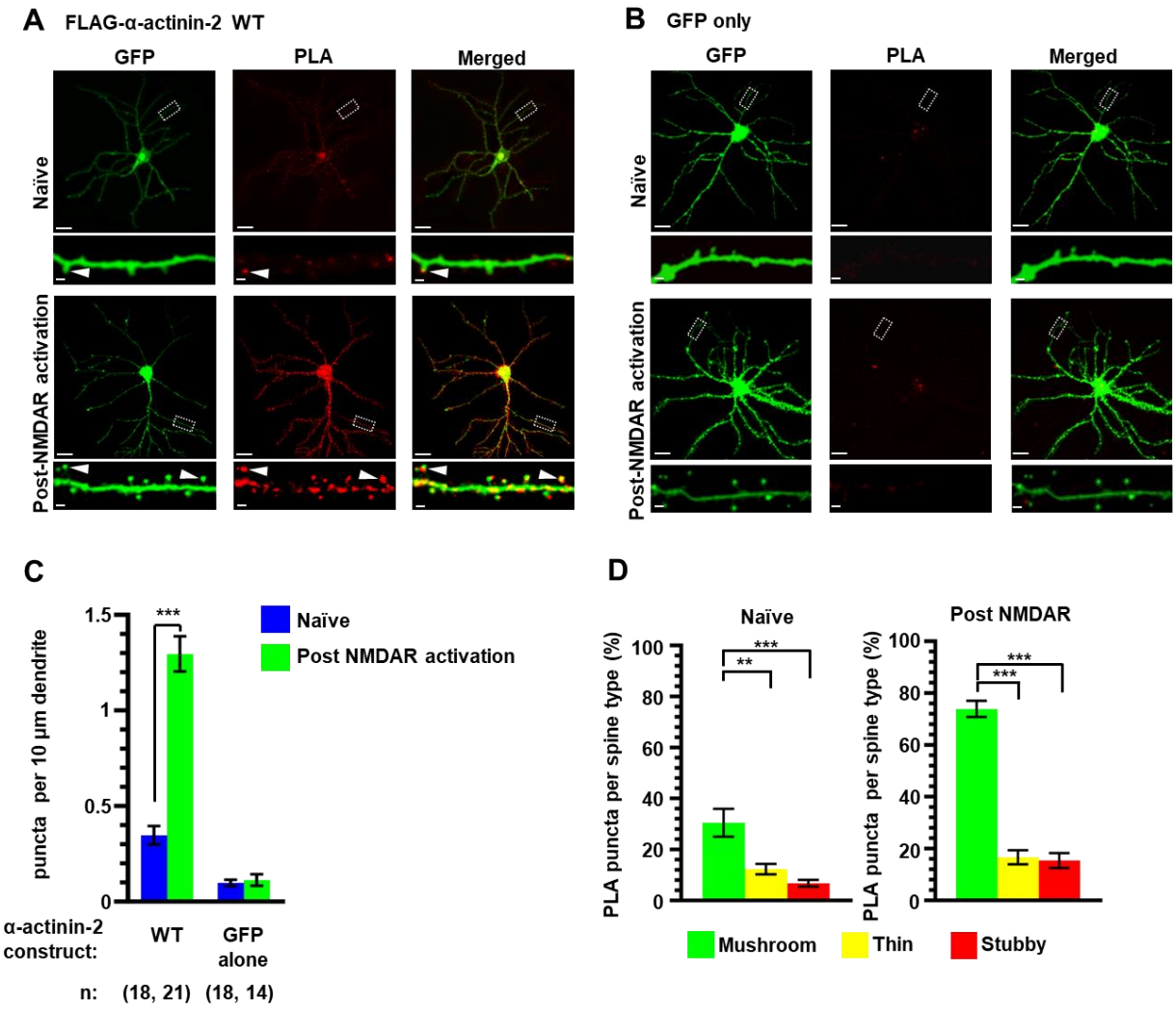

Figure 3.1. Changes in FLAG-α-actinin-2 WT and endogenous CaMKII association following NMDAR stimulation. Panels **A-B** are representative images for neurons expressing **(A)** FLAG-α-actinin-2 WT in tandem with GFP or **(B)** GFP alone. For panels **A-B**, the **a**nti-GFP immunofluorescence (left column), anti-FLAG/anti-CaMKII PLA puncta (middle column) and merged GFP and PLA puncta channels (right column) are shown either before (top row) or after (bottom row) NMDAR activation. Scale bars for **(A)** and **(B)** are 20 µm (whole cell images) and 1 µm (dendritic close-up). **(C)** Quantitation of PLA puncta per 10 µm dendrite before (blue) or after (green) NMDAR activations for the full set of FLAG-α-actinin-2 constructs. **(D)** Percentage of mushroom, thin and stubby type spines which contain PLA puncta in FLAG-α-actinin 2 WT transfected neurons**.** Data are presented as the mean ± standard error (SE) and were collected from three independent E18 preparations. The number of neurons analysed for each construct is shown in parentheses.

For full-length WT FLAG-α-actinin-2, PLA puncta were observed in unstimulated neurons at a density of 0.35 ± 0.05 puncta per 10 μm dendrite (**Figure 3.1C**) which was 3.5-fold higher (p=2.2×10^{-5}) than in unstimulated neurons expressing GFP alone (0.10 ± 0.05) (**Figure 3.1C** & **Figure 3.1B**). Imaging GFP-immunofluorescence from NMDAR-activated neurons transfected with WT α-actinin-2 revealed the development of mushroom-type spines, as expected, indicative of sLTP (**Figure 3.1A**, left panel). NMDAR-activated neurons also exhibited PLA puncta density of 1.30 ± 0.09 per 10 μm dendrite (**Figure 3.1C**), which is 3.7-fold higher (p=1.6×10^{-10}) compared to unstimulated, naïve neurons. These PLA puncta were localised to enlarged mushroom-type spines (**Figure 3.1A**, arrows), consistent with a role for α-actinin-2-CaMKIIα interactions in stabilizing the structure of potentiated spines: 44 ± 7 % of mushroom-type spines contained PLA puncta in naïve neurons, rising to 82 ± 3 % after NMDAR activation (**Figure 3.1D**). In comparison, lower proportions of thin (19 ± 5 % pre activation; 31 ± 5 % post-activation) and stubby (10 ± 2 % pre; 35 ± 5 % post) spines exhibited PLA puncta. In sum, this data is consistent with a role for α-actinin-2-CaMKIIα interactions in stabilizing the enlarged structure of potentiated spines.

I next compared PLA puncta formation in neurons expressing different fragments of α-actinin-2 (**Figure 3.2A**). Consistent with a key role for α-actinin-2 EF hands in mediating interactions with CaMKIIα (Jalan-Sakrikar et al., 2012; Robison et al., 2005a): expression of a fragment limited to the EF hand motifs ('EF1-4') generated similar levels of PLA puncta compared to the WT fragment, with a puncta density of 0.41 ± 0.04 per 10 μm dendrite rising to 1.01 ± 0.06 (p=6.8×10^{-11}) following NMDAR activation (**Figure 3.2F** & **Figure 3.2C**). Deletion of the EF hand motif ('ΔEF1-4') produced PLA puncta densities close to GFP control, irrespective of NMDAR activation, with 0.18 ± 0.04 and 0.21 ± 0.03 puncta/10 μm dendrite before and after NMDAR activation, respectively. (**Figure 3.2F** & **Figure 3.2E**). Although PLA signal is a measure of protein proximity rather than direct protein-protein interaction, the low levels of puncta formation observed with the ΔEF1-4 construct indicate that puncta formation in this case is likely to correspond to direct interaction between CaMKII and a-actinin-2.

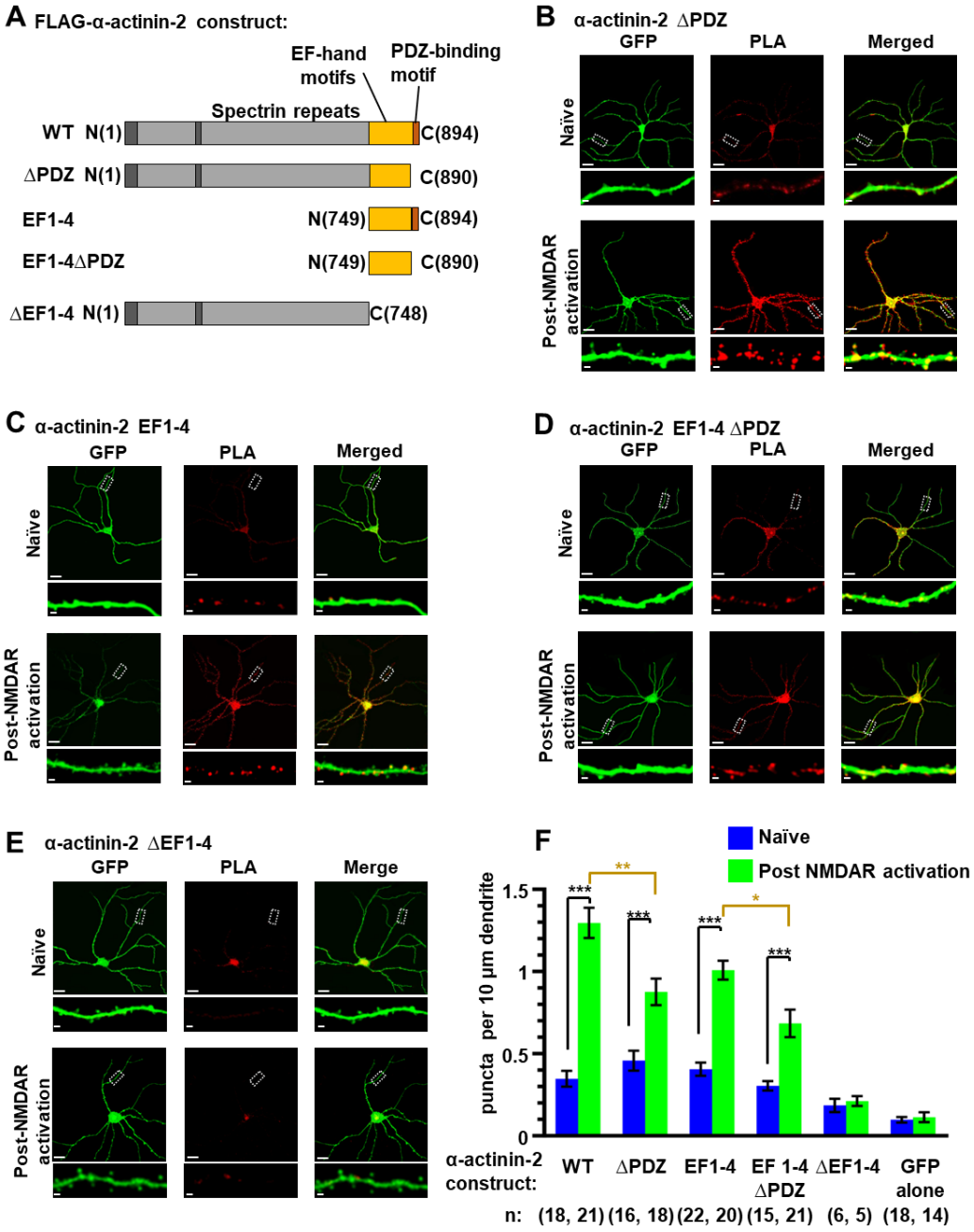

Figure 3.2. PLA imaging of CaMKIIα association with fragments of α-actinin-2 in primary hippocampal neurons. (A) Topologies of FLAG-α-actinin-2 constructs used for expression in primary hippocampal neurons. Panels **B-E** shows anti-GFP immunofluorescence (left column), anti-CaMKIIα/anti-FLAG PLA puncta (middle column) and GFP/PLA channels merged, either before (upper row) or after (lower row) NMDAR activation. The images correspond to transfections with α-actinin-2: **(B)** ΔPDZ; **(C)** EF1-4; **(D)** EF1-4 ΔPDZ; **(E)** ΔEF1-4. Scale bars correspond to 20 µm (whole neuron images) and 1 µm (dendrite close-up). **(F)** Quantitation of PLA puncta per 10 µm dendrite before (blue) or after (green) NMDAR activations for the full set of FLAG-α-actinin-2 constructs. Data are presented as the mean ± standard error (SE), and were collected from three independent E18 preparations with the exception of ΔEF1-4 (one animal). The number of neurons analysed for each construct is shown in parentheses.

The last four amino acids of α-actinin-2 (ESDL) can bind to the PDZ domain of densin-180 *in vitro* (Walikonis et al., 2001), and cooperative interactions between the three proteins have been suggested to support the structure of dendritic spines (Robison et al., 2005a; Walikonis et al., 2001). Expression of FLAG-α-actinin-2 lacking the last four amino acids ('ΔPDZ') yielded 0.46 ± 0.06 PLA puncta per 10 μm in naïve neurons, increasing to 0.88 ± 0.08/10 μm (p=2.9×10^{-4}) following NMDAR activation (**Figure 3.2F** & **Figure 3.2B**). Comparable results were also observed with an EF hand construct lacking the PDZ motif ('EF1-4ΔPDZ') with 0.30 ± 0.03 puncta per 10 μm dendrite rising to 0.72 ± 0.07/10 μm dendrite (p=1.1×10^{-5}) following NMDAR activation (**Figure 3.2F** & **Figure 3.2D**). These mild attenuations in puncta formation from the deleted PDZ motif, was most pronounced in the context of the full-length protein following NMDAR activation (1.48-fold reduction in puncta density, p=0.0017), suggesting an additional minor role in the PDZ motif contributing to CaMKII binding. Together, the data indicates that the actinin EF hands are sufficient for robust α-actinin-2 – CaMKII interactions, and this region underlies the marked elevation in interaction of the two proteins in enlarged spines.

3.2. densin-180 supports α-actinin-2 & CaMKII interactions *in vitro*

The previous section revealed the essential function of α-actinin-2 EF hand motifs in binding to CaMKII in synapses, while the PDZ ligand may provide additional CaMKII association. To investigate the notion that densin-180 can facilitate *in vitro* CaMKII-α-actinin-2 association, I performed pull-down assays and isothermal titration calorimetry (ITC) **(Figure 3.3)**. I developed and purified a fragment of densin-180 spanning from 1266-C (hereafter referred to as densin-180c) which contains both the CaMKII binding region and the PDZ domain to associate with α-actinin-2 (**Figure 3.3A**). I also purified GST fused to a fragment of α-actinin-2 EF hands 1-4 ('GST-EF1-4) and full-length version CaMKIIα WT.

Pull-down assays were performed using magnetic glutathione beads charged with either GST or GST- EF1-4 as 'bait' and full-length CaMKIIα as 'prey' with or without densin-180c (**Figure 3.3B,** see methods **Section 2.7**). The recovery of CaMKIIα alone was 18.8 ± 1.3 % which increased modestly to 32.7 ± 1.3 % (p= 0.015) in the presence of densin-180c (**Figure 3.3B** & **C**). These results are consistent with previous results showing the

facilitation of α-actinin-2 and CaMKII interaction through densin-180 (Robison et al., 2005a).

Next, I performed ITC (see methods, **Section 2.4**) experiments to quantify the affinity of densin-180-α-actinin-2 PDZ interactions and densin-180-CaMKII interactions as this has not been established to date (**Table 3.1**). Titrations of α-actinin-2 EF1-4 containing the four amino acid PDZ ligand, bound to densin-180c in an exothermic manner with a moderately high affinity (K_d= 2.35 ± 0.09 μM) (**Figure 3.3D**). To test the affinity of the CaMKII association domain and densin-180c, I purified a fragment of CaMKII (336-C) containing only the association domain of CaMKII. I titrated 300 μM of densin-180c against 30 μM CaMKIIα association domain. Surprisingly, no binding was detected in ITC experiments performed at 10 ^{o}C (endothermic binding) or at 25 ^{o}C (exothermic binding) (**Figure 3.3 E** & **F**). Together these *in vitro* experiments suggest that densin-180 can support CaMKII-α-actin-2 association to a limited extent, which is consistent with the mild attenuation in PLA puncta observed with α-actinin-2 'ΔPDZ' constructs (**Section 3.1**).

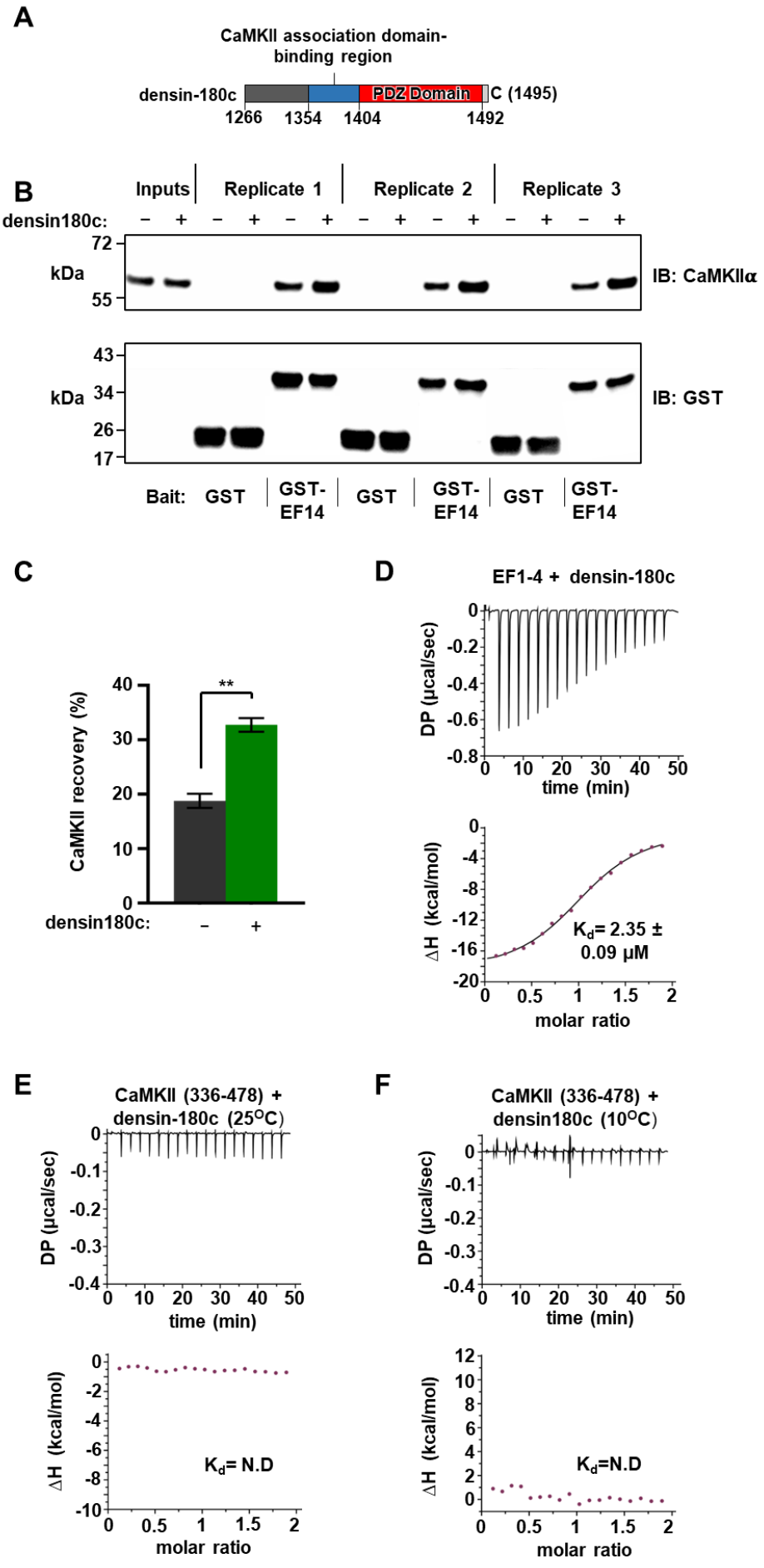
A
CaMKII association domain-binding region
densin-180c
PDZ Domain
C (1495)
1266
1354
1404
1492
B
Inputs
Replicate 1
Replicate 2
Replicate 3
densin180c:
kDa
72
55
IB: CaMKIIα
43
34
26
17
IB: GST
Bait: GST
GST-EF14
C
CaMKII recovery (%)
densin180c:
**
D
EF1-4 + densin-180c
DP (µcal/sec)
time (min)
ΔH (kcal/mol)
Kd= 2.35 ± 0.09 µM
molar ratio
E
CaMKII (336-478) + densin-180c (25°C)
Kd= N.D
F
CaMKII (336-478) + densin180c (10°C)

Figure 3.3. The effect of densin-180c on CaMKII & α-actinin-2 interaction. **(A)** Topology of densin-180c fragment**. (B)** Pull-down of purified CaMKIIα to GST or GST-EF1-4. CaMKII pull-down was compared +/− densin-180c fragment as indicated. CaMKIIα and GST/GST-EF1-4 were detected by anti-CaMKIIα (upper) and anti-GST (lower) immunoblots (IBs). **(C)** Densitometry for pull-down experiments shown in the preceding panel showing CaMKII recovery either with (green) or without (black) densin-180c (n=3 for all conditions). **(D-F)** ITC of interactions with α-actinin-2, CaMKII and densin-180 constructs**.** Representative isotherms showing binding of **(D)** α-actinin-2 EF1-4 with densin-180c; **(B)** and **(C)** CaMKII association domain with densin-180c at 25 ^{o}C **(B)** and **(C)** 10 ^{o}C. In all cases, the top sub-panels show the raw power output (µcal/s) per unit time; the bottom sub-panels show the integrated data including a line of best fit to a single site binding model. Stated K_d values are averages from experimental replicates. ND = not determined.

Cell	Syringe	reps	n	K_d (µM)	ΔH (kcal/mol)	-TΔS (kcal/mol)
densin-180c (1266-C)	EF1-4	3	1.00 ± 0.06	2.35 ± 0.09	-16.97 ± 1.52	9.16 ± 1.45
CaMKIIα association domain (336-C)	densin-180c (1266-C)	5	ND	ND	ND	ND

Table 3.1. Thermodynamic parameters for ITC measurements with densin-180c. Data is given as mean ± SE, Rep = replicates, ND = not determined, n is stoichiometry of binding, K_d is the dissociation constant.

3.3. α-actinin-2 and CaMKII associate within two minutes of LTP induction

The timescale of CaMKII activation during LTP is believed to be in the order of seconds to up to a minute (Yasuda et al., 2022). On the other hand, actin polymerisation to build enlarged synapses is thought to occur after one minute and persist for hours following NMDAR activation (Yasuda et al., 2022). To investigate how quickly CaMKII and α-actinin-2 associate following NMDAR activation, I decided to measure PLA puncta in neurons that were fixed 10, 30, 120, 600 & 3600 seconds following cLTP induction (**Figure 3.4**). I found that the PLA puncta levels saturated at ~2 min post NMDAR activation. Fitting the timepoint data to a Hill function reveals that CaMKII-α-actinin-2 interactions reach 50 % maximal levels after 22 ± 1 seconds. This rate of accumulation is consistent with a recently-proposed hypothetical time-scale of CaMKII signalling in dendritic spines following the induction of LTP (Yasuda et al., 2022). Careful observation of the representative images in **figure 3.4** also reveals a gradual increase in PLA puncta

of the soma with slower kinetics relative to the dendrites. This may reflect increased CaMKII activity within the soma following neuronal stimulation (Zalcman et al., 2018).

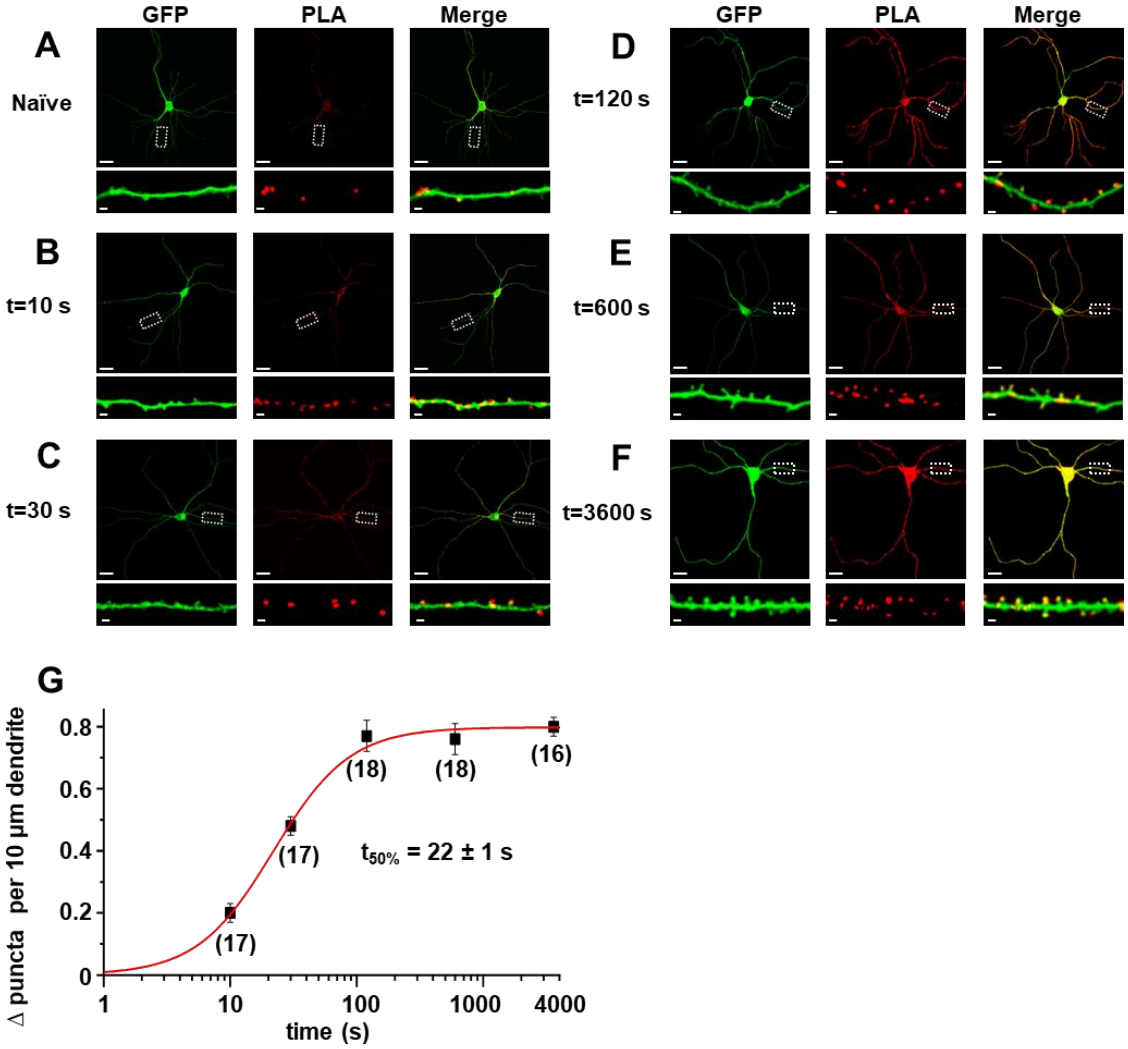

Figure 3.4. Time course of CaMKIIα/α-actinin-2 puncta following NMDAR activation assessed by PLA. Each panel shows anti-GFP immunofluorescence (left column), anti-CaMKIIα/anti-FLAG PLA puncta (middle column) and GFP/PLA channels merged (right column). The image rows correspond to timepoints post NMDAR activation for: **(A)** 0 seconds (control); **(B)** 10 seconds; **(C)** 30 seconds; **(D)** 120 seconds; **(E)** 600 seconds; **(F)** 3600 seconds. Scale bars correspond to 20 µm (whole neuron images) and 1 µm (dendrite close-up). **(G)** Time dependence of CaMKII-α-actinin-2 association in primary hippocampal neurons. PLA puncta baselined at the pre-activation level and fitted to a Hill function with max=0.80 ± 0.01, n=1.4 ± 0.1, and $t_{50\%}$=22 ± 1 s. Data are presented as the mean ± SE, and were collected from three independent E18 preparations. The number of neurons analysed for each timepoint is shown underneath each datapoint.

3.4. Disrupting α-actinin-2-CaMKII interactions prevents structural LTP following NMDAR activation.

We noticed during PLA analysis (**Section 3.1**) that neurons expressing α-actinin-2 EF1-4 generated fewer mushroom-type spines following NMDAR activation compared to full-length α-actinin-2 (compare **Figure 3.1A & D** & **Figure 3.2C**). The α-actinin-2 EF1-4 construct (**Figure 3.2A**) lacks the actin-binding domain and therefore can be expected to operate as a disruptor of endogenous actinin-CaMKII interactions thereby breaking the actinin-mediated link between CaMKII and the actin cytoskeleton. Additionally, other than CaMKII, the only other known interaction partner for the EF1-4 region is the muscle-specific titin (Young and Gautel, 2000), so any effect of EF1-4 in neurons is likely to correspond to disruption of CaMKII-α-actinin-2 interactions. To investigate this disruption effect further, I decided to compare the type of dendritic spines generated in neurons expressing α-actinin-2 EF1-4 WT or L854R mutant. The L854R mutation lies within the fourth EF hand and disrupts α-actinin-2 binding to the CaMKII regulatory segment (Jalan-Sakrikar et al., 2012), thus in this case it serves as a negative control.

To confirm that α-actinin-2 EF1-4 L854R does not bind endogenous CaMKII, I performed PLA experiments (**Figure 3.5A** & **B**) similar to the experiments with the other α-actinin-2 fragments **(Section 3.1).** In naïve neurons, 0.12 ± 0.06 puncta per 10 μm dendrite were found in neurons expressing EF1-4 L854R mutant which was 5-fold lower compared to EF1-4 WT neurons (0.58 ± 0.09/10 μm dendrite, $p=1.0\times10^{-5}$). In contrast to neurons expressing EF1-4 WT, neurons expressing the EF1-4 L854R mutant failed to exhibit elevated PLA puncta following NMDAR activation with puncta densities of 1.25 ± 0.15 and 0.21 ± 0.04/10 μm dendrite respectively ($p=6.0\times10^{-6}$) (**Figure 3.5C**). Overall, these measurements show that, as expected, α-actinin-2 EF1-4 L854R does not bind to CaMKII and is a suitable negative control for investigating the disruptor action of WT EF1-4.

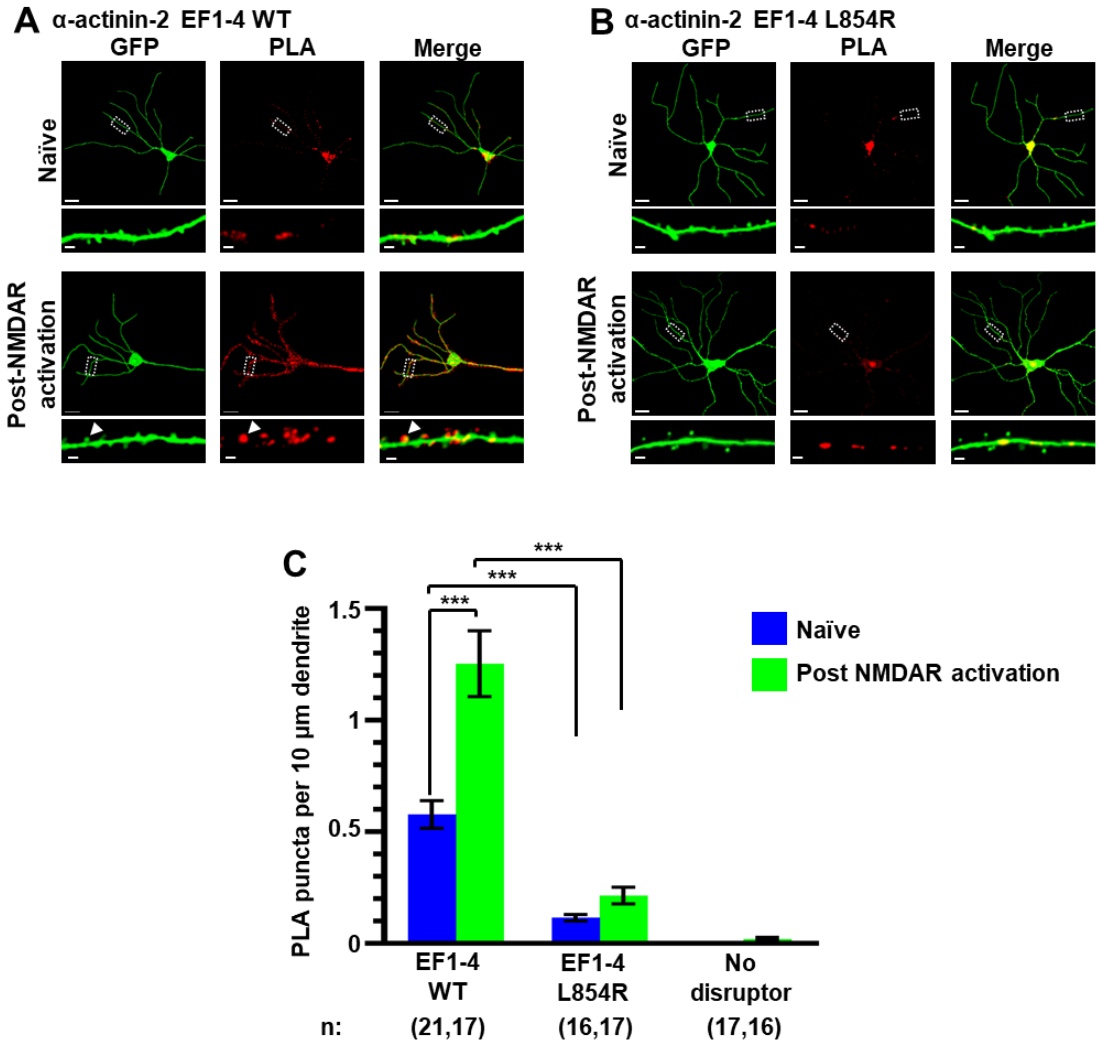

Figure 3.5. PLA of CaMKIIα association with α-actinin-2 EF1-4 disruptors. Anti-GFP immunofluorescence (left columns), anti-CaMKIIα/anti-FLAG PLA puncta (middle columns) and GFP/PLA channels merged, either before (upper row) or after (lower row) NMDAR activation for either WT **(A)** or L854R **(B)** α-actinin-2 EF1-4. Scale bars correspond to 20 µm (whole neuron images) and 1 µm (dendrite close-ups). **(C)** Quantitation of dendritic PLA puncta density before (blue) and after (green) NMDAR activation.

Next, I investigated the effect of α-actinin-2 EF1-4 on dendritic spine morphology. I compared the numbers of stubby (red), thin (yellow) and mature mushroom-type (green) spines in neurons expressing either α-actinin-2 EF1-4 WT (**Figure 3.6A**), α-actinin-2 EF1-4 L854R (**Figure 3.6B**), or GFP alone (**Figure 3.6C**). Prior to NMDAR activation, the total number of spines was approximately one third lower in neurons expressing the WT EF1-4 construct than in the other two conditions (**Figure 3.7A**). For all three conditions, the distribution of spine types was initially similar (**Figure 3.6D**), with stubby spines predominating at ~ 1.5 stubby spines per 10 µm dendrite prior to NMDAR activation. However, whereas NMDAR activation triggered a transition from stubby to mushroom type spines in neurons expressing GFP alone (**Figure 3.6C**) or GFP/EF1-4

L854R (**Figure 3.6B**), no such transformation occurred in neurons expressing the WT EF1-4 disruptor (**Figure 3.6A**).

Four hours after NMDAR activation (**Figure 3.6F**), stubby spines had decreased in abundance from 1.50 ± 0.19 to 0.67 ± 0.10/10 µm in GFP-only neurons (p=0.0013), and from 1.64 ± 0.15 to 0.65 ± 0.10/10 µm in neurons expressing L854R EF1-4 (p=7.2x10^{-6}). Furthermore, mushroom spines accounted for approximately half of all spines four hours after NMDAR activation (**Figure 3.6F**). In contrast, mushroom spines did not accumulate in neurons expressing WT EF1-4 disruptor, such that after 4 hours there were 7.2-fold fewer mushroom spines in these neurons than in GFP control neurons (p=3.43x10^{-11}) and 6.8-fold fewer than in L854R EF1-4 neurons (p=4.81x10^{-6}). The number of stubby spines also remained unchanged in WT EF1-4 neurons (1.24 ± 0.16 before vs 1.22 ± 0.18/10 µm four hours after NDMAR activation). The lack of plasticity in neurons expressing the WT EF1-4 disruptor was also reflected in analysis of changes in the average spine diameter upon NMDAR activation (**Figure 3.7B**). Mean spine diameter increased by 58.3 % (p=7.1x10^{-8}) and 65.5 % (p=1.3x10^{-4}) over four hours in GFP-only and L854R EF1-4 neurons, respectively whereas expression of the WT EF1-4 disruptor limited the increase to only 11 % (p=0.17). These results build on previous reports that siRNA-mediated knockdown of α-actinin-2 reduces mushroom-type spine formation following NMDAR activation (Hodges et al., 2014) by resolving a key role for the interface with CaMKII in this process. In sum, our PLA and spine imaging data indicate that α-actinin-2-CaMKII interactions accumulate upon induction of sLTP via NMDAR activation, and that interaction between the two is necessary to support the formation of enlarged mushroom-type spines. Together, the PLA imaging and spine width analysis indicate that α-actinin-2-CaMKII interactions accumulate upon induction of sLTP following NMDAR activation, and that interaction between the two is necessary to support the formation of enlarged mushroom-type spines.

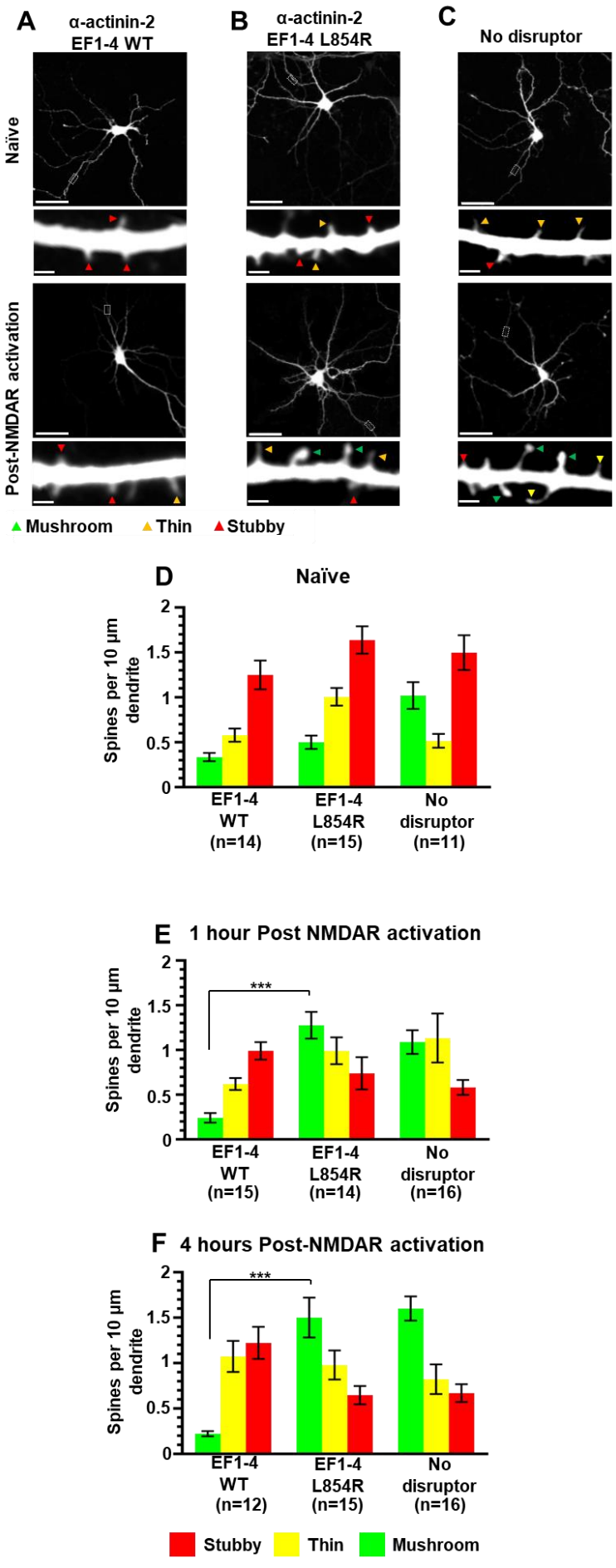

Figure 3.6. Effect of EF hand disruptors on spine morphology. Panels **A-C** show GFP imaging of primary hippocampal neurons transfected with either α-actinin-2 EF1-4 WT with GFP **(A)**, EF1-4 L854R with GFP **(B)** or GFP alone **(C)**. For **A-C**, the upper rows show imaging of naïve synapses, and the lower rows shows imaging 4 hours after NMDAR activation. Stubby (red), thin (yellow), and mushroom (green) type synapses are highlighted with arrows. Scale bars correspond to 20 µm (whole neuron images) and 1 µm (dendrite zoom-ins). Panels **D-F** show quantification of spine types across the three conditions either before NMDAR activation **(D)**, 1 hour after NMDAR activation **(E)**, or 4 hours after activation **(F)**. Red, yellow, and green bars indicate stubby, thin, and mushroom spine numbers respectively. Numbers of neurons analysed for each condition are shown in parentheses. Data were obtained from 3 independent cultures.

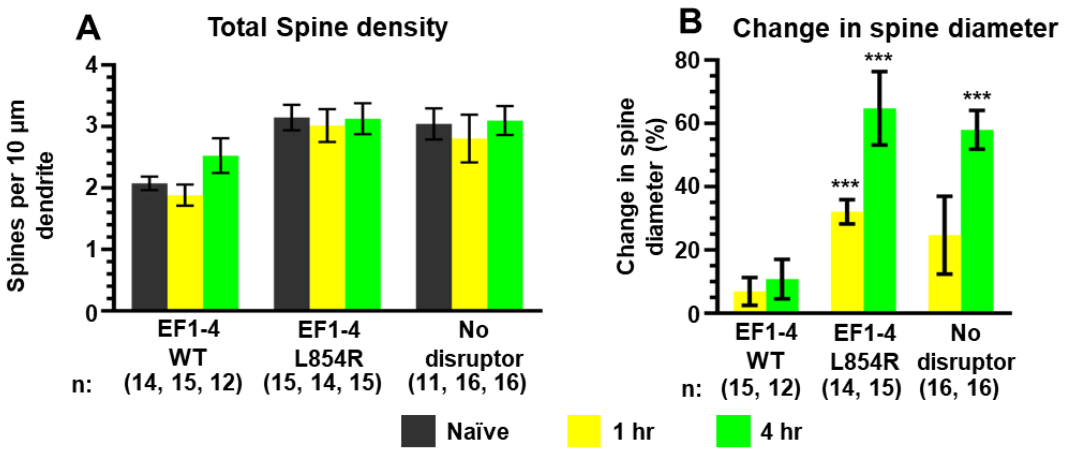

Figure 3.7. Effect of EF hand disruptors on spine density and width. (A) Total spine density primary hippocampal neurons transfected with either α-actinin-2 EF1-4 WT with GFP, EF1-4 L854R with GFP or GFP alone. Mean spine number ± SE per 10 µm dendrite is shown before NMDAR activation (black), and 1 hour (yellow) and 4 hours (green) after activation. **(B)** Changes in spine diameter (mean ± SE) are shown either 1 hour (yellow) or 4 hours (green) hour after NMDAR activation. Numbers of neurons analysed for each condition are shown in parentheses. Data were obtained from 3 independent cultures.

3.5. Concluding remarks

In this Chapter, I have shown using PLA measurements that, contrary to previous assumptions, CaMKII-α-actinin-2 interactions are elevated following NMDAR activation. The EF hand motifs of α-actinin-2 are essential for rapid binding to CaMKII which occurs within 2 min following cLTP induction, while the PDZ ligand which mediates indirect binding to CaMKII via densin-180 appears to facilitate interactions to a limited extend. Finally, I show that disruption of endogenous CaMKII-α-actinin-2 interactions prevents sLTP, underlining the key role for this interaction in the formation of enlarged dendritic spines.

Chapter 4. Molecular basis of elevated CaMKII - α-actinin-2 interactions that underlie structural LTP

In the previous chapter we observed an increased association between α-actinin-2 and CaMKII in dendritic spines following NMDAR activation according to PLA imaging (**Section 3.1**). This increase in association occurred quickly with $t_{50\%}$ = 22 s (**Section 3.3**). We also found that disrupting actinin-CaMKII interactions prevented the accumulation of mushroom-type dendritic spines following chemical LTP (**Section 3.4**). Taken together, these findings indicate that elevated interactions between the two proteins are fundamental to sLTP. In this chapter, I focus on understanding how this interaction might be upregulated following the induction of LTP at the molecular level. A molecular mechanism was not immediately obvious given that Ca^{2+}/CaM – the activator of CaMKII – was known to antagonise interactions between actinin and the CaMKII regulatory segment (Robison et al., 2005b). I first use calorimetry to determine binding affinities for association between different fragments of the two proteins (**Section 4.1**). Cross-referencing to crystal structures, including a structure of α-actinin-2 EF3-4 in complex with the CaMKIIα regulatory segment, suggests that the regulatory segment is not fully accessible to α-actinin-2 in inactive CaMKIIα (**Section 4.2**) Additionally, I investigate the idea that CaMKII docking to GluN2B could provide a mechanism for increasing access to α-actinin-2 by conducting pull-down experiments (**Section 4.3)**, performing additional PLA measurements involving GluN2B subunits (**Section 4.4**) and CaMKII T286A (**Section 4.5**). Finally, I utilise cross-linking coupled to mass spectrometry (XL-MS) to investigate the structure of purified actinin-CaMKII-GluN2B complexes (**Section 4.6**).

4.1. The CaMKII kinase domain decreases the affinity of α-actinin-2 towards the regulatory segment

Previous studies have shown that EF hands 3 and 4 of α-actinin-2 (hereafter referred to as 'EF3-4') are sufficient for binding CaMKIIα via its regulatory segment (Jalan-Sakrikar et al., 2012; Robison et al., 2005a), unlike Ca^{2+}/CaM which utilises all 4 EF hands to wrap around the regulatory segment. Since the regulatory segment is docked against the kinase domain in autoinhibited CaMKII, Ca^{2+}/CaM can bind much more tightly to isolated regulatory segment than to constructs that include the kinase domain (Chao et al., 2010;

Forest et al., 2008; Rellos et al., 2010). This is important since factors that alter the accessibility of the regulatory segment, including T286 autophosphorylation (Singla et al., 2001) and association with NMDARs (Bayer et al., 2001), can trap CaM. The assumption has been that α-actinin-2 is able to fully access the regulatory segment in inactive CaMKII since only EF3-4 are involved in the interaction. However, my PLA data challenges this assumption, with the observation of increased interactions between actinin and CaMKII following NMDAR activation. I therefore employed isothermal titration calorimetry (ITC) (see methods **Section 2.4**) to investigate whether the kinase domain inhibits access of α-actinin-2 to the regulatory segment in inactive CaMKII. I specifically compared the affinity of EF3-4 towards a peptide corresponding to the regulatory segment (positions 294-315), and to a longer construct (1-315) that includes the kinase domain. An N-terminal thioredoxin (Trx) tag was fused at the N-terminus of the longer construct to ensure the protein remained soluble at high concentrations necessary for ITC (Costa et al., 2014). This N-terminal tag is not expected to affect interactions with the regulatory segment (Rellos et al., 2010).

EF3-4 bound to the regulatory segment peptide (294-315) in an exothermic manner with a dissociation constant (K_d) = 32 ± 1 μM (**Figure 4.1A**). In contrast, the longer construct (1-315) failed to generate detectable heat changes upon mixing – indicative of a weak interaction – so it was not possible to determine a K_d for binding for this construct (**Figure 4.1B**). Control experiments using CaM confirmed that, as expected, CaM binds more tightly to isolated regulatory segment with a K_d = 11 ± 1 nM (**Figure 4.1C**) compared to Trx-CaMKIIα 1-315 (K_d = 2.8 ± 0.2 μM, **Figure 4.1D**), consistent with previous studies (Rellos et al., 2010).

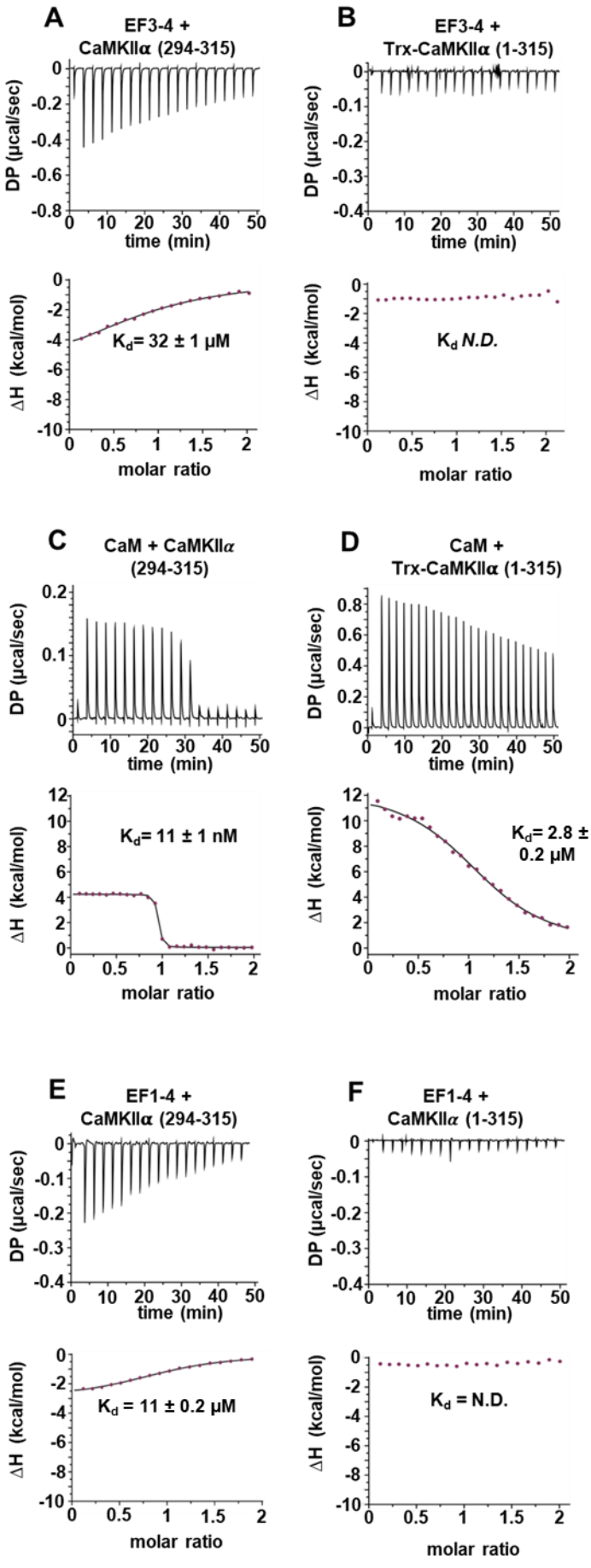

Figure 4.1. ITC measurements for EF hand association with the CaMKIIα regulatory segment. Representative isotherms showing binding of α-actinin-2 EF3-4 to **(A)** peptide corresponding to CaMKIIα regulatory segment (294-315) and **(B)** a construct (1-315) corresponding to the kinase and regulatory segment regions of CaMKIIα. Binding of CaM and α-actinin-2 EF1-4 to the same two CaMKII regions is shown in panel **C & D** and **E & F**, respectively. In all cases, the top sub-panels show the raw power output (µcal/s) per unit time; the bottom sub-panels show the integrated data including a line of best fit to a single site binding model. Stated K_d values are averages from experimental replicates. ND = not determined.

Next, I examined the contribution of EF hands 1-2 towards the binding to the CaMKII regulatory segment, using the purified fragment α-actinin-2 EF hand motif 1-4 (herein referred to as EF1-4). Like the shorter fragment EF3-4, I could not detect any binding with EF1-4 Trx-CaMKIIα (1-315) (**Figure 4.1F**). However, EF1-4 bound to the isolated regulatory segment (294-315) with K_d=11 ± 0.2 μM (**Figure 4.1E**) – an approximate 3-fold lower concentration than EF3-4 alone. This is similar to K_d = ~4 μM recorded for association of EF1-4 with peptide corresponding to titin Z repeat 7 (Young and Gautel, 2000). Overall, the ITC measurements show that – like CaM – α-actinin-2 is unable to fully access the CaMKII regulatory segment in the presence of the autoinhibited kinase. Furthermore, the data reveal that while EF hands 3-4 are sufficient for binding, the highest affinity binding is achieved when EF hands 1-2 are also present. Full thermodynamic parameters obtained for all ITC measurements are shown in **table 4.1**.

Cell	**Syringe**	**Rep**	**n**	**K_d (μM)**	**ΔH (kcal/mol)**	**-TΔS (kcal/mol)**
EF3-4	CaMKIIα 294-315	3	0.98 ± 0.04	32.13 ± 0.86	-6.7 ± 0.06	0.61 ± 0.06
CaMKIIα 1-315	EF3-4	3	ND	ND	ND	ND
EF1-4	CaMKIIα 294-315	3	0.98 ± 0.01	11.37 ± 0.15	-3 ± 0.005	-3.7 ± 0.01
CaMKIIα 1-315	EF1-4	3	0.99 ± 0.03	ND	ND	ND
CaM	CaMKIIα 294-315	3	0.99 ± 0.03	0.011 ± 0.0007	4.3 ± 0.2	-14.6 ± 0.2
CaMKIIα 1-315	CaM	2	1.06 ± 0.02	2.8 ± 0.2	11.3 ± 0.1	-18.5 ± 0.07
EF3-4	CaMKIIα 299-315	3	0.66 ± 0.02	17.76 ± 1.49	-11.24 ± 0.54	4.74 ± 0.59
CaM	CaMKIIα 299-315	3	1 ± 0.01	0.047 ± 0.001	4.51 ± 0.04	-14.04 ± 0.05

Table 4.1. Thermodynamic parameters for interactions between CaMKII constructs and either α-actinin-2 or CaM. Data is given as mean ± SE, Rep = replicates, n is stoichiometry of binding, K_d is the dissociation constant, ΔH is enthalpy, and -TΔS is entropy.

4.2. Structure of the α-actinin-2-CaMKII core interface

Previous structural models of α-actinin-2-CaMKII interaction have assumed that the third and fourth EF hands of α-actinin-2 bind to the CaMKII regulatory segment in a similar mode to the third and fourth EF hands of Ca^{2+} /CaM in such a way that α-actinin-2 could fully access the regulatory segment in the inhibited kinase (Jalan-Sakrikar et al., 2012). However, during my PhD, Dr. Jian Zhu (Gold lab) solved the crystal structure of α-actinin-2 EF3-4 in complex with a peptide corresponding to the CaMKIIα regulatory segment (positions 294-315) to a 1.28 Å resolution (**Figure 4.2A**). This has allowed me to cross-reference my ITC measurements against the structure.

The asymmetric unit of the crystal structure contains two highly similar copies of the complex (RMSD 0.202 Å for all atoms). The analysis focuses on the first copy of the complex (chains A & B in PDB: 6TS3) for which it was possible to position the full EF3-4 region (824-894) and positions 294-313 of the CaMKIIα regulatory segment in electron density. In the complex, the CaMKII regulatory segment forms an amphipathic helix with four hydrophobic residues (L299, I303, M307, F313) engaged in van der Waals interactions with α-actinin-2 EF3-4 (orange, **Figure 4.2A**). $M307_{CaMKII}$ is buried closest to the centre of the EF3-4 domain, where it contacts the sidechains of EF3-4 residues F835 and L854. This binding mode is consistent with the observation of reduced PLA puncta targeting FLAG- α-actinin-2 EF3-4 L854R mutant & endogenous CaMKII in primary neurons. Residues S834 and Y861 of α-actinin-2 directly contact the CaMKII regulatory segment and mutations in these residues have been shown to inhibit binding to CaMKII (Jalan-Sakrikar et al., 2012)

The last four amino acids of α-actinin-2 (ESDL) can bind to the PDZ domain of densin-180 *in vitro*, and cooperative interactions between the three proteins have been suggested to from stable ternary complexes to support the structure of dendritic spines (Robison et al., 2005a; Walikonis et al., 2001). In the structure, the PDZ ligand is re-orientated away from the CaMKII interface by $G890_{EF3-4}$ such that is accessible to bind to PDZ domains (**Figure 4.2B**).

The phosphorylation of CaMKII inhibitory residues T305 and T306 prevent Ca^{2+}/CaM binding acting as a negative feedback mechanism to prevent maximally stimulated Ca^{2+}/CaM bound activity of CaMKII. Mutational analyses has previously shown that phosphorylation at T306 but not T305 reduces binding to α-actinin-2 (Jalan-Sakrikar et al., 2012). This is in agreement with the crystal structure (**Figure 4.2C**) in which T305 projects away from the binding interface, whereas the hydroxyl group of T306 engages in a H-bond network that includes $Gln858_{EF3\text{-}4}$, and its Cγ atom is packed against $P885_{EF3\text{-}4}$.

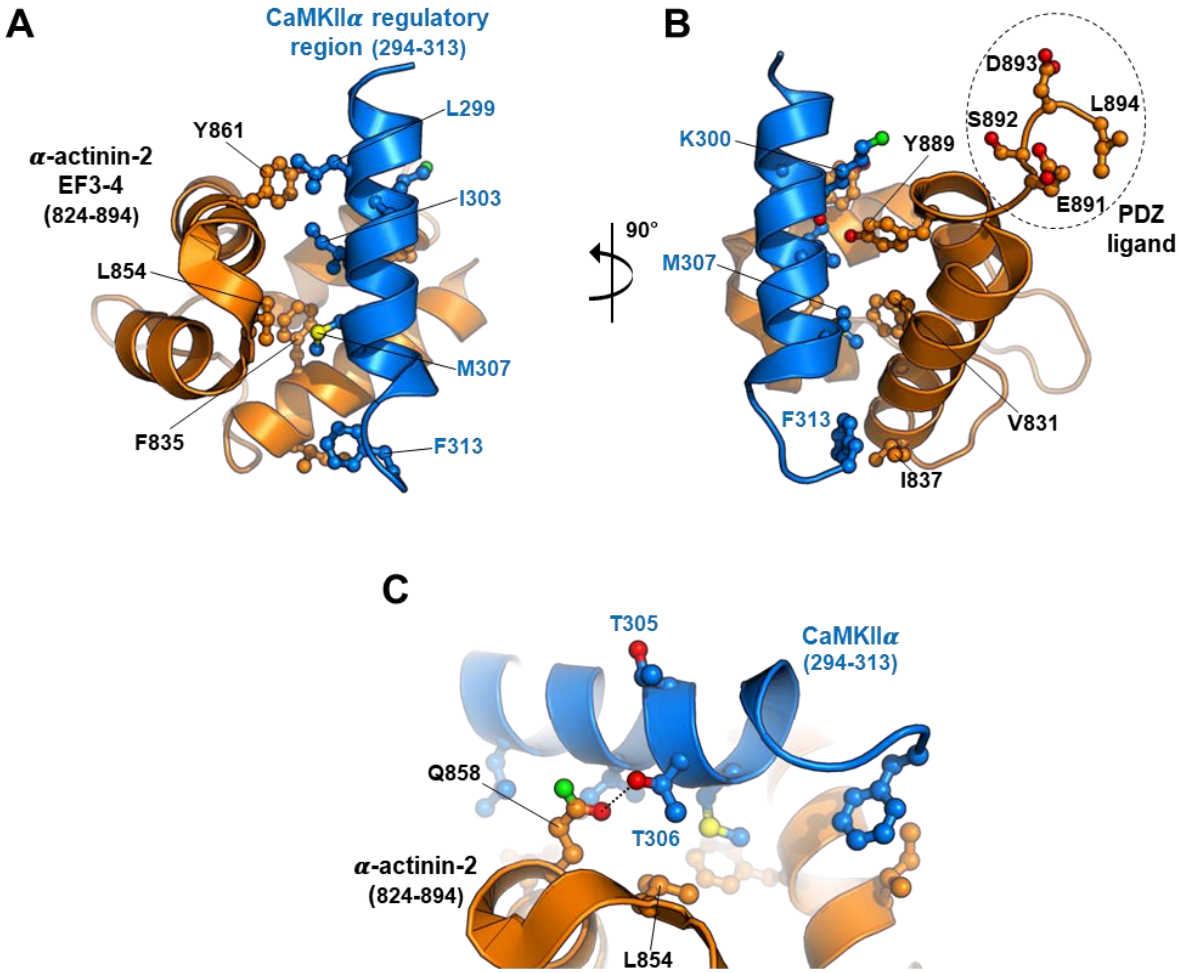

Figure 4.2. Structure of the core α-actinin-2 - CaMKIIα interface. **(A)** and **(B)** show two views of the complex between α-actinin-2 EF3-4 (orange) and a peptide corresponding to the CaMKIIα regulatory segment (blue). The C-terminal tetrapeptide that is a ligand for PDZ domain-containing proteins including densin-180 is highlighted. **(C)** Close-up highlighting the positions of CaMKIIα threonine 305 and 306 in the complex showing their orientations relative to the binding interface. PDB: 6TS3

Previous modelling of the CaMKII-actinin interaction has been built on the assumption that α-actinin-2 EF3-4 binds to CaMKII using the same binding mode as the CaM C-lobe (Jalan-Sakrikar et al., 2012). However, comparison to the crystal structure of CaMKIIδ (11-315) in complex with Ca^{2+}/CaM (Rellos et al., 2010) shows that the binding modes are distinct. Ca^{2+}/CaM fully encompasses the regulatory segment (whose sequence is identical between the α and δ isoforms) with the C-lobe (light purple, **Figure 4.3A**) mediating most interactions to the hydrophobic face of the helix. The N-lobe (deep purple) is responsible for the bulk of H-bonding to the helical side that is solvent exposed in complex with α-actinin-2 EF3-4 (**Figure 4.3B**). The centre of mass of EF3-4 is rotated by ~ 50 ° relative to the CaM C-lobe when viewed along the central axis of the regulatory segment (lower panels, **Figure 4.3A** & **B**). In addition, the CaM C-lobe engages the regulatory segment approximately one helical turn further to its N-terminus than α-actinin-2 EF3-4, including interactions with positions A295 and K298. The conformation of the regulatory segment itself also differs between the two complexes. In complex with α-actinin-2 EF3-4, the helical structure breaks down at the C-terminal end to re-orient F313 for interaction with $I837_{EF3-4}$ (blue, **Figure 4.3C**). In complex with Ca^{2+}/CaM, alpha-helicity is maintained for the full length of the regulatory segment, which directs F313 in the opposite direction for interaction with the CaM N-lobe (grey, **Figure 4.3C**).

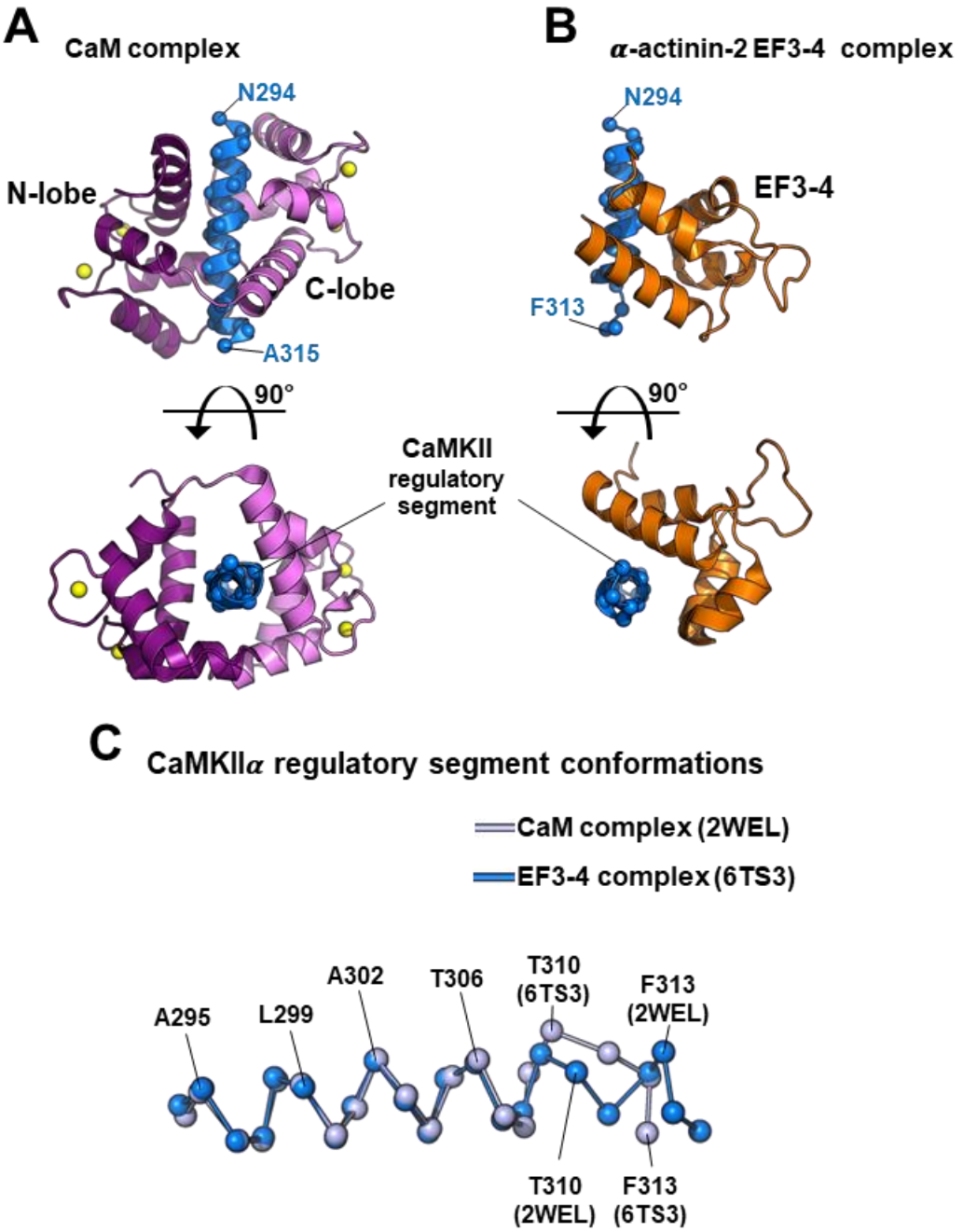

Figure 4.3. Comparison of the Ca^{2+}/CaM and α-actinin-2 binding modes on the CaMKIIα regulatory segment. For each complex two views are shown for CaM **(A)** and α-actinin-2 EF3-4 **(B)** association with the CaMKIIα regulatory segment. The structures were aligned through the regulatory segment (blue in both panels). For the CaM complex (2WEL), the N-lobe is coloured dark purple; the C-lobe is light purple. For α-actinin-2 EF3-4 complex, EF hands 3-4 is coloured in orange. **(C)** Conformation of CaMKIIα regulatory helix in complex with CaM (grey) and α-actinin-2 EF3-4 (blue).

Since CaMKIIα positions 294-298 are solvent exposed in the complex with α-actinin-2 EF3-4 but not CaM, I performed further ITC measurements with a truncated regulatory segment peptide (299-315) to corroborate the binding mode observed in the crystal structure. α-actinin-2 EF3-4 bound CaMKIIα 299-315 peptide with K_d = 17.8 ± 1.5 μM (**Figure 4.4A**) – comparable to its affinity for CaMKIIα 294-315 (K_d = 32 ± 1). Consistent with the crystal structures, CaM associated with CaMKIIα (299-315) with K_d = 47 ± 1 nM (**Figure 4.4B**) approximately 5-fold higher than for the longer peptide (K_d =11 ± 1 nM). This also tallies with previous reports that positions 293-295 in the regulatory segment mediate interactions with CaM that markedly reduce the off-rate (Putkey and Waxham, 1996; Waxham et al., 1998). Overall, our structural data show how α-actinin-2 employs a unique binding mode to interact with the CaMKII regulatory segment.

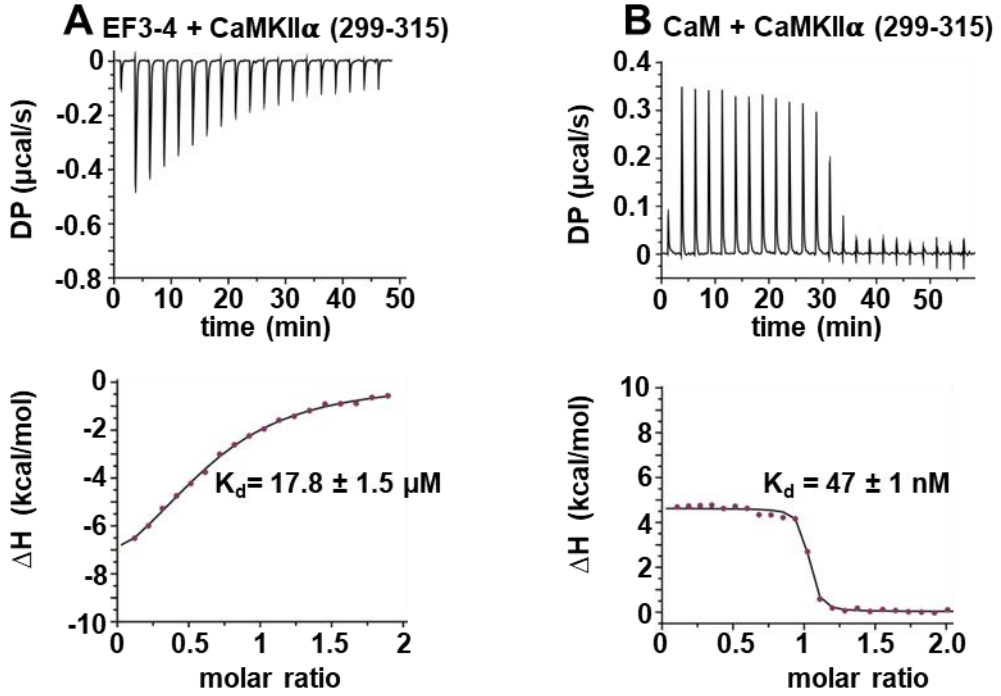

Figure 4.4. ITC measurements with CaMKIIα 299-315 peptide. Representative isotherms showing binding of CaMKIIα (299-315) to **(A)** α-actinin-2 EF3-4 and **(B)** Ca^{2+}/CaM. The top sub-panels show the raw power output (μcal/s) per unit time; the bottom sub-panels show the integrated data including a line of best fit to a single site binding model. Stated K_d values are averages from experimental replicates.

The reduced affinity for α-actinin-2 EF hands 3-4/1-4 to the regulatory segment in the presence of the kinase domain, suggests that the kinase inhibits α-actinin-2 access to the regulatory segment. To understand the structural details underlying this phenomenon, the structure of α-actinin-2 EF3-4-CaMKIIα (294-315) complex was superimposed on a previously solved structure of CaMKIIα (13-302) bound to the inhibitor indirubin, where L299 is the last visible residue in CaMKII (Rellos et al., 2010). The RMSD was 0.2 Å for backbone carbon and oxygen atoms in the common aligned residues 294-299 (**Figure 4.5A**). The superimposition shows that without the release of the regulatory segment from the kinase, both termini of the EF3-4 region will sterically clash with the kinase domain (**Figure 4.5B** & **C**). This steric clash is most prominent in the vicinity the kinase domain aG helix (**Figure 4.5C**), located in the equivalent position to the last 5 amino acids of α-actinin-2. The α-actinin-2 EF3-4-CaMKIIα (294-315) complex was also superimposed onto the crystal structure of a chimeric form of full-length CaMKII, which incorporates WT sequence for CaMKIIα up to position T305 (Chao et al., 2011). The two structures were aligned on the basis of the common positions 294-305. In this case, steric clashing was more pronounced since the regulatory segment kinks towards the kinase domain in this case (**Figure 4.5D** & **E**).

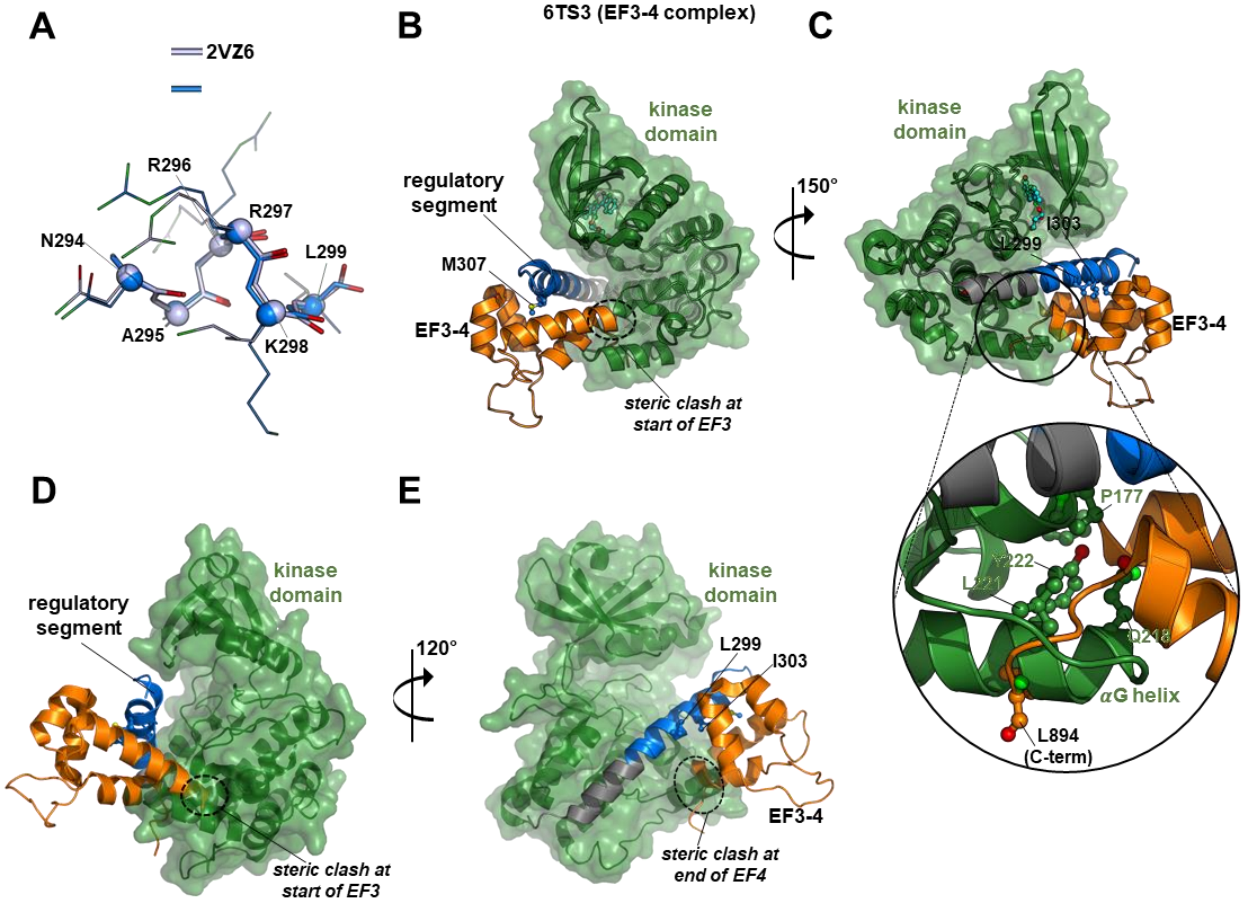

Figure 4.5. Superimposition of the α-actinin-2/CaMKII complex with earlier crystal structures of CaMKII. (A) Alignment of all atoms for CaMKIIα positions 294-299 in crystal structures 2VZ6 and 6TS3. Cα atoms are shown as spheres. Panels **(B)** and **(C)** show two views of the superimposition of the α-actinin-2 – regulatory segment complex (6TS3) onto the structure of CaMKIIα 1-299 (2VZ6). The structures were aligned using positions 294-299 of the regulatory segment. Regions of steric incompatibility between the kinase (green) and EF3-4 domain (orange) are highlighted. Panel C shows a close-up highlighting clashing in the vicinity of the CaMKII αG helix. Panels **(D)** and **(E)** show two views of the superimposition of the α-actinin-2 – regulatory segment complex (6TS3) onto the structure of CaMKIIα (3SOA – *β*7 linker and hub domain are not shown). The structures were aligned through positions 294-305 of the regulatory segment.

4.3. Docking of CaMKII to the GluN2B C-terminal tail facilitates CaMKII-α-actinin-2 association *in vitro*

We found that α-actinin-2 association with CaMKII markedly increased in dendritic spines four hours after NMDAR activation in cLTP (**chapter 3**). Since our structural and calorimetry data show that the kinase domain occludes α-actinin-2 access to the regulatory segment in autoinhibited CaMKII, the mechanism underlying this increase in association is likely to involve regulatory segment release. Existing knowledge of CaMKII regulation during LTP suggests two possibilities: autophosphorylation at T286, and formation of NMDAR-CaMKII complexes (Yasuda et al., 2022). During the initial phase of LTP induction, CaMKII autophosphorylates at T286 to generate an autonomously active form with partial activity (Barcomb et al., 2014). The pT286 modification is likely to partially disengage the regulatory segment from the kinase domain, however this modification does not endure for more than ~ 10 s following the induction of LTP (Chang et al., 2017; Yasuda et al., 2022). A more logical possibility to explain increased actinin-CaMKII association hours after LTP induction is the formation of NMDAR-CaMKII complexes that endure hours following CaMKII activation (Bayer et al., 2001; Yasuda et al., 2022). CaMKII binds tightly to a site centred on S1303 in the GluN2B C-terminal tail (Strack et al., 2000a), and recent crystallographic work shows how this sequence wraps around the kinase domain using a binding mode that necessitates full displacement of the regulatory segment from the kinase domain (Özden et al., 2022). To investigate the possibility that GluN2B supports CaMKIIα binding to α-actinin-2, I compared pull-down (methods **Section 2.7**) of full-length CaMKIIα with magnetic glutathione beads charged with either GST or GST-EF1-4 and determined the effect of including a purified fragment of the GluN2B tail spanning positions 1260-C– hereafter referred to as 'GluN2Bc'.

In all cases, an initial pre-incubation step was included to enable CaMKII-GluN2B association (0.1 μM CaMKIIα, 3 μM CaM, 1.5 μM GluN2Bc incubated for 1 hour in buffer including 2 mM $CaCl_2$ and 0.5 mM ADP). Samples were then supplemented with 2% BSA and incubated with the magnetic beads for 20 minutes to reduce basal pull-down in the absence of GluN2Bc. Following incubation with magnetic beads, EGTA was then added to samples at three different final concentrations: 10, 2.5, or 1.8 mM corresponding to final approximate free Ca^{2+} concentrations of 10 nM, 200 nM, and 200 Mm and incubated for a further 20 mins (**Figure 4.6A**).

In the absence of GluN2B CaMKII recovery from GST EF1-4 was reduced from 2.5 ± 0.8 % to 0 ± 0.1 % (p=0.027, **figure 4.6B**) moving from low to high final Ca^{2+} (lanes 5 & 13, **Figure 4.6A**), consistent with previous reports that Ca^{2+}/CaM alone outcompetes α-actinin-2 for binding to CaMKII (Robison et al., 2005b). Some association without GluN2Bc is seen at low Ca^{2+} levels, consistent with previous PLA imaging (**Figure 3.1**) and with the original identification of the actinin-CaMKII interaction by the yeast two-hybrid method (Walikonis et al., 2001) and it should be noted that this baseline interaction is more pronounced under less stringent binding conditions (Jalan-Sakrikar et al., 2012). Surprisingly, in the presence of GluN2Bc, CaMKII recovery markedly increased irrespective of EGTA concentrations: at ~10 nM free Ca^{2+}, GluN2Bc increased recovery from 2.5 ± 0.8 % to 33 ± 0.5 % (lanes 5 & 6, **Figure 4.6A**, $p=5.0\times10^{-6}$). At 200 nM Ca^{2+}, recovery increased from 1.7 ± 0.3% to 31 ± 11 % (lanes 9 & 10, **Figure 4.6A**, p=0.055). The effect was even maintained at 200 μM free Ca^{2+}, with GluN2Bc increasing recovery from 0 ± 0.1 % to 40 ± 13 % (lanes 13 & 14, **Figure 4.6A**, p=0.032). The effects of GluN2Bc on CaMKII recovery are summarised in **figure 4.6B**. Overall, these experiments indicate that association of CaMKII with GluN2B subunits following LTP is a plausible mechanism to enable increased interaction between the kinase and α-actinin-2 in sLTP even in the presence of excess Ca^{2+}/CaM.

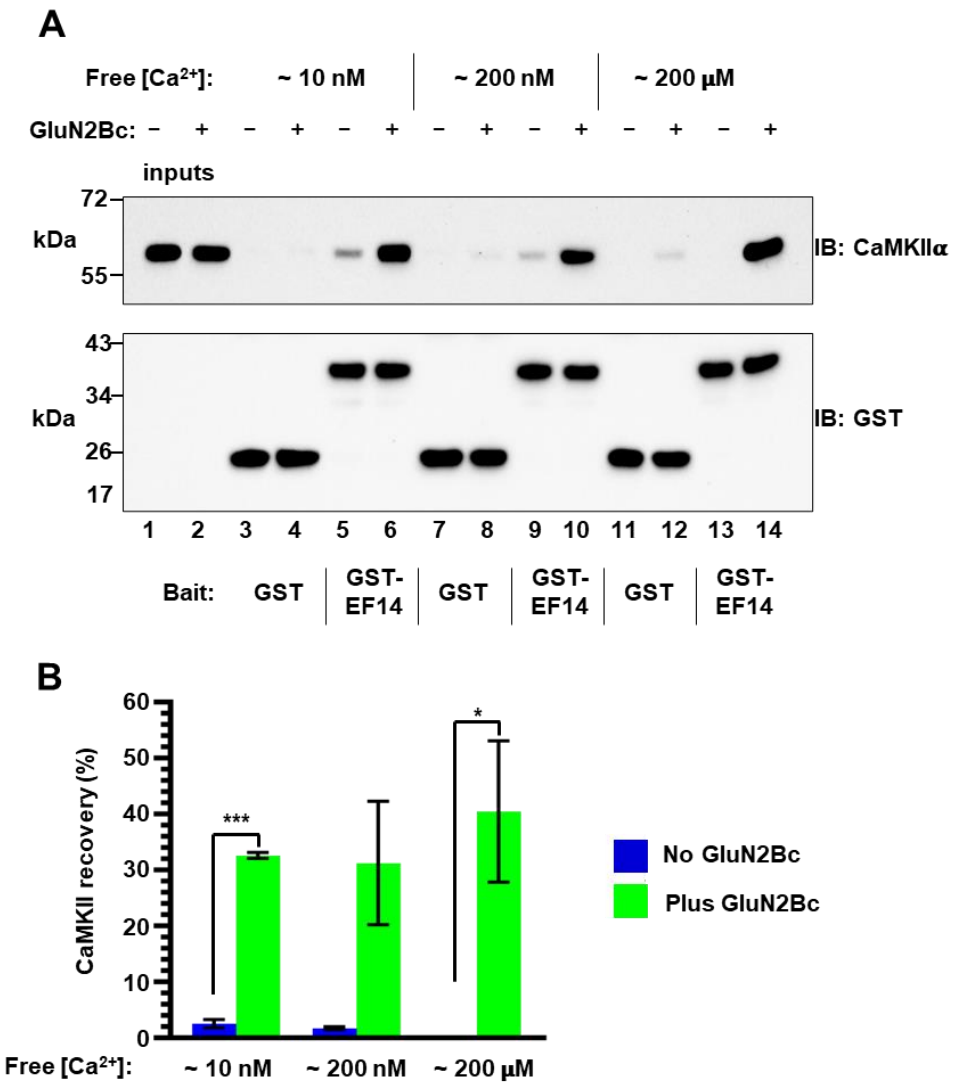

Figure 4.6. The effect of GluN2B on EF hand access to the CaMKII regulatory segment. (A) Pull-down of purified CaMKIIα with magnetic beads charged with either GST or GST-EF1-4. CaMKII pull-down was compared +/− GluN2Bc fragment, and at three different final free Ca^{2+} concentrations, as indicated. CaMKIIα and GST/GST-EF1-4 were detected by anti-CaMKIIα (upper) and anti-GST (lower) immunoblots (IB). **(B)** Densitometry for pull-down experiments shown in the preceding panel showing CaMKII recovery at each free Ca^{2+} concentration either with (green) or without (black) GluN2Bc (n=3 for all conditions).

4.4. GluN2B associates with both CaMKII and α-actinin-2 following NMDAR activation in dendritic spines

The *in vitro* finding that GluN2Bc promotes CaMKII-α-actinin-2 interactions prompted me to explore whether the phenomenon holds true in dendritic spines. Therefore, I turned to PLA assays to measure the association of GluN2B with α-actinin-2 and CaMKII in primary hippocampal neurons. A GluN2B subunit was constructed with an internal HA tag ('WT GluN2B-iHA') inserted between positions G1211 & G1212 that lies close to

CaMKII binding region (1290-1309) (**Figure 4.7A**). The tag includes four glycine residues at both the N & C- termini, in this way the final construct includes 5 Gly at either end of the epitope tag. Additionally, I generated a GluN2B variant ('GluN2B-iHAΔCaMKII') which possesses L1298A/R1300Q mutations, rendering the subunit incapable of binding to CaMKII (Halt et al., 2012).

Primary hippocampal neurons were first transfected with WT GluN2B-iHA, GluN2B-iHA ΔCaMKII or an empty GFP vector on DIV10, and fixed on DIV14, where a subset of neurons was subject to chemical LTP before fixation. Neurons were then subsequently labelled with appropriate anti-GFP antibody and PLA probes for imaging anti-GFP immunofluorescence and GluN2B-CaMKIIα PLA puncta respectively (**Figure 4.7B-D**). It should be noted that the GluN2B variants used in these experiments are fused to GFP at their N-termini, hence the observation of non-uniform GFP expression with GluN2B vectors compared to GFP control.

For WT GluN2B-iHA, PLA puncta were observed in stimulated neurons at a density of 1.23 ± 0.04 puncta per 10 μm dendrite (**Figure 4.7E**) which was ~2-fold higher than in unstimulated neurons (0.66 ± 0.04, $p = 1.03 \times 10^{-11}$) (**Figure 4.7B**). Unstimulated neurons expressing GluN2B-iHAΔCaMKII had ~ 2-fold lower PLA puncta densities (0.29 ± 0.02) compared to their WT counterparts ($p = 3.09 \times 10^{-8}$) . Upon NMDAR activation, PLA puncta in GluN2B-ΔCaMKII neurons increased to a small but significant level (0.40 ± 0.02, $p = 0.02$). (**Figure 4.7D** & **E**). However, the PLA puncta observed in stimulated neurons expressing GluN2B-iHAΔCaMKII were significantly less than their WT counterparts ($p = 5.16 \times 10^{-16}$). Together these results: i) demonstrate that L1298A/R1300Q mutations in GluN2B abrogate CaMKII binding as expected, and ii) are consistent with the persistent binding of CaMKII to GluN2B following NMDAR activation (Barcomb et al., 2016; Bayer, 2006).

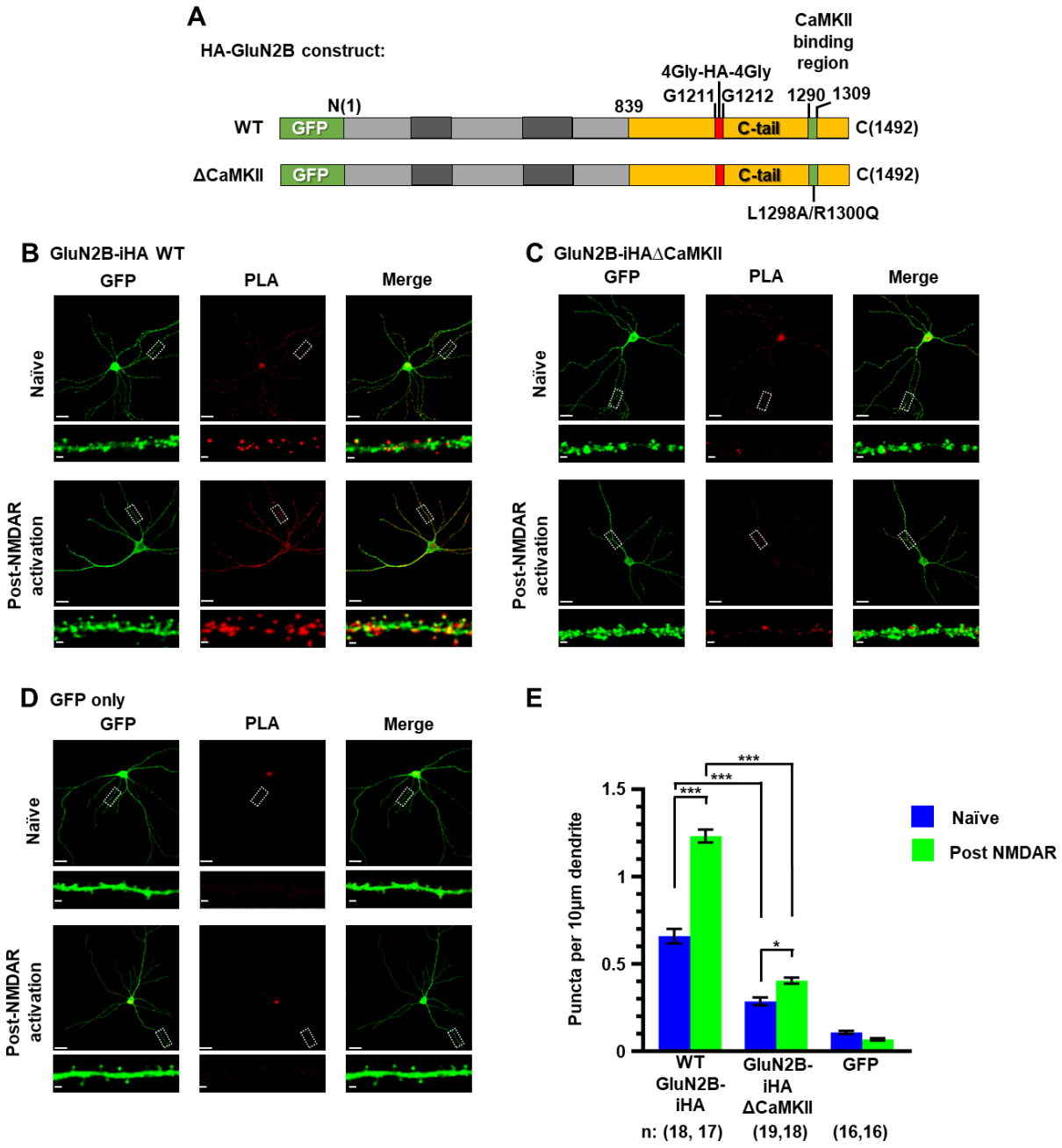

Figure 4.7. Changes in GluN2B and CaMKII association following NMDAR stimulation. (A) Topologies of HA-GluN2B constructs used for expression in primary hippocampal neurons. Representative images for neurons expressing **(B)** WT GluN2B-iHA, **(C)** GluN2B-iHAΔCaMKII, **(D)** empty GFP vector. In all cases for panels (**B-D),** images are shown for anti-GFP immunofluorescence (left column), anti-HA/anti-CaMKII PLA puncta (middle column) and merged GFP and PLA puncta channels (right column). Also for panels (**B-D)**, top row represent naïve neurons and bottom row represents NMDAR activated neurons. Scale bars for are 20 μm (whole cell images) and 1 μm (dendritic close-ups). **(E)** PLA puncta per 10 μm dendrite were calculated before (blue) or after (green) NMDAR activation for GluN2B constructs and GFP control. Data are presented as the mean ± SE and were collected from three independent preparations. The number of neurons analysed for each construct is shown in parentheses.

I next compared PLA puncta formation in neurons transfected with equal amounts of FLAG-α-actinin-2 and Glu2NB-iHA WT or GluN2B-iHAΔCaMKII (**Figure 4.8**). I found that PLA puncta per 10 μm dendrite in naïve neurons co-expressing FLAG-α-actinin-2 & WT GluN2B-iHA to be 0.47 ± 0.02, which rose to 0.61 ± 0.02 (p=2.45×10^{-6}) (**Figure 4.8A** & **E**). In neurons expressing FLAG-α-actinin-2 and Glu2NB-iHA ΔCaMKII, PLA puncta were observed at 0.38 ± 0.01 per 10 μm dendrite in naïve neurons, which only rose to 0.41 ± 0.01 following NMDAR activation (**Figure 4.8B** & **E**). Control experiments performed in neurons expressing either FLAG-α-actinin-2 or Glu2NB-iHA WT in isolation confirmed that PLA puncta formation depended on the presence of both proteins (**Figure 4.8C-E**). Analysis of the data presented in **figure 4.8** by two-way ANOVA indicates an interaction between the presence of the CaMKII anchoring site and NMDAR activation (p=9 x 10^{-3}), which supports the notion that docking to GluN2B plays at least some role in supporting elevated CaMKII-α-actinin-2 association following sLTP.

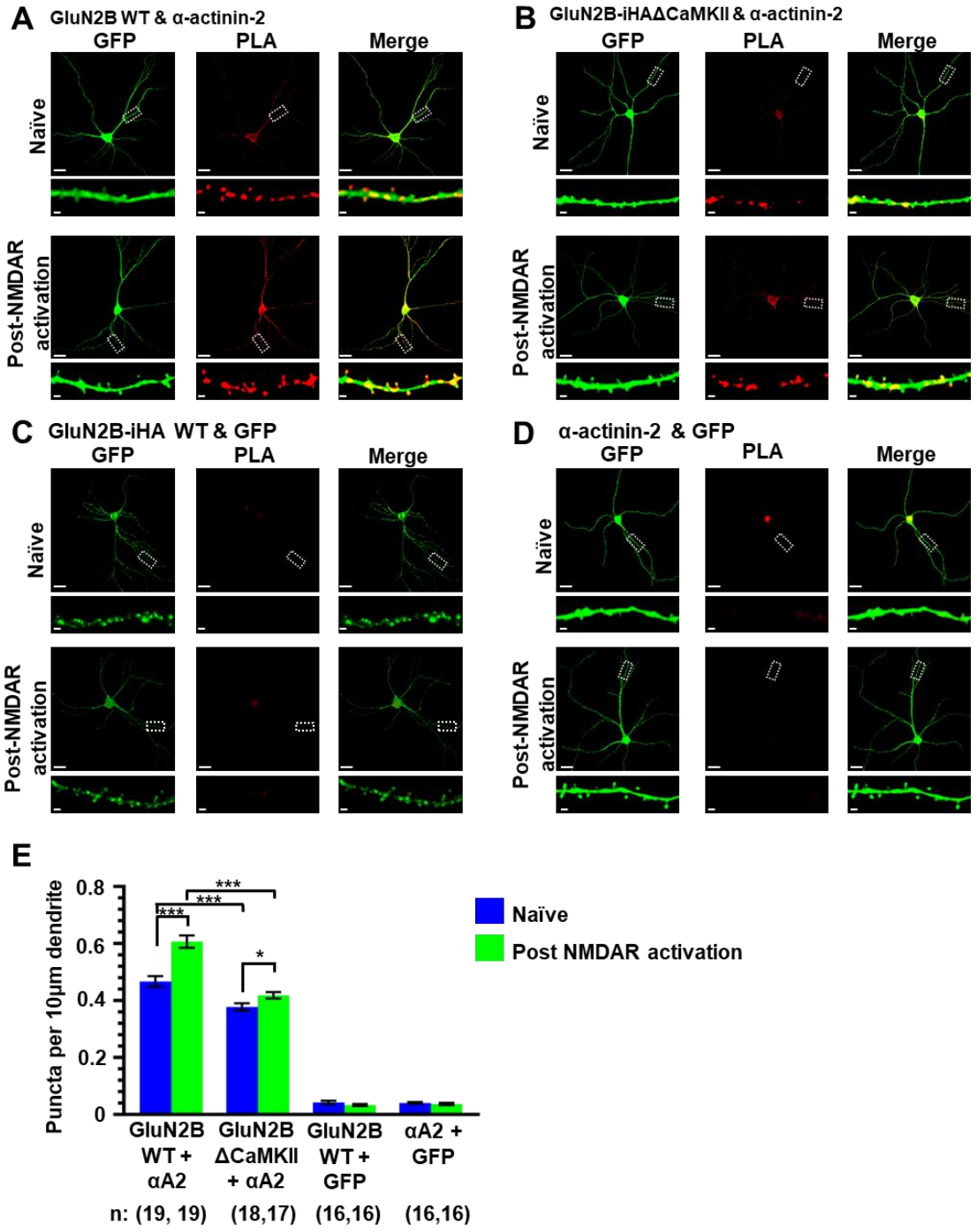

Figure 4.8. Changes in GluN2B and α-actinin-2 association following NMDAR activation. Representative images for neurons expressing **(A)** α-actinin-2 and WT GluN2B-iHA, **(B)** α-actinin-2 and GluN2B-iHAΔCaMKII, **(C)** WT GluN2B-iHA and GFP, **(D)** α-actinin-2 and GFP. In all cases images are shown for anti-GFP immunofluorescence (left column), anti-HA/anti-FLAG PLA puncta (middle column) and merged GFP and PLA puncta channels (right column). Also, for panels, top row represent naïve neurons and bottom row represents NMDAR activated neurons. Scale bars for are 20 µm (whole cell images) and 1 µm (dendritic close-ups). **(E)** PLA puncta per 10 µm dendrite were calculated before (blue) or after (green) NMDAR activation. Data are presented as the mean ± SE, and were collected from three independent preparations. The number of neurons analysed for each construct combination is shown in parentheses.

4.5. Phosphorylation at CaMKII T286 is not required for association with α-actinin-2

As discussed in **section 1.4**, CaMKII autophosphorylation at T286 is also thought to partially release the CaMKII regulatory segment from the kinase domain enabling constitutive low-level kinase activity (Barcomb et al., 2014). This form of CaMKII regulation is thought to be important in the initial induction but not maintenance of LTP (Yasuda et al., 2022). I therefore also investigated the possibility that phosphorylation at this site might be required to enable elevated interaction with α-actinin-2 following the induction of LTP. To explore a potential role for T286 phosphorylation, I performed further PLA measurements in primary hippocampal neurons expressing either WT or T286A variants of V5-CaMKIIα, monitoring association of the kinase in each case with FLAG-α-actinin-2 (**Figure 4.9**).

As with the PLA experiments monitoring FLAG-α-actinin-2/endogenous CaMKIIα, the PLA puncta per 10 μm dendrite in neurons expressing FLAG-α-actinin-2 & V5-CaMKIIα WT significantly increased following NMDAR activation (naïve: 0.38 ± 0.02 vs. NMDAR activated: 1.23 ± 0.02, p=2.022×10^{-25}, **Figure 4.9A** & **E**). Similar levels of PLA puncta increase were also seen in FLAG-α-actinin-2 & V5-CaMKIIα-T286A transfected neurons (naïve: 0.40 ± 0.01 vs. NMDAR activated: 1.17 ± 0.01, (p= 2.16×10^{-33}), **Figure 4.9B** & **E**), with no significant different in PLA puncta between stimulated neurons expressing CaMKII WT and T286A variant (p= 0.10). This indicates that T286 autophosphorylation is not a mechanism facilitating CaMKII-actinin association.

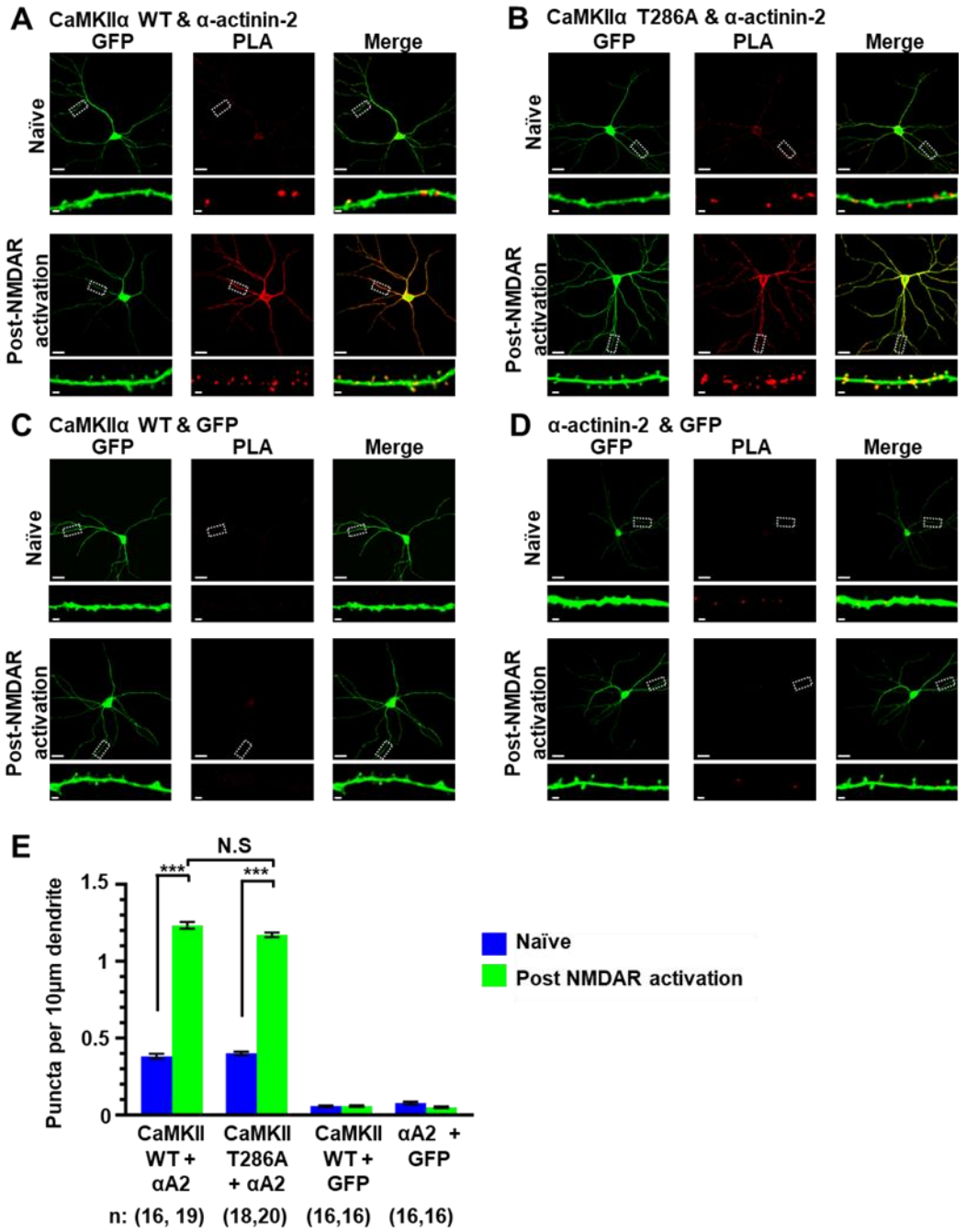

Figure 4.9 Changes in V5-CaMKII WT/T286A association with FLAG-α-actinin-2 following NMDAR stimulation. The panels show imaging of primary hippocampal neurons expressing **(A)** V5-CaMKII WT and FLAG-α-actinin-2, **(B)** V5-CaMKII T286A and FLAG-α-actinin-2, **(C)** V5-CaMKII WT alone, and **(D)** FLAG-α-actinin-2 alone. In all cases images are shown for anti-GFP immunofluorescence (left columns), anti-FLAG/anti-CaMKII PLA puncta (middle columns) and merged GFP and PLA puncta channels (right columns). For each panel, the upper row shows naïve neurons and the lower row shows neurons fixed after NMDAR activation. Scale bars are 20 µm (whole cell images) and 1 µm (dendritic close-ups). **(E)** PLA puncta per 10 µm dendrite were calculated before (blue) or after (green) NMDAR activation. Data are presented as the mean ± SE, and were collected from three independent preparations. The number of neurons analysed for each construct is shown in parentheses.

4.6. XL-MS with mixtures of purified CaMKII, α-actinin-2 and GluN2Bc

Given the *in vitro* observation that GluN2Bc increases CaMKII-α-actinin-2 association, and the PLA indication that all three proteins associate following LTP induction, I sought to understand the global assembly of this tri-partite complex with XL-MS (cross-linking coupled to mass-spectrometry). XL-MS is a developing structural technique well-suited to the investigation of large multi-protein complexes (see **Section 2.5**). XL-MS can provide key information regarding inter-protein domain interactions in multimeric assemblies and give low- resolution insights into the overall architecture of multimeric complexes.

Cross-linking experiments with CaMKIIα/ CaM/ α-actinin-2/ ± GluN2Bc mixtures in the presence or absence of 200 nM free-Ca^{2+} were performed at an approximate 3:3:1:3 molar ratio with CaMKIIα at 7.3 μM. Similar to pull-down assays in **section 4.3**, a pre-incubation step was included to allow CaMKIIα-GluN2B association (see **Section 2.5**). Final sample mixtures were then incubated in 2 mM D_{12}/H_{12}-DSS for 30 min at 30 °C and cross-linking was terminated with the addition of ammonium bicarbonate to a final concentration of 50 mM for a further 15 min. Each cross-linking sample was prepared in triplicate and 5 μL of each replicate was combined to examine cross-linked CaMKII complexes by western blot and Coomassie staining.

Figure 4.10 shows anti-CaMKII, anti-α-actinin-2, anti-CaM immunoblots and Coomassie staining for the different CaMKII mixtures both before and after DSS cross-linking. In all cross-linked conditions, CaMKIIα appears at higher molecular weight (MW) bands indicating successful cross-linking (lanes, 2, 4, 6, 8, **Figure 4.10A**). These cross-links are presumably within the association domains of the holoenzyme, however increased signal at higher MW band with the addition of Glun2Bc (compare lanes 6 & 8, with 2 & 4, **Figure 4.10A**) suggest increase in CaMKII cross-linking with GluN2Bc and possibly α-actinin-2.

Similar to CaMKIIα, α-actinin-2 polypeptides appears to cross-link efficiently with their associated protomer – in its case antiparallel dimers, with prominent bands at ~250 kDa following addition of DSS (lanes, 2, 4, 6, 8, **Figure 4.10B**). The immunoblot for α-actinin-2 also reveals a higher molecular weight band with a weaker signal just below the gel loading well for all cross-linked conditions (lanes, 2, 4, 6, 8, **Figure 4.10B**). This band

increases in intensity with the addition of GluN2Bc suggesting an increase in CaMKIIα-α-actinin-2~GluN2Bc assembly (compare lanes 6 & 8, with 2 & 4, **Figure 4.10B**). Interestingly, the anti-CaM immunoblot shows a decrease in CaM cross-linking in sample mixtures containing GluN2Bc (compare lanes 4 & 8, **Figure 4.10C**) further supporting the notion that GluN2Bc increases CaMKII association with α-actinin-2. Lastly, Coomassie staining shows an increase in cross-linking for GluN2Bc in the presence of Ca^{2+} (compare lanes 6 & 8, **Figure 4.10D**) which could be explained by increased CaMKIIα-GluN2Bc association following Ca^{2+}/CaM activation. Together these western blots and Coomassie staining support the idea that CaMKII-α-actinin-2 association is increased in the presence of GluN2Bc.

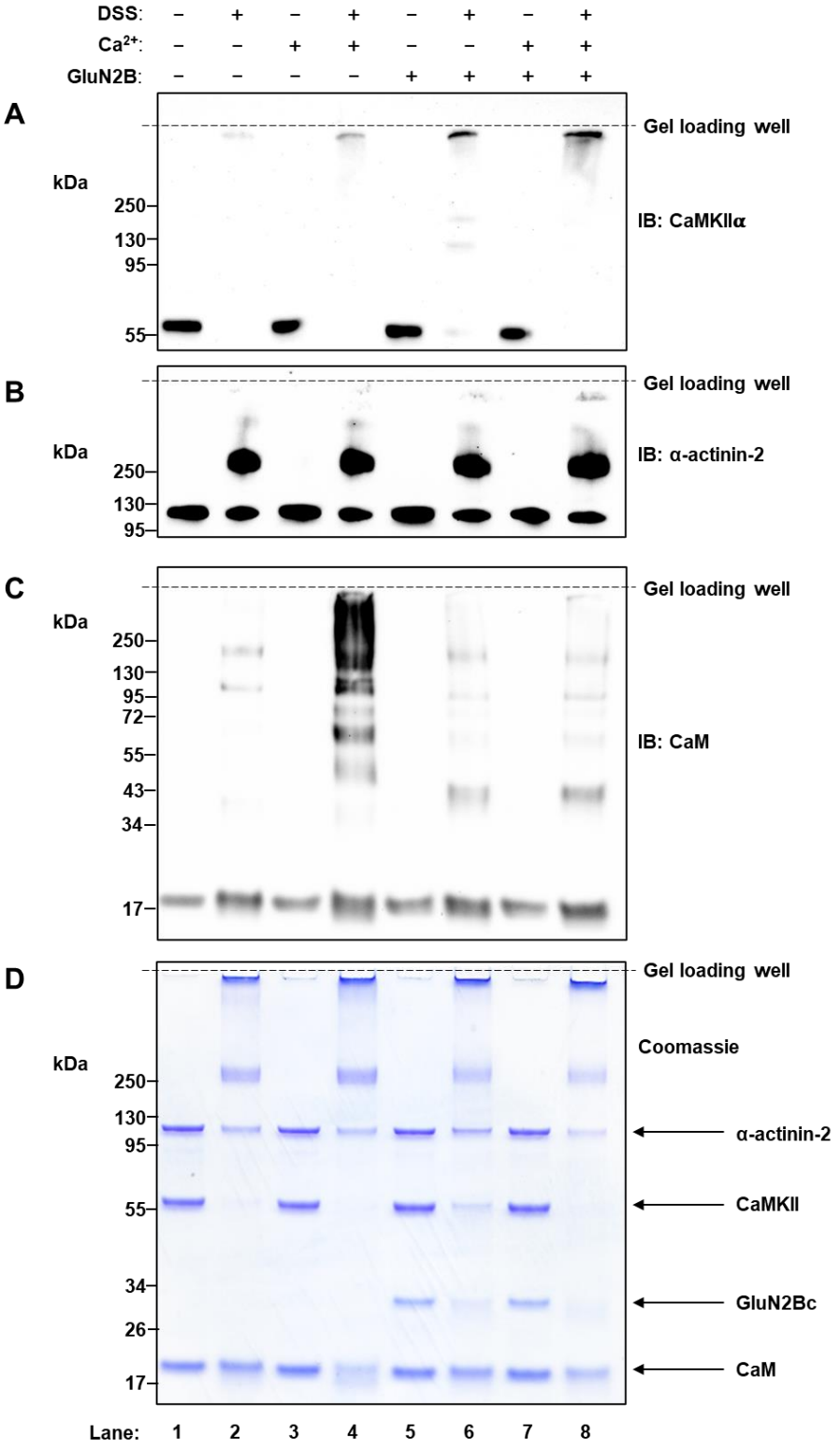

Figure 4.10. DSS cross-linking of CaMKII-α-actinin-2 purified protein mixtures. In all panels, the odd lanes represent the samples prior to DSS cross-linking, the even lanes represent cross-linked samples. The first four lanes are CaMKII mixed with calmodulin and α-actinin-2, while the last four lanes also include GluN2BC fragment. Lanes 3,4,7,8 include the addition of 2 mM final concentration of $CaCl_2$ to allow calmodulin/CaMKII binding. **(A)** Immunoblot for CaMKIIα, **(B)** Immunoblot for α-actinin-2 **(C)** Immunoblot for calmodulin, **(D)** Coomassie staining.

The cross-linked samples of CaMKII-α-actinin-2-GluN2Bc (lane 8, **Figure 4.10**) were analysed by mass-spectrometry. **Figure 4.11** and **table 4.2** illustrate the cross-linking map of the complex and the amino acid positions of the interlinks, respectively. The table shows cross-links that were identified in at least two of the three replicates with an ID score >20. A total of 9 interlinks were identified according to this criteria: 6 GluN2Bc-CaMKIIα interlinks, 2 GluN2Bc-α-actinin-2 and 1 CaMKII-α-actinin-2 interlink (**Table 4.2**). The full dataset of cross-links can be found in the **Appendix** (**Appendix 1** – interlinks; **Appendix 2** – Intralinks). All interlinks found in CaMKIIα occur at three sites (K56, K68, K148) within the kinase domain (**Figure 4.11B**), and each site cross-linked with a lysine within GluN2Bc, consistent with the role of GluN2B cytoplasmic tail binding to the CaMKII kinase domain following the release of the regulatory segment (Bayer et al., 2001; Özden et al., 2022). The α-actinin-2 interlinks with GluN2B & CaMKII kinase domain were found to be at position K86 located within the actin-binding domain, which lies opposite to the EF hand-motifs within the anti-parallel dimer. Although the cross-linking dataset is limited, this pattern of cross-linking is consistent with GluN2B docking to the CaMKII substrate binding groove to release the regulatory segment for interaction with the α-actinin-2 EF hands.

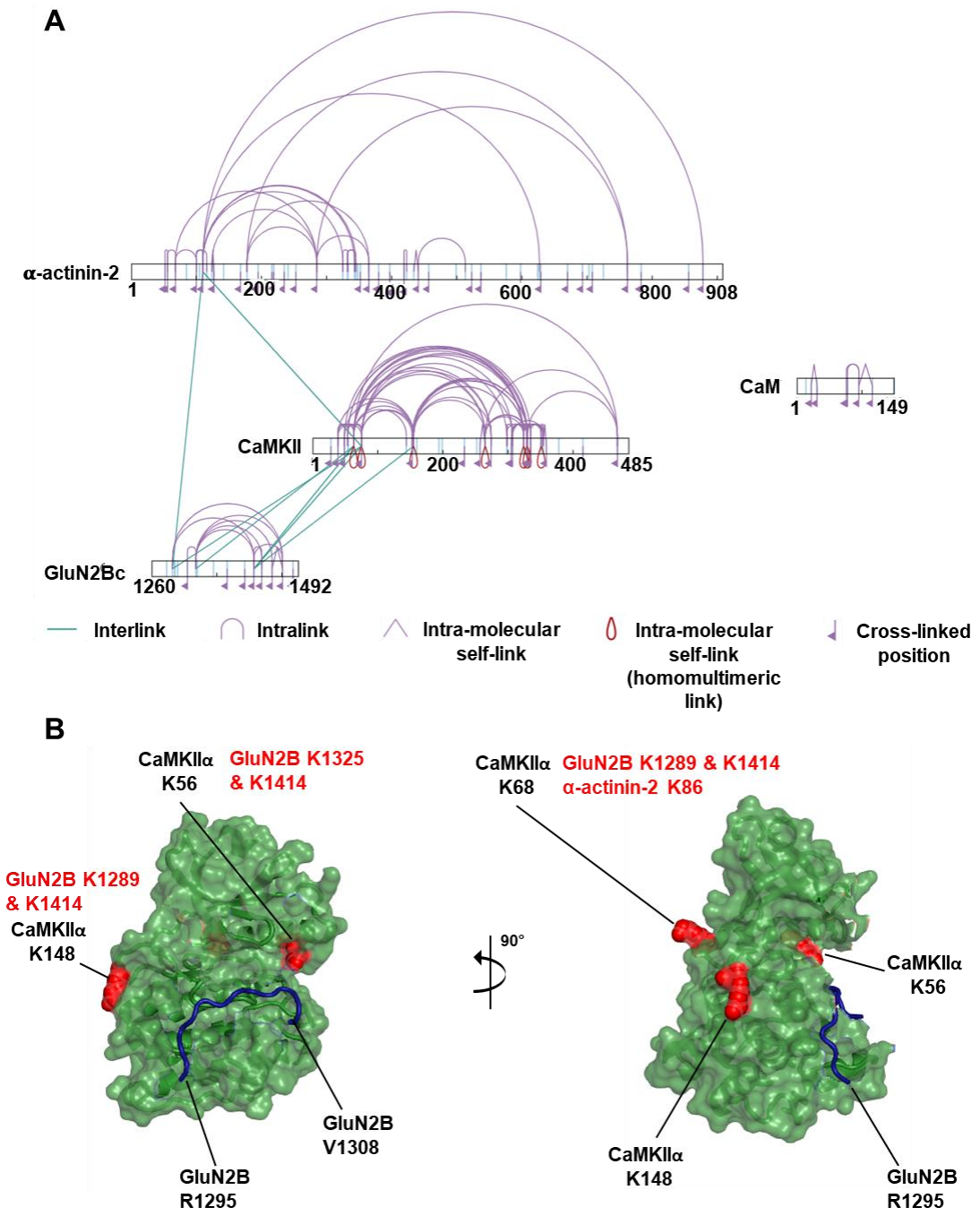

Figure 4.11. Cross-linking map of CaMKII-α-actinin-2-GluN2B. (A) Purple loops represent intralinks; blue lines represent interlinks. Purple flags highlight lysine residues that are present in the polypeptide chain. Map was generated from cross-links identified in at least 2 of the 3 biological replicates analysed with an ID score over 20. **(B)** Interlinks within CaMKII kinase domain are highlighted (red) and their links with GluN2Bc/α-actinin-2 are described (red font) in the crystal structure of CaMKII kinase (1-274) in complex with GluN2B peptide (1295-1308) (PDB:7UJQ).

Protein A Sequence Id-Protein B Sequence Id	Protein A	Protein B	Position A	Position B	Id-Score	Replicates
FHKIANVNK-LLKHPNIVR	α-actinin-2	CaMKII	86	68	38.94	2
YPQSPTNSKAQK-FHKIANVNK	GluN2B	α-actinin-2	1289	86	28.21	2
ALVTNKPVVSALHGAVPGR-KTAPYR	GluN2B	α-actinin-2	1269	164	25.03	2
QPTVAGASKTRPDFR-LKGAAVK	GluN2B	CaMKII	1414	148	25.44	3
YPQSPTNSKAQK-LKGAAVK	GluN2B	CaMKII	1289	148	20.9	2
QPTVAGASKTRPDFR-DHQKLER	GluN2B	CaMKII	1414	56	25.63	3
DHQKLER-SVSLKDK	GluN2B	CaMKII	1325	56	24.67	2
QPTVAGASKTRPDFR-LLKHPNIVR	GluN2B	CaMKII	1414	68	32.01	3
YPQSPTNSKAQK-LLKHPNIVR	GluN2B	CaMKII	1289	68	21.83	3

Table 4.2. Sequence and amino acid position of the identified interlinks in CaMKII/α-actinin-2/GluN2B samples. The table includes biological ID score of the interlinks and the number of replicates possessing the interlinks from the XLMS study. Cross-linked lysines are highlighted in yellow.

4.7. Concluding remarks

In this Chapter, I utilised ITC measurements, cross-referencing to a crystal structure, to understand the structural basis underlying elevated CaMKII-α-actinin-2 association in synapses following LTP. Additionally, I provide *in vitro* and *in situ* evidence to support the hypothesis that docking of CaMKII to the GluN2B C-tail promotes α-actinin-2 association through the displacement of the regulatory segment, even in the presence of Ca^{2+}/CaM. PLA studies contribute to the notion that all three proteins can associate following NMDAR activation and re-enforce existing data for the persistent GluN2B-CaMKII interactions in synapses. Finally, I attempted to analyse the structure of CaMKIIα-α-actinin-2-GluN2B assemblies *in vitro* using XL-MS, and identified a limited number of interlinks in agreement with my other observations.

Chapter 5. The T305A/T306A variant of CaMKIIα binds tightly to α-actinin-2 to enlarge dendritic spines irrespective of NMDAR stimulation

My results (chapters 3 and 4) show that elevated interactions between α-actinin-2 and CaMKIIα underlie the formation of enlarged dendritic spines following NMDAR activation. Intriguingly, earlier studies of this interaction have taken advantage of the CaMKIIα variant T305A/T306A since this mutant version of the kinase is more effectively pulled down by α-actinin-2 EF3-4 *in vitro* (Jalan-Sakrikar et al., 2012, see Supplementary Figure 4B). The T305A/T306A variant of CaMKIIα has also been utilised in many studies to investigate the role of CaMKII regulatory phosphorylation at T305 or T306 that it thought to constitute an important form of negative feedback by preventing further activation by Ca^{2+}/CaM (Barcomb et al., 2014; Colbran and Soderling, 1990b; Patton et al., 1990). Studies incorporating experiments with CaMKIIα T305A/T306A have concluded, for example, that T305 & T306 phosphorylation inhibits CaMKII binding to GluN2B (Barcomb et al., 2014) and promotes dissociation of CaMKII from the PSD (Barcomb et al., 2014; Elgersma et al., 2002; Shen et al., 2000). However, if CaMKII T305A/T306A binds more tightly to α-actinin-2, the effects of this mutant on CaMKII localisation in the PSD could also be attributed a gain-of-function ability to interact with α-actinin-2 as well as its interaction with GluN2B.

To investigate the possibility of an actinin-binding gain-of-function effect in CaMKIIα T305A/T306A, I first used PLA to determine whether alanine substitution of either or both of T305 and T306 alters interactions with α-actinin-2 either before or after chemical LTP (**Section 5.1**). Next, I determined whether expression of CaMKIIα T305A/T306A alters dendritic spine morphology either before or after NDMAR activation (**Section 5.2**). To quantify the effect of alanine substitutions at T305A and T306A on interaction with α-actinin-2, I performed ITC (**Section 5.3**). Cross-referencing to a recently determined crystal structure of CaMKIIα (1-315) in complex with α-actinin-2 EF3-4 provides a potential explanation for higher affinity interaction with the T305A/T306A variant that I was able to corroborate using further ITC experiments (**Section 5.4**). Together, these experiments call for a re-evaluation of earlier studies involving CaMKIIα T305A/T306A.

5.1. The effect CaMKII T305A and T306A mutations on α-actinin-2 association in synapses

To investigate the difference in association between α-actinin-2 and CaMKIIα WT and CaMKIIα T305A and/or T306A mutants, I returned to *in situ* PLA experiments. I developed expression vectors for these CaMKII mutants bearing N-terminal V5 tags and co-transfected the vectors in tandem with FLAG-α-actinin-2 in primary hippocampal neurons. I then compared PLA puncta formation using anti-V5/anti-FLAG antibodies in neurons before and after NMDAR activation that elicits sLTP in wild-type neurons.

I first compared anti-V5/anti-FLAG PLA puncta in neurons expressing FLAG-α-actinin-2 with either V5-CaMKIIα WT, V5-CaMKIIα T305A, or V5-CaMKII T306A. As expected, PLA puncta per 10 μm dendrite in V5-CaMKII WT transfected neurons increased by ~ 3-fold following NMDAR activation (naïve: 0.38 ± 0.02 vs. NMDAR activated: 1.23 ± 0.02, p=2.02×10^{-25}, **Figure 5.1A** & **F**). PLA puncta remained at baseline levels irrespective of NMDAR activation if either V5-CaMKII or FLAG-α-actinin-2 was expressed in isolation (**Figure 5.1D-F**). Puncta levels were little changed by alanine substitutions at either position 305 (0.32 ± 0.01 rising to 1.12 ± 0.02, p=4.90×10^{-24}, **Figure 5.1B** & **F**), or position 306 (0.44 ± 0.01 rising to 1.24 ± 0.02, p=2.10×10^{-26}, **Figure 5.1C** & **F**). Moreover, spine morphology was consistent with all three CaMKII variants. The absence of substantial PLA changes compared to WT in either the T305A and T306A variants of CaMKII indicates that single T305A or T306A mutations does not affect the affinity for CaMKII-α-actinin-2 binding and that phosphorylation at either side is not an important factor in dictating interactions between actinin and CaMKII.

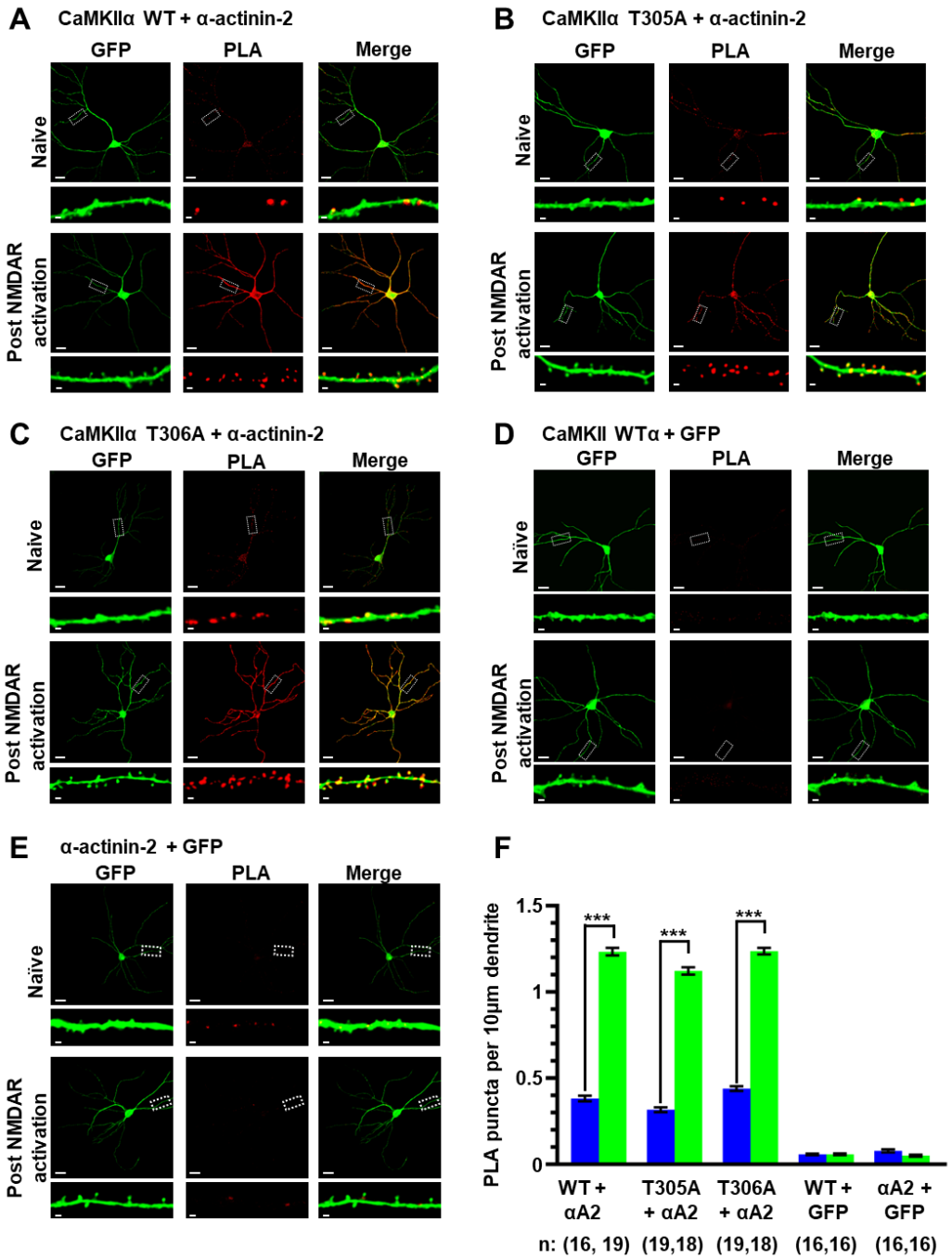

Figure 5.1. Comparison of WT, T305A, and T306A CaMKIIα association with α-actinin-2 in primary hippocampal neurons. **(A)** CaMKII WT and α-actinin-2, **(B)** CaMKII T305A and α-actinin-2, **(C)** CaMKII T306A and α-actinin-2, **(D)** CaMKII-WT and GFP, **(E)** α-actinin-2 and GFP. In all cases images are shown for anti-GFP immunofluorescence (left column), anti-FLAG/anti-CaMKII PLA puncta (middle column) and merged GFP and PLA puncta channels (right column). Also for panel, top row represent naïve neurons and bottom row represents NMDAR activated neurons. Scale bars for are 20 µm (whole cell images) and 1 µm (dendritic close-ups). **(F)** Quantitation of CaMKIIα - α-actinin-2 (αA2) PLA puncta**.** PLA puncta per 10 µm dendrite were calculated before (blue) or after (green) NMDAR activation. Data are presented as the mean ± SE and were collected from three animals. The number of neurons analysed for each construct is shown in parentheses.

I next performed PLA experiments to compare the difference in puncta from neurons expressing FLAG-α-actinin-2 in tandem with either WT or T305A/T306A V5-CaMKIIα. Unstimulated hippocampal neurons co-expressing V5-CaMKIIα WT and FLAG-α-actinin-2 exhibited PLA puncta with a density of 0.41 ± 0.05/ 10 μm dendrite (**Figure 5.2A** & **C**), increasing ~3-fold (1.27 ± 0.06 puncta/10 μm dendrite) in NMDAR activated neurons (p=2.60×10^{-8}). Imaging GFP-immunofluorescence from NMDAR activated CaMKII WT/α-actinin-2 neurons revealed the development of mushroom-type spines, as expected, indicative of sLTP (**Figure 5.2 A**, left panels). Surprisingly, PLA imaging of unstimulated neurons co-expressing CaMKIIα T305A/T306A & α-actinin-2 revealed ~3-fold higher levels of PLA puncta compared to the CaMKIIα WT equivalent (1.14 ± 0.02 puncta/10 μm dendrite, p= 1.17×10^{-8}) (**Figure 5.2 B** & **C**). NMDAR activated neurons co-transfected with α-actinin-2 and CaMKII WT or T305A/T306A displayed similar levels of PLA puncta densities with no statistical difference between groups (p= 0.43, **Figure 5.2C** & **Figure 5.2 A** & **B,** bottom rows). Finally, neurons transfected with single expression vectors for either V5-CaMKII WT, V5-CaMKII T305A/T306A or FLAG-α-actinin-2 displayed baseline levels PLA puncta (**Figure 5.3A-C**), confirming the specificity of the assay. Together, the PLA data indicates a marked increase in association of α-actinin-2 and CaMKII T305A/T306A compared to CaMKII WT in unstimulated primary hippocampal neurons, with interaction with the mutant form in naïve neurons at comparable levels to the WT following NMDAR activation.

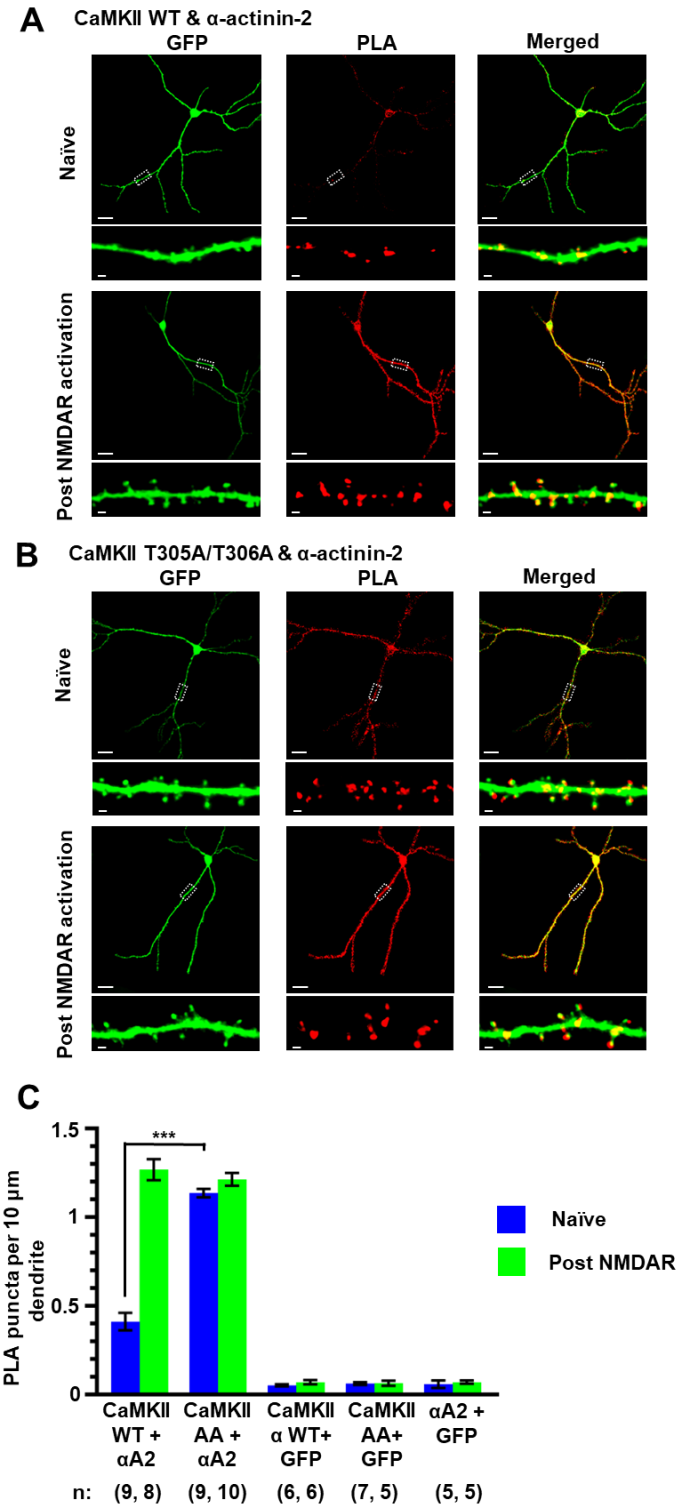

Figure 5.2. Comparison of WT and T305A/T306A CaMKIIα association with α-actinin-2 in primary hippocampal neurons. **(A)** and **(B)** Anti-GFP immunofluorescence (left column), anti-FLAG/anti-V5 PLA puncta (middle column) and merged GFP and PLA puncta channels (right column) for naïve neurons (top rows) or NMDAR stimulated neurons (bottom rows) expressing FLAG-α-actinin-2 and V5-CaMKII WT **(A)** or FLAG-α-actinin-2 and V5-CaMKII T305A/T306A **(B)**. Scale bars for **(A)** and **(B)** are 20 µm (whole cell images) and 1 µm (dendritic close-ups). **(C)** Quantitation of PLA puncta per 10 µm dendrite before (blue) or after (green) NMDAR activations for the full set of FLAG-α-actinin-2 and V5-CaMKII constructs. Data are presented as the mean ± SE. The number of neurons analysed for each construct is shown in parentheses.

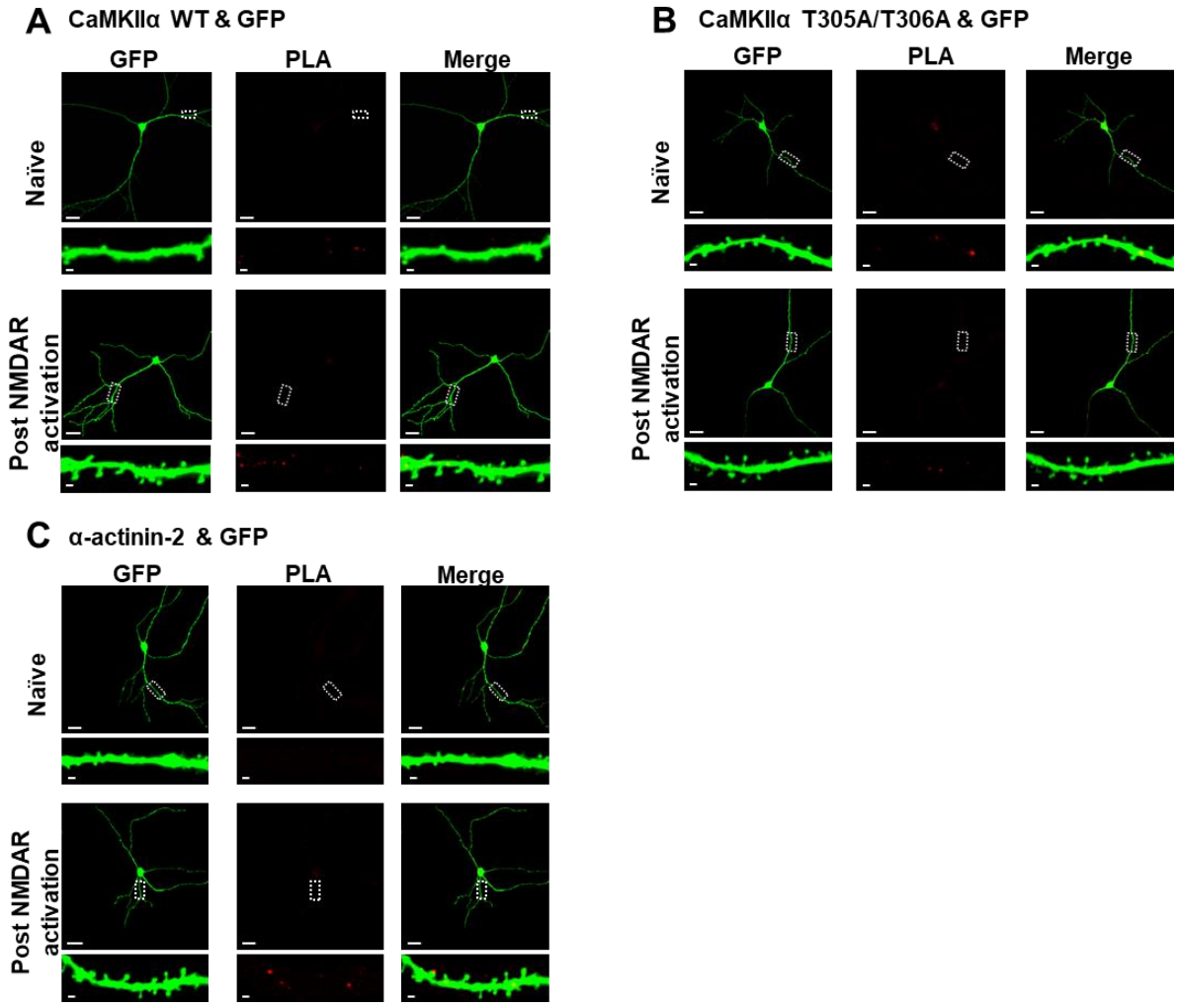

Figure 5.3. Imaging data for primary hippocampal neurons co-expressing CaMKIIα WT, T305A/T306A or α-actinin-2 with GFP. Each panel shows anti-GFP immunofluorescence (left columns), anti-FLAG/anti-V5 PLA puncta (middle columns) and GFP/PLA channels merged.**A-C** Upper panels show images for naïve neurons, lower panels show images for NMDAR activated neurons for; **(A)** V5-CaMKII WT and GFP; **(B)** V5-CaMKII T305A/T306A and GFP; **(C)** FLAG-α-actinin-2 and GFP. Scale bars correspond to 20 μm (whole neuron images) and 1 μm (dendrite close-ups).

5.2. CaMKII T305A/T306A mutations increase spine volume in unstimulated neurons

While analysing PLA puncta in neurons expressing CaMKII variants it was noticeable that neurons expressing the T305A/T306A variant of CaMKII exhibited many more mushroom type spines in naïve neurons compared to WT CaMKII (**Figure 5.2A** & **B**, left panel). Enhanced association between CaMKII T305A/T306A and α-actinin-2 in unstimulated neurons could upregulate CaMKII linking to the actin cytoskeleton and therefore drive premature sLTP prior to NMDAR activation. To investigate this hypothesis, I decided to compare the width and spine type of neurons co-transfected with V5-CaMKII WT or T305A/T306A, in tandem with FLAG-α-actinin-2 or GFP only (**Figure 5.4**).

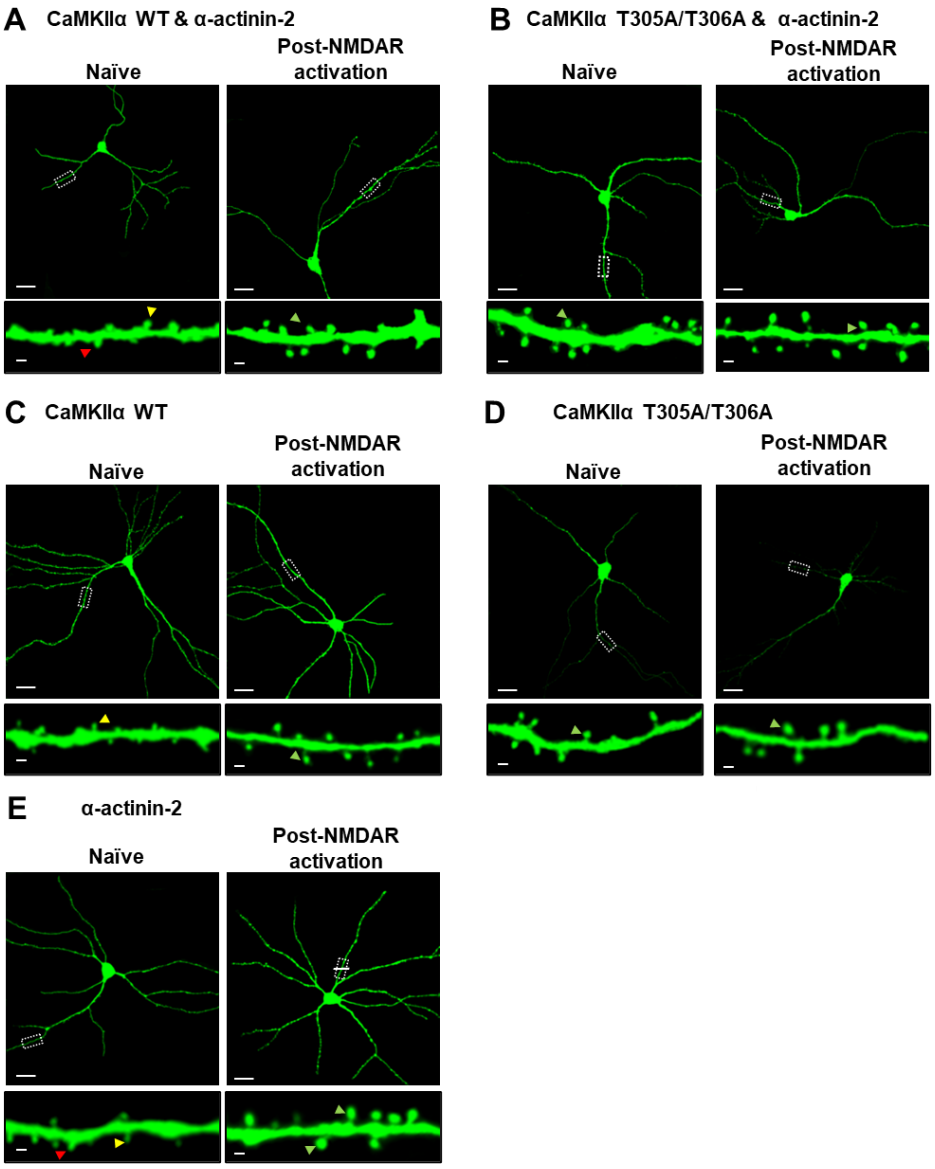

Figure 5.4. Effect of CaMKII and actinin transfections on spine morphology. Panels **A-E** show GFP imaging of primary hippocampal neurons transfected with either **(A)** V5-CaMKII WT and FLAG-α-actinin-2, **(B)** V5-CaMKII T305A/T306A and FLAG-α-actinin-2. **(C)** V5-CaMKII WT alone, **(D)** V5-CaMKII T305A/T306A alone, or **(E)** FLAG-α-actinin-2 alone. Stubby (red), thin (yellow), and mushroom (green) type synapses are highlighted with arrows. Scale bars correspond to 20 *μm* (whole neuron images) and 1 *μm* (dendrite close-ups).

Neurons transfected with each vector displayed similar spine densities with no statistical difference between groups (**Figure 5.5B**). For neurons transfected with V5-CaMKIIα WT & FLAG-α-actinin-2, V5-CaMKIIα WT alone or FLAG-α-actinin-2 alone, the majority of the spines observed in naïve neurons were thin or stubby (**Figure 5.4A,C** & **E** & **Figure 5.5C**). Upon NMDAR stimulation, average spine width in these neurons increased by ~1.7-fold, with the appearance of many mushroom type spines (**Figure 5.5D**) characteristic of sLTP. Surprisingly, expression of V5-CaMKIIα T305A/T306A with FLAG-α-actinin-2, or V5-CaMKIIα T305A/T306A alone led to the formation of large numbers of mushroom-type spines in naïve neurons (**Figure 5.4B** & **D** & **Figure 5.5C**). Quantification of spine diameters revealed that expression of V5-CaMKIIα T305A/T306A with FLAG-α-actinin-2 generated spine diameters ~1.75-fold ($p=2.9\times10^{-8}$) larger than the CaMKIIα WT counterpart (**Figure 5.5A**). Similar results were also observed in naïve neurons expressing V5-CaMKIIα variants alone, with the mutant variant producing ~1.65-fold wide spines on average than the WT sequence ($p=1.7\times10^{-7}$) (**Figure 5.5A**). Spine diameters, morphology, and total spine densities were comparable between all conditions post NMDAR activation with no statistical difference between groups. Overall, analysis of dendritic spines shows that CaMKIIα T305A/T306A mediates development of mushroom type spines, characteristic of spines that have undergone sLTP, irrespective of NMDAR activation to LTP induction.

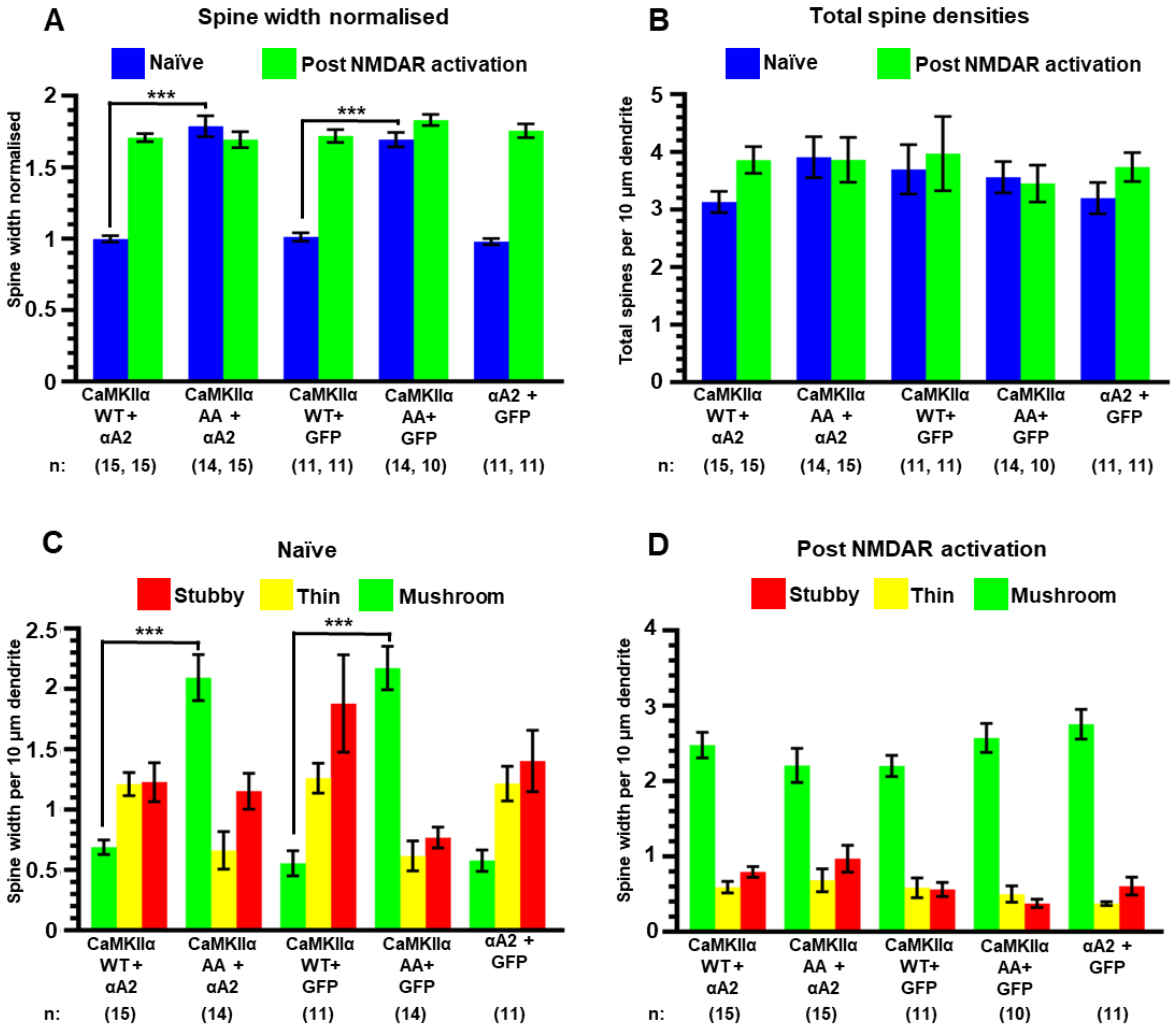

Figure 5.5. Quantification of spine morphology in neurons transfected with CaMKII and actinin constructs. (A) Quantification of spine width (mean ± SE) normalised to V5-CaMKII WT and FLAG-α-actinin-2 naïve neurons, either before NMDAR activation (blue) or after NMDAR activation (green). Numbers of neurons analysed for each condition are shown in parentheses. **(B)** Total spine density (mean spine number ± SE per 10 µm dendrite) in primary hippocampal neurons transfected with, either before NMDAR activation (blue) or after NMDAR activation (green). **(C)** and **(D)** Quantification of spine types in naïve neurons **(C)** or NMDAR activated neurons **(D)** transfected with V5-CaMKII and/or FLAG-α-actinin-2. Data are presented as mean ± SE spines per 10 *µm* dendritic length. The number of neurons analysed for each condition is shown in parentheses. Red, yellow, and green bars indicate stubby, thin, and mushroom spine numbers respectively.

5.3. CaMKII T305A/T306A double mutant increases α-actinin-2 affinity for the regulatory region

Given the observed increase in PLA puncta between α-actinin-2 and CaMKII T305A/T306A in naïve neurons, I sought to directly determine the affinity between α-actinin-2 EF hands 3-4 and the CaMKII regulatory segment with T305A/T306A mutations. Similar to ITC experiments performed in **section 4.1**, I compared the affinity of α-actinin-2 EF3-4 towards a CaMKII T305A/T306A peptide corresponding to the regulatory segment (294-315), and to a longer construct (CaMKIIα 1-315 T305A/T306A) that includes the autoinhibited kinase domain. The complete thermodynamic parameters obtained from ITC experiments are shown in **table 5.1**. EF3-4 bound to the T305A/T306A regulatory segment peptide (294-315) in an exothermic manner with a dissociation constant (K_d) = 15 ± 1 μM (**Figure 5.6A**), a modest ~2-fold higher affinity compared to the WT equivalent peptide (K_d=32 ± 1 μM). Remarkably, EF3-4 bound to CaMKII 1-315 T305/T306A with a K_d = 150 ± 10 nM (**Figure 5.6B**), ~100-fold stronger binding compared to the regulatory segment peptide alone. This finding was of surprise as the presence of the kinase domain was expected to reduce the affinity of EF3-4 towards the regulatory segment. To confirm T305A/T306A constructs were performing as expected, I examined the affinity of the mutated constructs with Ca^{2+}/CaM (**Figure 5.6C** & **D**). The dissociation constant of CaM to T305A/T306A regulatory peptide was 12 ± 1 nM, comparable to WT peptide (K_d = 11 ± 1 nM). Ca^{2+}/CaM also bound to the longer CaMKIIα 1-315 T305A/T306A construct in a similar fashion to the WT variant, with a dissociation constant of ~2.5 μM. Thus, the T305A/T306A mutation does not alter CaM binding to CaMKII. Together the ITC measurements demonstrate that T305A/T306A substitutions generate a version of CaMKII with a remarkable gain-of-function property of tight α-actinin-2 binding although strangely this property did not present in peptides limited to residues 294 to 315.

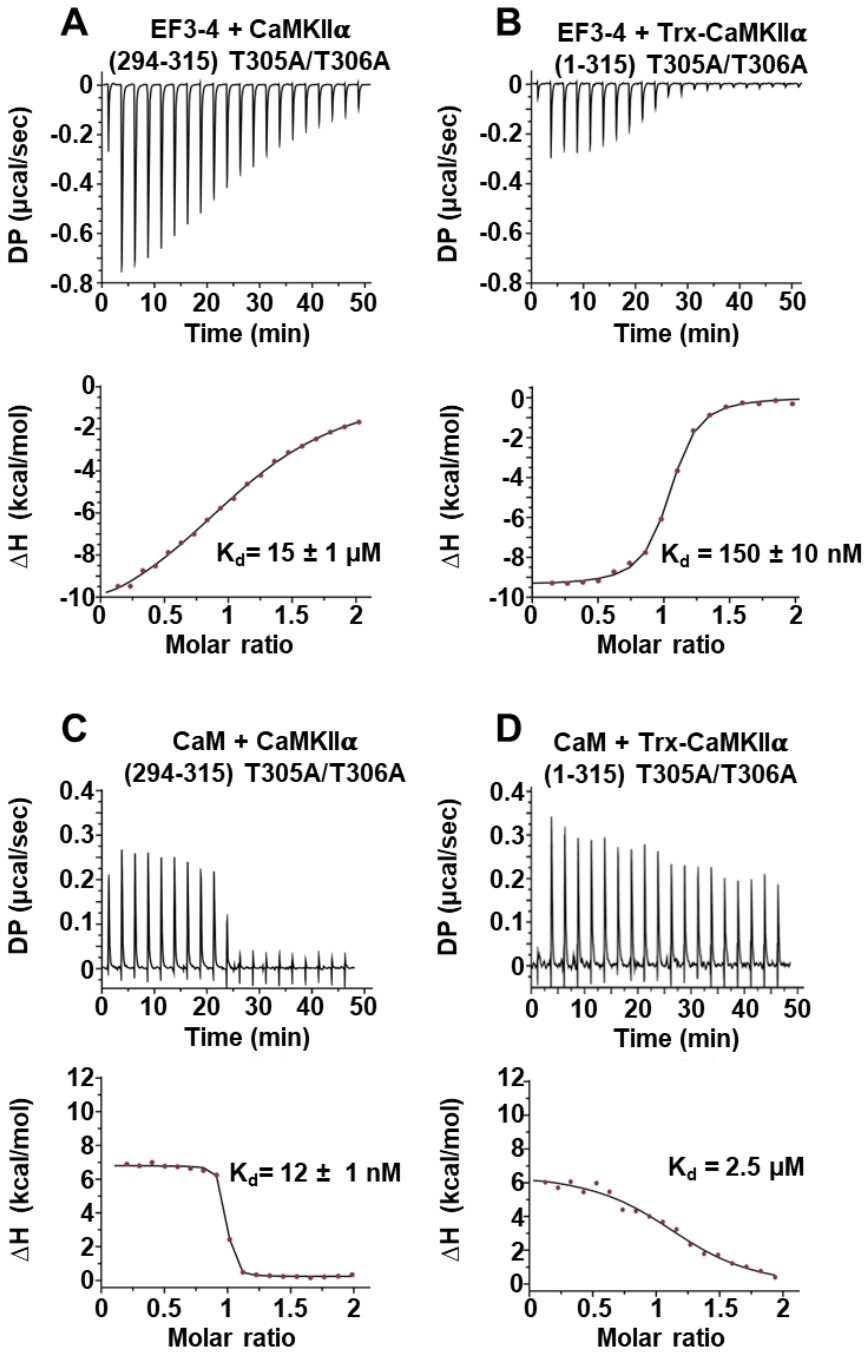

Figure 5.6. ITC recordings involving T305A/T306A CaMKIIα constructs. Representative isotherms showing binding of α-actinin-2 EF3-4 to **(A)** CaMKIIα regulatory segment (294-315) T305A/T306A peptide, and **(B)** Trx-CaMKII 1-315 T305A/T306A. Representative isotherms showing the binding of CaM to **(C)** CaMKIIα regulatory segment (294-315) T305A/T306A peptide, and **(D)** Trx-CaMKII 1-315 T305A/T306A. In all cases, the top sub-panels show the raw power output (µcal/s) per unit time; the bottom sub-panels show the integrated data including a line of best fit to a single site binding model. Stated K_d values are averages from experimental replicates.

I also performed equivalent experiments using T305A and T306A variants of CaMKII. EF3-4 bound to T305A and T306A regulatory segment peptides (294-315) at almost identical affinities with K_d = 19 ± 1 μM and 20 ± 2 μM, respectively (**Figure 5.7A** & **C**). These results suggest that in the context of the peptide alone, the T305A and T306A residues equally contribute to the binding of actinin-2 with a slightly higher affinity compared to the WT peptide (K_d = 32 ± 1 μM), and slightly lower affinity compared to T305A/T306A peptide (K_d = 15 ± 1 μM). Importantly, in contrast to CaMKII 1-315 T305A/T306A, neither single substitution facilitated the binding of EF3-4 to CaMKII – in fact, like the WT construct, it was not possible to establish a K_d for these constructs since the heat changes were barely detectable (**Figure 5.7B** & **D**). The combination of these results reveals that both T305A and T306A substitutions act in tandem to greatly enhance the interaction of actinin-2 to the regulatory segment of autoinhibited CaMKII, whereas either mutation in isolation has no significant effect on the affinity.

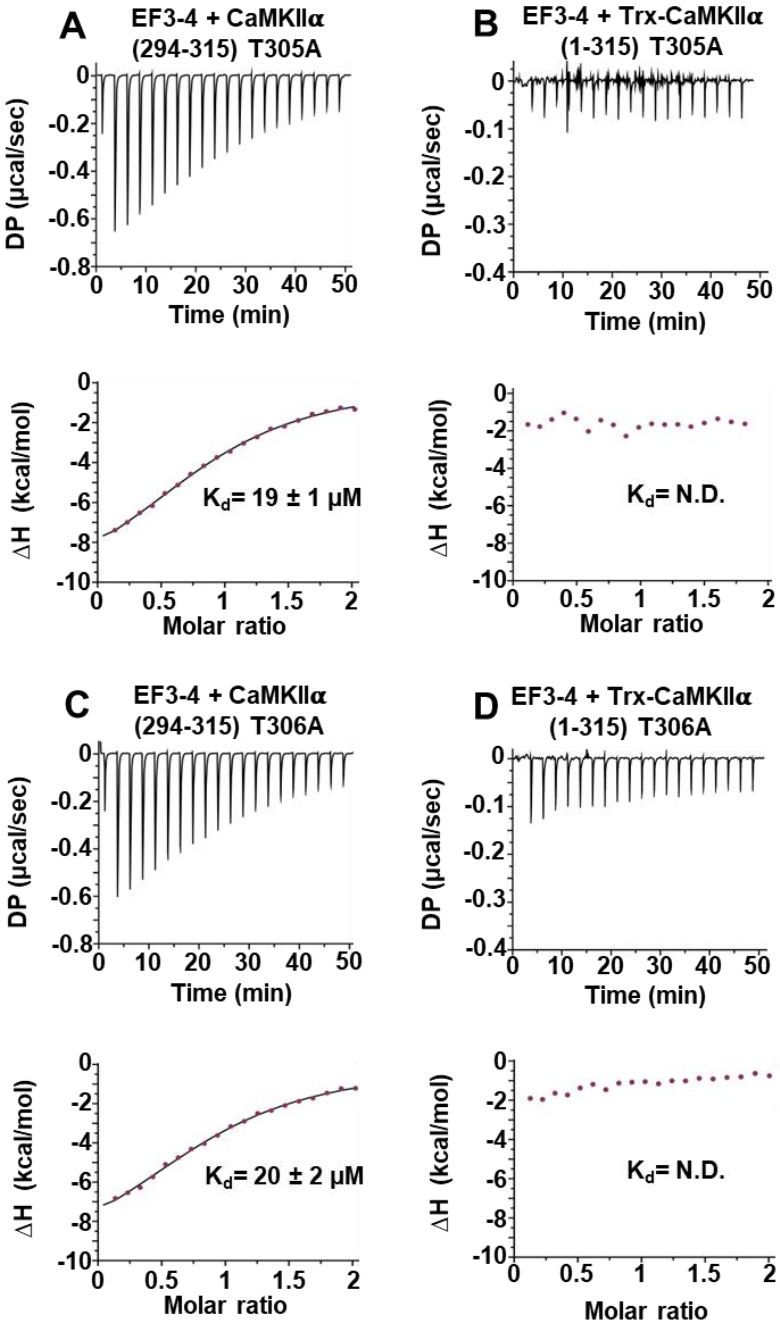

Figure 5.7. ITC measurements involving T305A and T306A CaMKIIα constructs. Representative isotherms showing binding of α-actinin-2 EF3-4 to **(A)** CaMKIIα regulatory segment (294-315) T305A peptide, **(B)** Trx-CaMKIIα 1-315 T305A , **(C)** CaMKIIα regulatory segment (294-315) T306A peptide, **(D)** Trx-CaMKIIα 1-315 T306A. In all cases, the top sub-panels show the raw power output (µcal/s) per unit time; the bottom sub-panels show the integrated data including a line of best fit to a single site binding model. Stated K_d values are averages from experimental replicates.

Cell	Syringe	Rep	n	K_d (μM)	ΔH (kcal/mol)	-TΔS (kcal/mol)
EF3-4	CaMKIIα 294-315 T305A/T306A	3	1.15 ± 0.02	14.67 ± 1.25	-12.5 ± 0.60	5.64 ± 0.62
CaMKIIα 1-315 T305A/T306A	EF3-4	3	0.99 ± 0.03	0.15 ± 0.01	-9.79 ± 0.56	0.49 ± 0.53
CaM	CaMKIIα 294-315 T305A/T306A	2	0.95 ± 0.01	0.01 ± 0.001	6.44 ± 0.15	-16.75 ± 0.11
CaMKIIα 1-315 T305A/T306A	CaM	1	0.97	2.43	6.34	-16.5
EF3-4	CaMKIIα 294-315 T305A	3	0.98 ± 0.03	19.40 ± 0.70	-11.83 ± 0.60	5.46 ± 0.60
CaMKIIα 1-315 T305A	EF3-4	3	ND	ND	ND	ND
EF3-4	CaMKIIα 294-315 T306A	3	0.91 ± 0.01	19.83 ± 1.93	-10.31 ± 0.54	3.89 ± 0.60
CaMKIIα 1-315 T306A	EF3-4	3	ND	ND	ND	ND
EF3-4	CaMKIIα 290-309 WT	3	1.03 ± 0.01	3.46 ± 0.08	-7.02 ± 0.17	-0.43 ± 0.02
EF3-4	CaMKIIα 290-309 T305A/T306A	3	0.99 ± 0.02	0.146 ± 0.001	-9.05 ± 0.21	-0.43 ± 0.12

Table 5.1. Full thermodynamic parameters for ITC measurements to investigate effect of alanine substitutions at CaMKII positions 305 and 306. Data is given as mean ± SE, Rep = replicates, ND = not determined, n is stoichiometry of binding, K_d is the dissociation constant, ΔH is enthalpy, -TΔS is entropy**.**

5.4. Structure of the CaMKIIα T305A/T306A & α-actinin-2 interface.

The enhanced affinity of α-actinin-2 towards CaMKII T305A/T306A regulatory region in the context of the autoinhibited kinase led us to investigate the structural basis of this phenomenon. Dr. Jian Zhu (Gold lab) solved the crystal structure of CaMKIIα T305A/T306A (1-315) bound to α-actinin-2 EF3-4 at 1.60 Å resolution (**Figure 5.8**). Initial observations from the complex reveal that, in contrast to CaMKIIα WT (**Figure 4.2**), α-actinin-2 EF hand motif 3 does not sterically clash with the kinase of CaMKIIα T305A/T306A (**Figure 5.8A**, left panel). This is consistent with previous data in this chapter and illustrates that α-actinin-2 is fully accessible to CaMKII regulatory segment in the context of T305A/T306A double mutation.

Closer inspection of the CaMKII T305A/T306A-EF3-4 binding interface reveals an expected amphipathic helix formed by the CaMKII regulatory region (**Figure 5.8B,** left panel). Compared to CaMKII WT regulatory segment (**Figure 5.8B,** right panel), α-actinin-2 EF3-4 binds to CaMKII T305A/T306A with a relative 180^{o} rotation. The EF3-4 motif also engages one helical turn further to the N-terminus of the regulatory segment peptide compared to the WT complex, with four hydrophobic residues (A295, L299, I303, M307) engaged in van der Waals interactions with α-actinin-2 EF3-4 (orange, **Figure 5.8B** & **C**). Additionally, the crystal structure shows that I303 in the mutant variant of CaMKII is buried closest to the centre of the hydrophobic pocket (as compared to M307 for CaMKII WT) where it contacts side chains of EF3-4 residues V831 and L850. The hydroxyl group from the threonine side chains of positions 305 and 306 in WT CaMKII would disrupt these van der waals arrangements observed with CaMKII T305A/T306A complex. Hence why the substitution allows for the phenomenon to occur.

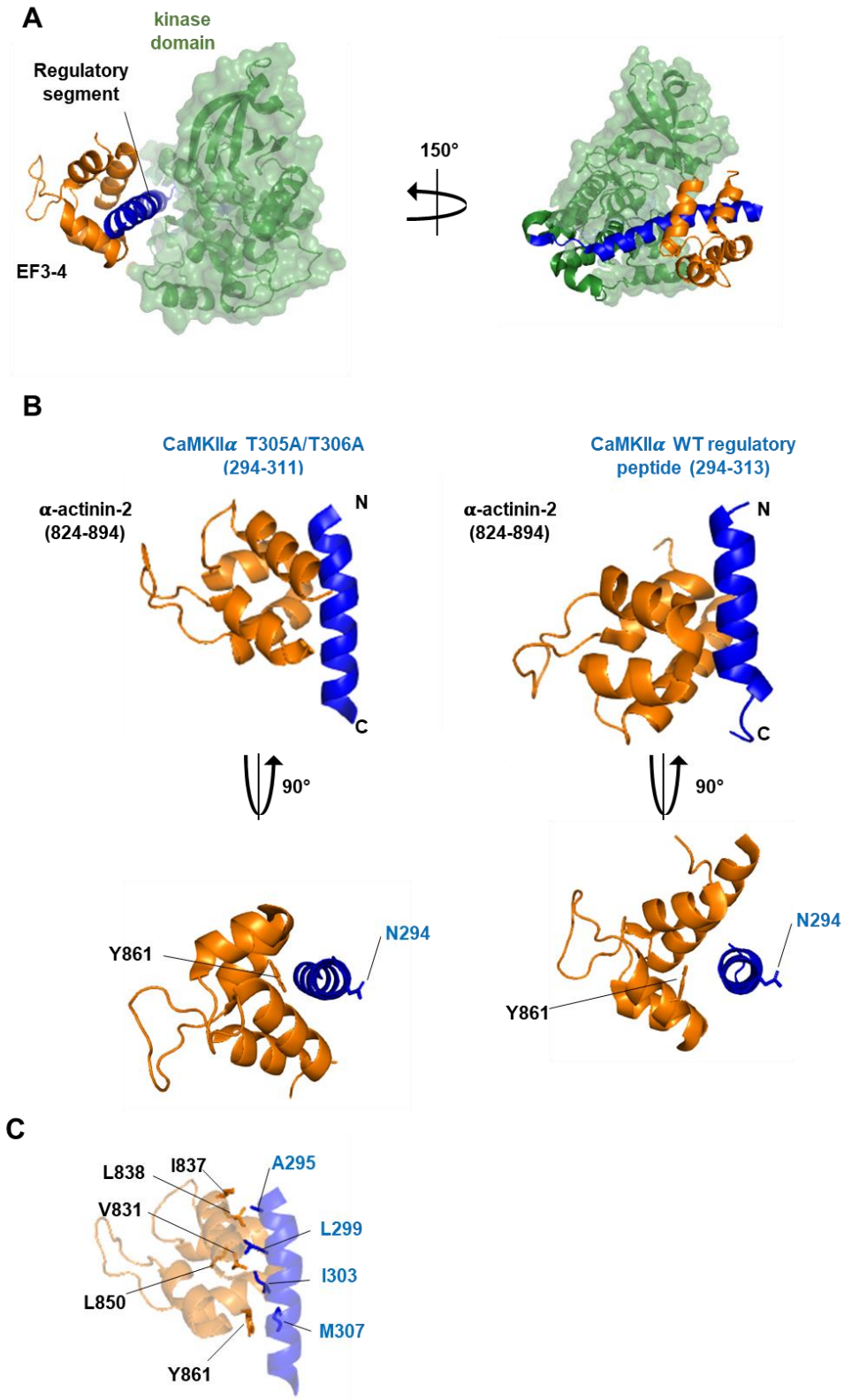

Figure 5.8. Crystal structure of α-actinin-2 EF3-4 – CaMKIIα T305A/T306A (1-315) complex. (A) Two views of the complex between α-actinin-2 EF3-4 (orange) and CaMKII 1-315 T305A/T306A containing the autoinhibited kinase (green) and regulatory region (blue). PDB:7B55. **(B)** Comparison of the interface between α-actinin-2 EF3-4 and CaMKII T305A/T306A (left panels) or CaMKII WT (right panels). **(C)** Close-up highlighting the residues which form the hydrophobic binding pocket of α-actinin-2 EF3-4 (orange) and CaMKIIα T305A/T306A in the complex showing their orientations relative to the binding interface.

To corroborate the binding mode observed in the crystal structure, with an important role for positions in the regulatory segment prior to 295, I performed further ITC experiments. Specifically, I measured the binding of EF3-4 to CaMKII WT and T305A/T306A peptides shifted on helical turn to the N-terminus spanning residues 290-309 (rather than 294-315, see **Section 5.5**). CaMKIIα WT (290-309) peptide bound to EF3-4 at a K_d= 3.5 ± 0.1 μM (**Figure 5.9A**) which is ~10-fold higher than equivalent peptide spanning residues 294-315. On the other hand, CaMKIIα T305A/T306A (290-309) bound to EF3-4 at a K_d=146 ± 1 nM (**Figure 5.9B**), which is ~100-fold tighter binding compared to the equivalent peptide spanning residues 294-315. The affinity of EF3-4 to CaMKII T305A/T306A (290-309) is almost identical to the longer CaMKII 1-315 construct (compare **Figure 5.6B** & **Figure 5.9B**). Taken together these results imply that the CaMKII epitope for α-actinin-2 EF hands extends beyond residues 294-315, and also confirm that the interface observed in the crystal structure of CaMKIIα 1-315 T305/T306A-EF34 is likely to represent the binding mode in solution.

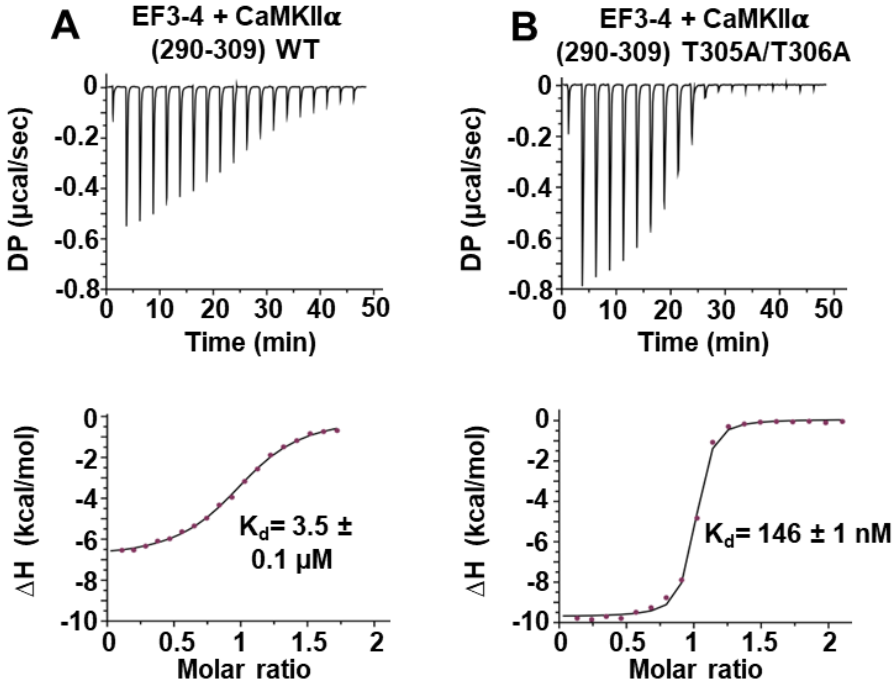

Figure 5.9. ITC measurements of α-actinin-2 EF3-4 with WT and T305A/T306A CaMKIIα 290-309 peptide. Representative isotherms showing binding of α-actinin-2 EF3-4 to **(A)** CaMKIIα WT regulatory peptide, **(B)** CaMKIIα T305A/T306A regulatory peptide, In all cases, the top sub-panels show the raw power output (μcal/s) per unit time; the bottom sub-panels show the integrated data including a line of best fit to a single site binding model. Stated K_d values are averages from experimental replicates.

5.5. Concluding remarks

The combination of PLA and ITC data in this chapter demonstrates that neither individual CaMKII T305A or T306A mutations affect CaMKIIα-α-actinin-2 association at dendritic spines in isolation. However, the combination T305A/T306A leads to a marked enhancement in CaMKIIα-α-actinin-2 interactions leading to premature sLTP. ITC measurements, and cross-referencing to a crystal structure, show that this is an inherent property of the CaMKII variant and not dependent on additional factors such as reduced phosphorylation at positions 305 and 306. Together these data call for a re-evaluation of the results of earlier studies with the T305A/T306A CaMKII variant (Jalan-Sakrikar et al., 2012; Pi et al., 2010), which were built on the assumption that the only significant characteristic of this variant is that it cannot be regulated at these sites by phosphorylation.

Chapter 6. Discussion

6.1. Summary of key findings

6.1.1. Role of CaMKII-α-actinin-2 interactions during structural LTP

In Chapter 3, I employed PLA to measure the association of CaMKII and α-actinin-2 in primary hippocampal neurons. The data shows CaMKII-α-actinin-2 complexes form after NMDAR activation. Formation of new CaMKII-α-actinin-2 complexes occurs in the range of seconds after NMDAR activation, and is dependent on the EF hands motifs of α-actinin-2 with the PDZ ligand somewhat facilitating the interaction through densin-180. Additionally, disrupting endogenous CaMKII-α-actinin-2 binding with fragments of α-actinin-2 prevents generation of the canonical enlarged mushroom type spines that accumulate during sLTP. This finding is consistent with the notion that α-actinin-2, which is known to bind both CaMKII and actin filaments, acts as a bridge between CaMKII and the cytoskeleton during structural reorganisation of spines in LTP.

6.1.2. The molecular basis of elevated CaMKII-α-actinin-2 interaction in sLTP

In Chapter 4, I cross-referenced ITC data with a crystal structure solved in the Gold lab to understand CaMKII-α-actinin-2 interactions at a molecular level. Together the data suggests that α-actinin-2 EF hands are not fully accessible to the regulatory segment of inactive CaMKII due to the steric hindrance of EF hands and autoinhibited kinase. I investigated the hypothesis that CaMKII docking onto the GluN2B C-tail supports the formation of CaMKII-α-actinin-2 complexes and provide *in vitro* evidence in support of this hypothesis. Further PLA imaging of neurons transfected with an exogenously-tagged GluN2B subunit revealed that both CaMKII and α-actinin-2 association with GluN2B subunits is elevated following NMDAR activation. Moreover, this increase in association of both CaMKII and actinin was attenuated in experiments with a CaMKII-binding deficient variant of GluN2B. Together this data suggests that CaMKII acts as a bridge between GluN2B and α-actinin-2 to form a tripartite complex. XL-MS experiments were broadly consistent with mechanism although this dataset suffered from a limited number of detected cross-links.

6.1.3. The CaMKIIα T305A/T306A variant artificially enhances CaMKII-α-actinin-2 complex formation

In Chapter 5, I investigated the effect of T305A/T306A substitutions in CaMKII. These substitutions have been used to investigate the role of negative feedback phosphorylation at these sites. However, I found that this CaMKII has an unexpected and pronounced gain-of-function ability of tight α-actinin-2 binding. My combined PLA and ITC data, in combination with structural data collected by Jian Zhu in the Gold lab, show that α-actinin-2 can fully access the regulatory segment within inactivated CaMKII mutant, and moreover that it adopts a novel binding mode and is able to bind tightly in doing so. This leads to elevated CaMKII-α-actinin-2 association prior to the activation of NMDARs and the generation of premature sLTP in unstimulated neurons. The findings of this chapter highlight that care should be taken in interpreting earlier studies involving the CaMKII T305A/T306A variant. Moreover, it should be noted that while the findings of this study illustrate the impacts of T305A/T306A mutations on α-actinin-2 affinity and consequently dendritic spine volume. The consequence of CaMKII T305A/T306A & α-actinin-2 interactions have not been directly investigated.

6.2. A revised mechanism for CaMKII mediated spine enlargement in structural LTP.

From the findings of this project, I propose a revised mechanism for spine enlargement in sLTP (**Figure 6.1**). In naïve spines, the regulatory segment of CaMKII is sequestered by its kinase domain (**Figure 6.1A**) within inactive dodecamers, ensuring only limited association with α-actinin-2 in the basal state. Initiation of LTP through Ca^{2+} influx via NMDARs triggers Ca^{2+}/CaM association to the regulatory segment of CaMKII, which in turn, exposes the substrate binding groove of the kinase domain. The active kinase phosphorylates key substrates such as AMPARs and forms a highly stable complex with the C-tail of NMDAR GluN2B subunits (**Figure 6.1 B**). CaMKII activity endures beyond the duration of Ca^{2+} elevation by auto-phosphorylation at T286 (Yasuda et al., 2022) which is longer lasting than the initial stimulus and potentiates CaMKII binding with GluN2B subunits of NMDARs(Özden et al., 2022), thereby promoting regulatory segment access for α-actinin-2 EF hand motifs and enabling new interactions between the two to be established within the first two minutes of LTP induction. In this way, α-actinin-2 is enriched in dendritic spine heads where it supports spine head enlargement

through its ability to cross-link actin filaments via its N-terminal actin-binding domain (**Figure 6.1C**). This updated mechanism fits with an influential 'synaptic tagging' theory (Sanhueza et al., 2011), whereby long-lasting CaMKII-NMDAR complexes formed during LTP induction serve as primers for more global structural changes in dendritic spines that occur after the initial Ca^{2+} signal has subsided. In the case of the CaMKII T305A/T306A mutant, we propose that artificial enhancement of α-actinin-2 – CaMKII interactions leads to elevated actin remodelling of dendritic spines into mushroom-type structures regardless of NMDAR activation.

The simplified model presented in **figure 6.1** is broadly consistent with previous reports identifying protein-protein interactions that are involved in the positioning of CaMKII and α-actinin-2. For example densin-180 includes a C-terminal PDZ domain that binds to the PDZ ligand at the C-terminus of α-actinin-2 (Walikonis et al., 2001), and a motif ~100-150 amino acids from its C-terminus that associates with the CaMKII hub domain (Strack et al., 2000b). In the crystal structure (**Figure 4.2**), the PDZ ligand at the C-terminus of EF3-4 is available for interaction which suggests that densin-180 could form a tripartite complex with CaMKII and α-actinin including a single CaMKII protomer. Additionally, α-actinin-2 is known bind to the C-tail of NMDAR GluN1 subunits through its spectrin repeats (Wyszynski et al., 1997), and also the N-terminal 13 amino acids of PSD-95, which underlie spine formation (Matt et al., 2018). These interactions are compatible with α-actinin-2 binding to CaMKII-GluN2B complexes at the synapse. The model is also consistent with recent studies demonstrating liquid-liquid phase separation of auto phosphorylated CaMKII and GluN2B following enzyme activation which serves as a platform for synaptic potentiation (Hosokawa et al., 2021).

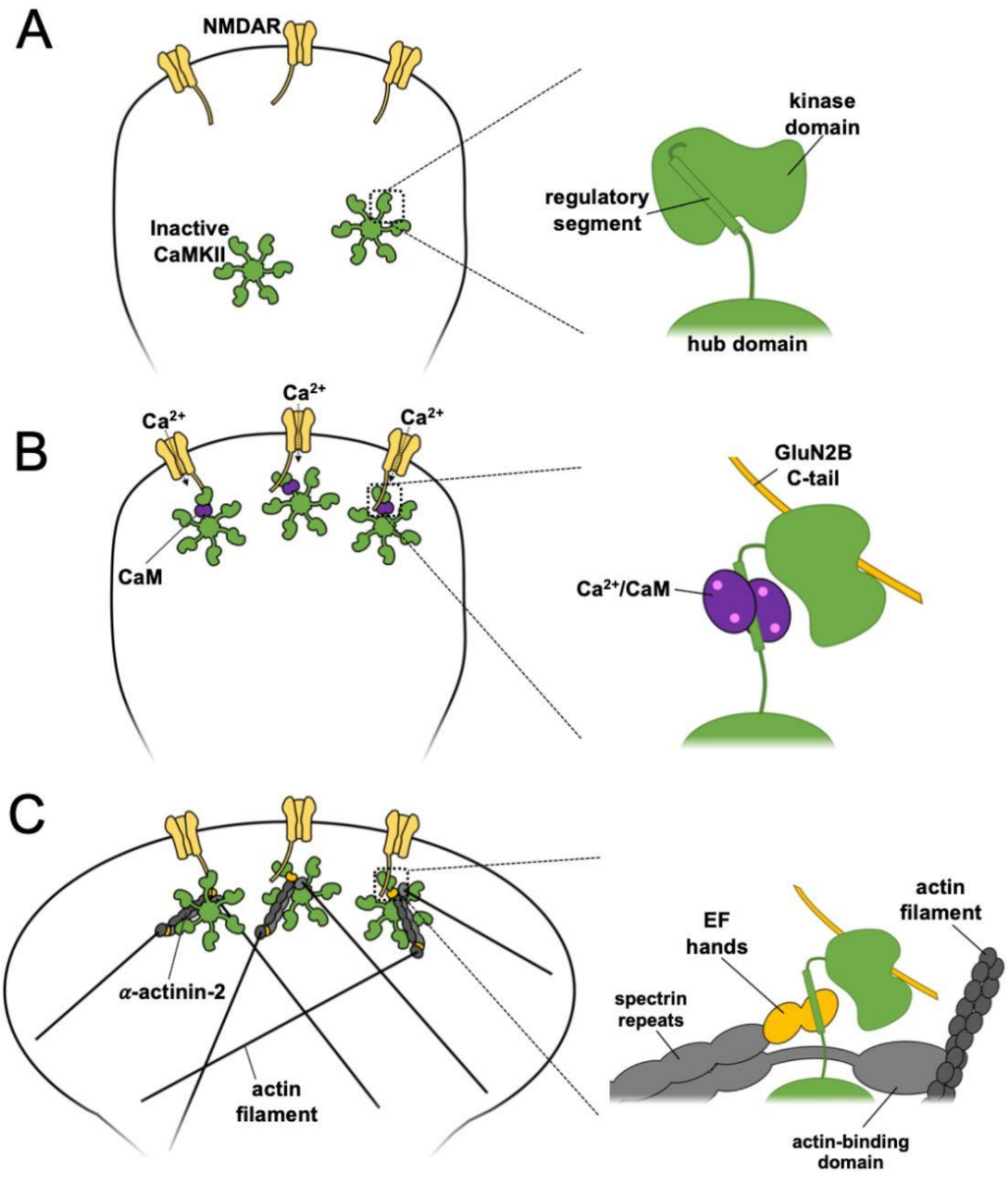

Figure 6.1 Updated model of actinin-CaMKII dynamics underlying sLTP. A three-stage model is presented with close-up illustrations on the right of each stage illustrating CaMKII protein interactions. **(A)** In naïve synapses prior to Ca^{2+} entry, the CaMKII regulatory segment is docked to the kinase domain and is largely inaccessible to α-actinin-2. **(B)** Ca^{2+} influx through NMDARs (yellow) sparks binding of Ca^{2+}/CaM (purple) to the regulatory segment, enabling the association of the kinase domain to the C-terminal tail of GluN2B (gold) subunits. **(C)** Following return of intracellular [Ca^{2+}] to baseline levels, Ca^{2+}/CaM dissociates whereas CaMKII-NMDAR interactions persist. This combination enables α-actinin-2 to dock to the kinase domain, thereby linking the kinase to the actin cytoskeleton in support of spine enlargement.

6.3 Caveats & Limitations

In this project I employed a chemically-induced LTP (cLTP) protocol to investigate the association of CaMKII with its interaction partners and their role in sLTP. While cLTP is suitable for potentiating synapses in bulk, it can be limited when investigating the temporal aspect of CaMKII association with its interaction partners. This should be particularly noted in PLA experiments to measure CaMKII-actinin association rate and investigating the effects of T286A on complex formation. Another method would be electrical stimulation protocols, however these protocols are not well suited to the biochemical approaches that I employed in this investigation. A caveat to the PLA experiments was the lack of endogenous protein knockdown, particularly in the case of GluN2B subunits. NMDARs assemble as tetramers (Hansen et al., 2018), therefore it is possible that the GluN2B-iHAΔCaMKII subunits expressed in neurons oligomerise with endogenous GluN2B subunits within a single NMDA receptor. While the data in this project were able to reveal difference in PLA puncta formation between WT and ΔCaMKII variants of GluN2B, these effects might be more pronounced in a GluN2B knock-down environment.

The data provided in this project infers that GluN2B docking onto the substrate binding groove of CaMKII kinase renders the regulatory segment accessible for α-actinin-2 binding. However, it is conceivable if not likely that other proteins that dock to the kinase domain of activated CaMKII serve a similar function. For example, both TIAM-1 and densin-180 associate with the CaMKII kinase domain following LTP induction (Özden et al., 2022). Future studies may investigate the notion that these proteins can also promote CaMKII-α-actinin-2 interactions in support of sLTP.

I attempted to understand the structural basis of CaMKII-GluN2B-α-actinin-2 assemblies with XL-MS. While I could identify cross-links between GluN2B and CaMKII, the full set of interlinks identified in these experiments was limited. This suggests that the three proteins may have not bound properly in our experimental conditions, or that the cross-linking conditions need to be optimised. One variable to consider is the presence of phosphatidylinositol 4,5-bisphosphate (PIP_2) which is known promote the exposure of EF hand motifs within α-actinin-2 dimers (Ribeiro et al., 2014) – this may be required to enable the EF hands to access CaMKII in the context of the full-length dimeric protein.

6.4. Future directions

To consolidate GluN2B's role in CaMKII-actinin interactions I would perform further PLA experiments in GluN2B KO (knock-out) primary hippocampal neurons transfected with GluN2B WT or ΔCaMKII. I would then perform PLA experiments to identify CaMKII-α-actinin-2 puncta. This experiment would provide direct evidence for the role of GluN2B in facilitating CaMKII-α-actinin-2 interactions in synapses.

The findings with CaMKIIα T305A/T306A mutant could be built upon with PLA experiments in neurons co-expressing the CaMKII mutant with GluN2B WT or ΔCaMKII. If PLA puncta are similar in both groups of neurons, it would suggest the binding of CaMKII T305A/T306A and α-actinin-2 is enhanced irrespective of GluN2B C-tail binding to the CaMKII kinase domain. The data in this project shows that CaMKII T305A/T306A triggers premature sLTP through an ability to bind α-actinin-2 tightly regardless of NMDAR activation so this mutant is not appropriate for investigating the role of CaMKII phosphorylation at these sites. It would be valuable if a less perturbing phospho-null CaMKII mutant could be identified. One way to go about this would be to screen the affinity of different phosphodeficient mutants for α-actinin-2 EF hand motifs and CaM to identify mutations that prevent phosphorylation but that do not alter the affinity of interactions with CaM or actinin. These mutations could then be taken forward for studies in neurons.

The project has focused on the structural consequence of CaMKII and α-actinin-2 interactions in LTP, however the physiological changes e.g. EPSPs of binding remains to be explored. One future direction could investigate the physiological effect of CaMKII and α-actinin-2 interactions on LTP through electrophysiological experiments performed on primary hippocampal neurons. Briefly endogenous α-actinin-2 could be knocked out and replaced with CaMKII binding deficient mutant or WT and the EPSP from LTP induction can be measured to probe the functional. While there is no clinical data from patients revealing mutations which affect CaMKII and α-actinin-2 complex formation, the experimentally designed α-actinin-2 L854R mutation can be used for a future study. Further work beyond confocal data presented and electrophysiological experiments suggested could be to examine the effect of the interaction on a behavioural level in mice.

Accurately conceptualising interactions between CaMKII interacting proteins in the PSD is complicated by the potential for cooperative interactions since many of the relevant proteins are oligomeric. For example, each protomeric EF hand motif in an α-actinin-2 dimer is spaced ~28 nm from each other (Ribeiro et al., 2014), while the maximum extended conformation of a CaMKII holoenzyme is ~ 35 nm in length (**Figure 6.2A**) (Myers et al., 2017). Therefore, there are two plausible modes of assembly (**Figure 6.2B**): a single actinin dimer can simultaneously bridge two regulatory segments within a CaMKII dodecamer, in a 'steering wheel lock' conformation (Hell, 2014); alternatively α-actinin-2, may radiate away from the holoenzyme to form an overall extended conformation (Robison et al., 2005b). Furthermore, NMDAR receptors themselves are spaced at regular intervals of ~ 30 nm in the PSD (Chen et al., 2008) – a similar scale to the width of CaMKII dodecamers and the length of α-actinin-2 dimers– raising the possibility of cooperative interactions spanning multiple receptors.

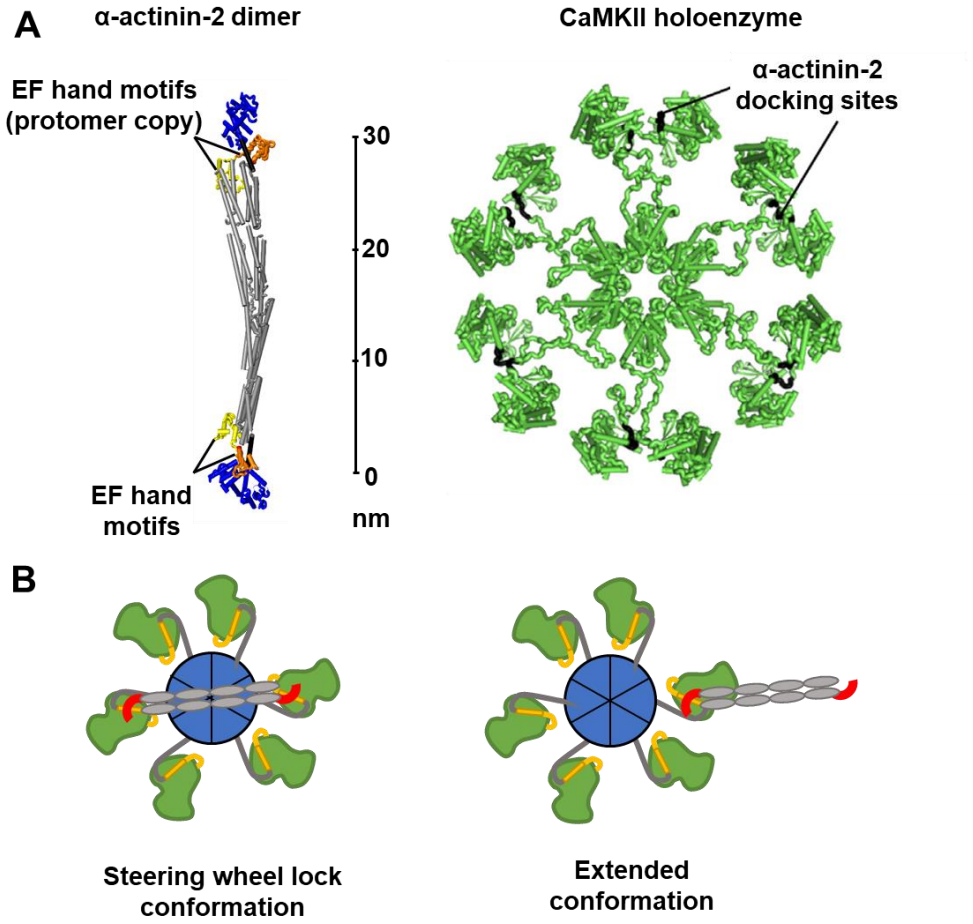

Figure 6.2 Potential higher order assemblies of α-actinin-2 and CaMKII. (A) The crystal structure of dimeric α-actinin-2 (PDB: 4D1E) is shown to scale alongside the most extended structural model of CaMKIIα to date, which was determined by cryo-EM (PDB ID 5U6Y). The EF hand motifs 1-2 (yellow), 3-4 (orange) and CaMKII regulatory region (black) are highlighted in both structures. **(B)** Two hypothetical models for the assembly of α-actinin-2 and CaMKII complexes. (left) α-actinin-2 can bridge a CaMKII holoenzyme in a steering wheel lock conformation or (right) α-actinin-2 can bridge away from CaMKII in an extended conformation.

Developments in techniques for *in situ* imaging including cryo-electron tomography (Van Den Hoek et al., 2022) will be required to resolve the extent to which cooperative interactions support the structure of potentiated dendritic spines. Furthermore, acquiring high-quality 2D images of CaMKII complexes assembled from purified proteins using negative-stain EM can be feasible. Images obtained from negative-stain-EM have a resolution ~2 nm. This resolution is appropriate for imaging CaMKII-α-actinin-2-GluN2B complexes given that the diameter of CaMKII is approximately ~35 nm, while the length of an α-actinin-2 dimer is ~28 nm.

Over the past decade, there has been significant progress and widespread adoption of the BioID (Proximity-dependent biotin identification) technique for the identification of native protein-protein interaction (Roux et al., 2012). This method utilises a mutated form *E.coli* biotin ligase BirA, which is capable of biotinylating proteins within a 10 nm radius (Kim et al., 2014). The protein of interest can therefore be fused with BioID to allow for the biotinylation of proximal or binding partners which can subsequently be isolated and identified through mass-spectrometry (Sears et al., 2019). Neurons transfected with BioID-α-actinin-2 and BioID-densin-180 could reveal important binding partners before or after LTP. This could aid the understanding of other CaMKII associated partners and mechanisms in synaptic potentiation.

6.5. Concluding statement

Synaptic plasticity is a process thought to be essential for information processing and storage in the brain. LTP is a major form of synaptic plasticity and is known to be mediated by central synaptic enzyme CaMKII. While the catalytic role of CaMKII has been well characterised, the multivalent interactions with its partners and their structural effect on synaptic morphology were less well understood. In this project, I showed how CaMKII-α-actinin-2 interactions contribute to sLTP and established how they interact at the molecular level. Additionally, I showed a commonly-used T305A/T306A variant of CaMKII is actually a gain-of-function binder of actinin, and the effects of this variant in neurons underscore the importance of actinin-CaMKII interactions in regulating spine morphology. Together these results clarify our understanding of LTP and contribute to a better understanding of synaptic plasticity in the brain.

References

Alam, M. (2018). Proximity Ligation Assay (PLA). Curr. Protoc. Immunol. *123*, e58.

Allison, D.W., Gelfand, V.I., Spector, I., and Craig, A.M. (1998). Role of Actin in Anchoring Postsynaptic Receptors in Cultured Hippocampal Neurons: Differential Attachment of NMDA versus AMPA Receptors. J. Neurosci. *18*, 2423–2436.

Apperson, M.L., Moon, I.S., and Kennedy, M.B. (1996). Characterization of densin-180, a new brain-specific synaptic protein of the O-sialoglycoprotein family. J. Neurosci. *16*, 6839–6852.

Araki, Y., Zeng, M., Zhang, M., and Huganir, R.L. (2015). Rapid Dispersion of SynGAP from Synaptic Spines Triggers AMPA Receptor Insertion and Spine Enlargement during LTP. Neuron *85*, 173–189.

Barcomb, K., Buard, I., Coultrap, S.J., Kulbe, J.R., O'Leary, H., Benke, T.A., and Bayer, K.U. (2014). Autonomous CaMKII requires further stimulation by Ca2+/ calmodulin for enhancing synaptic strength. FASEB J. *28*, 3810–3819.

Barcomb, K., Hell, J.W., Benke, T.A., and Bayer, K.U. (2016). The CaMKII / GluN2B Protein Interaction Maintains Synaptic strength. J. Biol. Chem.*291*, 16082–16089.

Barnes, S.J., Opitz, T., Merkens, M., Kelly, T., Von Der Brelie, C., Krueppel, R., and Beck, H. (2010). Stable mossy fiber long-term potentiation requires calcium influx at the granule cell soma, protein synthesis, and microtubule-dependent axonal transport. J. Neurosci. *30*, 12996–13004.

Barria, A., and Malinow, R. (2002). Subunit-Specific NMDA Receptor Trafficking to Synapses. Neuron *35*, 345–353.

Barria, A., Muller, D., Derkach, V., Griffith, L.C., and Soderling, T.R. (1997). Regulatory phosphorylation of AMPA-type glutamate receptors by CaM-KII during long-term potentiation. Science *276*, 2042–2045.

Bats, C., Groc, L., and Choquet, D. (2007). The Interaction between Stargazin and PSD-95 Regulates AMPA Receptor Surface Trafficking. Neuron *53*, 719–734.

Bayer, K.U. (2006). Transition from Reversible to Persistent Binding of CaMKII to Postsynaptic Sites and NR2B. J. Neurosci. *26*, 1164–1174.

Bayer, K.U., De Koninck, P., Leonard, A.S., Hell, J.W., and Schulman, H. (2001). Interaction with the NMDA receptor locks CaMKII in an active conformation. Nature *411*, 801–805.

Bear, M.F. (2003). Bidirectional synaptic plasticity: from theory to reality. Philos. Trans. R. Soc. Lond. B. Biol. Sci. *358*, 649–655.

Bers, D.., Patton, C.., and Nuccitelli, R. (2010). A practical guide to the preparation of Ca(2+) buffers. Method Celullar Biol. *99*, 1–26.

Bliss, T., and Lomo, T. (1973). Long-lasting potentiation of synaptic transmission in the dentate area of the anaesthetized rabbit following stimulation of the perforant path. J. Physiol. *232*, 331–356.

Buard, I., Coultrap, S.J., Freund, R.K., Lee, Y.S., Dell'Acqua, M.L., Silva, A.J., and Bayer, K.U. (2010). CaMKII "autonomy" is required for initiating but not for maintaining neuronal long-term information storage. J. Neurosci. *30*, 8214–8220.

Carlisle, H.J., Luong, T.N., Medina-Marino, A., Schenker, L., Khorosheva, E., Indersmitten, T., Gunapala, K.M., Steele, A.D., O'Dell, T.J., Patterson, P.H. (2011). Deletion of Densin-180 Results in Abnormal Behaviors Associated with Mental Illness and Reduces mGluR5 and DISC1 in the Postsynaptic Density Fraction. J. Neurosci. *31*, 16194–16207.

Chang, J.Y., Parra-Bueno, P., Laviv, T., Szatmari, E.M., Lee, S.J.R., and Yasuda, R. (2017). CaMKII Autophosphorylation Is Necessary for Optimal Integration of Ca2+ Signals during LTP Induction, but Not Maintenance. Neuron *94*, 800-808.e4.

Chang, J.Y., Nakahata, Y., Hayano, Y., and Yasuda, R. (2019). Mechanisms of Ca2+/calmodulin-dependent kinase II activation in single dendritic spines. Nat. Commun. *10*, 1–12.

Chao, L.H., Pellicena, P., Deindl, S., Barclay, L.A., Schulman, H., and Kuriyan, J. (2010). Intersubunit capture of regulatory segments is a component of cooperative CaMKII activation. Nat. Struct. Mol. Biol. *17*, 264–272.

Chao, L.H., Stratton, M.M., Lee, I.H., Rosenberg, O.S., Levitz, J., Mandell, D.J., Kortemme, T., Groves, J.T., Schulman, H., and Kuriyan, J. (2011). A mechanism for tunable autoinhibition in the structure of a human Ca 2+/calmodulin-dependent kinase II holoenzyme. Cell *146*, 732–745.

Chen, H.J., Rojas-Soto, M., Oguni, A., and Kennedy, M.B. (1998). A synaptic Ras-GTPase activating protein (p135 SynGAP) inhibited by CaM kinase II. Neuron *20*, 895–904.

Chen, X., Vinade, L., Leapman, R.D., Petersen, J.D., Nakagawa, T., Phillips, T.M., Sheng, M., and Reese, T.S. (2005). Mass of the postsynaptic density and enumeration of three key molecules. Proc. Natl. Acad. Sci. U. S. A. *102*, 11551–11556.

Chen, X., Winters, C., Azzam, R., Li, X., Galbraith, J. a, Leapman, R.D., and Reese, T.S. (2008). Organization of the core structure of the postsynaptic density. Proc. Natl. Acad. Sci. U. S. A. *105*, 4453–4458.

Cheng, D., Hoogenraad, C.C., Rush, J., Ramm, E., Schlager, M. a, Duong, D.M., Xu, P., Wijayawardana, S.R., Hanfelt, J., Nakagawa, T., et al. (2006). Relative and absolute quantification of postsynaptic density proteome isolated from rat forebrain and cerebellum. Mol. Cell. Proteomics *5*, 1158–1170.

Cobb, M. (2021). The idea of the brain: A history. Profile Books .Ltd.

Colbran, R.J., and Soderling, R. (1990a). Calcium / Calmodulin-independent Autophosphorylation Sites of Calcium / Calmodulin-dependent Autophosphorylation Protein Kinase II. J. Biol. Chem. *265*, 11213–11219.

Colbran, R.J., and Soderling, T.R. (1990b). Calcium/calmodulin-independent autophosphorylation sites of calcium/calmodulin-dependent protein kinase II. Studies on the effect of phosphorylation of threonine 305/306 and serine 314 on calmodulin binding using synthetic peptides. J. Biol. Chem. *265*, 11213–11219.

Collingridge, G., Kehl, S., and McLennan, H. (1983). Excitatory amino acids in synaptic transmission in the Schaffer collateral-commissural pathway of the rat hippocampus. J. Physiol. *334*, 33–46.

Costa, S., Almeida, A., Castro, A., and Domingues, L. (2014). Fusion tags for protein solubility , purification , and immunogenicity in Escherichia coli : the novel Fh8 system. *5*, 1–20.

Coultrap, S.J., Buard, I., Kulbe, J.R., Acqua, M.L.D., and Bayer, K.U. (2010). CaMKII Autonomy Is Substrate-dependent and Further Stimulated by Ca 2+/ Calmodulin. J. Biol. Chem. *285*, 17930–17937.

Curtis, A.J., Dowsell, R.S., and Gold, M.G. (2022). Assaying Protein Kinase A Activity Using a FRET-Based Sensor Purified from Mammalian Cells. In Methods in Molecular Biology, p. 15–31.

Dosemeci, A., Weinberg, R.J., Reese, T.S., and Tao-Cheng, J.-H. (2016). The Postsynaptic Density: There Is More than Meets the Eye. Front. Synaptic Neurosci. *8*, 1–8.

Dosemeci, A., Tao-Cheng, J.H., Loo, H., and Reese, T.S. (2018). Distribution of densin in neurons. PLoS One *13*, 1–11.

Dudek, S.M., and Bear, M.F. (1992). Homosynaptic long-term depression in area CA1 of hippocampus and effects of N-methyl-D-aspartate receptor blockade. Proc. Natl. Acad. Sci. *89*, 4363–4367.

Ehlers, M.D. (2000). Reinsertion or degradation of AMPA receptors determined by activity-dependent endocytic sorting. Neuron *28*, 511–525.

Elgersma, Y., Fedorov, N.B., Ikonen, S., Choi, E.S., Elgersma, M., Carvalho, O.M., Giese, K.P., and Silva, A.J. (2002). Inhibitory autophosphorylation of CaMKII controls PSD association, plasticity, and learning. Neuron *36*, 493–505.

Erondu, N.E., and Kennedy, M.B. (1985). Regional distribution of type II Ca2+/calmodulin-dependent protein kinase in rat brain. J. Neurosci. *5*, 3270–3277.

Feng, B., Raghavachari, S., and Lisman, J. (2011). Quantitative estimates of the cytoplasmic, PSD, and NMDAR-bound pools of CaMKII in dendritic spines. Brain Res. *1419*, 46–52.

Forest, A., Swulius, M.T., Tse, J.K.Y., Bradshaw, J.M., Gaertner, T., and Waxham, M.N. (2008). Role of the N- and C-lobes of calmodulin in the activation of Ca(2+)/calmodulin-dependent protein kinase II. Biochemistry *47*, 10587–10599.

Fortin, D.A., Davare, M.A., Srivastava, T., Brady, J.D., Nygaard, S., Derkach, V.A., and Soderling, T.R. (2010). Long-term potentiation-dependent spine enlargement requires synaptic Ca2+-permeable AMPA receptors recruited by CaM-kinase I. J. Neurosci. *30*, 11565–11575.

Fredriksson, S., Gullberg, M., Jarvius, J., Olsson, C., Pietras, K., Gústafsdóttir, S.M., Östman, A., and Landegren, U. (2002). Protein detection using proximity-dependent DNA Ligation Assays. Nat. Biotechnol. *20*, 473–477.

Gasteiger, E., Gattiker, A., Hoogland, C., Ivanyi, I., Appel, R.D., and Bairoch, A. (2003). ExPASy: The proteomics server for in-depth protein knowledge and analysis. Nucleic Acids Res. *31*, 3784–3788.

Giese, K.P., Fedorov, N.B., Filipkowski, R.K., and Silva, A.J. (1998). Autophosphorylation at Thr286 of the alpha calcium-calmodulin kinase II in LTP and learning. Science *279*, 870–873.

Gilles, J.F., Dos Santos, M., Boudier, T., Bolte, S., Heck, N., (2017). DiAna, an ImageJ tool for object-based 3D co-localization and distance analysis. Methods 115:55-64.

Gold, M.G. (2012). A frontier in the understanding of synaptic plasticity: Solving the structure of the postsynaptic density. BioEssays *34*, 599–608.

Gray, E. (1959). Electron Microscopy of Synaptic Contacts on Dendrite Spines of the Cerebral Cortex. Nature *183*, 1592–1593.

Halt, A.R., Dallapiazza, R.F., Zhou, Y., Stein, I.S., Qian, H., Juntti, S., Wojcik, S., Brose, N., Silva, A.J., and Hell, J.W. (2012). CaMKII binding to GluN2B is critical during memory consolidation. EMBO J. *31*, 1203–1216.

Hamilton, A.M., Oh, W.C., Vega-Ramirez, H., Stein, I.S., Hell, J.W., Patrick, G.N., and Zito, K. (2012). Activity-Dependent Growth of New Dendritic Spines Is Regulated by the Proteasome. Neuron *74*, 1023–1030.

Hansen, K.B., Yi, F., Perszyk, R.E., Furukawa, H., Wollmuth, L.P., Gibb, A.J., and Traynelis, S.F. (2018). Structure , function , and allosteric modulation of NMDA receptors. J. Gen. Physiol. *150*, 1081–1105.

Hanson, P.I., Meyer, T., Stryer, L., and Schulman, H. (1994). Dual role of calmodulin in autophosphorylation of multifunctional cam kinase may underlie decoding of calcium signals. Neuron *12*, 943–956.

Van Harreveld, A., and Fifkova, E. (1975). Swelling of dendritic spines in the fascia dentata after stimulation of the perforant fibers as a mechanism of post-tetanic potentiation. Exp. Neurol. *49*, 736–749.

Harris, K.M., Jensen, F.E., and Tsao, B. (1992). Three-dimensional structure of dendritic spines and synapses in rat hippocampus (CA1) at postnatal day 15 and adult ages: implications for the maturation of synaptic physiology and long-term potentiation. J. Neurosci. *12*, 2685–2705.

Hell, J.W. (2014). CaMKII: Claiming center stage in postsynaptic function and organization. Neuron *81*, 249–265.

Hodges, J.L., Vilchez, S.M., Asmussen, H., Whitmore, L.A., and Horwitz, A.R. (2014). alpha-Actinin-2 mediates spine morphology and assembly of the post-synaptic density in hippocampal neurons. PLoS One *9 (7): e101770.*

Hosokawa, T., Liu, P,W., Cai, Q., Ferreira, J,S., Levet, F., Butler, C., Sibarita, J,B., Choquet, D., Groc, Hosy, E., Zhang, M., Hayashi, Y. (2021). CaMKII activation persistently segregates postsynaptic proteins via liquid phase separation. Nat. Neur. 6: 777-785

Van Den Hoek, H., Klena, N., Jordan, M.A., Viar, G.A., Righetto, R.D., Schaffer, M., Erdmann, P.S., Wan, W., Geimer, S., Plitzko, J.M., et al. (2022). In situ architecture of the ciliary base reveals the stepwise assembly of intraflagellar transport trains. Science *548*, 543–548.

Huijstee, A.N. Van, and Mansvelder, H.D. (2015). Glutamatergic synaptic plasticity in the mesocorticolimbic system in addiction. Front. Cellular Neuroscience. *8*, 1–13.

Huttner, W., and Greengard, P. (1979). Multiple phosphorylation sites in protein I and their differential regulation by cyclic AMP and calcium. Proc. Natl. Acad. Sci. *76*, 5402–5406.

Jalan-Sakrikar, N., Bartlett, R.K., Baucum, A.J., and Colbran, R.J. (2012). Substrate-selective and calcium-independent activation of CaMKII by α-actinin. J. Biol. Chem. *287*, 15275–15283.

Jiao, Y., Jalan-Sakrikar, N., Robison, A.J., Baucum, A.J., Bass, M.A., and Colbran, R.J. (2011). Characterization of a central Ca2+/calmodulin-dependent protein kinase IIα/β binding domain in densin that selectively modulates glutamate receptor subunit phosphorylation. J. Biol. Chem. *286*, 24806–24818.

Kandel, E., Carew, T., and Castellucci, V. (1970). An Analysis of Dishabituation and Sensitization of The Gill-Withdrawal Reflex In Aplysia. Int. J. Neurosci. *2*, 79–98.

Kennedy, M.B., and Greengard, P. (1981). Two calcium/calmodulin-dependent protein kinases, which are highly concentrated in brain, phosphorylate protein I at distinct sites. Proc. Natl. Acad. Sci. *78*, 1293–1297.

Kim, D.I., Birendra, K.C., Zhu, W., Motamedchaboki, K., Doye, V., and Roux, K.J. (2014). Probing nuclear pore complex architecture with proximity-dependent biotinylation. Proc. Natl. Acad. Sci. U. S. A. *111*, 2453–2461.

Kojima, H., Rosendale, M., Sugiyama, Y., Hayashi, M., Horiguchi, Y., Yoshihara, T., Ikegaya, Y., Saneyoshi, T., and Hayashi, Y. (2019). The role of CaMKII-Tiam1 complex on learning and memory. Neurobiol. Learn. Mem. *166*, 107070.

Kuner, R., and Flor, H., (2016). Structural plasticity and reorganisation in chronic pain. Nat Rev Neurosci
18(1):20-30.

Kuret, J., and Schulman, H. (1985). Mechanism of autophosphorylation of the multifunctional Ca2+/calmodulin-dependent protein kinase. J. Biol. Chem. *260*, 6427–6433.

Lee, H.K., Kameyama, K., Huganir, R.L., and Bear, M. (1998). NMDA induces long-term synaptic depression and dephosphorylation of the GluR1 subunit of AMPA receptors in hippocampus. Neuron *21*. 1151-1162

Lee, S.J.R., Escobedo-Lozoya, Y., Szatmari, E.M., and Yasuda, R. (2009). Activation of CaMKII in single dendritic spines during long-term potentiation. Nature *458*, 299–304.

Leitner, A., Walzthoeni, T., Kahraman, A., Herzog, F., Rinner, O., Beck, M., and Aebersold, R. (2010). Probing native protein structures by chemical cross-linking, mass spectrometry, and bioinformatics. Mol. Cell. Proteomics *9*, 1634–1649.

Leonard, A.S., Lim, I.A., Hemsworth, D.E., Horne, M.C., and Hell, J.W. (1999). Calcium/calmodulin-dependent protein kinase II is associated with the N-methyl-D-aspartate receptor. Proc. Natl. Acad. Sci. U. S. A. *96*, 3239–3244.

Lin, D.T., Makino, Y., Sharma, K., Hayashi, T., Neve, R., Takamiya, K., and Huganir, R.L. (2009). Regulation of AMPA receptor extrasynaptic insertion by 4.1N, phosphorylation and palmitoylation. Nat. Neurosci. *12*, 879–887.

Liu, D.C., Jow, G.M., Chuang, C.C., Peng, Y.J., Hsu, P.H., and Tang, C.Y. (2013). Densin-180 is Not a Transmembrane Protein. Cell Biochem. Biophys. *67*, 773–783.

Lu, W.Y., Man, H.Y., Ju, W., Trimble, W.S., MacDonald, J.F., and Wang, Y.T. (2001). Activation of synaptic NMDA receptors induces membrane insertion of new AMPA receptors and LTP in cultured hippocampal neurons. Neuron *29*, 243–254.

Lynch, G., Larson, J., Kelson, S., Barrinuevo, G., and Schottler, F. (1983). Intracellular injections of EGTA block induction of hippocampal long-term potentiation. Nature *305*, 719–721.

Mahan, A.L., and Ressler, K.J. (2012). Fear conditioning , synaptic plasticity and the amygdala : implications for posttraumatic stress disorder. Trends Neurosci. *35*, 24–35.

Malinow, R., Schulman, H., and Tsien, R.W. (1989). Inhibition of postsynaptic PKC or CaMKII blocks induction but not expression of LTP. Science *245*, 862–866.

Mammen, A.L., Kameyama, K., Roche, K.W., and Huganir, R.L. (1997). Phosphorylation of the α-amino-3-hydroxy-5-methylisoxazole-4-propionic Acid receptor GluR1 subunit by calcium/calmodulin-dependent kinase II. J. Biol. Chem. *272*, 32528–32533.

Marcora, E., Carlisle, H.J., and Kennedy, M.B. (2007). The role of the postsynaptic density and the spine cytoskeleton in synaptic plasticity. Learn. Mem. A Compr. Ref. 649–673.

Markram, H., Lübke, J., Frotscher, M., and Sakmann, B. (1997). Regulation of synaptic efficacy by coincidence of postsynaptic APs and EPSPs. Science *275*, 213–215.

Masaki, T., Endo, M., and Ebashi, S. (1967). Localization of 6S component of a alpha-actinin at Z-band. J. Biol. Chem. *62*, 630–632.

Matsuzaki, M., Honkura, N., Ellis-Davies, C.R.., and Kasai, H. (2004). Structural basis of long-term potentiation in single dendritic spines. Nature *429*, 761–766.

Matt, L., Kim, K., Hergarden, A.C., Patriarchi, T., Malik, Z.A., Park, D.K., Chowdhury, D., Buonarati, O.R., Henderson, P.B., Gökçek Saraç, Ç. (2018). α-Actinin Anchors PSD-95 at Postsynaptic Sites. Neuron *97*, 1094-1109.e9.

McBain, C.., and Mayer, M.. (1994). N-Methyl-D-Aspartic Acid Receptor Structure. Physiol. Rev. *74*, 723-760

McLeod, F., Bossio, A., Marzo, A., Ciani, L., Sibilla, S., Hannan, S., Wilson, G.A., Palomer, E., Smart, T.G., Gibb, A., et al. (2018). Wnt Signaling Mediates LTP-Dependent Spine Plasticity and AMPAR Localization through Frizzled-7 Receptors. Cell Rep. *23*, 1060–1071.

Merkley, E.D., Rysavy, S., Kahraman, A., Hafen, R.P., Daggett, V., and Adkins, J.N. (2014). Distance restraints from crosslinking mass spectrometry: Mining a molecular dynamics simulation database to evaluate lysine-lysine distances. Protein Sci. *23*, 747–759.

Miller, S.G., and Kennedy, M.B. (1985). Distinct forebrain and cerebellar isozymes of type II Ca2+/calmodulin-dependent protein kinase associate differently with the postsynaptic density fraction. J. Biol. Chem. *260*, 9039–9046.

Miller, S.., Patton, B.L., and Kennedy, M.B. (1988). Sequences in autophosphorylation sites in neuronal type II CaM kinase that controls Ca2+ independent activity. Cell *1*, 593–604.

Morris, R.G.., Davis, S., and Butcher, S.. (1990). Hippocampal synaptic plasticity and NMDA receptors: a role in information storage? Philos. Trans. R. Soc. Lond. B. Biol. Sci. *329*, 187–204.

Myers, J.B., Zaegel, V., Coultrap, S.J., Miller, A.P., Bayer, K.U., and Reichow, S.L. (2017). The CaMKII holoenzyme structure in activation-competent conformations. Nat. Commun. *8*, 1–14.

Nakagawa, T., Engler, J., and Sheng, M. (2004). The dynamic turnover and functional roles of alpha-actinin in dendritic spines. Neuropharmacology *47*, 734–745.

O'Leary, H., Lasda, E., and Bayer, K.-U. (2006). CaMKIIbeta Association with the Actin Cytoskeleton Is Regulated by Alternative Splicing. Mol. Biol. Cell *17*, 4656–4665.

Oh, J.S., Manzerra, P., and Kennedy, M.B. (2004). Regulation of the Neuron-specific Ras GTPase-activating Protein, synGAP, by Ca2+/Calmodulin-dependent Protein Kinase II. J. Biol. Chem. *279*, 17980–17988.

Okabe, S. (2007). Molecular anatomy of the postsynaptic density. Mol. Cell. Neurosci. *34*, 503–518.

Okamoto, K.I., Narayanan, R., Lee, S.H., Murata, K., and Hayashi, Y. (2007). The role of CaMKII as an F-actin-bundling protein crucial for maintenance of dendritic spine structure. Proc. Natl. Acad. Sci. U. S. A. *104*, 6418–6423.

Opazo, P., Labrecque, S., Tigaret, C.M., Frouin, A., Wiseman, P.W., De Koninck, P., and Choquet, D. (2010). CaMKII triggers the diffusional trapping of surface AMPARs through phosphorylation of stargazin. Neuron *67*, 239–252.

Özden, C., Sloutsky, R., Mitsugi, T., Santos, N., Agnello, E., Gaubitz, C., Foster, J., Lapinskas, E., Esposito, E.A., Saneyoshi, T., et al. (2022). CaMKII binds both substrates and activators at the active site. Cell Rep. *40*, 1–14.

Palay, S.L., and Palade, G.E. (1955). The fine structure of neurons. J. Biophys. Biochem. Cytol. *1*, 69–88.

Patel, N., Stengel, F., Aebersold, R., and Gold, M.G. (2017). Molecular basis of AKAP79 regulation by calmodulin. Nat. Commun. *8*, 1681.

Patton, B.L., Miller, S.G., and Kennedy, M.B. (1990). Activation of type II calcium/calmodulin-dependent protein kinase by Ca2+/calmodulin is inhibited by autophosphorylation of threonine within the calmodulin-binding domain. J. Biol. Chem. *265*, 11204–11212.

Payne, M.., and Sorderling, T.. (1980). Calmodulin-dependent Glycogen Synthase Kinase. J. Biol. Chem. *255*, 8054–8056.

Penny, C.J., and Gold, M.G. (2018). Mechanisms for localising calcineurin and CaMKII in dendritic spines. Cell. Signal. *49*, 46–58.

Pettit, D.L., Perlman, S., and Malinow, R. (1994). Potentiated transmission and prevention of further LTP by increased CaMKII activity in postsynaptic hippocampal slice neurons. Science *266*, 1881–1885.

Pi, H.J., Otmakhov, N., Lemelin, D., De Koninck, P., and Lisman, J. (2010). Autonomous CaMKII Can Promote either Long-Term Potentiation or Long-Term Depression, Depending on the State of T305/T306 Phosphorylation. J. Neurosci. *30*, 8704–8709.

Putkey, J.A., and Waxham, M.N. (1996). A peptide model for calmodulin trapping by calcium/calmodulin-dependent protein kinase II. J. Biol. Chem. *271*, 29619–29623.

Quitsch, A. (2005). Postsynaptic Shank Antagonizes Dendrite Branching Induced by the Leucine-Rich Repeat Protein Densin-180. J. Neurosci. *25*, 479–487.

Ramon y Cajal, S. La fine structure des centres nerveux. Croonian Lecture Delivered at the Royal Society of London, 8th March 1894.

Rellos, P., Pike, A.C.W., Niesen, F.H., Salah, E., Lee, W.H., von Delft, F., and Knapp, S. (2010). Structure of the CaMKIIδ/calmodulin complex reveals the molecular mechanism of CamKII kinase activation. PLoS Biol. *8* (7): e1000426

Ribeiro, E.D.A., Pinotsis, N., Ghisleni, A., Salmazo, A., Konarev, P. V., Kostan, J., Sjöblom, B., Schreiner, C., Polyansky, A.A., Gkougkoulia, E.A., et al. (2014). The structure and regulation of human muscle α-Actinin. Cell *159*, 1447–1460.

Rinner, O., Seebacher, J., Walzthoeni, T., Mueller, L., Beck, M., Schmidt, A., Mueller, M., and Aebersold, R. (2008). Identification of cross-linked peptides from large sequence databases. Nat. Methods *5*, 315–318.

Robison, a J., Bartlett, R.K., Bass, M. a, and Colbran, R.J. (2005a). Differential modulation of Ca2+/calmodulin-dependent protein kinase II activity by regulated interactions with N-methyl-D-aspartate receptor NR2B subunits and alpha-actinin. J. Biol. Chem. *280*, 39316–39323.

Robison, A.J., Bass, M.A., Jiao, Y., MacMillan, L.B., Carmody, L.C., Bartlett, R.K., and Colbran, R.J. (2005b). Multivalent interactions of calcium/calmodulin-dependent protein kinase II with the postsynaptic density proteins NR2B, densin-180, and ??-actinin-2. J. Biol. Chem. *280*, 35329–35336.

Roux, K.J., Kim, D.I., Raida, M., and Burke, B. (2012). A promiscuous biotin ligase fusion protein identifies proximal and interacting proteins in mammalian cells. J. Cell Biol. *196*, 801–810.

Saneyoshi, T., Matsuno, H., Suzuki, A., Murakoshi, H., Hedrick, N.G., Agnello, E., O'Connell, R., Stratton, M.M., Yasuda, R., and Hayashi, Y. (2019a). Reciprocal Activation within a Kinase-Effector Complex Underlying Persistence of Structural LTP. Neuron *102*, 1199-1210.e6.

Saneyoshi, T., Hitomi Matsuno, H., Suzuki, A., Murakoshi, H., Hedrick, N.G., Agnello, E., O'Connell, R., Stratton, M.M., Yasuda, R., and Hayashi, Y. (2019b). Reciprocal Activation within a Kinase-Effector Complex Underlying Persistence of Structural LTP Article Reciprocal Activation within a Kinase-Effector Complex Underlying Persistence of Structural LTP. Neuron *102*, 1199–1210.

Sanhueza, M., German Fernandez-Villalobos, I.S.S., Kasumova, G., Zhang, P., Bayer, K.U., Otmakhov, N., Hell, J.W., and Lisman, J. (2011). Role of the CaMKII/NMDA-receptor complex in the maintenance of synaptic strength. J Neurosci *31*, 9170–9178.

Savitsky, P., Bray, J., Cooper, C.D.O., Marsden, B.D., Mahajan, P., Burgess-brown, N.A., and Gileadi, O. (2010). High-throughput production of human proteins for crystallization : The SGC experience. J. Struct. Biol. *172*, 3–13.

Schulman, H., and Greengard, P. (1978a). Stimulation of brain membrane protein phosphorylation by calcium and an endogenous heat-stable protein. Nature;Biology,Physico-Chemical *271*, 478–479.

Schulman, H., and Greengard, P. (1978b). Ca2 + -dependent protein phosphorylation system in membranes from various tissues , and its activation by " calcium-dependent regulator ". Proc. Natl. Acad. Sci. *75*, 5432–5436.

Scoville, W.B., and Milner, B. (1957). Loss of recent memory after bilateral hippocampal lesions. J. Neuropsychiatry Clin. Neurosci. *12*, 103–113.

Sears, R.., May, D.., and Roux, K.. (2019). BioID as a Tool for Protein-Proximity Labeling in Living Cells. Methods Mol Biol. 2019:299-313

Shen, K., and Meyer, T. (1999). Dynamic control of caMKII translocation and localization in hippocampal neurons by NMDA receptor stimulation. Science *284*, 162–166.

Shen, K., Teruel, M.N., Connor, J.H., Shenolikar, S., and Meyer, T. (2000). Molecular memory by reversible translocation of calcium/calmodulin-dependent protein kinase II. Nat. Neurosci. *3*, 881–886.

Silva, A.J., Stevens, C.F., Tonegawa, S., and Wang, Y. (1992). Deficient hippocampal long-term potentiation in α-calcium-calmodulin kinase II mutant mice. Science *257*, 201–206.

Singla, S.I., Hudmon, A., Goldberg, J.M., Smith, J.L., and Schulman, H. (2001). Molecular Characterization of Calmodulin Trapping by Calcium / Calmodulin-dependent Protein Kinase II . J. Biol. Chem. *276*, 29353–29360.

Sjöblom, B., Salmazo, A., and Djinović-Carugo, K. (2008). α-Actinin structure and regulation. Cell. Mol. Life Sci. *65*, 2688–2701.

Sloutsky, R., Dziedzic, N., Dunn, M.J., Bates, R.M., Torres-ocampo, A.P., Boopathy, S., Page, B., Weeks, J.G., Chao, L.H., and Stratton, M.M. (2020). Heterogeneity in human hippocampal CaMKII transcripts reveals allosteric hub-dependent regulation. Sci. Signal. *0240*, 1–13.

Spacer, J., and Harris, K.M. (1998). Three-dimensional organization of cell adhesion junctions at synapses and dendritic spines in area CA1 of the rat hippocampus. J. Comp. Neurol. *393*, 58–68.

Strack, S., and Colbran, R.J. (1998). Autophosphorylation-dependent targeting of calcium/ calmodulin-dependent protein kinase II by the NR2B subunit of the N-methyl-D-aspartate receptor. J. Biol. Chem. *273*, 20689–20692.

Strack, S., McNeill, R.B., and Colbran, R.J. (2000a). Mechanism and regulation of calcium/calmodulin-dependent protein kinase II targeting to the NR2B subunit of the N-methyl-D-aspartate receptor. J. Biol. Chem. *275*, 23798–23806.

Strack, S., Robison, A.J., Bass, M.A., and Colbran, R.J. (2000b). Association of Calcium /Calmodulin- dependent Kinase II with Developmentally Regulated Splice Variants of the. J. Biol. Chem. *275*, 25061–25064.

Studier, F.W. (2005). Protein production by auto-induction in high density shaking cultures. Protein Expr. Purif. *41*, 207–234.

Tao-Cheng, J.H. (2020). Activity-dependent redistribution of CaMKII in the postsynaptic compartment of hippocampal neurons. Mol. Brain *13*, 1–9.

Thalhammer, A., Trinidad, J.C., Burlingame, A.L., and Schoepfer, R. (2009). Densin-180: Revised membrane topology, domain structure and phosphorylation status. J. Neurochem. *109*, 297–302.

Tombes, M.., Omar Faison, M., and Turbeville, J.. (2003). Organization and evolution of multifunctional Ca2+/CaM-dependent protein kinase genes. Gene *322*, 17–31.

Vest, R.S., Davies, K.D., O'Leary, H., Port, D.J., and Bayer, K.U. (2007). Dual Mechanism of a natural CaMKII Inhibitor. Mol. Biol. Cell *18*, 5024–5033.

Villers, A., Giese, K.P., and Ris, L. (2014). Long-term potentiation can be induced in the CA1 region of hippocampus in the absence of αCaMKII T286-autophosphorylation. Learn. Mem. *21*.(11):616–626.

Walikonis, R.S., Oguni, A., Khorosheva, E.M., Jeng, C.J., Asuncion, F.J., and Kennedy, M.B. (2001). Densin-180 forms a ternary complex with the (alpha)-subunit of Ca2+/calmodulin-dependent protein kinase II and (alpha)-actinin. J. Neurosci. *21*, 423–433.

Walkup, W.G., Washburn, L., Sweredoski, M.J., Carlisle, H.J., Graham, R.L., Hess, S., and Kennedy, M.B. (2015). Phosphorylation of synaptic GTPase-activating protein (synGAP) by Ca2+/Calmodulin-dependent protein kinase II (CaMKII) and cyclin-dependent kinase 5 (CDK5) alters the ratio of its GAP activity toward ras and rap GTPases. J. Biol. Chem. *290*, 4908–4927.

Wang, H., Ardiles, A.O., Yang, S., Tran, T., Posada-duque, R., Valdivia, G., Baek, M., Chuang, Y., Palacios, X.A.G., Gallagher, X.M., et al. (2016). Metabotropic Glutamate Receptors Induce a Form of LTP Controlled by Translation and Arc Signaling in the Hippocampus. *36*, 1723–1729.

Wang, Q., Chen, M., Schafer, N.P., Bueno, C., Song, S.S., Hudmon, A., Wolynes, P.G., Neal Waxham, M., and Cheung, M.S. (2019). Assemblies of calcium/calmodulin-dependent kinase II with actin and their dynamic regulation by calmodulin in dendritic spines. Proc. Natl. Acad. Sci. U. S. A. *116*, 18937–18942.

Waxham, M.N., Tsai, A.L., and Putkey, J.A. (1998). A mechanism for calmodulin (CaM) trapping by CaM-kinase II defined by a family of CaM-binding peptides. J. Biol. Chem. *273*, 17579–17584.

Wyszynski, M., Lin, J., Rao, A., Nigh, E., Beggst, A.H., Craig, A.M., and Sheng, M. (1997). Competitive binding of a-actinin and calmodulin to the NMDA receptor. Nature *2*, 439–442.

Yamagata, Y., Kobayashi, S., Umeda, T., Inoue, A., Sakagami, H., Fukaya, M., Watanabe, M., Hatanaka, N., Totsuka, M., Yagi, T., et al. (2009). Kinase-dead knock-in mouse reveals an essential role of kinase activity of Ca2+/calmodulin-dependent protein kinase IIα in dendritic spine enlargement, long-term potentiation, and learning. J. Neurosci. *29*, 7607–7618.

Yamauchi, T., and Fujisawa, H. (1981). A calmodulin-dependent protein kinase that is involved in the activation of tryptophan 5-monooxygenase is specifically distributed in brain tissues. FEBS Lett. *129*, 117–119.

Yasuda, R., Hayashi, Y., and Hell, J.W. (2022). CaMKII: a central molecular organizer of synaptic plasticity, learning and memory. Nat. Rev. Neurosci. *23*, 666–682.

Young, P., and Gautel, M. (2000). The interaction of titin and alpha-actinin is controlled by a phospholipid-regulated intramolecular pseudoligand mechanism. EMBO J. *19*, 6331–6340.

Zalcman, M., Federman, N., Romano, A., (2018). CaMKII isoforms in learning and memory: Localization and function. Front. Mol. Neur. 11, e445

Zhou, Q., Homma, K.J., and Poo, M.M. (2004). Shrinkage of dendritic spines associated with long-term depression of hippocampal synapses. Neuron *44*, 749–757.

Zhu, J.J.J., Qin, Y., Zhao, M., Van Aelst, L., Malinow, R., Antonarakis, S.., Aelst, L. Van, Benke, T.., Luthi, A., Isaac, J.., et al. (2002). Ras and Rap Control AMPA Receptor Trafficking during Synaptic Plasticity. Cell *110*, 443–455.

Appendix

Supplementary table 1. Full table of interlinks identified in XL-MS experiments with CaMKII-GluN2B-actinin. Note absolute position of proteins include also include their affinity tag and cleavage residues.

Sequence Id	Protein1	Protein2	XLType	AbsPos1	AbsPos2	ld-Score	FDR
FHKIANVNK-LLKHPNIVR-a3-b3	α-actinin-2	CaMKII	interlink	110	75	38.94	0
FHKIANVNK-LLKHPNIVR-a3-b3	α-actinin-2	CaMKII	interlink	110	75	26.42	0.167
YPQSPTNSKAQK-FHKIANVNK-a9-b3	GluN2B	α -actinin-2	interlink	32	110	28.21	0.182
YPQSPTNSKAQK-FHKIANVNK-a9-b3	GluN2B	α-actinin-2	interlink	32	110	32.42	0
ALVTNKPVVSALHGAVPGR-KTAPYR-a6-b1	GluN2B	α-actinin-2	interlink	169	178	25.03	0.182
ALVTNKPVVSALHGAVPGR-KTAPYR-a6-b1	GluN2B	α-actinin-2	interlink	169	178	21.88	0.3
QPTVAGASKTRPDFR-LKGAAVK-a9-b2	GluN2B	CaMKII	interlink	157	155	25.44	0.25
QPTVAGASKTRPDFR-LKGAAVK-a9-b2	GluN2B	CaMKII	interlink	157	155	26.75	0.182
QPTVAGASKTRPDFR-LKGAAVK-a9-b2	GluN2B	CaMKII	interlink	157	155	20.96	0.3
YPQSPTNSKAQK-LKGAAVK-a9-b2	GluN2B	CaMKII	interlink	32	155	24.98	0.182
YPQSPTNSKAQK-LKGAAVK-a9-b2	GluN2B	CaMKII	interlink	32	155	20.9	0.3
QPTVAGASKTRPDFR-DHQKLER-a9-b4	GluN2B	CaMKII	interlink	157	63	25.63	0.25
QPTVAGASKTRPDFR-DHQKLER-a9-b4	GluN2B	CaMKII	interlink	157	63	26.31	0.182
QPTVAGASKTRPDFR-DHQKLER-a9-b4	GluN2B	CaMKII	interlink	157	63	29.04	0.167
DHQKLER-SVSLKDK-a4-b5	CaMKII	GluN2B	interlink	63	68	24.67	0.182
DHQKLER-SVSLKDK-a4-b5	CaMKII	GluN2B	interlink	63	68	32.19	0

QPTVAGASKTRPDFR-LLKHPNIVR-a9-b3	GluN2B	CaMKII	interlink	157	75	32.01	0
QPTVAGASKTRPDFR-LLKHPNIVR-a9-b3	GluN2B	CaMKII	interlink	157	75	27.56	0.182
QPTVAGASKTRPDFR-LLKHPNIVR-a9-b3	GluN2B	CaMKII	interlink	157	75	23.9	0.286
YPQSPTNSKAQK-LLKHPNIVR-a9-b3	GluN2B	CaMKII	interlink	32	75	21.83	0.333
YPQSPTNSKAQK-LLKHPNIVR-a9-b3	GluN2B	CaMKII	interlink	32	75	20.31	0.385
YPQSPTNSKAQK-LLKHPNIVR-a9-b3	GluN2B	CaMKII	interlink	32	75	28.45	0.167

Supplementary table 2. Full table of intralinks identified in XL-MS experiments with CaMKII-GluN2B-actinin. Note absolute position of proteins include also include their affinity tag and cleavage residues.

Sequence Id	Protein1	Protein2	XLType	AbsPos1	AbsPos2	ld-Score	FDR
ALDYIASKGVKLVSIGAEEIVDGNVK-K8-K11	α-actinin-2	-	intralink	124	127	26.91	0
ALDYIASKGVKLVSIGAEEIVDGNVK-K8-K11	α-actinin-2	-	intralink	124	127	35.13	0
ASTHETWAYGKEQILLQKDYESASLTEVR-K11-K18	α-actinin-2	-	intralink	434	441	37.38	0
ASTHETWAYGKEQILLQKDYESASLTEVR-K11-K18	α-actinin-2	-	intralink	434	441	47.81	0
ASTHETWAYGKEQILLQKDYESASLTEVR-K11-K18	α-actinin-2	-	intralink	434	441	41.73	0
DLINKMLTINPSKR-K5-K13	CaMKII	-	intralink	257	265	29.58	0
DLINKMLTINPSKR-K5-K13	CaMKII	-	intralink	257	265	29.47	0
DLINKMLTINPSKR-K5-K13	CaMKII	-	intralink	257	265	34.86	0
QETVDCLKKFNAR-K8-K9	CaMKII	-	intralink	298	299	42.4	0
QETVDCLKKFNAR-K8-K9	CaMKII	-	intralink	298	299	38.73	0
QETVDCLKKFNAR-K8-K9	CaMKII	-	intralink	298	299	36.66	0
KLKGAILTTMLATR-K1-K3	CaMKII	-	intralink	305	307	39.31	0
KLKGAILTTMLATR-K1-K3	CaMKII	-	intralink	305	307	39.01	0
KLKGAILTTMLATR-K1-K3	CaMKII	-	intralink	305	307	38.87	0
KNDGVKESSESTNTTIEDEDTK-K1-K6	CaMKII	-	intralink	330	335	28.53	0
KQEIIKVTEQLIEAISNGDFESYTK-K1-K6	CaMKII	-	intralink	354	359	28.52	0

KQEIIKVTEQLIEAISNGDFESYTK-K1-K6	CaMKII	-	intralink	354	359	31.24	0
KQEIIKVTEQLIEAISNGDFESYTK-K1-K6	CaMKII	-	intralink	354	359	31.84	0
FQKDICIGNQSNPCVPNNKNPR-K3-K19	GluN2B	-	intralink	185	201	20.88	0
FQKDICIGNQSNPCVPNNKNPR-K3-K19	GluN2B	-	intralink	185	201	28.82	0
FQKDICIGNQSNPCVPNNKNPR-K3-K19	GluN2B	-	intralink	185	201	20.28	0
VFDKDGNGYISAAELRHVMTNLGEK-K4-K25	calmodulin	-	intralink	95	116	28.05	0
VFDKDGNGYISAAELRHVMTNLGEK-K4-K25	calmodulin	-	intralink	95	116	28.06	0
VFDKDGNGYISAAELRHVMTNLGEK-K4-K25	calmodulin	-	intralink	95	116	29.93	0
EAFSLFDKDGDGTITTKELGTVMR-K8-K17	calmodulin	-	intralink	22	31	33.1	0
EAFSLFDKDGDGTITTKELGTVMR-K8-K17	calmodulin	-	intralink	22	31	33.75	0
EAFSLFDKDGDGTITTKELGTVMR-K8-K17	calmodulin	-	intralink	22	31	31.97	0
FHKIANVNK-LPKPDR-a3-b3	α-actinin-2	α-actinin-2	intralink	110	100	40.01	0
FHKIANVNK-LPKPDR-a3-b3	α-actinin-2	α-actinin-2	intralink	110	100	38.03	0.016
FHKIANVNK-LPKPDR-a3-b3	α-actinin-2	α-actinin-2	intralink	110	100	40.86	0
IANVNKALDYIASK-LPKPDR-a6-b3	α-actinin-2	α-actinin-2	intralink	116	100	38.01	0
IANVNKALDYIASK-LPKPDR-a6-b3	α-actinin-2	α-actinin-2	intralink	116	100	37.28	0.016
IANVNKALDYIASK-LPKPDR-a6-b3	α-actinin-2	α-actinin-2	intralink	116	100	38.53	0
KAGTQIENIEEDFR-LPKPDR-a1-b3	α-actinin-2	α-actinin-2	intralink	68	100	35.66	0
KAGTQIENIEEDFR-LPKPDR-a1-b3	α-actinin-2	α-actinin-2	intralink	68	100	33.22	0.016
KAGTQIENIEEDFR-LPKPDR-a1-b3	α-actinin-2	α-actinin-2	intralink	68	100	32.08	0
TPEKTMQAMQK-FHKIANVNK-a4-b3	α-actinin-2	α-actinin-2	intralink	325	110	32.8	0.016
TPEKTMQAMQK-FHKIANVNK-a4-b3	α-actinin-2	α-actinin-2	intralink	325	110	30.61	0
FHKIANVNK-KHKPPK-a3-b1	α-actinin-2	α-actinin-2	intralink	110	343	33.64	0

FHKIANVNK-KHKPPK-a3-b1	α-actinin-2	α-actinin-2	intralink	110	343	28.54	0.032
FHKIANVNK-KHKPPK-a3-b1	α-actinin-2	α-actinin-2	intralink	110	343	27.29	0.044
FHKIANVNK-KHKPPK-a3-b3	α-actinin-2	α-actinin-2	intralink	110	345	32.1	0.023
FHKIANVNK-KHKPPK-a3-b3	α-actinin-2	α-actinin-2	intralink	110	345	30.1	0
FHKIANVNK-TKWDKVK-a3-b5	α-actinin-2	α-actinin-2	intralink	110	627	29.6	0
FHKIANVNK-TKWDKVK-a3-b5	α-actinin-2	α-actinin-2	intralink	110	627	32.15	0.023
FHKIANVNK-TKWDKVK-a3-b5	α-actinin-2	α-actinin-2	intralink	110	627	32.18	0
ELPPDQAQYCIKR-FHKIANVNK-a12-b3	α-actinin-2	α-actinin-2	intralink	878	110	20.25	0.058
ELPPDQAQYCIKR-FHKIANVNK-a12-b3	α-actinin-2	α-actinin-2	intralink	878	110	26.57	0.037
ICKVLAVNQENER-ALDYIASKGVK-a3-b8	α-actinin-2	α-actinin-2	intralink	285	124	22.87	0.033
ICKVLAVNQENER-ALDYIASKGVK-a3-b8	α-actinin-2	α-actinin-2	intralink	285	124	34.92	0.016
ICKVLAVNQENER-ALDYIASKGVK-a3-b8	α-actinin-2	α-actinin-2	intralink	285	124	25.67	0.068
ICKVLAVNQENER-KTAPYR-a3-b1	α-actinin-2	α-actinin-2	intralink	285	178	50.86	0
ICKVLAVNQENER-KTAPYR-a3-b1	α-actinin-2	α-actinin-2	intralink	285	178	53.43	0
ICKVLAVNQENER-KTAPYR-a3-b1	α-actinin-2	α-actinin-2	intralink	285	178	50.76	0
CQLEINFNTLQTKLR-KTAPYR-a13-b1	α-actinin-2	α-actinin-2	intralink	365	178	24.24	0.067
CQLEINFNTLQTKLR-KTAPYR-a13-b1	α-actinin-2	α-actinin-2	intralink	365	178	29.63	0
DAKGITQEQMNEFR-KTAPYR-a3-b1	α-actinin-2	α-actinin-2	intralink	762	178	29.81	0
DAKGITQEQMNEFR-KTAPYR-a3-b1	α-actinin-2	α-actinin-2	intralink	762	178	47.53	0
DAKGITQEQMNEFR-KTAPYR-a3-b1	α-actinin-2	α-actinin-2	intralink	762	178	36.88	0
CQLEINFNTLQTKLR-ICKVLAVNQENER-a13-b3	α-actinin-2	α-actinin-2	intralink	365	285	44.73	0

CQLEINFNTLQTKLR-ICKVLAVNQENER-a13-b3	α-actinin-2	α-actinin-2	intralink	365	285	46.89	0
CQLEINFNTLQTKLR-ICKVLAVNQENER-a13-b3	α-actinin-2	α-actinin-2	intralink	365	285	46.22	0
KAGTQIENIEEDFR-ICKVLAVNQENER-a1-b3	α-actinin-2	α-actinin-2	intralink	68	285	38.95	0
KAGTQIENIEEDFR-ICKVLAVNQENER-a1-b3	α-actinin-2	α-actinin-2	intralink	68	285	28.98	0
DAKGITQEQMNEFR-ICKVLAVNQENER-a3-b3	α-actinin-2	α-actinin-2	intralink	762	285	38.28	0
DAKGITQEQMNEFR-ICKVLAVNQENER-a3-b3	α-actinin-2	α-actinin-2	intralink	762	285	45.99	0
DAKGITQEQMNEFR-ICKVLAVNQENER-a3-b3	α-actinin-2	α-actinin-2	intralink	762	285	48.2	0
TPEKTMQAMQK-KLEDFR-a4-b1	α-actinin-2	α-actinin-2	intralink	325	333	33.29	0
TPEKTMQAMQK-KLEDFR-a4-b1	α-actinin-2	α-actinin-2	intralink	325	333	35.1	0.016
TPEKTMQAMQK-KLEDFR-a4-b1	α-actinin-2	α-actinin-2	intralink	325	333	33.82	0
TMQAMQKK-KHKPPK-a7-b1	α-actinin-2	α-actinin-2	intralink	332	343	34.67	0
TMQAMQKK-KHKPPK-a7-b1	α-actinin-2	α-actinin-2	intralink	332	343	30.33	0.023
TMQAMQKK-KHKPPK-a7-b1	α-actinin-2	α-actinin-2	intralink	332	343	27.72	0.011
TMQAMQKK-KHKPPK-a7-b3	α-actinin-2	α-actinin-2	intralink	332	345	32.77	0
TMQAMQKK-KHKPPK-a7-b3	α-actinin-2	α-actinin-2	intralink	332	345	28.19	0.037
TMQAMQKK-KHKPPK-a7-b3	α-actinin-2	α-actinin-2	intralink	332	345	31.89	0
QYEHNIINYKNNIDK-KHKPPK-a10-b1	α-actinin-2	α-actinin-2	intralink	703	343	20.74	0.08
QYEHNIINYKNNIDK-KHKPPK-a10-b1	α-actinin-2	α-actinin-2	intralink	703	343	20.63	0.071

QKASTHETWAYGK-LEHLAEKFR-a2-b7	α-actinin-2	α-actinin-2	intralink	423	419	24.73	0.067
QKASTHETWAYGK-LEHLAEKFR-a2-b7	α-actinin-2	α-actinin-2	intralink	423	419	25.91	0.06
EQILLQKDYESASLTEVR-LGTLTQKR-a7-b7	α-actinin-2	α-actinin-2	intralink	441	513	38.46	0
EQILLQKDYESASLTEVR-LGTLTQKR-a7-b7	α-actinin-2	α-actinin-2	intralink	441	513	37.44	0.016
EQILLQKDYESASLTEVR-LGTLTQKR-a7-b7	α-actinin-2	α-actinin-2	intralink	441	513	42.2	0
DLLLDPAWEKQQR-KTFTAWCNSHLR-a10-b1	α-actinin-2	α-actinin-2	intralink	52	56	36.1	0.016
DLLLDPAWEKQQR-KTFTAWCNSHLR-a10-b1	α-actinin-2	α-actinin-2	intralink	52	56	34.58	0
KAGTQIENIEEDFR-KTFTAWCNSHLR-a1-b1	α-actinin-2	α-actinin-2	intralink	68	56	38.18	0
KAGTQIENIEEDFR-KTFTAWCNSHLR-a1-b1	α-actinin-2	α-actinin-2	intralink	68	56	34.49	0.016
KAGTQIENIEEDFR-KTFTAWCNSHLR-a1-b1	α-actinin-2	α-actinin-2	intralink	68	56	31.4	0
DLKPENLLLASK-LKGAAVK-a3-b2	CaMKII	CaMKII	intralink	144	155	23.54	0.033
DLKPENLLLASK-LKGAAVK-a3-b2	CaMKII	CaMKII	intralink	144	155	20.11	0.08
DLKPENLLLASK-DHQKLER-a3-b4	CaMKII	CaMKII	intralink	144	63	29.62	0
DLKPENLLLASK-DHQKLER-a3-b4	CaMKII	CaMKII	intralink	144	63	35.63	0.016
DLKPENLLLASK-DHQKLER-a3-b4	CaMKII	CaMKII	intralink	144	63	33.17	0
DLKPENLLLASKLK-NFSGGKSGGNK-a12-b6	CaMKII	CaMKII	intralink	153	324	34.2	0
DLKPENLLLASKLK-NFSGGKSGGNK-a12-b6	CaMKII	CaMKII	intralink	153	324	31.86	0.023
DLKPENLLLASKLK-NFSGGKSGGNK-a12-b6	CaMKII	CaMKII	intralink	153	324	31.73	0
DLKPENLLLASKLK-KNDGVK-a12-b1	CaMKII	CaMKII	intralink	153	330	31.63	0
DLKPENLLLASKLK-KNDGVK-a12-b1	CaMKII	CaMKII	intralink	153	330	29.45	0.023
DLKPENLLLASKLK-KNDGVK-a12-b1	CaMKII	CaMKII	intralink	153	330	24.99	0.071

DLKPENLLLASKLK-LLKHPNIVR-a12-b3	CaMKII	CaMKII	intralink	153	75	34.36	0.016
DLKPENLLLASKLK-LLKHPNIVR-a12-b3	CaMKII	CaMKII	intralink	153	75	32.66	0
LKGAAVK-LKGAAVK-a2-b2	CaMKII	CaMKII	intralink	155	155	36.1	0
LKGAAVK-LKGAAVK-a2-b2	CaMKII	CaMKII	intralink	155	155	33.54	0.016
LKGAAVK-LKGAAVK-a2-b2	CaMKII	CaMKII	intralink	155	155	35.02	0
MLTINPSKR-LKGAAVK-a8-b2	CaMKII	CaMKII	intralink	265	155	28.95	0.016
MLTINPSKR-LKGAAVK-a8-b2	CaMKII	CaMKII	intralink	265	155	28.43	0.032
MLTINPSKR-LKGAAVK-a8-b2	CaMKII	CaMKII	intralink	265	155	24.92	0.071
ITAAEALKHPWISHR-LKGAAVK-a8-b2	CaMKII	CaMKII	intralink	274	155	26.86	0.026
ITAAEALKHPWISHR-LKGAAVK-a8-b2	CaMKII	CaMKII	intralink	274	155	31.27	0.023
ITAAEALKHPWISHR-LKGAAVK-a8-b2	CaMKII	CaMKII	intralink	274	155	28.7	0
LKGAILTTMLATR-LKGAAVK-a2-b2	CaMKII	CaMKII	intralink	307	155	36.11	0
LKGAILTTMLATR-LKGAAVK-a2-b2	CaMKII	CaMKII	intralink	307	155	26.73	0.037
LKGAILTTMLATR-LKGAAVK-a2-b2	CaMKII	CaMKII	intralink	307	155	28.37	0
NFSGGKSGGNKK-LKGAAVK-a6-b2	CaMKII	CaMKII	intralink	324	155	38.03	0
NFSGGKSGGNKK-LKGAAVK-a6-b2	CaMKII	CaMKII	intralink	324	155	37.92	0.016
NFSGGKSGGNK-LKGAAVK-a6-b2	CaMKII	CaMKII	intralink	324	155	39.04	0
LKGAAVK-KNDGVK-a2-b1	CaMKII	CaMKII	intralink	155	330	38.59	0
LKGAAVK-KNDGVK-a2-b1	CaMKII	CaMKII	intralink	155	330	37.42	0.016
LKGAAVK-KNDGVK-a2-b1	CaMKII	CaMKII	intralink	155	330	38.25	0
CVKVLAGQEYAAK-LKGAAVK-a3-b2	CaMKII	CaMKII	intralink	39	155	34.4	0
CVKVLAGQEYAAK-LKGAAVK-a3-b2	CaMKII	CaMKII	intralink	39	155	40.43	0
VLAGQEYAAKIINTK-LKGAAVK-a10-b2	CaMKII	CaMKII	intralink	49	155	25.06	0.033

VLAGQEYAAKIINTK-LKGAAVK-a10-b2	CaMKII	CaMKII	intralink	49	155	25.16	0.045
VLAGQEYAAKIINTK-LKGAAVK-a10-b2	CaMKII	CaMKII	intralink	49	155	23.31	0.071
DHQKLER-LKGAAVK-a4-b2	CaMKII	CaMKII	intralink	63	155	36.1	0
DHQKLER-LKGAAVK-a4-b2	CaMKII	CaMKII	intralink	63	155	33.98	0.016
DHQKLER-LKGAAVK-a4-b2	CaMKII	CaMKII	intralink	63	155	31.25	0
LLKHPNIVR-LKGAAVK-a3-b2	CaMKII	CaMKII	intralink	75	155	40.14	0
LLKHPNIVR-LKGAAVK-a3-b2	CaMKII	CaMKII	intralink	75	155	40.17	0
LLKHPNIVR-LKGAAVK-a3-b2	CaMKII	CaMKII	intralink	75	155	42.07	0
MLTINPSKR-MLTINPSKR-a8-b8	CaMKII	CaMKII	intralink	265	265	27.91	0.026
MLTINPSKR-MLTINPSKR-a8-b8	CaMKII	CaMKII	intralink	265	265	28.52	0.032
MLTINPSKR-MLTINPSKR-a8-b8	CaMKII	CaMKII	intralink	265	265	34.3	0
ITAAEALKHPWISHR-MLTINPSKR-a8-b8	CaMKII	CaMKII	intralink	274	265	29.47	0.016
ITAAEALKHPWISHR-MLTINPSKR-a8-b8	CaMKII	CaMKII	intralink	274	265	34.23	0.016
ITAAEALKHPWISHR-MLTINPSKR-a8-b8	CaMKII	CaMKII	intralink	274	265	35.5	0
NFSGGKSGGNK-MLTINPSKR-a6-b8	CaMKII	CaMKII	intralink	324	265	37.66	0
NFSGGKSGGNK-MLTINPSKR-a6-b8	CaMKII	CaMKII	intralink	324	265	31.09	0.023
NFSGGKSGGNKK-MLTINPSKR-a6-b8	CaMKII	CaMKII	intralink	324	265	34.11	0
MLTINPSKR-SGGNKK-a8-b5	CaMKII	CaMKII	intralink	265	329	27.38	0.026
NFSGGKSGGNKK-MLTINPSKR-a11-b8	CaMKII	CaMKII	intralink	329	265	20.89	0.08
NFSGGKSGGNKK-MLTINPSKR-a11-b8	CaMKII	CaMKII	intralink	329	265	21.09	0.071
MLTINPSKR-KNDGVK-a8-b1	CaMKII	CaMKII	intralink	265	330	32.56	0
MLTINPSKR-KNDGVK-a8-b1	CaMKII	CaMKII	intralink	265	330	28.25	0.032
MLTINPSKR-KNDGVK-a8-b1	CaMKII	CaMKII	intralink	265	330	31.94	0

DGKWQIVHFHR-MLTINPSKR-a3-b8	CaMKII	CaMKII	intralink	468	265	25.73	0.045
DGKWQIVHFHR-MLTINPSKR-a3-b8	CaMKII	CaMKII	intralink	468	265	32.77	0
MLTINPSKR-DHQKLER-a8-b4	CaMKII	CaMKII	intralink	265	63	30.67	0
MLTINPSKR-DHQKLER-a8-b4	CaMKII	CaMKII	intralink	265	63	31.26	0.023
MLTINPSKR-DHQKLER-a8-b4	CaMKII	CaMKII	intralink	265	63	32.44	0
LLKHPNIVR-MLTINPSKR-a3-b8	CaMKII	CaMKII	intralink	75	265	24.74	0.033
LLKHPNIVR-MLTINPSKR-a3-b8	CaMKII	CaMKII	intralink	75	265	34.26	0.016
LLKHPNIVR-MLTINPSKR-a3-b8	CaMKII	CaMKII	intralink	75	265	33.2	0
ITAAEALKHPWISHR-DHQKLER-a8-b4	CaMKII	CaMKII	intralink	274	63	32.46	0
ITAAEALKHPWISHR-DHQKLER-a8-b4	CaMKII	CaMKII	intralink	274	63	32.85	0.016
ITAAEALKHPWISHR-DHQKLER-a8-b4	CaMKII	CaMKII	intralink	274	63	36.53	0
ITAAEALKHPWISHR-LLKHPNIVR-a8-b3	CaMKII	CaMKII	intralink	274	75	33.06	0
ITAAEALKHPWISHR-LLKHPNIVR-a8-b3	CaMKII	CaMKII	intralink	274	75	34.16	0.016
ITAAEALKHPWISHR-LLKHPNIVR-a8-b3	CaMKII	CaMKII	intralink	274	75	36.08	0
LKGAILTTMLATR-QETVDCLKK-a2-b8	CaMKII	CaMKII	intralink	307	298	24.54	0.033
LKGAILTTMLATR-QETVDCLKK-a2-b8	CaMKII	CaMKII	intralink	307	298	28.94	0.023
NFSGGKSGGNK-QETVDCLKK-a6-b8	CaMKII	CaMKII	intralink	324	298	23.78	0.033
NFSGGKSGGNK-QETVDCLKK-a6-b8	CaMKII	CaMKII	intralink	324	298	33.49	0.016
NFSGGKSGGNK-QETVDCLKK-a6-b8	CaMKII	CaMKII	intralink	324	298	29.74	0
QETVDCLKK-SGGNKK-a8-b5	CaMKII	CaMKII	intralink	298	329	20.24	0.058
QETVDCLKK-SGGNKK-a8-b5	CaMKII	CaMKII	intralink	298	329	22.99	0.08
NFSGGKSGGNKK-QETVDCLKK-a11-b8	CaMKII	CaMKII	intralink	329	298	20.3	0.071
LLKHPNIVR-QETVDCLKK-a3-b8	CaMKII	CaMKII	intralink	75	298	24.1	0.075

LLKHPNIVR-QETVDCLKK-a3-b8	CaMKII	CaMKII	intralink	75	298	26.88	0.054
LKGAILTTMLATR-NFSGGKSGGNK-a2-b6	CaMKII	CaMKII	intralink	307	324	44.99	0
LKGAILTTMLATR-NFSGGKSGGNK-a2-b6	CaMKII	CaMKII	intralink	307	324	42.1	0
LKGAILTTMLATR-NFSGGKSGGNK-a2-b6	CaMKII	CaMKII	intralink	307	324	35.31	0
KLKGAILTTMLATR-NFSGGKSGGNKK-a3-b11	CaMKII	CaMKII	intralink	307	329	24.97	0.061
LKGAILTTMLATR-NFSGGKSGGNKK-a2-b11	CaMKII	CaMKII	intralink	307	329	28.46	0
LKGAILTTMLATR-KNDGVK-a2-b1	CaMKII	CaMKII	intralink	307	330	39.78	0
LKGAILTTMLATR-KNDGVK-a2-b1	CaMKII	CaMKII	intralink	307	330	35.8	0.016
LKGAILTTMLATR-KNDGVK-a2-b1	CaMKII	CaMKII	intralink	307	330	31.68	0
LKGAILTTMLATR-KQEIIK-a2-b1	CaMKII	CaMKII	intralink	307	354	26.84	0.026
LKGAILTTMLATR-KQEIIK-a2-b1	CaMKII	CaMKII	intralink	307	354	30.06	0.023
LKGAILTTMLATR-KQEIIK-a2-b1	CaMKII	CaMKII	intralink	307	354	31.79	0
LKGAILTTMLATR-DHQKLER-a2-b4	CaMKII	CaMKII	intralink	307	63	38.1	0
KLKGAILTTMLATR-DHQKLER-a3-b4	CaMKII	CaMKII	intralink	307	63	39.76	0
LKGAILTTMLATR-DHQKLER-a2-b4	CaMKII	CaMKII	intralink	307	63	39.97	0
NFSGGKSGGNKK-NFSGGKSGGNKK-a6-b6	CaMKII	CaMKII	intralink	324	324	32.23	0
NFSGGKSGGNK-NFSGGKSGGNK-a6-b6	CaMKII	CaMKII	intralink	324	324	31.4	0.023
NFSGGKSGGNK-NFSGGKSGGNK-a6-b6	CaMKII	CaMKII	intralink	324	324	29.89	0
NFSGGKSGGNK-KNDGVK-a6-b1	CaMKII	CaMKII	intralink	324	330	34.26	0
NFSGGKSGGNK-KNDGVK-a6-b1	CaMKII	CaMKII	intralink	324	330	38.05	0.016
NFSGGKSGGNK-KNDGVK-a6-b1	CaMKII	CaMKII	intralink	324	330	37.05	0

NDGVKESSESTNTTIEDEDTK-NFSGGKSGGNK-a5-b6	CaMKII	CaMKII	intralink	335	324	22.94	0.033
NDGVKESSESTNTTIEDEDTK-NFSGGKSGGNK-a5-b6	CaMKII	CaMKII	intralink	335	324	28.87	0.023
NDGVKESSESTNTTIEDEDTK-NFSGGKSGGNK-a5-b6	CaMKII	CaMKII	intralink	335	324	32.59	0
ESSESTNTTIEDEDTKVR-NFSGGKSGGNK-a16-b6	CaMKII	CaMKII	intralink	351	324	29.26	0.023
ESSESTNTTIEDEDTKVR-NFSGGKSGGNK-a16-b6	CaMKII	CaMKII	intralink	351	324	32.09	0
NFSGGKSGGNKK-KQEIIK-a6-b1	CaMKII	CaMKII	intralink	324	354	38.18	0
NFSGGKSGGNKK-KQEIIK-a6-b1	CaMKII	CaMKII	intralink	324	354	38.93	0
NFSGGKSGGNKK-KQEIIK-a6-b1	CaMKII	CaMKII	intralink	324	354	38.21	0
VLAGQEYAAKIINTK-NFSGGKSGGNK-a10-b6	CaMKII	CaMKII	intralink	49	324	33.84	0
VLAGQEYAAKIINTK-NFSGGKSGGNK-a10-b6	CaMKII	CaMKII	intralink	49	324	36.71	0.016
VLAGQEYAAKIINTK-NFSGGKSGGNK-a10-b6	CaMKII	CaMKII	intralink	49	324	33.49	0
NFSGGKSGGNK-IINTKK-a6-b5	CaMKII	CaMKII	intralink	324	54	35.18	0
NFSGGKSGGNK-IINTKK-a6-b5	CaMKII	CaMKII	intralink	324	54	31.94	0.023
NFSGGKSGGNKK-IINTKK-a6-b5	CaMKII	CaMKII	intralink	324	54	37.58	0
NFSGGKSGGNKK-DHQKLER-a6-b4	CaMKII	CaMKII	intralink	324	63	34.28	0
NFSGGKSGGNKK-DHQKLER-a6-b4	CaMKII	CaMKII	intralink	324	63	38.55	0

NFSGGKSGGNK-DHQKLER-a6-b4	CaMKII	CaMKII	intralink	324	63	39.45	0
NFSGGKSGGNK-LLKHPNIVR-a6-b3	CaMKII	CaMKII	intralink	324	75	24.42	0.033
NFSGGKSGGNKK-LLKHPNIVR-a6-b3	CaMKII	CaMKII	intralink	324	75	36.6	0.016
NFSGGKSGGNKK-LLKHPNIVR-a6-b3	CaMKII	CaMKII	intralink	324	75	36.77	0
NFSGGKSGGNKK-KNDGVK-a11-b1	CaMKII	CaMKII	intralink	329	330	27.8	0.026
NFSGGKSGGNKK-KNDGVK-a11-b1	CaMKII	CaMKII	intralink	329	330	27.07	0.037
NDGVKESSESTNTTIEDEDTK-NFSGGKSGGNKK-a5-b11	CaMKII	CaMKII	intralink	335	329	23.85	0.033
NDGVKESSESTNTTIEDEDTKVR-SGGNKK-a5-b5	CaMKII	CaMKII	intralink	335	329	29.93	0.023
NDGVKESSESTNTTIEDEDTK-SGGNKK-a5-b5	CaMKII	CaMKII	intralink	335	329	25.83	0.06
KQEIIK-SGGNKK-a1-b5	CaMKII	CaMKII	intralink	354	329	34.11	0
KQEIIK-SGGNKK-a1-b5	CaMKII	CaMKII	intralink	354	329	32.54	0.016
LLKHPNIVR-SGGNKK-a3-b5	CaMKII	CaMKII	intralink	75	329	34.39	0
LLKHPNIVR-SGGNKK-a3-b5	CaMKII	CaMKII	intralink	75	329	40.48	0
LLKHPNIVR-SGGNKK-a3-b5	CaMKII	CaMKII	intralink	75	329	38.81	0
NDGVKESSESTNTTIEDEDTK-KNDGVK-a5-b1	CaMKII	CaMKII	intralink	335	330	39.96	0
NDGVKESSESTNTTIEDEDTK-KNDGVK-a5-b1	CaMKII	CaMKII	intralink	335	330	38.1	0
ESSESTNTTIEDEDTKVR-KNDGVK-a16-b1	CaMKII	CaMKII	intralink	351	330	26.32	0.026
ESSESTNTTIEDEDTKVR-KNDGVK-a16-b1	CaMKII	CaMKII	intralink	351	330	23.63	0.08
KNDGVKESSESTNTTIEDEDTK-KQEIIK-a1-b1	CaMKII	CaMKII	intralink	330	354	23.75	0.033

KNDGVK-KQEIIK-a1-b1	CaMKII	CaMKII	intralink	330	354	32	0
DGKWQIVHFHR-KNDGVK-a3-b1	CaMKII	CaMKII	intralink	468	330	26.59	0.026
DGKWQIVHFHR-KNDGVK-a3-b1	CaMKII	CaMKII	intralink	468	330	35.84	0.016
DGKWQIVHFHR-KNDGVK-a3-b1	CaMKII	CaMKII	intralink	468	330	33.31	0
IINTKK-KNDGVK-a5-b1	CaMKII	CaMKII	intralink	54	330	23.61	0.033
IINTKK-KNDGVK-a5-b1	CaMKII	CaMKII	intralink	54	330	26.95	0.037
DHQKLER-KNDGVK-a4-b1	CaMKII	CaMKII	intralink	63	330	36.37	0
DHQKLER-KNDGVK-a4-b1	CaMKII	CaMKII	intralink	63	330	35.31	0.016
KNDGVKESSESTNTTIEDEDTK-DHQKLER-a1-b4	CaMKII	CaMKII	intralink	330	63	22.21	0.071
NDGVKESSESTNTTIEDEDTK-KQEIIK-a5-b1	CaMKII	CaMKII	intralink	335	354	49.75	0
NDGVKESSESTNTTIEDEDTK-KQEIIK-a5-b1	CaMKII	CaMKII	intralink	335	354	41.7	0
NDGVKESSESTNTTIEDEDTK-KQEIIK-a5-b1	CaMKII	CaMKII	intralink	335	354	43.17	0
NDGVKESSESTNTTIEDEDTK-DHQKLER-a5-b4	CaMKII	CaMKII	intralink	335	63	29.18	0.016
NDGVKESSESTNTTIEDEDTK-DHQKLER-a5-b4	CaMKII	CaMKII	intralink	335	63	23.89	0.08
NDGVKESSESTNTTIEDEDTK-DHQKLER-a5-b4	CaMKII	CaMKII	intralink	335	63	26.19	0.06
ESSESTNTTIEDEDTKVR-ESSESTNTTIEDEDTKVR-a16-b16	CaMKII	CaMKII	intralink	351	351	27.67	0.026
ESSESTNTTIEDEDTKVR-ESSESTNTTIEDEDTKVR-a16-b16	CaMKII	CaMKII	intralink	351	351	34.74	0.016

ESSESTNTTIEDEDTKVR-ESSESTNTTIEDEDTKVR-a16-b16	CaMKII	CaMKII	intralink	351	351	30.21	0
ESSESTNTTIEDEDTKVR-KQEIIK-a16-b1	CaMKII	CaMKII	intralink	351	354	28.12	0.026
ESSESTNTTIEDEDTKVR-KQEIIK-a16-b1	CaMKII	CaMKII	intralink	351	354	31.38	0.023
ESSESTNTTIEDEDTKVR-KQEIIK-a16-b1	CaMKII	CaMKII	intralink	351	354	30.99	0
CVKVLAGQEYAAK-IINTKK-a3-b5	CaMKII	CaMKII	intralink	39	54	33.97	0.016
CVKVLAGQEYAAK-IINTKK-a3-b5	CaMKII	CaMKII	intralink	39	54	34.15	0
CVKVLAGQEYAAK-DHQKLER-a3-b4	CaMKII	CaMKII	intralink	39	63	28.38	0.032
CVKVLAGQEYAAK-DHQKLER-a3-b4	CaMKII	CaMKII	intralink	39	63	24.65	0.071
CVKVLAGQEYAAK-LLKHPNIVR-a3-b3	CaMKII	CaMKII	intralink	39	75	28.47	0.026
CVKVLAGQEYAAK-LLKHPNIVR-a3-b3	CaMKII	CaMKII	intralink	39	75	36.44	0.016
CVKVLAGQEYAAK-LLKHPNIVR-a3-b3	CaMKII	CaMKII	intralink	39	75	38.75	0
DGKWQIVHFHR-DHQKLER-a3-b4	CaMKII	CaMKII	intralink	468	63	24.25	0.067
DGKWQIVHFHR-DHQKLER-a3-b4	CaMKII	CaMKII	intralink	468	63	26.62	0.06
VLAGQEYAAKIINTK-DHQKLER-a10-b4	CaMKII	CaMKII	intralink	49	63	36.53	0
VLAGQEYAAKIINTK-DHQKLER-a10-b4	CaMKII	CaMKII	intralink	49	63	32.23	0.023
VLAGQEYAAKIINTK-DHQKLER-a10-b4	CaMKII	CaMKII	intralink	49	63	37.87	0
DHQKLER-IINTKK-a4-b5	CaMKII	CaMKII	intralink	63	54	30.62	0
DHQKLER-IINTKK-a4-b5	CaMKII	CaMKII	intralink	63	54	28.77	0.023
DHQKLER-IINTKK-a4-b5	CaMKII	CaMKII	intralink	63	54	31.36	0
LLKHPNIVR-IINTKK-a3-b5	CaMKII	CaMKII	intralink	75	54	31.24	0
LLKHPNIVR-IINTKK-a3-b5	CaMKII	CaMKII	intralink	75	54	32.6	0.016
LLKHPNIVR-IINTKK-a3-b5	CaMKII	CaMKII	intralink	75	54	30.72	0

LSARDHQKLER-DHQKLEREAR-a8-b4	CaMKII	CaMKII	intralink	63	63	24.47	0.033
DHQKLER-DHQKLER-a4-b4	CaMKII	CaMKII	intralink	63	63	33.39	0
LLKHPNIVR-DHQKLER-a3-b4	CaMKII	CaMKII	intralink	75	63	45.2	0
LLKHPNIVR-DHQKLER-a3-b4	CaMKII	CaMKII	intralink	75	63	42.51	0
LLKHPNIVR-DHQKLER-a3-b4	CaMKII	CaMKII	intralink	75	63	43.17	0
LLKHPNIVR-LLKHPNIVR-a3-b3	CaMKII	CaMKII	intralink	75	75	40.91	0
LLKHPNIVR-LLKHPNIVR-a3-b3	CaMKII	CaMKII	intralink	75	75	40.58	0
LLKHPNIVR-LLKHPNIVR-a3-b3	CaMKII	CaMKII	intralink	75	75	41.21	0
ALVTNKPVVSALHGAVPGR-QPTVAGASKTRPDFR-a6-b9	GluN2B	GluN2B	intralink	169	157	20.79	0.058
ALVTNKPVVSALHGAVPGR-QPTVAGASKTRPDFR-a6-b9	GluN2B	GluN2B	intralink	169	157	23.04	0.08
ALVTNKPVVSALHGAVPGR-QPTVAGASKTRPDFR-a6-b9	GluN2B	GluN2B	intralink	169	157	26.81	0.054
DICIGNQSNPCVPNNKNPR-QPTVAGASKTRPDFR-a16-b9	GluN2B	GluN2B	intralink	201	157	26.93	0.026
DICIGNQSNPCVPNNKNPR-QPTVAGASKTRPDFR-a16-b9	GluN2B	GluN2B	intralink	201	157	26.12	0.037
DICIGNQSNPCVPNNKNPR-QPTVAGASKTRPDFR-a16-b9	GluN2B	GluN2B	intralink	201	157	28.3	0
QPTVAGASKTRPDFR-YPQSPTNSKAQK-a9-b9	GluN2B	GluN2B	intralink	157	32	20.61	0.058
QPTVAGASKTRPDFR-YPQSPTNSKAQK-a9-b9	GluN2B	GluN2B	intralink	157	32	25.44	0.045

QPTVAGASKTRPDFR-YPQSPTNSKAQK-a9-b9	GluN2B	GluN2B	intralink	157	32	23.09	0.071
QPTVAGASKTRPDFR-SVSLKDK-a9-b5	GluN2B	GluN2B	intralink	157	68	25.4	0.033
QPTVAGASKTRPDFR-SVSLKDK-a9-b5	GluN2B	GluN2B	intralink	157	68	25.01	0.053
QPTVAGASKTRPDFR-SVSLKDK-a9-b5	GluN2B	GluN2B	intralink	157	68	25.61	0.068
ALVTNKPVVSALHGAVPGR-SVSLKDK-a6-b5	GluN2B	GluN2B	intralink	169	68	30.99	0
ALVTNKPVVSALHGAVPGR-SVSLKDK-a6-b5	GluN2B	GluN2B	intralink	169	68	30.47	0.023
ALVTNKPVVSALHGAVPGR-SVSLKDK-a6-b5	GluN2B	GluN2B	intralink	169	68	30.64	0
FQKDICIGNQSNPCVPNNKNPR-SVSLKDK-a3-b5	GluN2B	GluN2B	intralink	185	68	21.74	0.054
FQKDICIGNQSNPCVPNNKNPR-SVSLKDK-a3-b5	GluN2B	GluN2B	intralink	185	68	32.38	0.016
FQKDICIGNQSNPCVPNNK-SVSLKDK-a3-b5	GluN2B	GluN2B	intralink	185	68	30.32	0
DICIGNQSNPCVPNNKNPR-YPQSPTNSKAQK-a16-b9	GluN2B	GluN2B	intralink	201	32	26.6	0.026
DICIGNQSNPCVPNNKNPR-YPQSPTNSKAQK-a16-b9	GluN2B	GluN2B	intralink	201	32	27.73	0.037
DICIGNQSNPCVPNNKNPR-YPQSPTNSKAQK-a16-b9	GluN2B	GluN2B	intralink	201	32	28.36	0
DICIGNQSNPCVPNNKNPR-SVSLKDK-a16-b5	GluN2B	GluN2B	intralink	201	68	33.19	0.016
DICIGNQSNPCVPNNKNPR-SVSLKDK-a16-b5	GluN2B	GluN2B	intralink	201	68	33.66	0
QHSYDTFVDLQKEEAALAPR-SVSLKDK-a12-b5	GluN2B	GluN2B	intralink	55	68	41.3	0

QHSYDTFVDLQKEEAALAPR-SVSLKDK-a12-b5	GluN2B	GluN2B	intralink	55	68	41.39	0
RQHSYDTFVDLQKEEAALAPR-SVSLKDK-a13-b5	GluN2B	GluN2B	intralink	55	68	42.5	0
VFDKDGNGYISAAELR-KMKDTDSEEEIR-a4-b1	CaM	CaM	intralink	95	76	46.41	0
VFDKDGNGYISAAELR-KMKDTDSEEEIR-a4-b1	CaM	CaM	intralink	95	76	34.36	0
VFDKDGNGYISAAELR-MKDTDSEEEIR-a4-b2	CaM	CaM	intralink	95	78	40.09	0
VFDKDGNGYISAAELR-MKDTDSEEEIR-a4-b2	CaM	CaM	intralink	95	78	47.66	0
VFDKDGNGYISAAELR-MKDTDSEEEIR-a4-b2	CaM	CaM	intralink	95	78	49.48	0

Supplementary table 2. Raw table of XL-MS identified monolink in CaMKII-GluN2B-actinin mixtures. Note absolute position of proteins include also include their affinity tag and cleavage residues

Sequence Id	Protein1	Protein2	XLType	AbsPos1	AbsPos2	ld-Score	FDR
LMLLLEVISGERLPKPDR-K15-156	α-actinin-2	-	monolink	100		44.71	0
LMLLLEVISGERLPKPDR-K15-156	α-actinin-2	-	monolink	100		42.74	0
FHKIANVNK-K3-155	α-actinin-2	-	monolink	110		41.37	0
FHKIANVNK-K3-155	α-actinin-2	-	monolink	110		42.86	0

FHKIANVNK-K3-155	α-actinin-2	-	monolink	110		39.65	0
GVKLVSIGAEEIVDGNVK-K3-156	α-actinin-2	-	monolink	127		29.03	0
GVKLVSIGAEEIVDGNVK-K3-156	α-actinin-2	-	monolink	127		27.79	0
GVKLVSIGAEEIVDGNVK-K3-156	α-actinin-2	-	monolink	127		29.09	0
FAIQDISVEETSAKEGLLLWCQR-K14-155	α-actinin-2	-	monolink	168		27.46	0
FAIQDISVEETSAKEGLLLWCQR-K14-156	α-actinin-2	-	monolink	168		42.1	0
FAIQDISVEETSAKEGLLLWCQR-K14-156	α-actinin-2	-	monolink	168		41.91	0
NVNIQNFHTSWKDGLGLCALIHR-K12-156	α-actinin-2	-	monolink	195		46.96	0
NVNIQNFHTSWKDGLGLCALIHR-K12-156	α-actinin-2	-	monolink	195		47.29	0
NVNIQNFHTSWKDGLGLCALIHR-K12-155	α-actinin-2	-	monolink	195		46.96	0
HRPDLIDYSKLNK-K10-155	α-actinin-2	-	monolink	216		43.88	0
HRPDLIDYSKLNK-K10-155	α-actinin-2	-	monolink	216		43.51	0
HRPDLIDYSKLNK-K10-155	α-actinin-2	-	monolink	216		43.74	0
LNKDDPIGNINLAMEIAEK-K3-156	α-actinin-2	-	monolink	219		30.94	0
LNKDDPIGNINLAMEIAEK-K3-156	α-actinin-2	-	monolink	219		33.83	0
LNKDDPIGNINLAMEIAEK-K3-156	α-actinin-2	-	monolink	219		42.49	0
LNKDDPIGNINLAMEIAEKHLDIPK-K19-156	α-actinin-2	-	monolink	235		36.54	0
LNKDDPIGNINLAMEIAEKHLDIPK-K19-156	α-actinin-2	-	monolink	235		41.62	0
LNKDDPIGNINLAMEIAEKHLDIPK-K19-156	α-actinin-2	-	monolink	235		41.03	0
MLDAEDIVNTPKPDER-K12-156	α-actinin-2	-	monolink	253		33.53	0
MLDAEDIVNTPKPDER-K12-156	α-actinin-2	-	monolink	253		32.77	0
MLDAEDIVNTPKPDER-K12-156	α-actinin-2	-	monolink	253		29.55	0
ICKVLAVNQENER-K3-156	α-actinin-2	-	monolink	285		44.73	0

ICKVLAVNQENER-K3-156	α-actinin-2	-	monolink	285		48.95	0
ICKVLAVNQENER-K3-156	α-actinin-2	-	monolink	285		47.96	0
VQEKCQLEINFNTLQTK-K4-156	α-actinin-2	-	monolink	352		47.61	0
VQEKCQLEINFNTLQTK-K4-156	α-actinin-2	-	monolink	352		49.89	0
VQEKCQLEINFNTLQTK-K4-156	α-actinin-2	-	monolink	352		49.33	0
CQLEINFNTLQTKLR-K13-155	α-actinin-2	-	monolink	365		38.17	0
CQLEINFNTLQTKLR-K13-155	α-actinin-2	-	monolink	365		39.09	0
CQLEINFNTLQTKLR-K13-155	α-actinin-2	-	monolink	365		37.89	0
ISNRPAFMPSEGKMVSDIAGAWQR-K13-156	α-actinin-2	-	monolink	380		39.8	0
ISNRPAFMPSEGKMVSDIAGAWQR-K13-155	α-actinin-2	-	monolink	380		42.96	0
ISNRPAFMPSEGKMVSDIAGAWQR-K13-156	α-actinin-2	-	monolink	380		43.35	0
LEQAEKGYEEWLLNEIR-K6-156	α-actinin-2	-	monolink	397		46.13	0
LEQAEKGYEEWLLNEIR-K6-155	α-actinin-2	-	monolink	397		45.77	0
LEQAEKGYEEWLLNEIR-K6-156	α-actinin-2	-	monolink	397		46.92	0
LEHLAEKFR-K7-155	α-actinin-2	-	monolink	419		40.27	0
LEHLAEKFR-K7-156	α-actinin-2	-	monolink	419		38.93	0
LEHLAEKFR-K7-156	α-actinin-2	-	monolink	419		38.94	0
EQILLQKDYESASLTEVR-K7-156	α-actinin-2	-	monolink	441		33.33	0
EQILLQKDYESASLTEVR-K7-156	α-actinin-2	-	monolink	441		47.11	0
EQILLQKDYESASLTEVR-K7-156	α-actinin-2	-	monolink	441		43.63	0
KHEAFESDLAAHQDR-K1-156	α-actinin-2	-	monolink	457		50.36	0
KHEAFESDLAAHQDR-K1-156	α-actinin-2	-	monolink	457		50.53	0
KHEAFESDLAAHQDR-K1-156	α-actinin-2	-	monolink	457		50.01	0

DLLLDPAWEKQQR-K10-156	α-actinin-2	-	monolink	52		41.45	0
DLLLDPAWEKQQR-K10-156	α-actinin-2	-	monolink	52		39.76	0
MEKLLETIDQLHLEFAK-K3-155	α-actinin-2	-	monolink	523		33.83	0
MEKLLETIDQLHLEFAK-K3-155	α-actinin-2	-	monolink	523		40.7	0
MEKLLETIDQLHLEFAK-K3-156	α-actinin-2	-	monolink	523		30.72	0
LLETIDQLHLEFAKR-K14-156	α-actinin-2	-	monolink	537		38.23	0
LLETIDQLHLEFAKR-K14-155	α-actinin-2	-	monolink	537		36.48	0
LLETIDQLHLEFAKR-K14-156	α-actinin-2	-	monolink	537		36.97	0
KTFTAWCNSHLR-K1-155	α-actinin-2	-	monolink	56		31.63	0
KTFTAWCNSHLR-K1-155	α-actinin-2	-	monolink	56		35.61	0
QSIMAIQNEVEKVIQSYNIR-K12-155	α-actinin-2	-	monolink	598		43.26	0
QSIMAIQNEVEKVIQSYNIR-K12-155	α-actinin-2	-	monolink	598		41.97	0
QSIMAIQNEVEKVIQSYNIR-K12-155	α-actinin-2	-	monolink	598		44.41	0
VKQLVPIRDQSLQEELAR-K2-155	α-actinin-2	-	monolink	629		30.91	0
VKQLVPIRDQSLQEELAR-K2-155	α-actinin-2	-	monolink	629		30.18	0
VKQLVPIRDQSLQEELAR-K2-156	α-actinin-2	-	monolink	629		27.58	0
QFAAQANAIGPWIQNKMEEIAR-K16-156	α-actinin-2	-	monolink	670		28.51	0
QFAAQANAIGPWIQNKMEEIAR-K16-156	α-actinin-2	-	monolink	670		34.27	0
RQFAAQANAIGPWIQNKMEEIAR-K17-156	α-actinin-2	-	monolink	670		31.25	0
KAGTQIENIEEDFR-K1-156	α-actinin-2	-	monolink	68		40.03	0
KAGTQIENIEEDFR-K1-155	α-actinin-2	-	monolink	68		43.28	0
KAGTQIENIEEDFR-K1-155	α-actinin-2	-	monolink	68		37.16	0

SSIQITGALEDQMNQLKQYEHNIINYK-K17-156	α-actinin-2	-	monolink	693		34.81	0
SSIQITGALEDQMNQLKQYEHNIINYK-K17-156	α-actinin-2	-	monolink	693		36.43	0
SSIQITGALEDQMNQLKQYEHNIINYK-K17-156	α-actinin-2	-	monolink	693		37.14	0
NNIDKLEGDHQLIQEALVFDNK-K5-156	α-actinin-2	-	monolink	708		44.27	0
NNIDKLEGDHQLIQEALVFDNK-K5-155	α-actinin-2	-	monolink	708		46.13	0
NNIDKLEGDHQLIQEALVFDNK-K5-155	α-actinin-2	-	monolink	708		45.46	0
DAKGITQEQMNEFR-K3-156	α-actinin-2	-	monolink	762		29.19	0
DAKGITQEQMNEFR-K3-156	α-actinin-2	-	monolink	762		33.86	0
KNGLMDHEDFR-K1-156	α-actinin-2	-	monolink	783		26.06	0
RKNGLMDHEDFR-K2-156	α-actinin-2	-	monolink	783		27.41	0
KNGLMDHEDFR-K1-156	α-actinin-2	-	monolink	783		32.4	0
ILASDKPYILAEELRR-K6-156	α-actinin-2	-	monolink	856		25.19	0
ILASDKPYILAEELRR-K6-155	α-actinin-2	-	monolink	856		22	0
ILASDKPYILAEELRR-K6-156	α-actinin-2	-	monolink	856		25.17	0
ELPPDQAQYCIKR-K12-156	α-actinin-2	-	monolink	878		41.73	0
ELPPDQAQYCIKR-K12-156	α-actinin-2	-	monolink	878		45	0
ELPPDQAQYCIKR-K12-156	α-actinin-2	-	monolink	878		46.3	0
DLKPENLLLASKLK-K12-156	CaMKII	-	monolink	153		47.48	0
DLKPENLLLASKLK-K12-156	CaMKII	-	monolink	153		48.49	0
DLKPENLLLASKLK-K12-155	CaMKII	-	monolink	153		49.1	0
LYQQIKAGAYDFPSPEWDTVTPEAK-K6-155	CaMKII	-	monolink	233		52.01	0

LYQQIKAGAYDFPSPEWDTVTPEAK-K6-156	CaMKII	-	monolink	233		43.45	0
DLINKMLTINPSKR-K5-155	CaMKII	-	monolink	257		35.65	0
DLINKMLTINPSKR-K5-155	CaMKII	-	monolink	257		37.62	0
DLINKMLTINPSKR-K5-155	CaMKII	-	monolink	257		33.79	0
ITAAEALKHPWISHR-K8-156	CaMKII	-	monolink	274		44.68	0
ITAAEALKHPWISHR-K8-156	CaMKII	-	monolink	274		42.18	0
ITAAEALKHPWISHR-K8-156	CaMKII	-	monolink	274		43.79	0
FTEEYQLFEELGKGAFSVVR-K13-156	CaMKII	-	monolink	28		39.42	0
FTEEYQLFEELGKGAFSVVR-K13-156	CaMKII	-	monolink	28		44.29	0
FTEEYQLFEELGKGAFSVVR-K13-156	CaMKII	-	monolink	28		46.42	0
QETVDCLKKFNAR-K8-156	CaMKII	-	monolink	298		21.89	0
QETVDCLKKFNAR-K8-156	CaMKII	-	monolink	298		22.93	0
KLKGAILTTMLATR-K1-155	CaMKII	-	monolink	305		37.24	0
KLKGAILTTMLATR-K1-155	CaMKII	-	monolink	305		35.31	0
KLKGAILTTMLATR-K1-155	CaMKII	-	monolink	305		34.97	0
KLKGAILTTMLATR-K3-156	CaMKII	-	monolink	307		38.89	0
LKGAILTTMLATR-K2-156	CaMKII	-	monolink	307		36.93	0
LKGAILTTMLATR-K2-156	CaMKII	-	monolink	307		38.44	0
KNDGVKESSESTNTTIEDEDTK-K1-156	CaMKII	-	monolink	330		30.18	0
KNDGVKESSESTNTTIEDEDTK-K1-156	CaMKII	-	monolink	330		38.48	0
KNDGVKESSESTNTTIEDEDTK-K1-156	CaMKII	-	monolink	330		24.54	0
KNDGVKESSESTNTTIEDEDTK-K6-155	CaMKII	-	monolink	335		34.2	0
KNDGVKESSESTNTTIEDEDTK-K6-155	CaMKII	-	monolink	335		35.7	0

KNDGVKESSESTNTTIEDEDTK-K6-155	CaMKII	-	monolink	335		35.13	0
ESSESTNTTIEDEDTKVR-K16-155	CaMKII	-	monolink	351		20.51	0
NDGVKESSESTNTTIEDEDTKVR-K21-156	CaMKII	-	monolink	351		20.45	0
KQEIIKVTEQLIEAISNGDFESYTK-K6-156	CaMKII	-	monolink	359		43.68	0
KQEIIKVTEQLIEAISNGDFESYTK-K6-156	CaMKII	-	monolink	359		42.17	0
KQEIIKVTEQLIEAISNGDFESYTK-K6-155	CaMKII	-	monolink	359		40.91	0
RCVKVLAGQEYAAK-K4-156	CaMKII	-	monolink	39		39.92	0
RCVKVLAGQEYAAK-K4-156	CaMKII	-	monolink	39		43.3	0
RCVKVLAGQEYAAK-K4-156	CaMKII	-	monolink	39		42.86	0
NSKPVHTTILNPHIHLMGDESACIAYIR-K3-156	CaMKII	-	monolink	415		29.9	0
NSKPVHTTILNPHIHLMGDESACIAYIR-K3-156	CaMKII	-	monolink	415		34.42	0
NSKPVHTTILNPHIHLMGDESACIAYIR-K3-156	CaMKII	-	monolink	415		35.11	0
DGKWQIVHFHR-K3-156	CaMKII	-	monolink	468		32.45	0
DGKWQIVHFHR-K3-156	CaMKII	-	monolink	468		30.99	0
DGKWQIVHFHR-K3-156	CaMKII	-	monolink	468		30.9	0
VLAGQEYAAKIINTK-K10-156	CaMKII	-	monolink	49		43.15	0
VLAGQEYAAKIINTK-K10-156	CaMKII	-	monolink	49		44.39	0
VLAGQEYAAKIINTK-K10-156	CaMKII	-	monolink	49		46.07	0
LLKHPNIVR-K3-155	CaMKII	-	monolink	75		39.83	0
LLKHPNIVR-K3-155	CaMKII	-	monolink	75		39.68	0
LLKHPNIVR-K3-155	CaMKII	-	monolink	75		36.2	0

SSVPTAGHHHNNPGSGYMLSKSLYPDR-K21-156	GluN2B	-	monolink	116		35.57	0
SSVPTAGHHHNNPGSGYMLSKSLYPDR-K21-156	GluN2B	-	monolink	116		38.03	0
SSVPTAGHHHNNPGSGYMLSKSLYPDR-K21-155	GluN2B	-	monolink	116		37.35	0
VTQNPFIPTFGDDQCLLHGSKSYFFR-K21-156	GluN2B	-	monolink	143		44.55	0
VTQNPFIPTFGDDQCLLHGSKSYFFR-K21-156	GluN2B	-	monolink	143		43.67	0
VTQNPFIPTFGDDQCLLHGSKSYFFR-K21-156	GluN2B	-	monolink	143		43.82	0
QPTVAGASKTRPDFR-K9-156	GluN2B	-	monolink	157		34.45	0
QPTVAGASKTRPDFR-K9-156	GluN2B	-	monolink	157		34.12	0
QPTVAGASKTRPDFR-K9-156	GluN2B	-	monolink	157		34.07	0
ALVTNKPVVSALHGAVPGR-K6-156	GluN2B	-	monolink	169		38.26	0
ALVTNKPVVSALHGAVPGR-K6-156	GluN2B	-	monolink	169		40.45	0
ALVTNKPVVSALHGAVPGR-K6-156	GluN2B	-	monolink	169		39.28	0
FQKDICIGNQSNPCVPNNK-K3-155	GluN2B	-	monolink	185		38.43	0
FQKDICIGNQSNPCVPNNK-K3-156	GluN2B	-	monolink	185		38.05	0
FQKDICIGNQSNPCVPNNKNPR-K3-155	GluN2B	-	monolink	185		40.45	0
DICIGNQSNPCVPNNKNPR-K16-155	GluN2B	-	monolink	201		37.54	0
DICIGNQSNPCVPNNKNPR-K16-156	GluN2B	-	monolink	201		38.82	0
DICIGNQSNPCVPNNKNPR-K16-156	GluN2B	-	monolink	201		40.86	0
AFNGSSNGHVYEKLSSIESDV-K13-155	GluN2B	-	monolink	217		31.76	0
AFNGSSNGHVYEKLSSIESDV-K13-155	GluN2B	-	monolink	217		29	0
AFNGSSNGHVYEKLSSIESDV-K13-155	GluN2B	-	monolink	217		34.47	0

QHSYDTFVDLQKEEAALAPR-K12-156	GluN2B	-	monolink	55		43.84	0
QHSYDTFVDLQKEEAALAPR-K12-156	GluN2B	-	monolink	55		49.03	0
RQHSYDTFVDLQKEEAALAPR-K13-156	GluN2B	-	monolink	55		42.49	0
HVMTNLGEKLTDEEVDEMIR-K9-156	CaM	-	monolink	116		40.11	0
HVMTNLGEKLTDEEVDEMIR-K9-155	CaM	-	monolink	116		40.23	0
HVMTNLGEKLTDEEVDEMIR-K9-156	CaM	-	monolink	116		40.01	0
EAFSLFDKDGDGTITTK-K8-156	CaM	-	monolink	22		40.61	0
EAFSLFDKDGDGTITTK-K8-156	CaM	-	monolink	22		41.97	0
EAFSLFDKDGDGTITTK-K8-155	CaM	-	monolink	22		41.36	0
EAFSLFDKDGDGTITTKELGTVMR-K17-156	CaM	-	monolink	31		42.85	0
EAFSLFDKDGDGTITTKELGTVMR-K17-156	CaM	-	monolink	31		35.42	0
EAFSLFDKDGDGTITTKELGTVMR-K17-156	CaM	-	monolink	31		34.71	0
KMKDTDSEEEIR-K1-155	CaM	-	monolink	76		36.71	0
KMKDTDSEEEIR-K1-155	CaM	-	monolink	76		38.58	0
KMKDTDSEEEIR-K1-155	CaM	-	monolink	76		38.44	0
KMKDTDSEEEIR-K3-155	CaM	-	monolink	78		37.89	0
KMKDTDSEEEIR-K3-155	CaM	-	monolink	78		41.54	0
KMKDTDSEEEIR-K3-155	CaM	-	monolink	78		40.92	0
VFDKDGNGYISAAELR-K4-156	CaM	-	monolink	95		42.8	0
VFDKDGNGYISAAELR-K4-156	CaM	-	monolink	95		44.17	0
VFDKDGNGYISAAELR-K4-156	CaM	-	monolink	95		43.48	0